

**Structural Studies and Gene Silencing Activities of Chemically
Modified Nucleic Acids:
Effect of C2' Sugar Modifications and Iso-nucleobases on the
Stability and Polarity of Duplex and Tetraplex Structures**

Maryam Yahyae Anzae

Department of Chemistry
McGill University, Montréal
December, 2014

A thesis submitted to McGill University in partial fulfillment of the requirements of the degree
of
Doctor of Philosophy

©Maryam Yahyae Anzae, 2014

To my mom and dad,

COPYRIGHT STATEMENT

Some of the material presented in this thesis work has been adapted from published manuscripts and is under copyright:

Content in **Chapter 2** has been reproduced and adapted in part from the following two papers:

[Yahyaee Anzahaee, M. *et al.* (2011) Energetically Important C-H...F-C Pseudohydrogen Bonding in Water: Evidence and Application to Rational Design of Oligonucleotides with High Binding Affinity; *J. Am. Chem. Soc.* 133: 728–731]. Permission obtained from American Chemical Society publications.

[Martín-Pintado, N., Yahyaee Anzahaee, M. *et al.* (2013) Dramatic Effect of Furanose C2' Substitution on Structure and Stability: Directing the Folding of the Human Telomeric Quadruplex with a Single Fluorine Atom; *J. Am. Chem. Soc.* 135: 5344-5347]. Permission obtained from American Chemical Society publications.

Content in **Chapter 3** has been reproduced and adapted in part from [Martín-Pintado, N., Yahyaee Anzahaee, M. *et al.* (2012) The solution structure of double helical arabino-nucleic acids (ANA and 2'F-ANA): effect of arabinoses in duplex-hairpin interconversion; *Nucleic Acids Research*, 40: 9329–9339]. Permission obtained from Oxford University Press.

Content in **Chapter 4** has been reproduced and adapted in part from [Yahyaee Anzahaee, M. *et al.* (2014) Arabinonucleic Acids: 2'-Stereoisomeric Modulators of siRNA Activity; *Nucleic Acids Therapeutics*, 24: 336-343]. Permission obtained from Mary Ann Liebert, Inc.

ABSTRACT

The increasing number of promising applications for chemically modified nucleic acid analogues range from new oligonucleotide therapeutics to the design of DNA-based nanodevices, diagnostics, functional genomics and target validation. Among the many modified nucleic acids, and specifically those with modifications in their sugar moiety, arabinonucleic acid (ANA) and its 2'-fluorinated derivative (2'-F-ANA) are particularly interesting to our group, and this thesis is primarily focused on understanding the structural basis for the interesting properties imparted by these analogues, with a focus on their structure, stability, and activity in cell based systems.

Our work has led to the finding that the high binding affinity of 2'-F-ANA for RNA or itself is, in part, due to a hydrogen bonding interaction between the organic fluorine of the 2'-F-ANA nucleotides and the H8 of the proximal purine. The same conformational configuration leads to an unfavorable 2'-OH–nucleobase steric clash in the case of ANA:RNA and ANA:ANA duplexes. These results have been used as an additional design rule for the creation of therapeutically relevant 2'-F-ANA modified antisense oligonucleotides.

Our studies on substituted G-quadruplex structures have revealed that the same fluorine-mediated hydrogen bonding interactions observed in 2'-F-ANA modified double helices also contribute to the stability of 2'-F-ANA substituted G-quadruplex structures found in the human telomeric sequence. We have shown that a single 2'-F-ANA substitution stabilizes only the propeller parallel G-quadruplex form over all competing conformers, and that this stabilization is in most part related to the formation of C-H8...2'-F-C and 2'-F-CH...O4' noncovalent interactions.

Our studies showed that while stable ANA:ANA duplexes are too unstable to form via ANA+ANA bimolecular association, an appropriate combination of ANA and 2'-F-ANA nucleotides into a gapmer containing a central segment ('gap') of ANA nucleotides flanked by

two 2'F-ANA ‘wings’ will yield oligonucleotides that can adopt monomeric hairpin (with the unpaired ANA nucleotides on the loop) and bimolecular duplex structures of comparable thermal stabilities. This tendency of ANA nucleotide tracts to form loop structures offers a range of new applications for this modification, particularly in applications where a duplex/hairpin conformational switch is desirable.

A screen of arabinose modified siRNA constructs revealed that ANA has a place among chemically modified oligonucleotides known to be compatible with siRNA-mediated gene silencing in mammalian cells. Taking advantage of ANA’s destabilizing effects, we have shown that ANA in combination with RNA and 2'F-ANA allows the siRNA duplex thermodynamics to be finely tuned to produce heavily-modified siRNA duplexes that are capable of potent silencing of Luciferase and DRR, a gene linked to malignant glioma.

The impact of several sugar and nucleobase substitutions on the formation of parallel-stranded duplexes at neutral pH was investigated. Our results open up new perspectives for the development of parallel-stranded double helices at physiological-like conditions. We have demonstrated that rWC parallel hybridization incorporating iC/iG nucleobases occurs not only in *ps*-DNA:DNA, but also in *ps*-DNA:RNA, *ps*-DNA:2'F-RNA, and *ps*-DNA:2'F-ANA hybrids. This observation is of importance for potential future applications of parallel hybridization, and in particular in the design of novel oligonucleotide hybridization probes or oligonucleotide-based therapeutics.

RÉSUMÉ

Les applications prometteuses des analogues d'acides nucléiques chimiquement modifiés, dont le nombre est en constante progression, couvrent un large champ s'étirant des thérapies à oligonucléotides aux nanotechnologies d'ADN et outils de diagnostic, à la génomique fonctionnelle et à la validation de cible. Parmi les très nombreuses variétés d'acides nucléiques modifiés qui ont été développées, et plus encore parmi celles dont le sucre central n'est pas naturel, l'acide arabinonucléique (« *arabinonucleic acid* », ANA) et son dérivé fluoré en position 2' (2'F-ANA) nous sont particulièrement importants. La présente thèse se focalise en premier lieu sur la compréhension et l'élucidation des causes structurelles à l'origine des propriétés intéressantes qu'ont ces analogues nucléosidiques, et plus spécifiquement sur leurs structures, leurs stabilités et leur activité en milieu cellulaire.

Notre travail a permis d'établir que la grande affinité de 2'F-ANA pour l'ARN ou pour lui-même est en partie due à des interactions de type liaison hydrogène entre l'atome de fluor sur le carbone 2' des nucléotides 2'F-ANA et l'atome d'hydrogène sur le carbone 8 d'une purine consécutive. Au contraire, pour des duplexes ANA:ARN ou ANA:ANA, une configuration équivalente aboutit à une gêne stérique entre l'hydroxyle 2' et la base purique. Ces résultats se sont traduits par la mise en place d'une règle additionnelle pour la conception d'oligonucléotides modifiés 2'F-ANA antisens à visée thérapeutique.

Nos études sur des G-quadruplexes substitués ont révélé qu'une liaison hydrogène similaire impliquant l'atome de fluor de 2'F-ANA contribue de la même manière à la stabilité de ces structures secondaires présentes dans les séquences télomériques de l'homme. Nous avons montré qu'une seule incorporation d'un nucléotide 2'F-ANA suffit à stabiliser la forme en hélice de G-quadruplexes hybridés parallèlement uniquement, et ce parmi un certain nombre d'autres

conformères structurels, et cette stabilisation est l'œuvre d'interactions non-covalentes entre C-H8...2'F-C et 2'F-CH...O4'.

Bien que des duplexes stables ANA:ANA soient trop instables pour se former par association bimoléculaire, nos études ont montré qu'une combinaison adéquate de nucléotides ANA et 2'F-ANA selon laquelle le segment central de la séquence (« *gap* ») est composé d'ANA et les parties 5' et 3' terminales de 2'F-ANA (stratégie dite « *gapmer* ») permet d'obtenir des oligonucléotides qui peuvent adopter une structure monomérique en épingle (où les nucléotides ANA non-appariés se trouvent sur la boucle) ou s'apparier en duplexes, et ces structures bénéficient de stabilités thermiques comparables. Cette tendance qu'ont des séries de nucléotides ANA à former des structures en forme de boucle étoffe la panoplie d'applications des acides arabinonucléiques, en particulier là où un basculement conformationnel duplex/épingle est souhaitable.

Un criblage de différents siARN modifiés avec des arabinonucléotides a prouvé qu'ANA a sa place parmi les oligonucléotides chimiquement modifiés compatibles avec la machinerie cellulaire d'extinction de gène chez les mammifères. En prenant en compte l'effet déstabilisant provoqué par l'insertion de nucléotides ANA, il a été démontré que des combinaisons ANA, ARN et 2'F-ANA dans des siARN permettent de façonner avec précision la thermodynamique de ces duplexes et, ce faisant, des siARN largement modifiés ont été préparés qui se sont révélés capable de réduire l'expression des gènes de la luciférase et de DRR (« *Down-Regulated in Renal Cell Carcinoma* »), un gène impliqué dans le développement de gliomes malins.

L'effet provoqué par la substitution de sucres et de nucléobases sur la formation, à pH neutre, de duplexes dont les brins sont appariés parallèlement a également été analysé. Nos résultats ouvrent de nouvelles voies sur le développement d'hélices doubles appariées

parallèlement dans des conditions proches du milieu physiologique. Contrairement à la plupart des études publiées à ce jour sur l'interférence à l'ARN et sur les siARN chimiquement modifiés, nous avons prouvé que l'hybridation parallèle selon les règles d'appariement de type Watson-Crick inversé (« *reverse Watson-Crick* », rWC) à l'aide de nucléobases iC et iG se produit non seulement pour des duplexes *ps*-DNA:DNA (« *parallel-stranded* », *ps*), mais aussi *ps*-DNA:RNA, *ps*-DNA:2'F-RNA et *ps*-DNA:2'F-ANA. Cette observation renforce le potentiel thérapeutique et diagnostique des oligonucléotides dont les brins sont hybridés parallèlement.

ACKNOWLEDGEMENTS

I would like to sincerely thank all those who proffered their time and support over the last six years. First and foremost, I am truly grateful to my mentor Dr. Damha. My appreciation for him is beyond words as his guidance and kind support has brought me to a new place in life. He has been a major inspiration and has helped me improve my creativity, scientific curiosity, and my ability to think critically.

My very special thanks also go out to all members of the Damha group, past and present; for all their friendships, their shared knowledge and excellent suggestions, and for their skillful proofreading of this thesis and manuscripts written throughout my degree. I have learnt a great deal from you all!

McGill University is a wonderful school filled with excellent faculty and extremely helpful staff. In particular I would like to thank all members of the Department of Chemistry; all the professors who generously shared their knowledge with me, and all the kind staff who helped me with the administrative work, and provided me with trainings and technical support.

I should also mention that some of the research presented in this thesis is a result of a team effort. In particular I would like to thank Dr. Carlos Gonzales and Nerea Martin Pintado at the CSIC in Spain for a very productive and devoted collaboration.

And yet my deepest thanks are saved for my dearest parents, brother and sister for their unconditional love, encouragements and ongoing support.

*To my mom and dad, whom I doubt I will ever be able to convey
my appreciation and gratitude fully...*

PREFACE

During the course of my PhD studies in the laboratory of Dr. Damha at McGill University, I had the opportunity to interact and collaborate productively with several great scientists and researchers from other national and international laboratories, and I would like to sincerely thank all of them for their invaluable guidance and kind efforts. In summer 2011 I had the opportunity to travel to Spain as a visiting PhD student and receive training in the field of nucleic acid NMR structural studies under the direction of Dr. Carlos González in the Structural Biology Department of Instituto de Química Física Rocasolano (the CSIC) in Madrid. There, and at McGill, I conducted many of the NMR experiments described in Chapter 2. I would like to thank Dr. Damha and Dr. González for their kind support, both scientifically and financially, which made it possible for me to gain such a great experience.

Recognition of all contributions to the research presented in this thesis is included within the thesis and also here:

In Chapter 2, Nageswara R. Alla from Dr. Allen Nicholson's laboratory conducted RNase H assays, and Nerea Martin-Pintado from Dr. Gonzalez's lab solved the NMR structures of the chemically modified G-quadruplexes. In Chapter 3, Nerea Martin-Pintado from Dr. Gonzalez's lab solved the NMR structures of the gap(FA) duplex and performed the computational analysis of gap(FA) in order to calculate its 3D structure. In Chapter 4, Johans Fakhoury from Dr. Sleiman's lab conducted the luciferase silencing assays in Hela cells, and Dr. Phuong Le from Dr. Petrecca's lab conducted the DRR silencing assays in glioma cells. In Chapter 5, Nerea Martin-Pintado from Dr. Gonzalez's lab performed the 1D NMR experiments, and Elena Moroz from Dr. Jean Christophe Leroux conducted the Bcl-2 silencing assays in Caco-2 cells.

Table of Contents

COPYRIGHT STATEMENT.....	v
ABSTRACT	vii
RÉSUMÉ.....	ix
ACKNOWLEDGEMENTS.....	xiii
PREFACE.....	xv
LIST OF FIGURES	xxv
LIST OF TABLES	xxix
LIST OF SCHEMES.....	xxx
LIST OF ABBREVIATIONS.....	xxxii
CHAPTER 1: GENERAL INTRODUCTION	1
1.1 Nucleic Acid Structure and Function.....	2
1.1.1 Nucleosides, Nucleotides and Oligonucleotides	2
1.1.2 The Double Helix	7
1.2 Beyond the Watson-Crick Pairs	11
1.3 Synthetic Oligonucleotide as Therapeutics	16
1.4 Inhibitors of mRNA Translation	18
1.4.1 Antisense-Mediated Gene Silencing	18
1.4.2 siRNA-induced gene knockdown through RNAi	20
1.5 Challenges Facing the Development of Oligonucleotide Therapeutics.....	23
1.5.1 Overview.....	23

1.5.2 Optimization of AON and siRNA Therapeutics: Chemical Modifications.....	24
1.5.3 Structural Considerations for Designing Chemically Modified ON Therapeutics	25
1.6 Techniques Used to Study Hybridization Properties of Nucleic Acids	29
1.6.1 UV-Absorbance and Thermal Denaturation Studies	30
1.6.2 Circular Dichroism	33
1.6.3 NMR	35
1.7 Thesis Objectives and Layout	41
1.8 References	43
 CHAPTER 2: ENERGETICALLY IMPORTANT C-H...2'F-C PSEUDOHYDROGEN BONDING IN WATER: ORIGIN OF DIFFERENTIAL STABILITY OF 2'F-ANA:RNA AND ANA:RNA HYBRID DUPLEXES.....	 60
2.1 Differential Stability of 2'F-ANA:RNA and ANA:RNA Hybrid Duplexes	60
2.2 Nonconventional Hydrogen Bonding to Organic Fluorine	62
2.3 Sequence-Dependent C-2'F...H8-C Pseudohydrogen Bonding: A Testable Hypothesis.....	64
2.3.1 Background	64
2.3.2 Design and Evaluation of Thermal Stabilities of 2'F-ANA-Substituted Oligonucleotides Containing C-2'F...H8-C Pseudohydrogen Bonds.....	65
2.4 Characterization of Intra-Residual C-H...2'F-C Interactions by NMR Experiments.....	68
2.4.1 Evaluation of Deuterium Exchange Rates of H8 of Adenosine in D ₂ O at 37 °C.....	68
2.4.2 Evaluation of Thermal Stability of C-H8...2'F-C Interaction in D ₂ O or DMSO at Various Temperatures	72
2.4.3 Further Evaluation of H8/F2' Scalar Coupling Observed for 2'F-araA Nucleoside	73

2.5 “Cooperative” Inter- and Intra-Residual C-H...2’F-C Pseudohydrogen Bonding	74
2.6 Entropy and Enthalpy Contributions	76
2.7 Application of C-H8...2’F-C Hydrogen Bonding to Rationally Design Oligonucleotide Based Therapeutics with High Binding Affinity.....	81
2.7.1 Overview.....	81
2.7.2 Design and Evaluation of Thermal Stabilities of Modified Antisense Oligonucleotides Containing C-H8...2’F-C Pseudoydrogen Bonding	82
2.7.3 RNase H Cleavage Velocities of Designed Antisense Oligonucleotides	83
2.8 Directing the Folding of Human Telomeric Quadruplex with a Single Fluorine Atom: Evidence for C-H...2’F-C Pseudohydrogen Bonds in 2’F-Substituted Quadruplexes	85
2.8.1 Introduction.....	85
2.8.2 Design and Thermal Stability Evaluation of Substituted Human Telomeric DNA Quadruplexes	86
2.8.3 Structural Analysis of 2’F-Substituted Human Telomeric DNA Quadruplex Reveals Pseudohydrogen Bonds Contribute to Structure and Stability	87
2.9 Concluding Remarks.....	91
2.10 Experimental Methods	92
2.10.1 Oligonucleotide Synthesis and Purification.....	92
2.10.2 UV-Melting and Derivation of Thermodynamic Parameters of 2’F-Modified Duplexes.....	93
2.10.3 RNase H Assays on 2’F-modified Antisense Oligonucleotides Targeting COPD	94
2.10.4 CD Spectroscopy and Derivation of Thermodynamic Parameters of DNA Human Telomeric Quadruplex and Modified Structures	96

2.10.5 NMR experiments on DNA Human Telomeric Quadruplex Structures.....	96
2.11 References	98
CHAPTER 3: THE SOLUTION STRUCTURE OF DOUBLE HELICAL ARABINO NUCLEIC ACIDS: EFFECT OF ARABINOSES IN DUPLEX-HAIRPIN INTERCONVERSION	
3.1 ANA versus 2'F-ANA: An Overview	104
3.2 Sequence Design and Thermal Melting of Arabinose Modified Chimeric Dodecamers ..	107
3.3 Duplex-Hairpin Equilibrium	108
3.3.1 Evidence of Unimolecular Hairpin Structure	108
3.3.2 NMR Melting Experiments	110
3.3.3 Thermodynamic Parameters for the Hairpin to Duplex Equilibrium.....	113
3.4 NMR-Based Structure Determination of gap(FA)	114
3.4.1 Introduction.....	114
3.4.2 Description of the Duplex and Hairpin Structures Associated with gap(FA) Sequence	117
3.4.3 Structural Analysis of gap(FA) Reveals Electrostatic Interactions Contributing to Thermal Stability	120
3.5 Comparison of ANA and 2'F-ANA Modified Dodecamers with the Unmodified DNA ..	121
3.6 ANA Stabilizes Stem-Loop Structures	123
3.7 Alternative Genetic Systems Based on Arabinonucleic Acids?	125
3.8 Conclusions	126
3.9 Experimental Methods	128
3.9.1 Oligonucleotide Synthesis and Purification.....	128

3.9.2 UV Melting Experiments and Derivation of Thermodynamic Parameters	129
3.9.3 NMR Experiments.....	130
3.9.4 Experimental Constraints.....	131
3.9.5 Structure Determination of the Duplex	132
3.9.6 Molecular Modeling of the Hairpin Structure	133
3.10 References	133
CHAPTER 4: ARABINONUCLEIC ACIDS AS 2'-STEREOISOMERIC MODULATORS OF SIRNA ACTIVITY.....	139
4.1 Overview	139
4.2 RISC's Thermodynamic Bias.....	141
4.3 Targeting Firefly Luciferase by ANA-modified si-Duplexes	142
4.3.1 Sequence Design	142
4.3.2 Luciferase Gene Silencing	143
4.4 Targeting Down-Regulated in Renal Cell Carcinoma by ANA-modified si-Duplexes	148
4.4.1 siRNA Sequence Design and Knockdown of DRR Gene	149
4.5 Conclusions	153
4.6 Experimental Methods	154
4.6.1 Oligonucleotide Synthesis and Purification.....	154
4.6.2 siRNA Duplex Formation.....	156
4.6.3 Thermal Denaturation Experiments	156
4.6.4 Luciferase Assays.....	159
4.6.5 DRR Assays	162

4.7 References	164
CHAPTER 5: STRUCTURAL PROPERTIES AND GENE SILENCING ACTIVITY OF PARALLEL-STRANDED NUCLEIC ACID DUPLEXES AT PHYSIOLOGICAL CONDITIONS	
5.1 Parallel-Stranded DNA and RNA.....	168
5.2 Noncanonical Base Pairing Patterns in Parallel-Stranded Duplexes.....	169
5.3 Objectives.....	172
5.4 Parallel 12-bp Oligonucleotides	174
5.4.1 Design of 12-bp Parallel Hybrids and Thermal Denaturation Analysis.....	174
5.4.2 Circular Dichroism Studies of 12-bp Parallel Hybrids.....	176
5.4.3 ¹ H-NMR of 12-bp Parallel Hybrids	177
5.5 Parallel si-Duplexes	179
5.5.1 Design and Evaluation of Thermal Stabilities of Parallel si-Duplexes	179
5.5.2 Native Gel Electrophoretic Analysis	182
5.5.3 Determination of si-Duplex Parallel Chain Orientation by FRET Measurements	183
5.5.4 Induction of RNAi Activity by Parallel Hybrids	187
5.5.5 Can Parallel Hybridization Enhance the siRNA Properties?.....	189
5.6 Concluding Remarks and Future Work	191
5.7 Experimental Methods	191
5.7.1 Synthesis and Purification of Oligonucleotides Containing Isoguanine and Isocytosine	191
5.7.2 Synthesis and Purification of Oligonucleotides Labeled with Cyanine Dyes	193

5.7.3 Thermal Denaturation Experiments and Circular Dichroism Studies	194
5.7.4 NMR Experiments.....	196
5.7.5 Characterization of Duplex Formation by Gel Electrophoresis	196
5.7.6 FRET Assays	198
5.7.7 Bcl-2 si-Duplex Formation and <i>in Vitro</i> Bcl-2 Assays	199
5.8 References	200
CHAPTER 6: CONTRIBUTIONS TO KNOWLEDGE	209
6.1 Summary of Research	209
6.1.1 Structural Effects Determining the High Thermal Stability of 2'F-ANA:RNA Hybrids	209
6.1.2 Directing the Folding of Human Telomeric Quadruplex with a single 2'F-arabinose substitution	209
6.1.3 Effect of ANA and 2'F-ANA on Duplex-Hairpin Interconversion.....	210
6.1.4 ANA as Modulators of siRNA Activity	210
6.1.5 Development of Novel Chemically Modified Parallel-Stranded Duplexes	211
6.1.6 Parallel-Stranded Duplexes are Compatible with RNAi	211
6.2 Papers, and Conference Presentations	212
6.2.1 Papers published.....	212
6.2.2 Papers in preparation	213
6.2.3 Conference Attendance.....	213

LIST OF FIGURES

Figure 1.1: Structural components of nucleic acids.....	4
Figure 1.2: Nomenclature for torsion angles of the sugar-phosphate backbone of nucleic acids...5	
Figure 1.3: Furanose Ring Conformations.....	7
Figure 1.4: Schematic representations of the canonical Watson-Crick base pairs.....	8
Figure 1.5: Chemical groups exposed in the grooves of B-DNA from the edges of base pairs.....	9
Figure 1.6: Identification of the hydrogen bonding edges in RNA.....	11
Figure 1.7: Representations of some common noncanonical hydrogen bonding schemes found in nucleic acid structures.....	13
Figure 1.8: Schematic representations of G-quadruplexes and parallel-stranded duplexes.....	15
Figure 1.9: AON-mediated gene silencing.....	19
Figure 1.10: siRNA-mediated gene silencing.....	21
Figure 1.11: Schematic representation of classical siRNA duplex.....	22
Figure 1.12: Chemical structures of (a) Phosphorothioate backbone; (b) Selected C2'-sugar modifications	28
Figure 1.13: Example thermal Denaturation curve of a 12-nt DNA:RNA hybrid	32
Figure 1.14: Example CD spectra of 12-nt B-DNA and A-form DNA:RNA duplexes.....	34
Figure 1.15: Illustration of indicative 3J scalar couplings for South & North conformations.....	37
Figure 1.16: Representation of non-exchangeable and labile protons of natural nucleobases.....	38
Figure 1.17: Illustration of some strong base-sugar NOEs in B-type DNA.....	39
Figure 2.1: Chemical structures of ANA and 2'F-ANA.....	60

Figure 2.2: Selected previous results from structural analysis of 10mer 2'F-ANA:RNA hybrid by Damha lab.....	63
Figure 2.3: Thermal stability comparisons of A and B series upon 2'F-ANA modification.....	67
Figure 2.4: Illustration of inter- and intra-residual C-2'F...H8-C pseudohydrogen bonds.....	68
Figure 2.5: Monitoring exchange of H8 with deuterium in D ₂ O for different nucleosides.....	70
Figure 2.6: Rate constants for exchange reactions at H8 of DNA, RNA, 2'F-ANA and 2'F-RNA adenine nucleosides in D ₂ O.....	71
Figure 2.7: 2Hz splitting of H8 peak to a doublet observed for 2'F-araA nucleoside.....	72
Figure 2.8: Induction of a rigid northern conformation in 2'F-araA nucleoside.....	73
Figure 2.9: ¹⁹ F- ¹ H HOESY spectra of 2'F-ANA modified <i>ss</i> -tetramers in D ₂ O.....	78
Figure 2.10: ¹⁹ F- ¹ H HOESY spectra of 2'F-RNA modified <i>ss</i> -tetramers in D ₂ O.....	79
Figure 2.11: Illustration of a ¹ J(N,H) scalar coupling.....	80
Figure 2.12: Cleavage of “X”-AON:RNA Hybrids by RNase H1.....	84
Figure 2.13: CD spectra, melting profiles, and imino region of ¹ H-NMR spectra at different temperatures for all five G-rich telomeric sequences.....	88
Figure 2.14: Distances between F _i -H8 _{i+1} and H2'' _i -O4' _{i+1} in AFtel and H2' _i -H8 _{i+1} and H2'' _i -O4' _{i+1} in 1K8P telomeric G-quadruplexes.....	89
Figure 2.15: Snapshots of the most relevant configuration of the rG and 2'F-rG in the quadruplex as found in our molecular dynamics simulations.....	91
Figure 3.1: Chemical structures of ANA and 2'F-ANA.....	104
Figure 3.2: Self-complementary gap(FA) dodecamer sequence.....	106

Figure 3.3: Schematic illustration of gap(FA) duplex-hairpin equilibrium.....	109
Figure 3.4: Imino region of ¹ H-NMR spectra of gap(FA) at two different concentrations.....	110
Figure 3.5: Temperature-dependent 1D ¹ H- and ¹⁹ F-NMR spectra of gap(FA).....	111
Figure 3.6: Comparison between ¹ H-NMR spectra of gap(FA) and DNA sequence (DD).....	112
Figure 3.7: van't Hoff plot of ln(K _{eq}) vs. 1/T for gap(FA).....	113
Figure 3.8: Illustration of some strong base-sugar NOEs in B-type gap(FA) duplex.....	118
Figure 3.9: J-coupling constant values for gap(FA) sequence.....	119
Figure 3.10: Comparison between gap(FA) structure and the unmodified Dickerson dodecamer DNA structure obtained by Tjandra <i>et al.</i>	123
Figure 3.11: Model of the hairpin structure of gap(FA) and detail of the ANA residues in the loop, showing hydrogen bonds between the 2'-OH and phosphate oxygen.....	124
Figure 3.12: Normalized UV melting profiles of chimeric dodecamer duplexes	130
Figure 4.1: Chemical structures of 2'F-ANA, ANA and 2'F-RNA.....	140
Figure 4.2: T _m values and gene silencing produced by arabinose modified siRNAs targeting firefly luciferase in HeLa cells (I).....	146
Figure 4.3: T _m values and gene silencing produced by arabinose modified siRNAs targeting firefly luciferase in HeLa cells (II).....	147
Figure 4.4: Gene silencing produced by arabinose modified siRNAs targeting DRR in invasive glioma cells.....	152
Figure 4.5: Melting profiles of arabinose modified siRNAs targeting luciferase.....	156
Figure 4.6: Melting profiles of arabinose modified siRNAs targeting DRR.....	157
Figure 4.7: Dose-response curves of arabinose modified siRNAs targeting luciferase.....	161

Figure 4.8: Densitometry analyses of four different western blots of DRR expression after treatment with arabinose modified siRNAs.....	163
Figure 5.1: Illustration of antiparallel and parallel chain orientation in double helices.....	168
Figure 5.2: Common base pairing schemes in antiparallel and parallel <i>ds</i> -DNA.....	171
Figure 5.3: Isoguanine-cytosine and guanine-isocytosine rWC hydrogen bonds.....	172
Figure 5.4: Structures of modified nucleotides incorporated to the parallel arrangement.....	174
Figure 5.5: Representation of parallel and antiparallel strand pairings of 12-nt sequences.....	175
Figure 5.6: CD spectra of parallel and antiparallel 12-bp hybrids.....	178
Figure 5.7: Schematic representation of classical antiparallel siRNA duplex.....	180
Figure 5.8: Strategies to design rWC parallel si-duplexes incorporating iG and iC.....	181
Figure 5.9: UV melting profiles of parallel si-duplexes targeting Bcl-2.....	182
Figure 5.10: Native gel electrophoretic analysis of Bcl-2 targeting si-duplexes.....	183
Figure 5.11: Schematic representation of spectral overlap integral of Cy3-Cy5 FRET pair.....	184
Figure 5.12: Emission signals of parallel probe and control systems at 7°C.....	186
Figure 5.13: Emission peaks of each labeled probe at all three experimental temperatures.....	187
Figure 5.14: Knockdown of Bcl-2 by parallel and antiparallel si-duplexes in Caco-2 cells.....	188
Figure 5.15: Normalized UV melting profiles of 12-bp parallel hybrids.....	195
Figure 5.16: Imino region of 1D ¹ H-NMR spectra of parallel and antiparallel 12-bp hybrids...	197

LIST OF TABLES

Table 1.1: Helical parameters for A-form and B-form duplexes.....	10
Table 1.2: Families of edge-to-edge base pairs formed by natural bases defined by the relative orientation of the glycosidic bonds of the interacting bases and the edges they use.....	12
Table 2.1: Sequences and T_m values of duplexes of A and B series.....	66
Table 2.2: Sequences of single-stranded tetramers.....	77
Table 2.3: Sequences, T_m values and RNase H cleavage velocities of designed AONs.....	83
Table 2.4: T_m values of DNA telomeric sequence and singly modified telomeric sequences.....	87
Table 2.5: Inter-residual 2'F...H8 and 2'H...H8 distances for AFtel and 1K8P.....	90
Table 2.6: Inter-residual 2'F...H8-C8 and H2'...H8-C8 angles for AFtel and 1KP8.....	90
Table 3.1: Sequences and T_m values of gap(FA) and other self-complementary dodecamers...	107
Table 3.2: MS characterization of gap(FA) and other self-complementary dodecamers.....	129
Table 4.1: Sequences and T_m values of arabinose modified siRNAs targeting DRR.....	150
Table 4.2: MS characterization of arabinose modified siRNAs targeting luciferase.....	155
Table 4.3: MS characterization of arabinose modified siRNAs targeting DRR.....	155

Table 5.1: Melting temperature and percent hyperchromicity values of 12-bp hybrids.....	176
Table 5.2: Melting temperatures of parallel and antiparallel si-duplexes targeting Bcl-2.....	182
Table 5.3: Probes for parallel chain verification employing Cy3-Cy5 FRET pair.....	185
Table 5.4: MS characterization of 12-nt oligonucleotides.....	193
Table 5.4: MS characterization of 21-nt oligonucleotides with Bcl-2 sequence.....	193

LIST OF SCHEMES

Scheme 2.1: Representation of the pseudo first-order kinetics for purine H8 exchange with deuterium in D ₂ O.....	69
Scheme 3.1: Description of general approach for 3D structure determination of oligonucleotides using NMR in conjunction with conformational searching procedures.....	116

LIST OF ABBREVIATIONS

2D	two dimensional
2'F-ANA	2'-deoxy-2'-fluoroarabinonucleic acid
2'F-araN	2'-deoxy-2'-fluoroarabinonucleoside
2'F-RNA	2'-deoxy-2'-fluororibonucleic acid
2'F-rN	2'-deoxy-2'-fluororibonucleoside
3D	three dimensional
A	adenosine
Å	Angstrom
A ₂₆₀	UV absorbance at 260nm
ACN	acetonitrile
Ago2	Argonaute 2
ANA	arabinonucleic acid
AON	antisense oligonucleotide
<i>aps</i>	antiparallel-stranded
Bcl-2	B-cell lymphoma 2
bp	base pair
C	cytidine
°C	celsius
CD	circular dichroism
COSY	correlation spectroscopy
CPG	controlled pore glass

Cy3	cyanine-3
Cy5	cyanine-5
DCM	dichloromethane
DEPC	diethylpyrocarbonate
Di-siRNA	dicer substrate siRNA
DMEM	dulbecco's modified eagle's medium
DMF	dimethylformamide
DMSO	dimethylsulfoxide
DMTr	4,4'-dimethoxytrityl
dN	2'-deoxyribonucleoside
DNA	2'-deoxyribonucleic acid
DQF-COSY	double-quantum filtered COSY
DRR	Down-Regulated in Renal Cell Carcinoma
<i>ds</i>	double-stranded
DTT	dithiothreitol
EC ₅₀	half maximal effective concentration
EDTA	ethylenediaminetetraacetic acid
ESI	electrospray ionization
EtOH	Ethanol
FBS	fetal bovine serum
FRET	förster resonance energy transfer
G	guanosine
%H	percent hyperchromicity; $(A_{\text{final}} - A_{\text{initial}}) / A_{\text{initial}}$

hAgo2	human Argonaute 2
HEPES	4-(2-hydroxyethyl)-1-piperazineethanesulfonic acid
His	histidine
HOESY	heteronuclear overhauser effect spectroscopy
HPLC	high performance liquid chromatography
HSQC	heteronuclear single quantum coherence
J	coupling constant (Hz)
k	reaction rate constant
LCMS	liquid chromatography–mass spectrometry
LNA	locked nucleic acid
Luc	luciferase
MeOH	methanol
MD	molecular dynamics
miRNA	microRNA
mM	mili-molar
μ M	micro-molar
mRNA	messenger RNA
MS	mass spectrometry
NCBI	national center for biotechnology information
nM	nano-molar
NMP	<i>N</i> -methyl pyrrolidinone
NMR	nuclear magnetic resonance
NOE	nuclear overhauser effect

NOESY	nuclear overhauser effect spectroscopy
nt	nucleotide
ON	oligonucleotide
OTE	off-target effect
<i>P</i>	phase angle
PAGE	polyacrylamide gel electrophoresis
PBS	phosphate-buffered saline
PCR	polymerase chain reaction
PDB	protein data bank
PKR	protein kinase R
pM	pico-molar
<i>ps</i>	parallel-stranded
PS	phosphorothioate
RBP	RNA binding protein
rWC	reverse Watson-Crick
RISC	RNA-induced silencing complex
RNA	ribonucleic acid
RNAi	RNA interference
Sc	scrambled
shRNA	short hairpin RNA
si	small interfering
ss	single-stranded
T	thymidine

TAE	(tris-acetate-EDTA) buffer
TBDMS	<i>tert</i> -butyldimethylsilyl
TCA	trichloroacetic acid
TEAA	triethylammonium acetate
TLR	toll-like receptor
T _m	melting temperature
TREAT-HF	triethylamine trihydrofluoride
U	uridine
UV	ultraviolet
VINC	vinculin
WC	Watson-Crick

CHAPTER 1: GENERAL INTRODUCTION

The discovery that DNA is the prime genetic molecule and the carrier of all hereditary information (1), immediately focused the attention on elucidation of its structure.

The primary structure of DNA was already known (2-6), before Watson and Crick proposed the double helix model, however, it did not lend itself well to explain how DNA functions as the genetic material; it was going to take a better understanding of the three dimensional structure of DNA to uncover how the genetic instructions are held and passed from generation to generation.

The three dimensional structure of DNA was discovered in 1953 by James Watson and Francis Crick (7), with major scientific contributions from Franklin, Goslin, and Wilkins (8,9). Their proposed model readily explained all the foregoing experimental observations, and offered a hypothesis for a strand replication mechanism based on complementary Watson-Crick base pairing.

Since then, nucleic acid chemistry and biology has significantly advanced, which in most part is due to the development of efficient and automated solid-phase synthesis of DNA (10), and RNA (11). The availability of synthetic nucleic acids has led to a widespread use of nucleic acids and their analogues in chemistry, biology and medicine. Nucleic acids are now being used both commercially and experimentally in molecular diagnostic strategies for identifying disease-related genes and pathogens (12,13). As well, they are routinely used in laboratory as a means to control the expression of therapeutically relevant genes (14).

The availability of synthetic nucleic acids also provided a drive for the study of nucleic acid structure. Given the scope and promise of nucleic acid research, it should come as no surprise that the technologies for their structural analysis have progressed at a rate as fast as the technologies developed for their efficient synthesis. Today, the structural parameters for a vast

collection of nucleic acid structures have been determined using X-ray crystallography or NMR techniques.

1.1 Nucleic Acid Structure and Function

Nucleic acids are among a large number of biopolymers present in living cells, and together with proteins and carbohydrates, they form the macromolecules vital for all forms of life. The two major classes of naturally occurring nucleic acids are deoxyribonucleic acid (DNA), and ribonucleic acid (RNA). DNA is the carrier of heritable genetic information (1), and RNA is implicated in a variety of biological roles including coding, decoding, regulation, and expression of genes.

Indeed, most, if not all versatile functions of nucleic acids rely on their ability to form specific complexes, either folded intra-molecularly or bound inter-molecularly to a target nucleic acid. Thus, to fully comprehend the nucleic acid function and exploit it to the fullest, it is important to have a complete understanding of their structural features, which in most part arise from the unique physical, chemical, and topological properties of their monomers.

1.1.1 Nucleosides, Nucleotides and Oligonucleotides

Both DNA and RNA biopolymers are made up of an array of monomers called nucleotides. As such, nucleic acids are also commonly referred to as oligonucleotides (ONs).

Each nucleotide is constructed from three components: a nitrogen-heterocyclic base, a pentose sugar, and a phosphate moiety (Figure 1.1) (15,16). A nucleic acid analogue may have any of these altered.

The bases, also termed as nucleobases, are planar aromatic heterocyclic molecules and fall into two classes, purines and pyrimidines. Each of these bases exist in two alternative tautomeric states, keto and enol forms, which are in equilibrium with each other (17,18). The equilibrium lies far to the side of the conventional structures shown in Figure 1.1a, which are the predominant keto states and the ones important for Watson-Crick base pairing. The purines, adenine and guanine, are found in both RNA and DNA. The pyrimidines, cytosine and uracil, are found in RNA whilst uracil is replaced by thymine (5-methyluracil) in DNA.

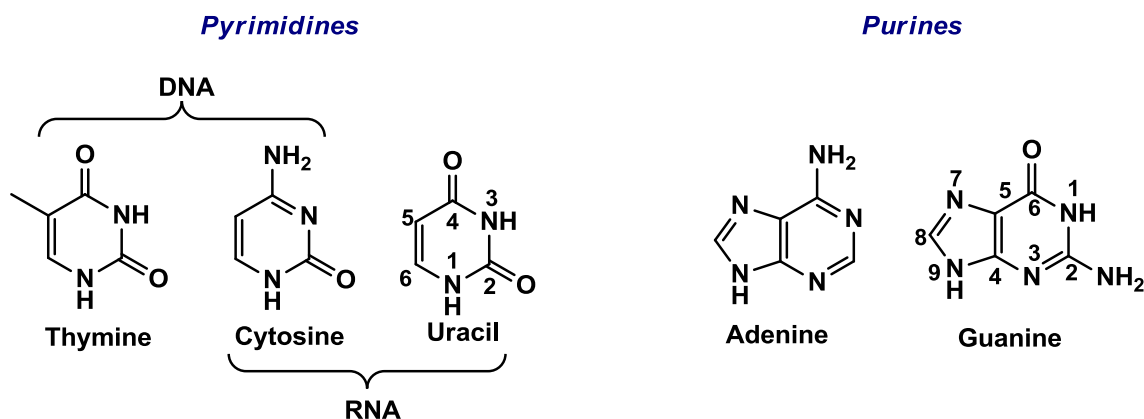
Nucleobases are attached to the C(1') position of the sugar moiety through N-glycosidic bonds, forming a nucleoside unit (Figure 1.1b). Only the D-pentose sugars are present in nucleic acids. D-ribose comprises RNA, and 2'-deoxy-D-ribose comprises DNA; both pentoses exist in the furanose form. The C(1')-N glycosidic bond involves the anomeric carbon of the sugar, and the stereochemistry of the glycosidic bonds found in natural nucleic acids is β .

The chemical linkage between nucleotide units in oligonucleotides is a phosphodiester linkage, which connects the 5'-hydroxyl group of one nucleotide to the 3'-hydroxyl group of the next nucleotide (Figure 1.1c). By convention, nucleic acid sequences are written from the 5'-end to the 3'-end and are usually written as the sequence of bases they contain. This linear sequence constitutes the primary structure of nucleic acids.

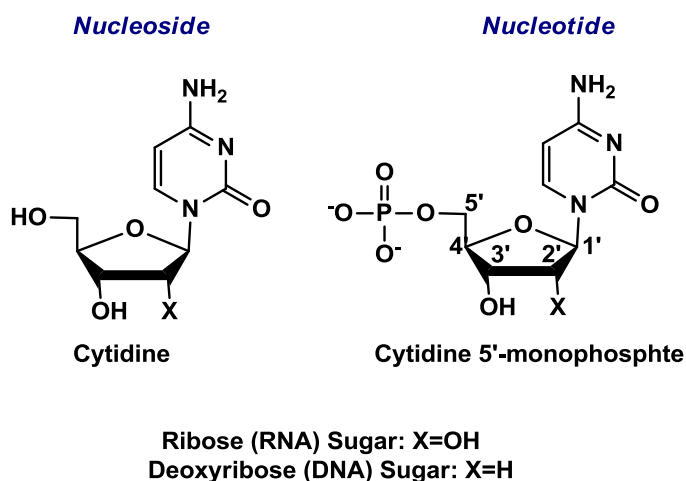
1.1.1.1 Conformation of Nucleosides and Nucleotides

Each nucleotide consists of three key conformational features: sugar-phosphate backbone, sugar ring, and the nucleobase with respect to the sugar ring. Generally, the conformation of each feature is described by bond lengths, bond angles, and specifically torsion angles (θ) (Figure 1.2a) (16,19).

a.



b.



c.

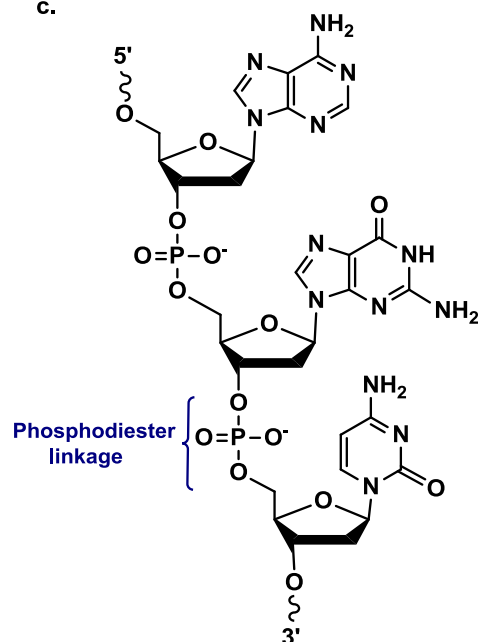


Figure 1.1 Structural components of nucleic acids. (a) The heterocyclic bases of DNA and RNA (pyrimidines and purines); (b) Example of a nucleoside unit and a nucleotide unit; (c) Example of a DNA oligonucleotide chain. Note that to distinguish between the sugar and base atoms, sugar atoms are numbered with a prime (').

Briefly, the sugar-phosphate backbone of a polynucleotide chain consists of a repeating unit of six single bonds, and the torsion angles about these bonds are denoted by α , β , γ , δ , ϵ , and ζ (Figure 1.2a). Because of the steric considerations, the backbone angles are not free to adopt any

value between 0° and 360° (20). Various torsion angle values for DNA backbone can be found in reference (19).

The torsion angle about the glycosidic C(1')-N bond that links the nucleobase to the sugar is denoted by the symbol χ . Depending on the rotation about the glycosidic bond, a nucleotide can be described as either “anti” or “syn” (Figure 1.2b). Because of steric constraints, nucleotides are generally found in the “anti” configuration. However, deoxyguanosine is sometimes found in a “syn” configuration, where the bulk of the purine ring is positioned directly over the plane of the sugar.

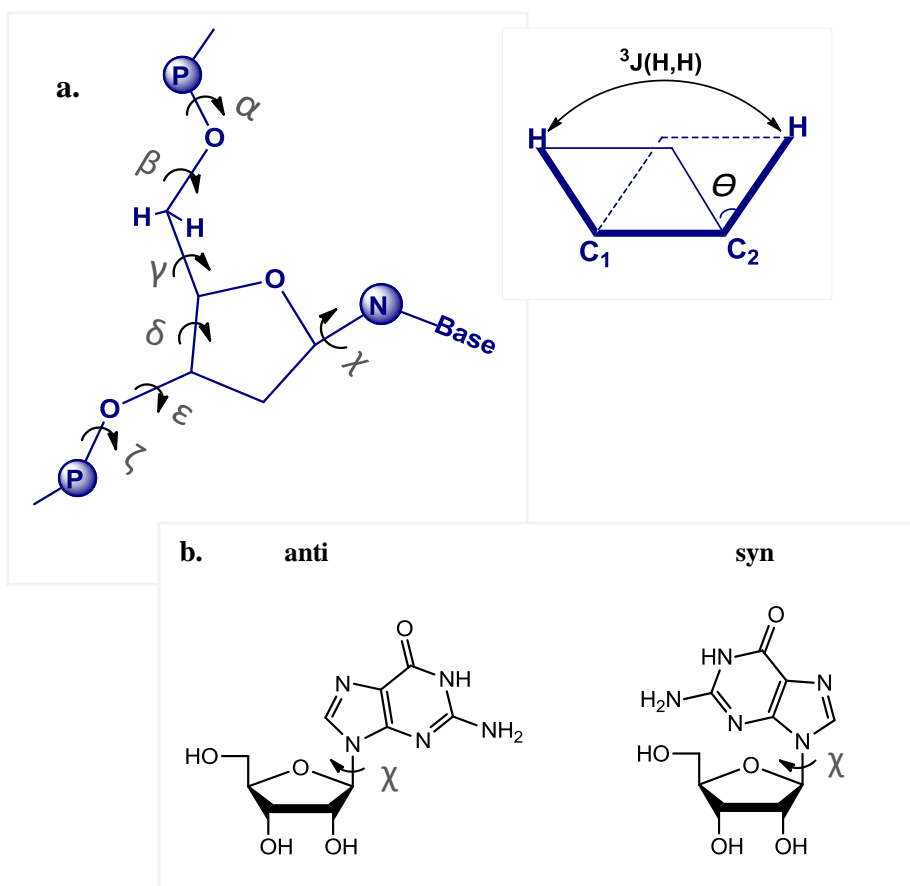


Figure 1.2 Nomenclature for torsion angles of the sugar-phosphate backbone of nucleic acids. (a) Schematic definition of torsion angle (θ) in general, and illustration of various torsion angles around the P-O(5'), O(5')-C(5'), C(5')-C(4'), C(4')-C(3'), C(3')-O(3') and O(3')-P single bonds of DNA backbone (α , β , γ , δ , ϵ , and ζ respectively). (b) syn and anti configurations around the C(1')-N glycosidic bond.

In order to provide a precise description of the sugar ring conformation, it is necessary to specify the five endocyclic torsion angles for the furanose sugar ring. These angles are denoted by the symbols, ν_0 , ν_1 , ν_2 , ν_3 and ν_4 for the O4'-C1', C1'-C2', C2'-C3', C3'-C4' and C4'-O4' bonds respectively (Figure 1.3). The furanose ring is inherently nonplanar, and this nonplanarity is termed puckering. The various puckers are produced by systematic changes in the ring torsion angles. The sugar may be puckered in an envelope form (*E*) with four of the five atoms coplanar and the fifth atom being out of this plane; or more commonly in a twist form (*T*) with two adjacent atoms displaced on opposite sides of the plane formed by the other three atoms (21,22). The direction of the atomic displacement from the plane is important. If a portion of the ring is bent upward toward the base, the conformation is known as *endo*, while if it is bent downward away from the base, this is known as *exo*.

In 1972 Altona and Sundaralingam introduced a new description for furanose ring puckering, which is based on the concept of pseudorotation and allows determination of the exact conformation of the furanose ring in terms of two parameters: the phase angle of pseudorotation (*P*) and the degree of pucker (τ_m); both of which are calculated from the known endocyclic torsion angles (23). In this approach, the phase angle values, the envelope (*E*)/twist (*T*) notations, and the *endo/exo* notations are all correlated on a pseudorotational wheel (Figure 1.3) (23).

DNA nucleosides exist in a rapid equilibrium between two puckered forms, the C3'-*endo*, and the C2'-*endo*, passing through the O4'-*endo* when moving between these conformational minima (24-26). The C3'-*endo* domain has *P* values in the range of -10 to $+40^\circ$, which falls into the northern half of the pseudorotational wheel and hence its conformation is termed "North". C2'-*endo* domain has *P* values ~ 144 - 180° in the southern half of the circle and is called "South" (21,23). Unlike DNA, for most substituted furanose sugars, a combination of steric, anomeric

and gauche effects of the substituents will shift the equilibrium towards only one of the puckers and significantly populate only a limited segment of pseudorotational wheel (21,23).

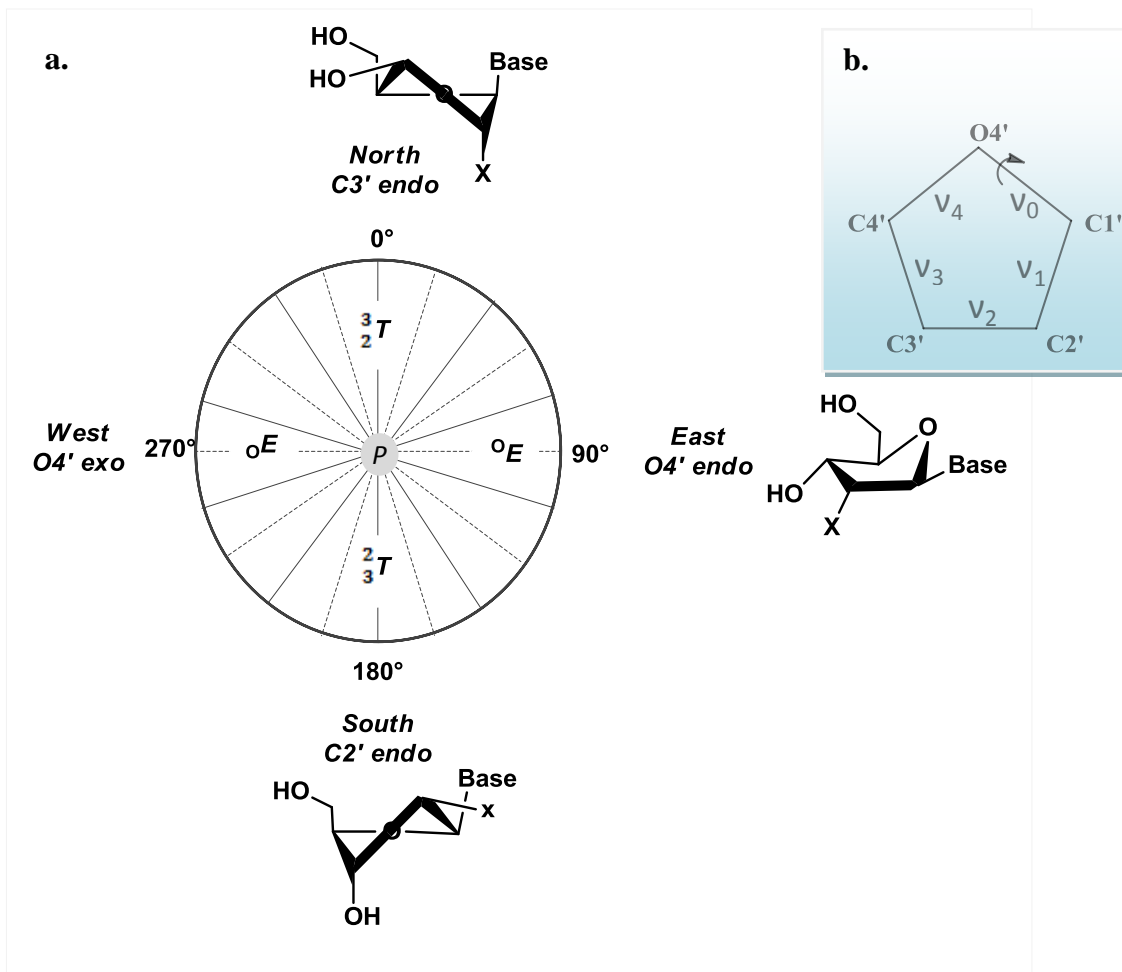


Figure 1.3 Furanose Ring Conformations. (a) The pseudorotational pathway of the furanose ring. (b) Nomenclature of endocyclic torsion angles of furanose ring. Note that the backbone torsion angle δ shown in Figure 1.2a and the endocyclic torsion angle v_3 both refer to rotation about the same bond (C4'-C3').

1.1.2 The Double Helix

In the model proposed by Watson and Crick (7), the double-stranded DNA (*ds*-DNA) is constituted of a right-handed helix in which the two strands are held together by noncovalent hydrogen bonds between the pairs of bases (A:T and C:G pairs; Figure 1.4).

Another characteristic of this model is the opposite polarity of the two strands of the duplex; that is the base at the 5' end of one strand is paired with the base at the 3' end of the other strand.

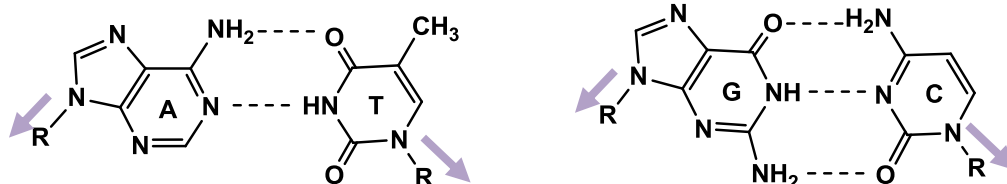


Figure 1.4 Schematic representations of the canonical Watson-Crick base pairs. The arrows show the cis geometry of glycosidic bonds of the two strands relative to each other and the axis of interaction in an antiparallel duplex with WC base pairs.

The Watson-Crick hydrogen bonds are fundamental features of the double helix and provide the genetic information content and replication. However, we recognize today that the structure, thermodynamic stability and dynamics of nucleic acid structures are governed not only by intra-strand Watson-Crick hydrogen bonds, but by a balance of a variety of noncovalent contributions (27-29); some of which are stabilizing like aromatic π - π base stacking of the adjacent bases (30-37), and some are destabilizing, like the electrostatic repulsion between the negatively charged phosphates along one strand and between the two strands of the double helix (38).

The exchange between these noncovalent forces is complex and it can be difficult to resolve between them. It is commonly concluded that because of the formation of many favorable hydrogen bonding and base stacking interactions upon hybridization, the helix formation process is enthalpically favored, and due to the restrictions imposed on the otherwise flexible backbone, the helix formation process is entropically disfavored (27,28,39). However, clearly this is an oversimplification since the impact of the solvent molecules and metal ions that surround both the single strands and the duplex must as well be considered when discussing the energetics of helix formation.

The Watson-Crick DNA double helix is known as B-form duplex (40-42). It is associated with C2'-*endo* sugar puckers, and as a consequence of the geometry of the base pairs and sugar puckers, it features two grooves of different sizes. There is a wide major groove, and a narrow minor groove. In each groove, the edges of base pairs are exposed, creating a pattern of hydrogen bond donors, hydrogen bond acceptors and hydrophobic moieties (Figure 1.5). Since the number and pattern of accessible functional groups are different in the two grooves, they differ in electrostatic potential, hydrogen bonding characteristics, sterics and hydration (43,44). The major groove of B-DNA exposes more functional groups that identify a base pair. Therefore, most proteins make sequence specific interactions with DNA in its major groove. The minor groove is not as rich in chemical information; however, some proteins and many small molecules interact with DNA in the minor groove (43,44).

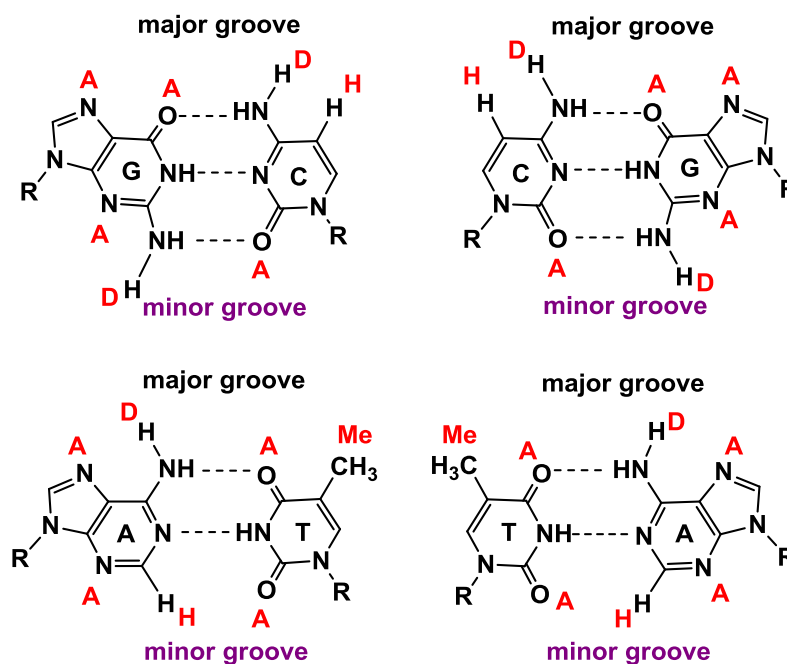


Figure 1.5 Chemical groups exposed in the major and minor grooves of B-DNA from the edges of the base pairs. The letters in red identify hydrogen bond acceptors (A), hydrogen bond donors (D), nonpolar hydrogen atoms (H), and methyl groups (Me).

While B-DNA is the major conformation of *ds*-DNA under physiological conditions (40-42), since the DNA sugars are flexible, depending on the sequence, solvent, ionic environment, or the presence of ligands, DNA can as well adopt a plethora of conformations far beyond the original B-form (45-48). Among them is the A-type conformation (49,50).

The A- and B-type duplexes are both right-handed helical structures with antiparallel orientation of strands; however they possess very different helical parameters and topologies (see Table 1.1) (49,50). The major groove of the A-duplex is narrow and deep while the major groove of the B-duplex is wide and shallow. These differences in helical geometry are mainly a consequence of their different sugar puckering. In B-type conformation, the furanose ring adopts a *C2'-endo* sugar pucker whereas A-type conformation is associated with a *C3'-endo* sugar pucker. Since the ribose sugars adopt a *C3'-endo* sugar pucker, the helical conformation of ribonucleic acid double helices is A-type (50-53).

Table 1.1 Helical parameters for A-form and B-form duplexes; adapted from reference (15).

Conformation	B-form	A-form
Helix sense	Right-handed	Right-handed
Sugar Pucker	<i>C3'-endo</i>	<i>C2'-endo</i>
Glycosidic Angle	anti	anti
Nucleotides per turn	10	11
Major Groove Depth	~8.8 Å	~13.5 Å
Major Groove Width	~11.7 Å	~2.7 Å
Minor Groove Width	~5.7 Å	~11 Å
Minor Groove Depth	~7.5 Å	~2.8 Å

1.2 Beyond the Watson-Crick Pairs

Today, some 60 years after the discovery of the *ds*-DNA structure, we know that although the Watson-Crick A:T and C:G base pairing is the dominant pattern known to stabilize the antiparallel *ds*-DNA and plays a vital role in the storage and replication of genetic information, a variety of other noncanonical arrangements have also been observed (54-57). Likewise for RNA; we now realize that RNA, which at the first might appear to be similar to DNA, has its own distinctive nonstandard structural features (56,58-61). It is important to realize that many of the cellular RNA molecules contain various modified nucleobases alongside the four canonical nucleobases. This enables the RNA strands to form various complex noncanonical structures with functions that are beyond the translation of DNA sequence information (56). The number of base modifications found in cellular DNA is smaller than those found for RNA (56).

The formation of the nonstandard structures (from either the four canonical nucleobases or the noncanonical modified bases) arises from the fact that nucleobases have multiple sites for base pairing. The multiple hydrogen bonding sites of purines and pyrimidines can be categorized into three groups (edges): the Watson-Crick (WC) edge, the Hoogsteen (H) or “C-H” edge, and the sugar edge (SE), which involves the ribose where the 2'-hydroxyl group is capable of forming efficient H-bonds, in contrast to deoxyribose in DNA (Figure 1.6) (62).

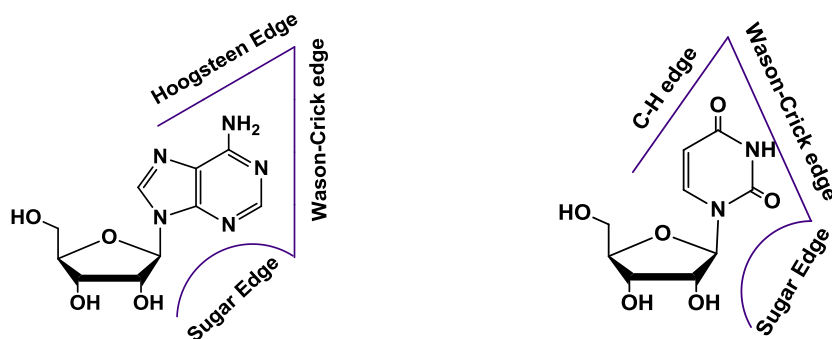


Figure 1.6 Identification of the hydrogen bonding edges in RNA. Figure adapted from reference (62).

The two nucleobases can interact with each other through any of these three edges; and depending on the edge of the interaction and the orientation of the glycosidic bonds relative to the axis of interaction (cis or trans), the type and geometry of the hydrogen bonding interaction is identified (Table 1.2) (62,63). The canonical hydrogen bonding motif is a Watson-Crick edge-to-Watson-Crick edge interaction, with the glycosidic bonds oriented cis relative to the axis of interaction (see entry 1 in Table 1.2, and Figure 1.4).

Table 1.2 Families of edge-to-edge base pairs formed by natural bases defined by the relative orientation of the glycosidic bonds of the interacting bases and the edges they use (62).

Glycosidic bond Orientation	Nucleobase Interacting Edge	Strand Orientation
Cis	Watson-Crick/Watson-Crick	Antiparallel
Trans	Watson-Crick/Watson-Crick	Parallel
Cis	Watson-Crick/Hoogsteen	Parallel
Trans	Watson-Crick/Hoogsteen	Antiparallel
Cis	Watson-Crick/Sugar Edge	Antiparallel
Trans	Watson-Crick/Sugar Edge	Parallel
Cis	Hoogsteen/Hoogsteen	Antiparallel
Trans	Hoogsteen/Hoogsteen	Parallel
Cis	Hoogsteen/Sugar Edge	Parallel
Trans	Hoogsteen/Sugar Edge	Antiparallel
Cis	Sugar Edge/Sugar Edge	Antiparallel
Trans	Sugar Edge/Sugar Edge	Parallel

Some examples of nucleic acid structures containing non-Watson-Crick hydrogen bonds include parallel-stranded duplexes (64-66), triplexes (67-71), G-quadruplexes (72-74) and i-motifs (75,76). The advances in X-ray diffraction and NMR spectroscopy techniques for structural analysis of nucleic acids (77), have led to the detection and detailed characterization of many of the nonstandard hydrogen bonding patterns; some of which are illustrated in Figure 1.7.

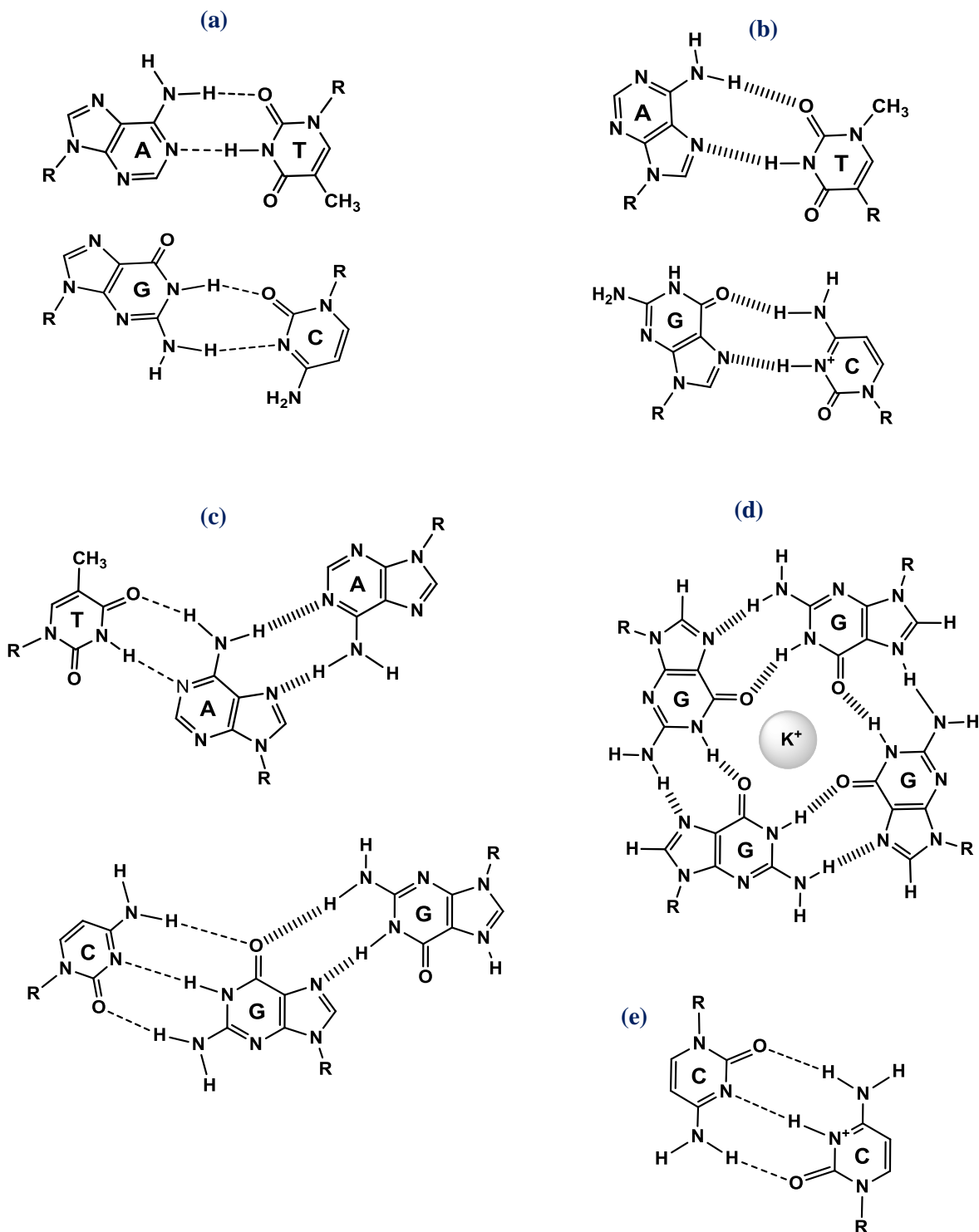


Figure 1.7 Representations of some common noncanonical hydrogen bonding schemes found in: **(a)** and **(b)** parallel duplexes; **(c)** Triplexes; **(d)** G-tetrads; **(e)** i-motifs. The Watson-Crick/reverse Watson-Crick base pairing is shown with dashed bonds, and Hoogsteen/reverse Hoogsteen base pairing is shown with hashed bonds.

Among these noncanonical structures, we are particularly interested in modulating the structural properties and function of G-quadruplexes and parallel-stranded duplexes.

G-quadruplexes are higher order nucleic acid structures composed of two or more stacked tetrads of hydrogen-bonded guanines (Figure 1.8a) (78-82). G-quadruplexes can display a wide variety of topologies based on variations in strand stoichiometry, strand polarity (Figure 1.8b-c), loop length and geometry (Figure 1.8d-f), and etc (72-74). Modulating the G-quadruplex folding and topology constitutes a part of the research presented in Chapter 2 of the present thesis, where we report on structural analysis of substituted human telomeric DNA G-quadruplexes containing several chemical modifications.

Parallel-stranded duplexes will be discussed in Chapter 5. Canonical double helices have their two strands arranged in an antiparallel orientation. However, under unnatural chemical and environmental conditions, a parallel-stranded hybridization is also feasible in which both strands adopt a 5'-3' direction (Figure 1.8h).

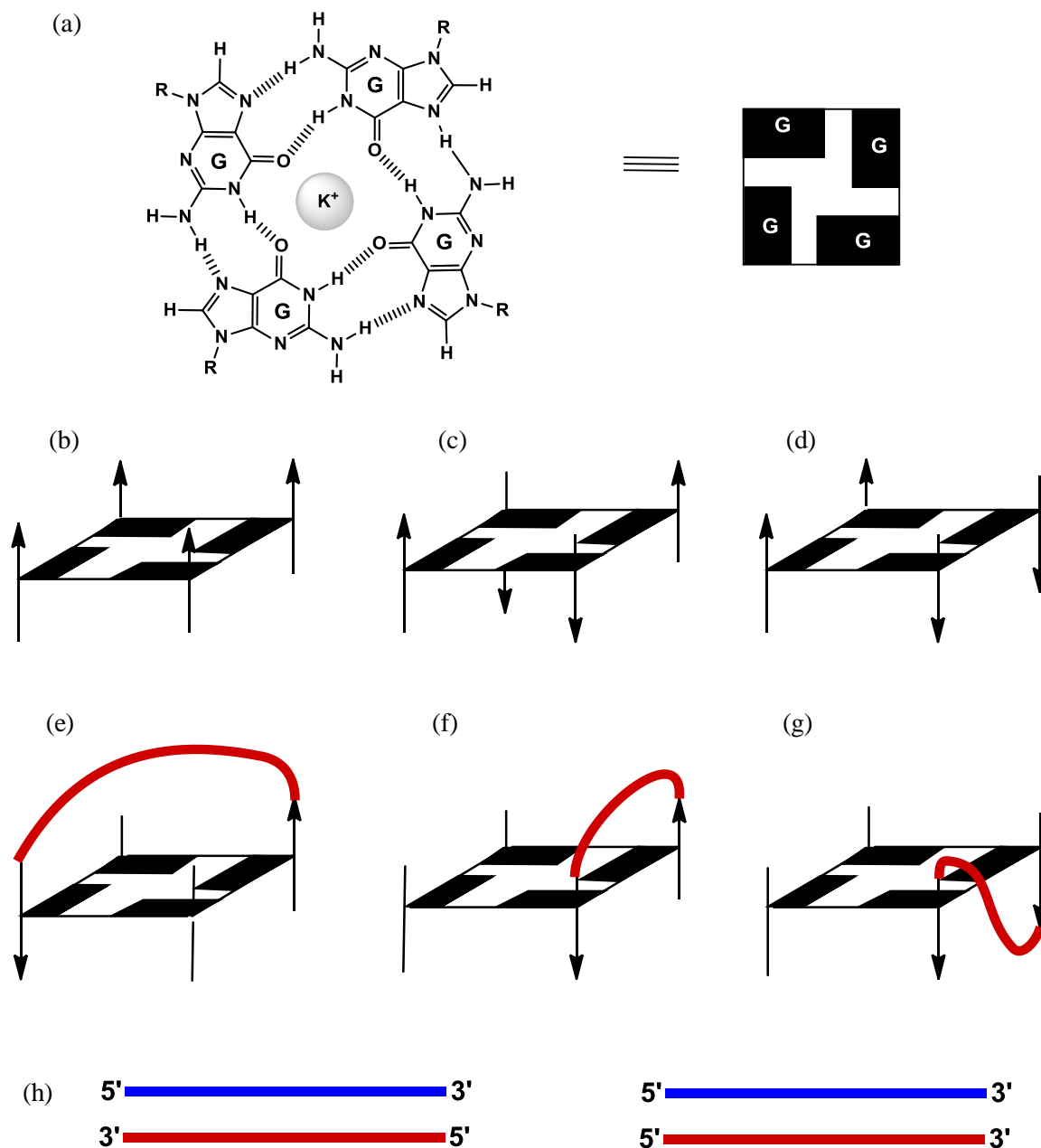


Figure 1.8 Schematic representations of G-quadruplexes and parallel-stranded duplexes. (a) Illustration of one G-tetrad as a square. (b-d) Three topologies for G-tetrad core (a) parallel: all four strands have the same polarity, with all their guanines adopting anti configurations; (b) alternating antiparallel; and (c) adjacent antiparallel. In both of the antiparallel topologies, the guanines alternate between syn and anti. Arrows indicate the strand orientations, from 5' to 3' direction. (e-g) Linkers connecting the G-rich strands are called loops, and there are three types of loops (colored red): (e) diagonal loop, (f) edgewise loop and (g) double-chain-reversal loop. (h) Illustration of antiparallel (left) and parallel (right) chain orientation in double helices.

1.3 Synthetic Oligonucleotide as Therapeutics

Gene-specific knockdown of pathological proteins through the use of synthetic oligonucleotides has become increasingly recognized therapeutically (14). The oligonucleotide-based therapeutics are commonly classified according to their structure, their target, and the mechanism of their action (14,83,84).

Most therapeutic oligonucleotides are antagonists of RNA. Common RNA targets include micro RNAs (miRNAs), precursor mRNA (pre-mRNAs), and messenger RNAs (mRNAs). All these RNA molecules are essential components to the synthesis of proteins– the genetic information contained within the chromosomes is typically passed from DNA to RNA to the resulting proteins (85).

During the past two decades, much effort has been focused on the development of antisense-oligonucleotides (AONs) and siRNAs which are both antagonists of messenger RNA (14,86). Other related RNA-targeting therapeutics include anti-miRNA oligonucleotides (87,88), ribozymes (89) and their DNA analogues DNAzymes (90), and pre-mRNA antagonists which are commonly used for exon skipping applications (91).

In addition to RNA antagonists, there are classes of oligonucleotides that are designed to act on chromosomal DNA and regulate the gene expression at its earliest stage. Such DNA-targeting ONs are called antigenes. One major challenge facing this approach is to develop oligonucleotides that can bind to chromosomal DNA, which is already a double-stranded molecule. To overcome this problem, chemically modified oligonucleotides with extremely high binding affinities towards DNA have been designed which can either replace one of the two strands of the DNA double helix (92-94), or can form triple-stranded structures with *ds*-DNA (95).

Oligonucleotides can also bind to proteins or small molecules, but, of course not through Watson-Crick base pairing. Famous examples include aptamers, decoys and immunostimulatory oligonucleotides.

Just as ribozymes and DNAzymes are nucleic acid analogous to enzymes, aptamers (96,97), are nucleic acids often considered as analogous to antibodies. And like antibodies, aptamers can be used to inhibit the action of pathological proteins (98). An example is pegaptanib (brand name Macugen) which is used for treatment of wet macular degeneration (99), and is the second oligonucleotide therapeutic that has received FDA approval.

Decoys are oligonucleotides that mimic the binding site of a specific transcription factor protein on DNA. The verb decoy itself means to lure. Thus, basically the decoy ONs are used to distract and lure the transcription factor proteins from their binding sites on DNA, and hence affect the rate of transcription of genetic information from DNA to mRNA (100,101).

The immunostimulatory oligonucleotides, also called CpG ONs, mimic bacterial DNA and bind to toll-like receptors (TLRs) and activate the innate immune response (102,103).

Taken together, all classes of oligonucleotides have great potential for research and various therapeutic applications. However, their mechanisms of action are extremely diverse, and a complete review of all would be beyond the scope of this thesis work. Thus, only the biological pathways relevant to the development of AONs and siRNAs, which are essential components of the research presented in this thesis work, will be reviewed below.

1.4 Inhibitors of mRNA Translation

1.4.1 Antisense-Mediated Gene Silencing

AONs are promising therapeutic agents against a variety of diseases. It was shown by Zamecnik and Stephenson for the first time in 1978 that mRNA-targeting DNA oligonucleotides can be utilized to effectively inhibit protein expression (104). Since then, immense progress has been made in the field (105-108), with two FDA approved AON drugs on the market: Formivirsen (brand name Vitravene) (109), and Mipomersen (brand name Kynamro) (110). Many other AON candidates are under study in early- to late-stage clinical trials (84,111,112).

From a chemical perspective, AONs are synthetic short single-stranded DNAs (13–25 nucleotides) which are Watson-Crick complements of the target mRNA. After delivery of AONs into the cytoplasm, antisense oligonucleotides hybridize to the complementary region on the target mRNA and induce silencing of gene expression via either arresting the mRNA translation, or inducing degradation of the target mRNA by RNase H. The basic concepts of these two major mechanisms are illustrated in Figure 1.9.

The first mode of action involves AONs that function by binding tightly to the mRNA. Such AONs contain chemical modifications that highly stabilize the DNA:RNA hybrids. The outcome of using such high-affinity AONs is essentially inhibiting the mRNA translation by blocking ribosomal assembly (112,113). However, it might also result in modulation of pre-mRNA splicing and inhibiting the production of the desired mRNA isoform (via tight binding of AON to the pre-mRNA) (114-117).

The second AON mode of action is an RNase H dependent mechanism. In this mechanism, the DNA antisense oligonucleotide does not only bind to mRNA, but also stimulates the cleavage of the pathological mRNA through the activation of an endogenous enzyme known as RNase H

(118). The RNase H enzymes are known to specifically recognize the DNA:RNA hybrids and cleave only the RNA strand of the hybrid duplex (119-121). The mechanism through which RNase H mediates the hydrolysis of the phosphodiester linkage of the RNA strand is under active investigation, and requires divalent cations (two highly coordinated Mg^{2+} cations) for the binding of the substrate to the active site and catalysis (122).

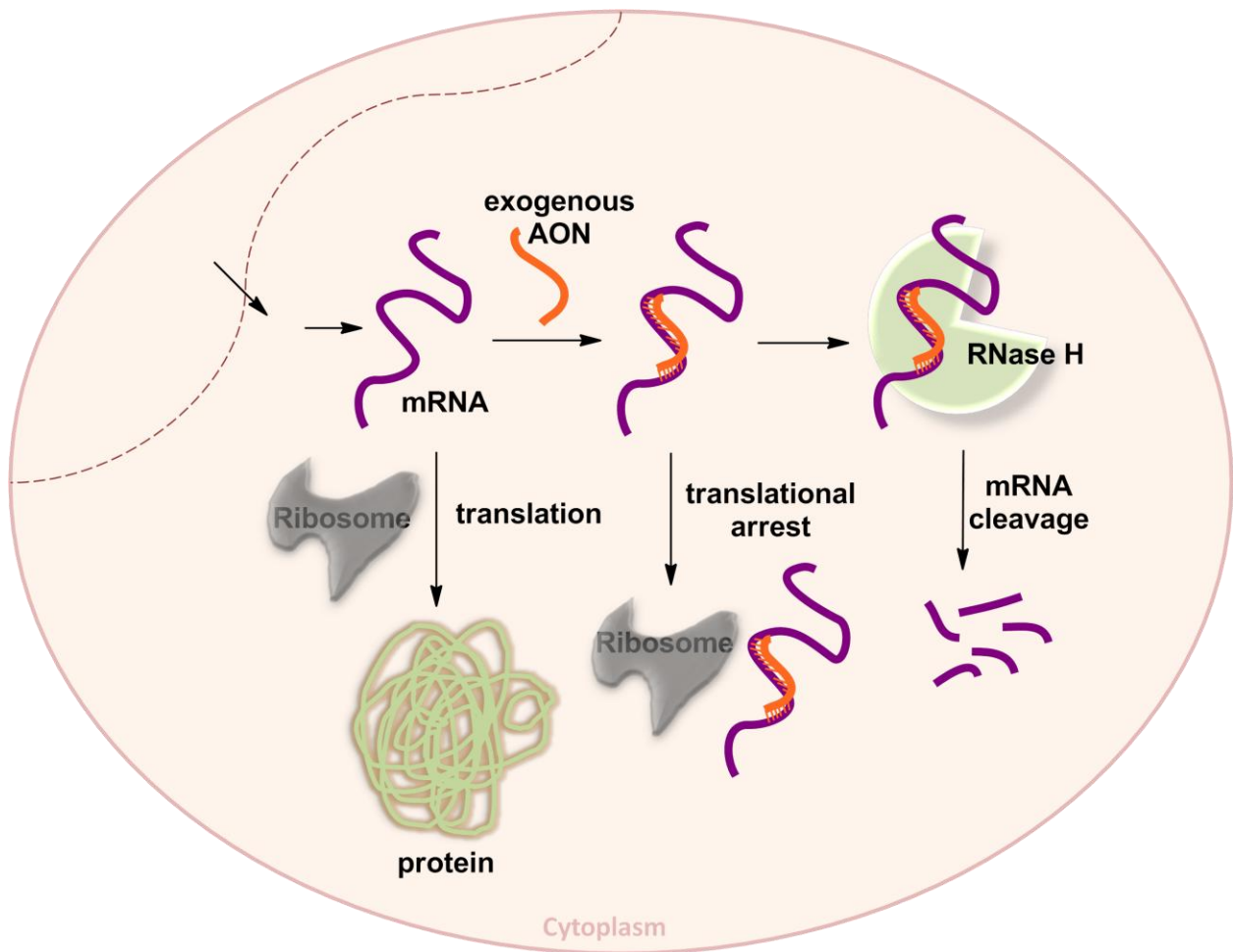


Figure 1.9 Fundamentals of mRNA targeting by antisense oligonucleotides (AONs). Exogenously introduced AONs can recognize and bind to target mRNA sequences and down-regulate the gene expression through either mRNA cleavage via RNase H1 (in humans), or translational arrest. Although shown in the cytoplasm, RNase H may also function in the nucleus.

1.4.2 siRNA-induced gene knockdown through RNAi

RNA interference (RNAi) is a natural cellular mechanism for post-transcriptional gene regulation in most eukaryotes, and was discovered in 1998 by Fire and Mello following the observation that in *C. elegans*, a *ds*-RNA sharing sequence with a cellular mRNA could knockdown the translation of that mRNA (123). Soon after this discovery, it was found that RNAi can also be triggered in mammalian cells using synthetic 21nt-long RNA duplexes (124).

A summary of the RNAi pathway is shown in Figure 1.10. Short double-stranded micro RNAs (miRNAs), present in the cytoplasm, are one major class of natural triggers of RNAi. It is estimated that around 30% of human genes are regulated by miRNAs (125).

Gene regulation by RNAi is mediated by the RNA-induced silencing complex (RISC)(126,127). RISC uses the *ds*-RNA as a guide for the sequence-specific silencing of messenger RNA through either inducing the degradation of the mRNA or translational arrest (87,128,129).

During RISC loading with *ds*-RNA, the strand of the RNA duplex that contains complementary sequence to the target mRNA (termed antisense or guide strand) is loaded into the RISC while the other strand (termed sense or passenger strand) is cleaved and unwound from the antisense strand to be discarded (130,131), although cleavage is not obligatory (131).

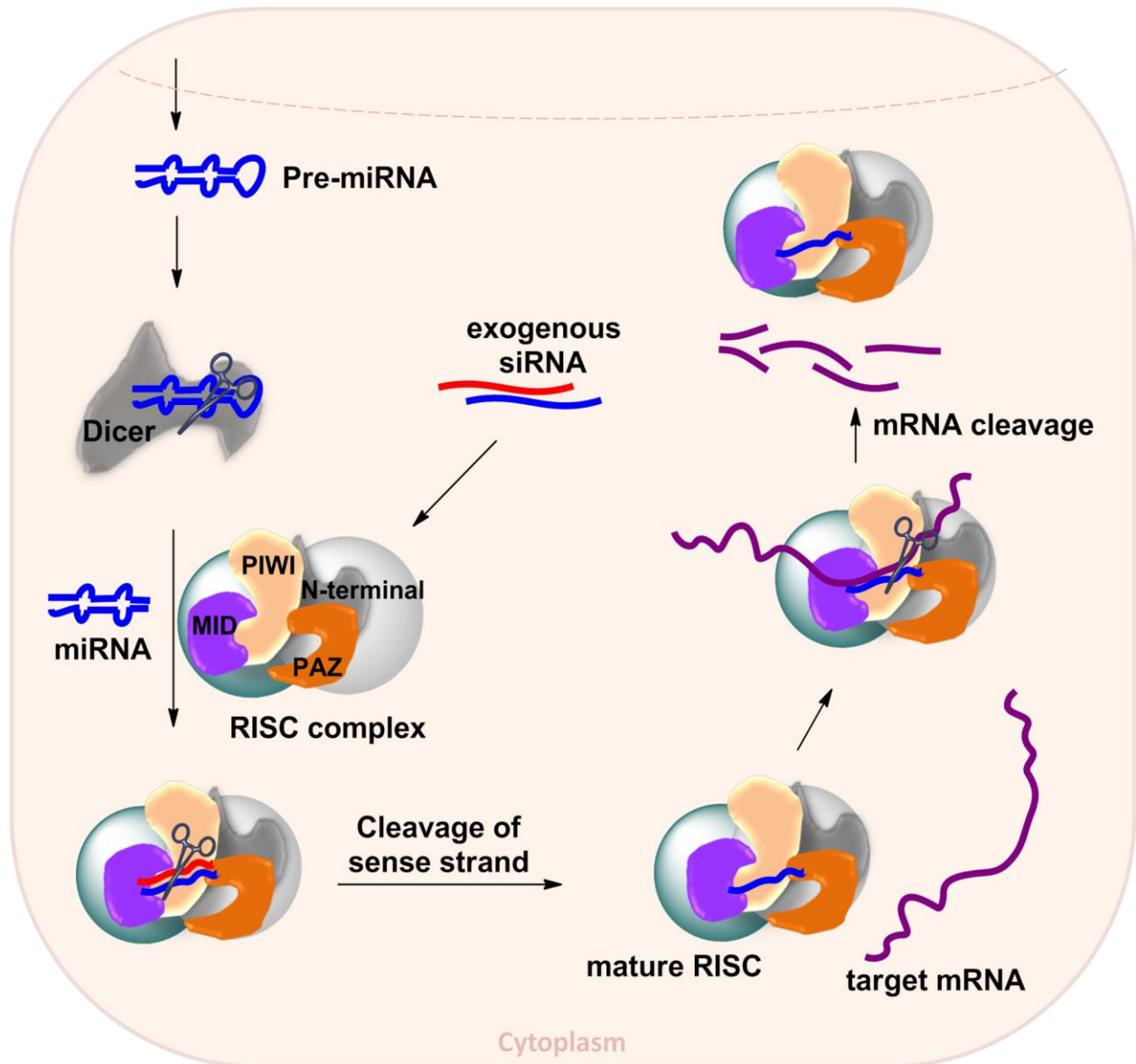


Figure 1.10 Fundamentals of mRNA targeting by miRNA and siRNA. Short *ds*-RNAs, loaded into RISC, are capable of recognizing and binding to the complementary mRNAs, resulting in a decrease in the expression of the corresponding gene.

From a chemical point of view, miRNAs are short RNA duplexes, mimics of which can be readily synthesized using automated solid-phase synthesis (124,132,133). Small interfering RNAs (siRNAs) are the synthetic *ds*-RNA mimics, which are 21-nt long duplexes with 2-nt 3' overhangs (Figure 1.11).

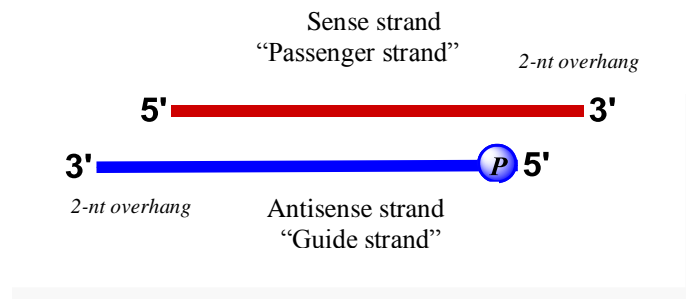


Figure 1.11 Schematic representation of classical siRNA duplex.

When designing chemically modified siRNAs, a detailed understanding of the mechanism of RNAi, guide strand selection/loading, and the enzymes involved in this process is of utmost importance. In a current model for RNAi mechanism, when siRNA duplex is introduced into mammalian cells, the 5'-end is phosphorylated by cellular kinases (134). The siRNA is then loaded into the RNA-induced silencing complex (RISC) and guides RISC to bind to the target mRNA and trigger the silencing of protein expression. RISC is a multiprotein complex that contains Argonaute2 (Ago2), Dicer, and two different double-stranded RNA binding proteins (*ds*-RBP) which are TRBP (trans-activation response RNA binding protein) and PACT (protein activator of PKR). In humans, the Argonaute2 itself is a multidomain protein that contains N-terminal, PAZ, middle (MID), and PIWI sub-domains (126,127). Structural studies have revealed specific interactions between hAgo2 sub-domains and siRNAs (135-137). The MID domain interacts with 5'-phosphate of the loaded guide strand. PIWI, which contains a ribonuclease (RNase) H-like fold, cleaves the passenger strand upon RISC loading. It also performs the mRNA cleavage event. The PAZ domain interacts with the 3'-OH of the loaded guide strand.

The extent to which these core components of RISC contribute to RNA guide strand selection is not fully understood yet (138-141). Recent elegant studies by Doudna and co-workers suggest

that Ago2 acts in concert with Dicer/*ds*-RBP “thermodynamic asymmetry sensors” to ensure proper strand selection, implying that Ago2 does not function exclusively in siRNA guide strand selection (142). In a proposed model, Dicer interacts with the *ds*-RNA on the less stable end of the duplex, and one of the *ds*-RNA binding proteins on the more stable end, spatially orienting the duplex for a subsequent Ago2 loading step in which *ds*-RBP may “hand off” the more stable end of the duplex to the PAZ domain (the guide strand 3'-binding domain) of Ago2 (139). This model suggests a mechanism through which guide strand selection can occur based on siRNA duplex thermodynamic asymmetry, correlating to the observation that the siRNA strand with the least tightly bound 5'-end frequently becomes the RISC guide (143,144).

1.5 Challenges Facing the Development of Oligonucleotide Therapeutics

1.5.1 Overview

All oligonucleotide-based therapeutics must successfully overcome similar obstacles if they are to achieve a high-enough concentration in the vicinity of their target. These obstacles include crossing the cell membrane and resisting nucleases (111). Within nuclease-rich cells or serum, unprotected oligonucleotides are rapidly degraded. Also, unmodified DNA and RNA bind weakly to plasma proteins and thus are filtered and excreted rather quickly resulting in poor pharmacokinetics.

A solution to overcome many of these shortcomings is the chemical modification of nucleic acid structure, which will provide a means to control and modulate many of the nucleic acid properties including binding affinity for their targets, structural preferences, and nuclease stability. Other approaches developed to achieve potent and efficient oligonucleotide therapeutics include conjugation of oligonucleotides with biologically relevant moieties (145-

148), or encapsulation of oligonucleotides within protective particles that shield them from degradation (147-150).

Clearly, since most oligonucleotides are from the same polyanionic nature, the strategies developed for improving drug-like properties of a specific class of ONs can apply to other classes as well.

1.5.2 Optimization of AON and siRNA Therapeutics: Chemical Modifications

Despite their immense therapeutic potential, siRNAs and AONs are disadvantaged by their poor nuclease stability, poor cellular uptake, and off-target effects arising from partial complementarities of ONs to unintended mRNA sequences and nonspecific immune responses (111,151,152). While double-stranded siRNAs are more nuclease-resistant than *ss*-DNA AONs, the unmodified siRNAs are still degraded *in vivo* resulting in a decrease in their half-life and poor delivery to the target (111,153).

From a chemist's perspective, the rational manipulation of nucleic acid structure through incorporation of chemical modifications can provide solutions to many of the hurdles facing oligonucleotide therapeutics, and thus, over the last two decades a large variety of chemically modified oligonucleotides have been synthesized and tested (154,155).

In general, chemical modification approaches of ONs can be classified into three main categories: (i) chemical modification of the internucleotide linkage; (ii) chemical modification of the sugar moiety; and (iii) chemical modification of the nucleobase.

Chemical modifications can improve the stability of ONs in serum. Also, they can improve potency and selectivity of ONs for their target by increasing the strength of their hybridization with target mRNA and thereby, minimizing the off target effects (OTEs). Since a detailed

discussion of all these chemical modifications lies beyond the scope of this chapter, only a few examples will be given below to emphasize their impact and outline the structural parameters required for the design of potent AONs and siRNAs. For thorough accounts, the reader is directed to references (155-157) for reviews on nucleic acid backbone modifications, to references (158-160) for reviews on nucleobase modifications, and to references (155,161-163) for reviews on sugar modifications.

1.5.3 Structural Considerations for Designing Chemically Modified ON Therapeutics

1.5.3.1 Antisense Design

The design of stable and RNase H-susceptible AON analogues is challenging. In order to maintain potency in cases where RNase H-mediated mRNA cleavage is desired, it is considered a requirement that AON analogues retain their polyanionic character (164), and as well form stable A-form heteroduplexes with target mRNA. The flexibility of the AON:mRNA hybrid is another critical factor for its recognition as a substrate by RNase H (165-167). It has been established that the more flexible strands may enable the enzyme to deform the duplex more easily and more quickly as required during binding (168-170). This latter observation may be employed to explain why RNase H enzymes react with A-form DNA:RNA hybrids but not with the A-form *ds*-RNAs (171-173). While *ds*-RNA is somehow similar in conformation to A-form DNA:RNA hybrid duplexes, it is the relatively inflexible nature of the two RNA strands that compromises its recognition by the RNase H. The sugars in RNA strand, perhaps as a result of strong gauche effects imparted by the 2'-OH substituents, are more conformationally pre-organized as compared to DNA sugars (24-26), a property that renders more rigidity to RNA:RNA duplexes as compared to RNA:DNA hybrids.

Considering these structural parameters, often when designing AON analogue that contain a combination of chemical modifications, the AON retains a continuous region of DNA or DNA-like modification in order to ensure the RNase H recruitment and cleavage (172).

Among the chemical modifications used for AON design, the introduction of phosphorothioate linkage (PS linkage; Figure 1.12a) in place of the phosphodiester bond is perhaps the earliest success (157). The PS-DNA forms A-form hybrids with RNA which are capable of activating RNase H activity. Moreover, it enhances the nuclease stability and improves ON binding to serum proteins *in vivo*, leading to improved pharmacokinetics and circulation time (174,175).

While PS modification is a very promising modification and is present in almost all the first generation AON designs, it has shown to induce sequence-independent toxicity (108). For this reason, to improve the suboptimal properties associated with PS-AONs, the second and third generation AONs often contain a combination of phosphorothioate backbone plus sugar modifications. A successful example of this approach is Kynamro, a second generation AON containing PS linkages and 2'-O-(2-methoxyethyl) sugars (2'-O-MOE; Figure 1.12b) (88).

The second and third generation sugar modifications are often employed in a "gapmer" design, in which sugar modified units are on the ends of the oligonucleotide, flanking a central DNA segment in the middle. The rationale is that because the sugar modifications are placed at the ends of the AON, they don't interfere with RNase H function. Both the DNA-like and RNA-like nucleotide analogues shown in Figure 1.12b have been successfully implemented into the gapmer AONs (176).

DNA-like sugars like 2'-fluoro-arabinonucleic acid (2'-F-ANA; Figure 1.12b) can also be successfully implemented into an "altimer" design, in which they are alternated with DNA units

every ~2-3 nucleotides (177,178). 2'F-ANA is particularly an interesting chemical modification for AON design (167,168,177,179). It is a DNA mimic that increases the binding affinity for RNA and improves the stability of AONs against degradation by nucleases and depurination. Moreover, 2'F-ANA substituted AONs activate the RNase H function when bound to target mRNA.

1.5.3.2 siRNA Design

The efficient control of gene regulation by siRNAs largely depends on their optimal design (180). Once the best sequence capable of potent knockdown of mRNA is selected (181), the function of siRNA can be enhanced through the incorporation of a variety of chemical and structural modifications. The double-stranded nature of siRNAs, and the fact that two strands serve very different functions, makes the siRNA design more complex than AON design. One must carefully consider each siRNA strand is modified at which positions and in what fashion (182).

As described earlier, RNAi is triggered by short A-form *ds*-RNAs. Thus, RNA mimics that retain a North sugar conformation are expected to be well tolerated in siRNAs (e.g. 2'F-RNA, 2'-O-Me RNA, 2'-O-MOE RNA and LNA; Figure 1.12b).

2'F-ribonucleic acid (2'F-RNA; Figure 1.12b) is a popular sugar modification in therapeutic oligonucleotide design (183). 2'F-RNA is an RNA mimic, adopting a C3'-*endo* sugar pucker (184), and is very well tolerated in both the guide and passenger strands of siRNA (183,185). 2'F-RNA increases the binding affinity for RNA (186,187) and enhances the ON, specifically pyrimidine-rich ON, resistance against endonucleases, however, they do not impart a significant resistance against exonucleases (176).

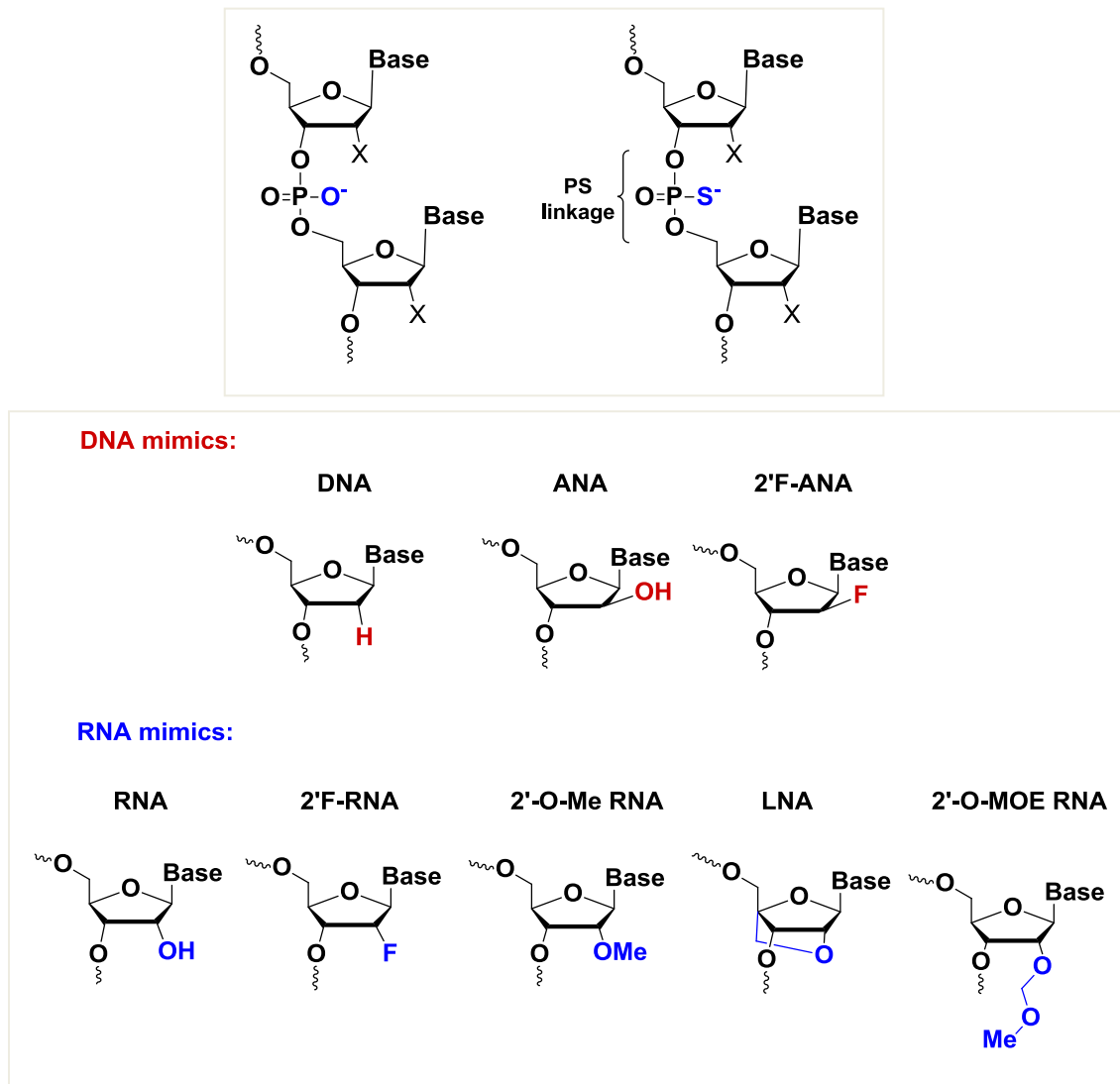


Figure 1.12 Chemical structures of (a) Phosphorothioate backbone; (b) Selected C2'-sugar modifications.

Based on the current model described earlier for the RNAi mechanism, we know that the siRNA guide strand selection relies on duplex thermodynamics, and the strand with the least tightly-bound 5'-end is typically selected and loaded as the guide strand (143,144). For this reason, chemical modifications should be introduced within the siRNA duplex in an arrangement that satisfies the thermal asymmetry required for guide strand loading into the RISC complex. This is a feature that will help enhance the siRNA potency and reduce off-target effects.

Off-target effects can also be reduced through chemical modifications incorporated to the sense strand in order to prevent its phosphorylation at the 5'-terminus. Cellular kinases add phosphate groups to the siRNA 5'-ends (134). These phosphates interact with the MID domain of Ago2 (188), and thereby play an important role in strand selection. Thus, adding chemical modifications that prevent the 5'-phosphorylation of the sense strand can be beneficial in preventing its loading to RISC and reducing the OTEs. As well, to ensure guide strand selection by RISC, 5'-phosphates are usually added chemically to the 5'-end of the antisense (guide) during siRNA synthesis.

The architecture of an siRNA duplex can also be modified. Classical 21-nt siRNA duplexes can be generated from longer RNAs (> 21-nt) by the act of upstream cellular enzymes, in a similar way that miRNAs are generated from pre-miRNAs by Dicer. Thus, RNAi-mediated gene silencing can be also triggered using a variety of longer RNA molecules including RNA hairpins (shRNAs) (189), long double-stranded siRNAs (also termed dicer-substrates) (190-192), and circular RNAs (193). Specifically, dicer substrate siRNAs demonstrate excellent potency and can often evoke more potent RNAi activity than the corresponding 21-nt siRNAs. Single-stranded antisense oligonucleotides have also been shown to function in RNAi, although in some cases reduced potency was observed versus standard duplex siRNAs (194-196).

1.6 Techniques Used to Study Hybridization Properties of Nucleic Acids

The following sections will briefly review three spectroscopic techniques that are commonly used to study the structure and hybridization properties of nucleic acids, and indeed have been essential to the advancement of the research presented in this thesis.

1.6.1 UV-Absorbance and Thermal Denaturation Studies

UV-absorbance experiments are highly useful for the study of nucleic acids. Because of their aromatic heterocyclic nucleobases, nucleic acids have a strong UV absorbance signature centered at about 260nm.

The absorbance of UV light at 260nm (A_{260}) and at a specific temperature can be used to measure the concentration of a nucleic acid solution. According to the Beer-Lambert law, the absorbance measured at a specific wavelength (260nm in this case), is given by $A = \epsilon lc$, where ϵ is the molar extinction coefficient given in [L/(mole.cm)], l is the sample thickness (typically 1cm), and c is the molar concentration of the sample [moles/L]. If the nucleic acid sequence is known, the molar extinction coefficient can be calculated from experimentally determined values for mono and di-nucleotides (197).

Heating a nucleic acid duplexes and multiplexes over a range of temperatures often leads to changes in absorbance properties, which reflects the conformational changes of the nucleic acid molecules in solution. The resulting profile of absorbance versus temperature is called a “melting” or a “thermal denaturation” curve (197-199).

A typical UV-absorbance melting curve of an antiparallel double-stranded duplex is given in Figure 1.13. At low temperatures, the oligonucleotide molecules are assumed to exist almost entirely in the duplex (annealed) state. As the temperature is increased, the duplex begins to unwind or “melt”, transitioning to the single-stranded state. The temperature at which 50% of the molecules exists in the duplex form and 50% exists as the single strands is known as the melting temperature (T_m) which is a value that can be determined from the thermal denaturation curve (198).

The melting process is associated with an increase in UV absorbance which is a result of decrease in base stacking. In the duplex state, the nucleobases of paired oligonucleotides are stacked on top of each other, causing dipole interactions that reduce the UV absorbance of the bases as compared to that of their free state. As the ordered regions of the base pairs are disrupted by increase in temperature, the stacking of the bases significantly decrease, leading to a decreased dipole interaction and thus a higher UV absorption. This increase in absorbance is called hyperchromicity (200), and together with the T_m value, provides a measure of the strength of base pairing and stacking of the nucleic acid secondary structure.

In principle, the thermal denaturation curves could also be obtained with other spectroscopic techniques. Monitoring a fluorescence emission signal (201), the intensity of an NMR peak (202), a circular dichroism signal (203), or a Raman signal (204,205) over a range of temperatures will produce a melting profile. Indeed the experimental settings as well as the Y-axis will be different, but the data analysis will be very similar. Nevertheless, in any of these procedures, it is essential to perform the melting experiments over a slow temperature gradient; specifically for those structures that have slow folding and unfolding kinetics like G-quadruplexes (199,206-208).

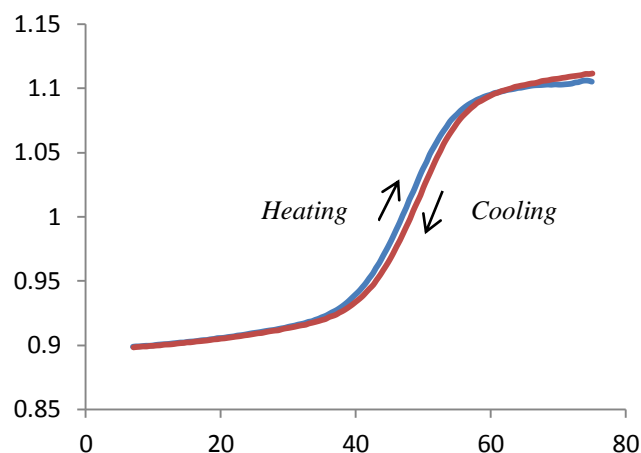


Figure 1.13 Example thermal denaturation curve corresponding to a 12-nt antiparallel DNA:RNA hybrid acquired on a Cary UV-Vis spectrophotometer (temperature ramp= 0.4 °C/min).

Analysis of melting curves of different nucleic acid structures (e.g. duplexes, triplexes, tetraplexes) enables the determination of the thermodynamic parameters (ΔH° , ΔG° or ΔS°) of the structures under study (198,209), providing an insight into the nature and strength of the forces that stabilize nucleic acids in their diverse structural states. As well, these studies have allowed the construction of thermodynamic databases and equations (210), that can be used to “predict” a secondary structure for a specific nucleic acid sequence and calculate the stability of the resulting structure (211-214). The method widely used for predicting nucleic acid duplex stability, pioneered by Tinoco and co-workers (215), employs a nearest-neighbor model for helix propagation. Such predictions can aid with the design and choice of the oligonucleotide sequences for a broad range of nucleic acid-based diagnostic and therapeutic protocols including PCR, sequencing by hybridization and antigen targeting (216-218). Nevertheless, these rules are empirical, and the actual secondary structure of a nucleic acid may differ significantly from the predicted structure, mostly because even short DNA or RNA may adopt unexpected nonstandard base pairing schemes, such as those described earlier (56-61).

1.6.2 Circular Dichroism

Circular Dichroism (CD) is a spectroscopic method which depends on the fact that the absorption of right- and left-handed circularly polarized light by chiral molecules differs. This difference is called CD (219).

The quantity used to describe circular dichroism is called ellipticity (Θ), and is expressed in degrees. Another convenient characterization of CD is the difference in the molar extinction coefficients, $\Delta\epsilon = \epsilon_L - \epsilon_R$ ($M^{-1}cm^{-1}$). Molar ellipticity and molar circular dichroism are related by the expression $\Theta = 3298\Delta\epsilon$ (220). Thorough reviews of the basic theory and practice of CD spectroscopy can be found in references (220,221).

In the case of nucleic acids, circular dichroism (CD) arises from the asymmetric helical structures they adopt, and thereby it is a powerful technique for studying the helical arrangement and secondary structure of nucleic acids (222-224). CD can be used for tracing the conformational transitions between discrete nucleic acid arrangements; many of which occur as a result of subtle changes in environmental conditions such as temperature, solvent ionic strength, and pH. Examples include monitoring B-DNA-to-A-DNA and B-DNA-to-Z-DNA conformational transitions (225,226), duplex-to-hairpin transitions (226), or as well for monitoring guanine quadruplexes topologies (225-227).

From a practical point of view, acquiring a CD spectrum for nucleic acids is a straightforward procedure and is operationally similar to recording a UV-absorbance spectrum. For guidelines on carrying out a CD experiment see reference (228).

Typical CD spectra of antiparallel Watson-Crick B-type and A-type duplexes are shown in Figure 1.14. Unmodified DNA with a mixed-base composition on average adopts a B-type conformation whose CD spectrum shows a positive band around 275-280nm and a negative band

around 245-250nm (225). The CD spectrum of an A-form DNA is characterized by a strong positive band around 260nm and a negative one at 240nm (225), and closely resembles the CD spectra of A-form *ds*-RNAs or RNA:DNA hybrids of the same base sequence. The position and amplitudes of the CD bands differ markedly with sequence; not only because chromophores (nucleobases) differ, but also because of the resulting changes in base stacking arrangements and overall conformational properties of the duplex (229,230).

The effect of heating on the CD spectrum has also been studied (203). The major change observed is that increasing the temperature decreases the intensity of the 275-280nm band, which is due to the unstacking of the bases with a decrease in the interaction between the neighboring bases.

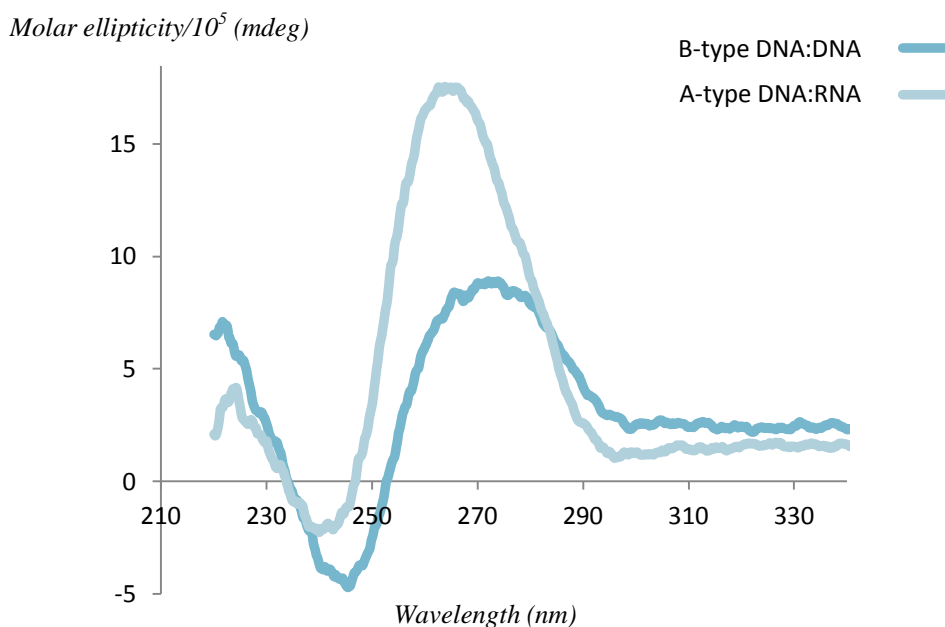


Figure 1.14 Example CD spectra of 12-nt B-DNA and A-form DNA:RNA antiparallel duplexes acquired on a JASCO J-810 circular dichroism spectrometer at 25°C.

CD spectroscopy has also been widely used to study G-quadruplexes (231-233). The parallel G-quartet structure (Figure 1.8), exhibits a CD spectrum characterized by a dominant positive band at 260nm and a negative band at 240nm (225-227). The CD spectrum of the antiparallel quadruplex (Figure 1.8), exhibits a CD spectrum with a positive band at 295 nm and a negative band at 260nm (225-227).

The different CD of the parallel and antiparallel quadruplexes mostly originates from different stacking interactions between the guanines that are differently oriented around their glycosidic bonds (227). The presence of two different glycosidic torsion angles allow for different base-stacking arrangements.

1.6.3 NMR

NMR spectroscopy is an extremely valuable technique to study the structure, conformation and interactions of nucleic acid duplexes (234-237), triplexes and tetraplexes (238-241).

In principal, all NMR active nuclei present in nucleic acids can be used to derive structural data. Among those, protons (^1H) can be detected with the highest sensitivity, and ^1H NMR is used by far the most extensively. Other nuclei are less sensitive than protons, and have low natural abundance but the high field strength of magnets used in NMR studies has made ^{13}C and ^{15}N -enriched oligonucleotides amenable to detailed studies.

NMR spectroscopy can be used for investigations of nucleic acids at various levels. 1D NMR studies of “nucleoside” and “nucleotide” monomers go back to the early days of NMR spectroscopy (242,243). The three principal parameters derived from 1D NMR of nucleic acid monomers are the chemical shift value (δ), the J-coupling constant or scalar coupling (which

provides information about the nuclei that are covalently bound), and the through-space or dipolar coupling (which provides information about the spatial proximity of nonbonded nuclei). The underlying principles of nuclear magnetic resonance spectroscopy can be found in reference (244). Reference (245) on the other hand provides a more practical approach and is for learning how to perform NMR experiments after having studied the theory.

The protons of the pyrimidine and purine nucleobases are found at $\delta \sim 5-9$ ppm. The sugar proton resonances are upfield at $\delta \sim 3-4$ ppm for the H2', H3', H4', H5' and H5'' protons and at $\delta \sim 5-6$ ppm for the H1' anomeric proton. These chemical shifts are rather conformation-dependent and vary according to the sugar pucker.

The three-bond $^1\text{H}, ^1\text{H}$ scalar couplings within the sugar moiety i.e. $^3\text{J}(\text{H},\text{H})$, also depend strongly on the sugar conformation, and thus are of diagnostic value for the determination of sugar pucker geometries. For example, a large $^3\text{J}(\text{H1}',\text{H2}')$ coupling together with a small $^3\text{J}(\text{H3}',\text{H4}')$ coupling is indicative of the C2'-*endo* conformation, while a large $^3\text{J}(\text{H3}',\text{H4}')$ coupling and a small $^3\text{J}(\text{H1}',\text{H2}')$ coupling are indicative of the C3'-*endo* conformation (Figure 1.15). Accordingly, the relative populations of puckers in solution can also be monitored directly by NMR measurements (246). The observed $^3\text{J}(\text{H1}',\text{H2}')$ and $^3\text{J}(\text{H3}',\text{H4}')$ coupling constant values obtained from basic ^1H -NMR experiments on a given nucleoside can be used to calculate an accurate approximation of the North/South conformational distribution of the nucleotide in solution (Figure 1.15) (246,247).

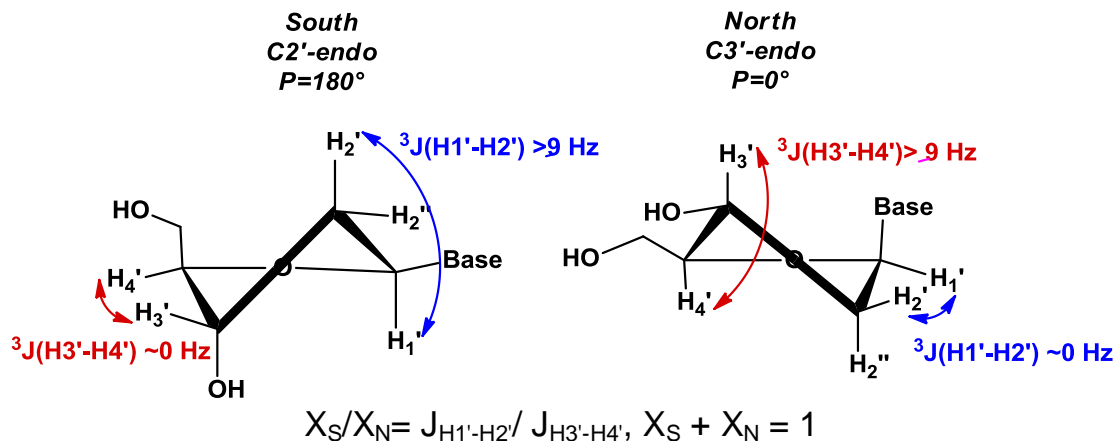


Figure 1.15 Illustration of indicative three-bond (3J) scalar couplings for South and North conformations, followed by the equation for approximating North/South conformational distribution of a nucleoside using 3J scalar coupling constants.

Besides nucleoside and nucleotide monomers, di-nucleotides have also been extensively studied by NMR and systematic classification of their 1H chemical shifts (δ) and coupling constants (J) data are available in the literature (248-250), which serve as a reference for oligomer spectra.

Perhaps the most challenging application of 1H NMR is the analysis of the spectra of nucleic acid “duplexes” and “multiplexes”, in which the oligomers are bound to each other (238,251-253).

Two classes of protons are particularly interesting (Figure 1.16): non-exchangeable protons, which are protons bonded to carbon atoms, both aromatic and sugar protons, and exchangeable (labile) protons that are attached to electronegative heteroatoms.

There are three types of exchangeable (labile) protons in natural oligonucleotides: imino protons, amino protons, and hydroxyl protons. The imino and amino protons are the $-NH$ and $-NH_2$ protons of the heterocyclic nucleobases that are involved in the formation of inter-chain hydrogen bonds. In general, both the imino and amino resonances exchange rapidly and won't be observed in D_2O solvent and they can only be detected in H_2O/D_2O solution (254).

The imino protons are particularly interesting moieties since they resonance far downfield from other protons (Watson-Crick [12-14.5 ppm]; Hoogsteen [10.5-12ppm], and C-C⁺ [15-16ppm]), and also only one imino resonance is contributed by each base pair.

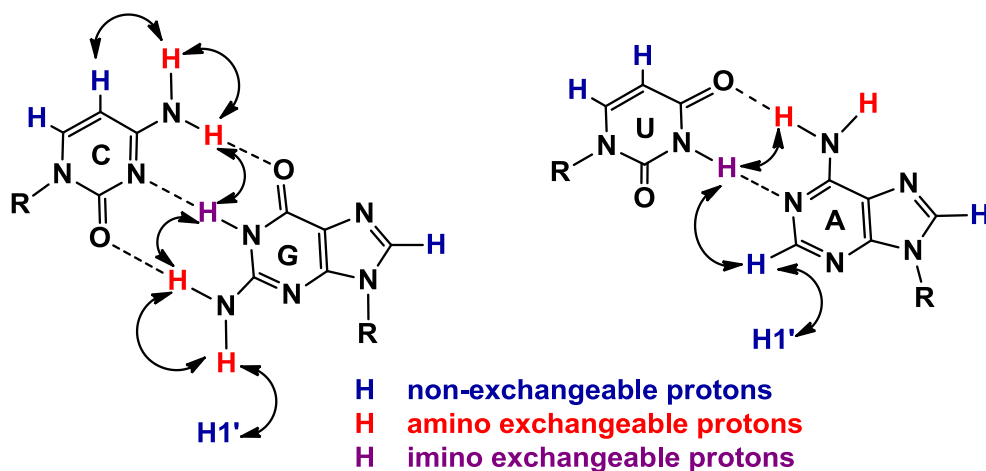


Figure 1.16 Schematic representation of non-exchangeable and labile protons of natural nucleobases, along with some NOEs observed over the canonical Watson-Crick hydrogen bonds. Arrows indicate the through-space connectivities.

While it is possible to obtain chemical-shift and coupling-constant information from a one dimensional (1D) NMR spectrum, it is necessary to run 2D (or sometimes 3D and 4D) NMR experiments in order to solve the structure of the nucleic acid structure (255-258). The most valuable data for DNA samples are obtained from variants of COSY (correlated spectroscopy), and NOESY (nuclear Overhauser effect spectroscopy) experiments. Since there is no spin-spin coupling between sugar protons and base protons, COSY spectra on their own are not sufficient and they are always used in combination with NOESY spectra.

The two-dimensional NOESY spectra obtained in D₂O will provide the cross peaks of the non-exchangeable protons and are valuable for sequential assignment of the duplex. This assignment is based on the NOE effects (Nuclear Overhauser Effects) originating from dipolar couplings

(through-space couplings) between the nuclei separated by $<4.5\text{-}5\text{\AA}$ (259,260). Shorter interproton distances lead to more intense NOE cross peaks. These distances change depending on the sugar pucker and glycosidic angles.

The assignment of nucleic acid duplex spectra is a complex task and has been very well reviewed in the literature (261-263). As an example, only a few important sequential connectivities of a B-DNA duplex are presented schematically in Figure 1.17. As illustrated by arrows, along each strand of the B-DNA helix (with C2'-endo sugar pucker and anti glycosidic bonds), there are a series of strong intranucleotide and sequential connectivities from H8 or H6 of the nucleobase to H1', H2', H2'' of the sugar in the 5'-to-3' direction. The connectivities between protons of a given sugar are obtained from correlated spectra (COSY, TOCSY, etc).

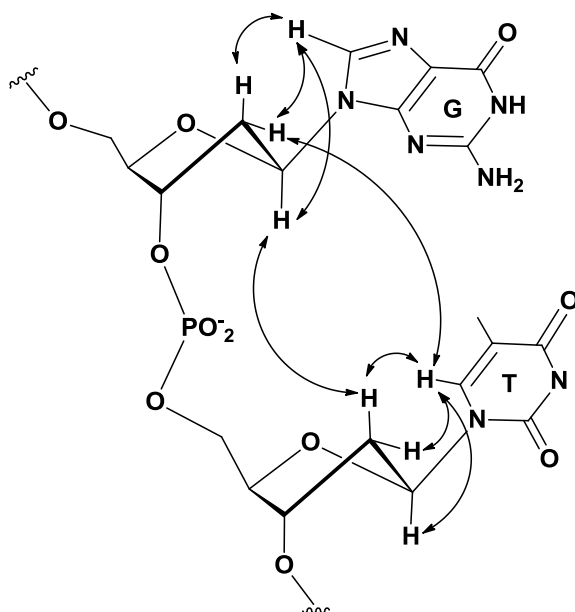


Figure 1.17 Illustration of some strong intra-nucleotide and inter-nucleotide (sequential) base-sugar NOEs in B-DNA. Arrows indicate the through-space connectivities. All-anti glycosidic torsion angles provide a pattern of strong H6,H8- H2',H2'' cross peaks and H6,H8- H1' cross peaks which are used to make sequential assignments. Although the shortest intra- and inter-nucleotide base-sugar connectivities are H6,H8-H2' and H6,H8- H2'', respectively, it is usually easiest to start sequential assignments via the H6,H8-H1' cross peaks. The more complicated H6,H8-H2',H2'' cross peak region can be used to confirm these assignments and to resolve ambiguities.

Alongside routine ^1H , ^1H homonuclear 2D NMR experiments (^1H , ^1H -COSY and NOESY), running heteronuclear variants of correlation and NOE spectroscopy will provide further structural information. For example, heteronuclear coupling between ^1H and ^{31}P obtained from ^{31}P - ^1H HSQC experiments can be useful for the determination of additional ^{31}P - ^1H coupling constants, which can be converted into semiquantitative backbone torsion angle restraints (262,264,265).

Heteronuclear NOESY spectroscopy (HOESY spectroscopy) (266,267) is also very helpful for studying nucleic acid structures. ^1H - ^{19}F HOESY in particular has been used vastly for structure determination of C2'-fluorinated nucleic acid analogues. In principal, ^1H - ^{19}F HOESY (also termed F-HOESY) originates from dipolar couplings between ^1H and ^{19}F nuclei in close proximity. If there are a proton and a fluorine (simplest case) close to each other (usually the distance $< 5 \text{ \AA}$), there will be a cross peak on the 2D HOESY map. The peak intensity indicates the distance between two atoms.

Once the 2D ^1H -NMR spectra are assigned as much as possible, accurate intensities of 2D NOE cross peaks are extracted and converted into distances via computational tools. Bond torsion angles on the other hand are determined using vicinal coupling constants (3J , obtained from various correlation spectroscopy) and Karplus-type relation ($^3J = A \cos^2 \theta + B \cos \theta + C$; where A , B , and C are empirically-derived parameters whose values depend on the substituents involved) (268-270). A brief overview on the process of generating three dimensional structures based on NMR data can be found in Chapter 3 of the present thesis (section 3.4.1). Thorough and detailed reviews on this topic can be found in references (236,271,272).

1.7 Thesis Objectives and Layout

The present thesis work is primarily focused on investigating the correlation between structure and functional properties of nucleic acid analogues. Our perspective is that many of the shortcomings associated with different nucleic acid applications can be solved through chemical modification of their nucleotide building blocks, and thus, gaining a detailed understanding on structural effects of chemical modifications is of significant interest to our laboratory.

Among the many modified nucleic acids, and specifically those with modifications in their sugar moiety, arabinonucleic acid (ANA) and its 2'-fluorinated derivative (2'-F-ANA) are particularly interesting to us. Hence the research presented in this thesis is directed particularly towards understanding the structural basis for the interesting properties imparted by these two analogues, with focus on their structure, stability, and activity in cell based systems.

The specific research projects of this thesis are presented as follows:

Chapter 2 provides a careful analysis of several 2'-F-arabinose modified duplexes and demonstrates that the greater stability of 2'-F-ANA:RNA hybrids relative to ANA:RNA hybrids originates, at least in part, from the formation of energetically important intra-strand hydrogen bonding interactions between F2' and the purine H8 of the 3'-proximal nucleotide. This contrasts the unfavorable 2'-OH–nucleobase steric interactions in the case of ANA:RNA hybrids. C2'-F...H8-C hydrogen bonding interactions, uncovered for the first time during the course of this work, are among the very rare examples of hydrogen bonds in which the organic fluorine acts as a hydrogen bond acceptor in water. In this chapter, we also report on structural analysis of substituted human telomeric DNA G-quadruplex containing several chemical modifications. Our study reveals that the same C2'-F...H8-C hydrogen bonding interactions observed in 2'-F-ANA

modified double-helices also contribute to the stability of 2'F-ANA substituted G-quadruplex structures found in the human telomeric sequence. Moreover, this favourable interaction was exploited to enhance the binding affinity and potency of therapeutically relevant 2'F-ANA substituted antisense oligonucleotides capable of eliciting RNase H-mediated cleavage of their complementary RNA target.

In an extension to this line of work, **Chapter 3** describes efforts aimed at determining the structure of 2'F-ANA:2'F-ANA and ANA:ANA duplexes, and further investigates the intra-chain noncovalent interactions between the C2' substituents (-OH and -F) and the proximal H8 of purine nucleobases. In this chapter, we show that while ANA binds very poorly to its complementary ANA strand, an appropriate combination of 2'F-ANA and ANA nucleotides in a gapmer design can form duplex and hairpin structures of similar thermal stability. The co-existence of the linear and hairpin duplex may be a particularly useful tool in applications where a duplex/hairpin conformational switch is desirable.

Chapter 4 describes how nucleotide analogues can be used to improve several aspects of siRNA molecules. Considering the current model for the RNAi mechanism and guide strand selection, ANA and 2'F-ANA nucleotides were introduced on the passenger strand in an arrangement that introduced thermal asymmetry within the siRNA duplex. During these studies, passenger and guide strands comprising exclusively arabinonucleic acid units were tested in the RNAi pathway for the first time.

As a part of our ongoing interest in chemically modified nucleic acid structures, **Chapter 5** examines the impact of several sugar and nucleobase substitutions on the formation of parallel-stranded duplexes at neutral pH. Our study is the first to incorporate isoguanosine and isocytidine into an RNA strand, assessing whether these modified nucleotides promote the

formation of stable parallel-stranded RNAs or DNA:RNA hybrids under physiological-like conditions. We also examine the impact of 2'-fluorinated sugar modifications (2'F-ANA, and its epimer 2'F-RNA) on parallel -stranded duplex strength and assess whether a similar stabilization to what is seen in conventional antiparallel arrangement, is obtained in the parallel arrangement. As well, the ability of developed parallel-stranded duplexes to participate in the RNAi gene silencing pathway is investigated for the first time.

1.8 References

1. Avery, O.T., Macleod, C.M. and McCarty, M. (1944) Studies on the chemical nature of the substance inducing transformation of pneumococcal types : induction of transformation by a desoxyribonucleic acid fraction isolated from pneumococcus type III. *J Exp Med*, **79**, 137-158.
2. Levene, P.A. (1919) The structure of yeast nucleic acid: IV. ammonia hydrolysis. *J. Biol. Chem.*, **40**, 415-424.
3. Levene, P.A. and Tipson, R.S. (1935) The ring structure of thymidine. *J. Biol. Chem.*, **109**, 623-630.
4. Griffith, F. (1928) The significance of pneumococcal types. *Epidemiology & Infection*, **27**, 113-159.
5. Chargaff, E. (1950) Chemical specificity of nucleic acids and mechanism of their enzymatic degradation. *Experientia*, **6**, 201-209.
6. Hayes, D.H., Michelson, A.M. and Todd, A.R. (1955) Nucleotides. Part XXX. Mononucleotides derived from deoxyadenosine and deoxyguanosine. *Journal of the Chemical Society (Resumed)*, 808-815.
7. Watson, J.D. and Crick, F.H.C. (1953) Molecular Structure of Nucleic Acids: A Structure for Deoxyribose Nucleic Acid. *Nature*, **171**, 737-738.
8. Franklin, R.E. and Gosling, R.G. (1953) Molecular Configuration in Sodium Thymonucleate. *Nature*, **171**, 740-741.
9. Wilkins, M.H.F., Stokes, A.R. and Wilson, H.R. (1953) Molecular Structure of Nucleic Acids: Molecular Structure of Deoxypentose Nucleic Acids. *Nature*, **171**, 738-740.
10. Beaucage, S.L. and Caruthers, M.H. (1981) Deoxynucleoside phosphoramidites—A new class of key intermediates for deoxypolynucleotide synthesis. *Tetrahedron Letters*, **22**, 1859-1862.

11. Usman, N., Ogilvie, K.K., Jiang, M.Y. and Cedergren, R.J. (1987) The automated chemical synthesis of long oligoribonucleotides using 2'-O-silylated ribonucleoside 3'-O-phosphoramidites on a controlled-pore glass support: synthesis of a 43-nucleotide sequence similar to the 3'-half molecule of an Escherichia coli formylmethionine tRNA. *Journal of the American Chemical Society*, **109**, 7845-7854.
12. Cotton, R.G.H. (1993) Current methods of mutation detection. *Mutation Research/Fundamental and Molecular Mechanisms of Mutagenesis*, **285**, 125-144.
13. O'Connor, L. and Glynn, B. (2010) Recent advances in the development of nucleic acid diagnostics. *Expert review of medical devices*, **7**, 529-539.
14. Goodchild, J. (2011) In Goodchild, J. (ed.), *Therapeutic Oligonucleotides*. Humana Press, Vol. 764, pp. 1-15.
15. Blackburn, G.M., M. J. Gait, and D. Loakes. (2006) *Nucleic Acids in Chemistry and Biology*. 3rd ed. RSC Publishing, UK.
16. Saenger, W. (1988) *Principles of Nucleic Acid Structure*. 2nd ed.
17. Shukla, M.K. and Leszczynski, J. (2013) Tautomerism in nucleic acid bases and base pairs: a brief overview. *Wiley Interdisciplinary Reviews: Computational Molecular Science*, **3**, 637-649.
18. Sepiol, J., Kazimierczuk, Z. and Shugar, D. (1976) Tautomerism of isoguanosine and solvent-induced keto-enol equilibrium. *Zeitschrift fur Naturforschung. Section C: Biosciences*, **31**, 361-370.
19. Davies, D.B. (1978) Conformations of nucleosides and nucleotides. *Progress in Nuclear Magnetic Resonance Spectroscopy*, **12**, 135-225.
20. Sundaralingam, M. (1969) Stereochemistry of nucleic acids and their constituents. IV. Allowed and preferred conformations of nucleosides, nucleoside mono-, di-, tri-, tetraphosphates, nucleic acids and polynucleotides. *Biopolymers*, **7**, 821-860.
21. Hall, L.D., Steiner, P.R. and Pedersen, C. (1970) Studies of specifically fluorinated carbohydrates. Part VI. Some pentofuranosyl fluorides. *Canadian Journal of Chemistry*, **48**, 1155-1165.
22. Sundaralingam, M. (1965) Conformations of the Furanose Ring in Nucleic Acids and Other Carbohydrate Derivatives in the Solid State¹. *Journal of the American Chemical Society*, **87**, 599-606.
23. Altona, C. and Sundaralingam, M. (1972) Conformational analysis of the sugar ring in nucleosides and nucleotides. New description using the concept of pseudorotation. *Journal of the American Chemical Society*, **94**, 8205-8212.
24. Gyi, J.I., Lane, A.N., Conn, G.L. and Brown, T. (1998) Solution Structures of DNA-RNA Hybrids with Purine-Rich and Pyrimidine-Rich Strands: Comparison with the Homologous DNA and RNA Duplexes. *Biochemistry*, **37**, 73-80.
25. Bachelin, M., Hessler, G., Kurz, G., Hacia, J.G., Dervan, P.B. and Kessler, H. (1998) Structure of a stereoregular phosphorothioate DNA/RNA duplex. *Nat Struct Mol Biol*, **5**, 271-276.
26. Gonzalez, C., Stec, W., Reynolds, M.A. and James, T.L. (1995) Structure and Dynamics of a DNA.cntdot.RNA Hybrid Duplex with a Chiral Phosphorothioate Moiety: NMR and Molecular Dynamics with Conventional and Time-Averaged Restraints. *Biochemistry*, **34**, 4969-4982.

27. Kool, E.T. (1997) Preorganization of DNA: Design Principles for Improving Nucleic Acid Recognition by Synthetic Oligonucleotides. *Chemical Reviews*, **97**, 1473-1488.
28. Kool, E.T. (2001) Hydrogen bonding, base stacking, and steric effects in dna replication. *Annual review of biophysics and biomolecular structure*, **30**, 1-22.
29. Šponer, J., Leszczynski, J. and Hobza, P. (2001) Electronic properties, hydrogen bonding, stacking, and cation binding of DNA and RNA bases. *Biopolymers*, **61**, 3-31.
30. Friedman, R.A. and Honig, B. (1992) The electrostatic contribution to DNA base-stacking interactions. *Biopolymers*, **32**, 145-159.
31. Maroun, R.C. and Olson, W.K. (1988) Base sequence effects in double-helical DNA. III. Average properties of curved dna. *Biopolymers*, **27**, 585-603.
32. Hunter, C.A. (1993) Sequence-dependent DNA Structure: The Role of Base Stacking Interactions. *Journal of Molecular Biology*, **230**, 1025-1054.
33. Lowe, M.J. and Schellman, J.A. (1972) Solvent effects on dinucleotide conformation. *Journal of Molecular Biology*, **65**, 91-109.
34. Guckian, K.M., Schweitzer, B.A., Ren, R.X.F., Sheils, C.J., Paris, P.L., Tahmassebi, D.C. and Kool, E.T. (1996) Experimental Measurement of Aromatic Stacking Affinities in the Context of Duplex DNA. *Journal of the American Chemical Society*, **118**, 8182-8183.
35. Guckian, K.M., Schweitzer, B.A., Ren, R.X.F., Sheils, C.J., Tahmassebi, D.C. and Kool, E.T. (2000) Factors Contributing to Aromatic Stacking in Water: Evaluation in the Context of DNA. *Journal of the American Chemical Society*, **122**, 2213-2222.
36. Kool, E.T., Morales, J.C. and Guckian, K.M. (2000) Mimicking the Structure and Function of DNA: Insights into DNA Stability and Replication. *Angewandte Chemie International Edition*, **39**, 990-1009.
37. Freier, S.M., Sugimoto, N., Sinclair, A., Alkema, D., Neilson, T., Kierzek, R., Caruthers, M.H. and Turner, D.H. (1986) Stability of XGCGCp, GCGCYp, and XGCGCYp helices: an empirical estimate of the energetics of hydrogen bonds in nucleic acids. *Biochemistry*, **25**, 3214-3219.
38. Manning, G.S. (1978) The molecular theory of polyelectrolyte solutions with applications to the electrostatic properties of polynucleotides. *Quarterly Reviews of Biophysics*, **11**, 179-246.
39. SantaLucia, J., Allawi, H.T. and Seneviratne, P.A. (1996) Improved Nearest-Neighbor Parameters for Predicting DNA Duplex Stability†. *Biochemistry*, **35**, 3555-3562.
40. Arnott, S. (1970) The geometry of nucleic acids. *Progress in Biophysics and Molecular Biology*, **21**, 265-319.
41. Drew, H.R., Wing, R.M., Takano, T., Broka, C., Tanaka, S., Itakura, K. and Dickerson, R.E. (1981) Structure of a B-DNA dodecamer: conformation and dynamics. *Proceedings of the National Academy of Sciences*, **78**, 2179-2183.
42. Ghosh, A. and Bansal, M. (2003) A glossary of DNA structures from A to Z. *Acta Crystallographica Section D*, **59**, 620-626.
43. Dervan, P.B. (1986) Design of sequence-specific DNA-binding molecules. *Science (New York, N.Y.)*, **232**, 464-471.
44. Zimmer, C. and Wähnert, U. (1986) Nonintercalating DNA-binding ligands: Specificity of the interaction and their use as tools in biophysical, biochemical and biological

- investigations of the genetic material. *Progress in Biophysics and Molecular Biology*, **47**, 31-112.
45. Egly, M. (1996) Structural Aspects of Nucleic Acid Analogs and Antisense Oligonucleotides. *Angewandte Chemie International Edition in English*, **35**, 1894-1909.
 46. Yanagi, K., Privé, G.G. and Dickerson, R.E. (1991) Analysis of local helix geometry in three B-DNA decamers and eight dodecamers. *Journal of Molecular Biology*, **217**, 201-214.
 47. Saenger, W., Hunter, W.N. and Kennard, O. (1986) DNA conformation is determined by economics in the hydration of phosphate groups. *Nature*, **324**, 385-388.
 48. Berman, H.M. (1991) Hydration of DNA. *Current Opinion in Structural Biology*, **1**, 423-427.
 49. Leslie, A.G.W., Arnott, S., Chandrasekaran, R. and Ratliff, R.L. (1980) Polymorphism of DNA double helices. *Journal of Molecular Biology*, **143**, 49-72.
 50. Arnott, S., Chandrasekaran, R., Millane, R.P. and Park, H.S. (1986) RNA-RNA, DNA-DNA, and DNA-RNA Polymorphism. *Biophys J*, **49**, 3-5.
 51. Conte, M.R., Conn, G.L., Brown, T. and Lane, A.N. (1997) Conformational properties and thermodynamics of the RNA duplex r(CGCAAUUUGCG)₂: comparison with the DNA analogue d(CGCAAATTTGCG)₂. *Nucleic Acids Research*, **25**, 2627-2634.
 52. Wang, A.H., Fujii, S., van Boom, J.H. and Rich, A. (1982) Molecular structure of the octamer d(G-G-C-C-G-G-C-C): modified A-DNA. *Proceedings of the National Academy of Sciences*, **79**, 3968-3972.
 53. Egly, M., Usman, N., Zhang, S.G. and Rich, A. (1992) Crystal structure of an Okazaki fragment at 2-Å resolution. *Proceedings of the National Academy of Sciences*, **89**, 534-538.
 54. Jissy, A.K. and Datta, A. (2013) Design and Applications of Noncanonical DNA Base Pairs. *The Journal of Physical Chemistry Letters*, **5**, 154-166.
 55. Mooers, B.H.M., Eichman, B.F. and Ho, P.S. (1997) The structures and relative stabilities of d(G · G) reverse Hoogsteen, d(G · T) reverse wobble, and d(G · C) reverse Watson-Crick base-pairs in DNA crystals. *Journal of Molecular Biology*, **269**, 796-810.
 56. Carell, T., Brandmayr, C., Hienzsch, A., Müller, M., Pearson, D., Reiter, V., Thoma, I., Thumbs, P. and Wagner, M. (2012) Structure and Function of Noncanonical Nucleobases. *Angewandte Chemie International Edition*, **51**, 7110-7131.
 57. Chou, S.H., Chin, K.H. and Wang, A.H. (2003) Unusual DNA duplex and hairpin motifs. *Nucleic Acids Res*, **31**, 2461-2474.
 58. Westhof, E. and Fritsch, V. (2000) RNA folding: beyond Watson-Crick pairs. *Structure*, **8**, R55-R65.
 59. Noller, H.F. (2005) RNA Structure: Reading the Ribosome. *Science (New York, N.Y.)*, **309**, 1508-1514.
 60. Luebke, K.J. and Tinoco, I., Jr. (1996) Sequence effects on RNA bulge-induced helix bending and a conserved five-nucleotide bulge from the group I introns. *Biochemistry*, **35**, 11677-11684.
 61. Varani, G. and McClain, W.H. (2000) The G · U wobble base pair: A fundamental building block of RNA structure crucial to RNA function in diverse biological systems. *EMBO reports*, **1**, 18-23.

62. Leontis, N.B., Stombaugh, J. and Westhof, E. (2002) The non-Watson–Crick base pairs and their associated isostericity matrices. *Nucleic Acids Research*, **30**, 3497-3531.
63. Šponer, J.E., Špačková, N.a., Kulhánek, P., Leszczynski, J. and Šponer, J. (2005) Non-Watson–Crick Base Pairing in RNA. Quantum Chemical Analysis of the cis Watson–Crick/Sugar Edge Base Pair Family. *The Journal of Physical Chemistry A*, **109**, 2292-2301.
64. van de Sande, J., Ramsing, N., Germann, M., Elhorst, W., Kalisch, B., von Kitzing, E., Pon, R., Clegg, R. and Jovin, T. (1988) Parallel stranded DNA. *Science (New York, N.Y.)*, **241**, 551-557.
65. Pattabiraman, N. (1986) Can the double helix be parallel? *Biopolymers*, **25**, 1603-1606.
66. Ramsing, N.B. and Jovin, T.M. (1988) Parallel stranded duplex DNA. *Nucleic Acids Res*, **16**, 6659-6676.
67. Frank-Kamenetskii, M.D. and Mirkin, S.M. (1995) Triplex DNA Structures. *Annual Review of Biochemistry*, **64**, 65-95.
68. Lavelle, L. and Fresco, J.R. (1995) UV spectroscopic identification and thermodynamic analysis of protonated third strand deoxycytidine residues at neutrality in the triplex d(C⁺-T)₆:[d(A-G)₆d(C⁻-T)₆]; evidence for a proton switch. *Nucleic Acids Research*, **23**, 2692-2705.
69. Marfurt, J. and Leumann, C. (1998) Evidence for C–H···O Hydrogen Bond Assisted Recognition of a Pyrimidine Base in the Parallel DNA Triple-Helical Motif. *Angewandte Chemie International Edition*, **37**, 175-177.
70. Marfurt, J., Parel, S.P. and Leumann, C.J. (1997) Strong, specific, monodentate G-C base pair recognition by N7-inosine derivatives in the pyrimidine•purine-pyrimidine triple-helical binding motif. *Nucleic Acids Research*, **25**, 1875-1882.
71. Sun, J.-s., Carestier, T. and Hélène, C. (1996) Oligonucleotide directed triple helix formation. *Current Opinion in Structural Biology*, **6**, 327-333.
72. Burge, S., Parkinson, G.N., Hazel, P., Todd, A.K. and Neidle, S. (2006) Quadruplex DNA: sequence, topology and structure. *Nucleic Acids Research*, **34**, 5402-5415.
73. Phan, A.T. (2010) Human telomeric G-quadruplex: structures of DNA and RNA sequences. *FEBS Journal*, **277**, 1107-1117.
74. Collie, G.W. and Parkinson, G.N. (2011) The application of DNA and RNA G-quadruplexes to therapeutic medicines. *Chemical Society Reviews*, **40**, 5867-5892.
75. Guéron, M. and Leroy, J.-L. (2000) The i-motif in nucleic acids. *Current Opinion in Structural Biology*, **10**, 326-331.
76. Völker, J., Klump, H.H. and Breslauer, K.J. (2007) The energetics of i-DNA tetraplex structures formed intermolecularly by d(TC5) and intramolecularly by d[(C5T3)3C5]. *Biopolymers*, **86**, 136-147.
77. Panigrahi, S., Pal, R. and Bhattacharyya, D. (2011) Structure and Energy of Non-Canonical Basepairs: Comparison of Various Computational Chemistry Methods with Crystallographic Ensembles. *Journal of Biomolecular Structure and Dynamics*, **29**, 541-556.
78. Blackburn, E.H. and Szostak, J.W. (1984) The Molecular Structure of Centromeres and Telomeres. *Annual Review of Biochemistry*, **53**, 163-194.

79. Sen, D. and Gilbert, W. (1992) Novel DNA superstructures formed by telomere-like oligomers. *Biochemistry*, **31**, 65-70.
80. Sundquist, W.I. and Klug, A. (1989) Telomeric DNA dimerizes by formation of guanine tetrads between hairpin loops. *Nature*, **342**, 825-829.
81. Williamson, J.R. (1994) G-quartet structures in telomeric DNA. *Annual review of biophysics and biomolecular structure*, **23**, 703-730.
82. Sen, D. and Gilbert, W. (1988) Formation of parallel four-stranded complexes by guanine-rich motifs in DNA and its implications for meiosis. *Nature*, **334**, 364-366.
83. Kole, R., Krainer, A.R. and Altman, S. (2012) RNA therapeutics: beyond RNA interference and antisense oligonucleotides. *Nature reviews. Drug discovery*, **11**, 125-140.
84. Burnett, J.C. and Rossi, J.J. (2012) RNA-based therapeutics: current progress and future prospects. *Chem Biol*, **19**, 60-71.
85. Weaver, R. (2011) *Molecular Biology*. McGraw-Hill Science/Engineering/Math; 5th edition
86. Kalota, A., Shetzline, S.E. and Gewirtz, A.M. (2004) Progress in the development of nucleic acid therapeutics for cancer. *Cancer biology & therapy*, **3**, 4-12.
87. Lennox, K.A. and Behlke, M.A. (2011) Chemical modification and design of anti-miRNA oligonucleotides. *Gene therapy*, **18**, 1111-1120.
88. Ambros, V. (2008) The evolution of our thinking about microRNAs. *Nat Med*, **14**, 1036-1040.
89. Goodchild, J. (2000) Hammerhead ribozymes: biochemical and chemical considerations. *Current opinion in molecular therapeutics*, **2**, 272-281.
90. Schlosser, K. and Li, Y. (2009) Biologically inspired synthetic enzymes made from DNA. *Chem Biol*, **16**, 311-322.
91. Saleh, A.F., Arzumanov, A.A. and Gait, M.J. (2012) Overview of alternative oligonucleotide chemistries for exon skipping. *Methods in molecular biology (Clifton, N.J.)*, **867**, 365-378.
92. Beane, R., Gabillet, S., Montallier, C., Arar, K. and Corey, D.R. (2008) Recognition of Chromosomal DNA inside Cells by Locked Nucleic Acids†. *Biochemistry*, **47**, 13147-13149.
93. Beane, R.L., Ram, R., Gabillet, S., Arar, K., Monia, B.P. and Corey, D.R. (2007) Inhibiting gene expression with locked nucleic acids (LNAs) that target chromosomal DNA. *Biochemistry*, **46**, 7572-7580.
94. Hu, J. and Corey, D.R. (2007) Inhibiting gene expression with peptide nucleic acid (PNA)--peptide conjugates that target chromosomal DNA. *Biochemistry*, **46**, 7581-7589.
95. Duca, M., Vekhoff, P., Oussedik, K., Halby, L. and Arimondo, P.B. (2008) The triple helix: 50 years later, the outcome. *Nucleic Acids Res*, **36**, 5123-5138.
96. Keefe, A.D., Pai, S. and Ellington, A. (2010) Aptamers as therapeutics. *Nature reviews. Drug discovery*, **9**, 537-550.
97. Thiel, K.W. and Giangrande, P.H. (2009) Therapeutic applications of DNA and RNA aptamers. *Oligonucleotides*, **19**, 209-222.
98. Blake, C.M., Sullenger, B.A., Lawrence, D.A. and Fortenberry, Y.M. (2009) Antimetastatic potential of PAI-1-specific RNA aptamers. *Oligonucleotides*, **19**, 117-128.

99. Fraunfelder, F.W. (2005) Pegaptanib for wet macular degeneration. *Drugs of today (Barcelona, Spain : 1998)*, **41**, 703-709.
100. Mann, M.J. and Dzau, V.J. (2000) Therapeutic applications of transcription factor decoy oligonucleotides. *The Journal of clinical investigation*, **106**, 1071-1075.
101. Morishita, R., Gibbons, G.H., Horiuchi, M., Ellison, K.E., Nakama, M., Zhang, L., Kaneda, Y., Ogihara, T. and Dzau, V.J. (1995) A gene therapy strategy using a transcription factor decoy of the E2F binding site inhibits smooth muscle proliferation in vivo. *Proceedings of the National Academy of Sciences of the United States of America*, **92**, 5855-5859.
102. Barchet, W., Wimmenauer, V., Schlee, M. and Hartmann, G. (2008) Accessing the therapeutic potential of immunostimulatory nucleic acids. *Current opinion in immunology*, **20**, 389-395.
103. Agrawal, S. and Kandimalla, E.R. (2001) Antisense and/or immunostimulatory oligonucleotide therapeutics. *Current cancer drug targets*, **1**, 197-209.
104. Zamecnik, P.C. and Stephenson, M.L. (1978) Inhibition of Rous sarcoma virus replication and cell transformation by a specific oligodeoxynucleotide. *Proceedings of the National Academy of Sciences*, **75**, 280-284.
105. Gewirtz, A.M. (2000) Oligonucleotide Therapeutics: A Step Forward. *Journal of Clinical Oncology*, **18**, 1809-1811.
106. Crooke, S.T. (2004) Antisense strategies. *Current molecular medicine*, **4**, 465-487.
107. Aboul-Fadl, T. (2005) Antisense oligonucleotides: the state of the art. *Current medicinal chemistry*, **12**, 2193-2214.
108. Dias, N. and Stein, C.A. (2002) Antisense oligonucleotides: basic concepts and mechanisms. *Molecular cancer therapeutics*, **1**, 347-355.
109. Marwick, C. (1998) First "antisense" drug will treat CMV retinitis. *Jama*, **280**, 871.
110. Crooke, S.T. and Geary, R.S. (2013) Clinical pharmacological properties of mipomersen (Kynamro), a second generation antisense inhibitor of apolipoprotein B. *British journal of clinical pharmacology*, **76**, 269-276.
111. Watts, J.K. and Corey, D.R. (2012) Silencing disease genes in the laboratory and the clinic. *The Journal of pathology*, **226**, 365-379.
112. Bennett, C.F. and Swayze, E.E. (2010) RNA targeting therapeutics: molecular mechanisms of antisense oligonucleotides as a therapeutic platform. *Annual review of pharmacology and toxicology*, **50**, 259-293.
113. Baker, B.F., Lot, S.S., Condon, T.P., Cheng-Flournoy, S., Lesnik, E.A., Sasmor, H.M. and Bennett, C.F. (1997) 2'-O-(2-Methoxy)ethyl-modified anti-intercellular adhesion molecule 1 (ICAM-1) oligonucleotides selectively increase the ICAM-1 mRNA level and inhibit formation of the ICAM-1 translation initiation complex in human umbilical vein endothelial cells. *The Journal of biological chemistry*, **272**, 11994-12000.
114. Alter, J., Lou, F., Rabinowitz, A., Yin, H., Rosenfeld, J., Wilton, S.D., Partridge, T.A. and Lu, Q.L. (2006) Systemic delivery of morpholino oligonucleotide restores dystrophin expression bodywide and improves dystrophic pathology. *Nat Med*, **12**, 175-177.
115. Aartsma-Rus, A. and van Ommen, G.-J.B. (2009) Less is more: therapeutic exon skipping for Duchenne muscular dystrophy. *The Lancet Neurology*, **8**, 873-875.
116. Bauman, J., Jearawiriyapaisarn, N. and Kole, R. (2009) Therapeutic potential of splice-switching oligonucleotides. *Oligonucleotides*, **19**, 1-13.

117. Dominski, Z. and Kole, R. (1993) Restoration of correct splicing in thalassemic pre-mRNA by antisense oligonucleotides. *Proceedings of the National Academy of Sciences of the United States of America*, **90**, 8673-8677.
118. Wu, H., Lima, W.F., Zhang, H., Fan, A., Sun, H. and Crooke, S.T. (2004) Determination of the Role of the Human RNase H1 in the Pharmacology of DNA-like Antisense Drugs. *J. Biol. Chem.*, **279**, 17181-17189.
119. Stein, H. and Hausen, P. (1969) Enzyme from calf thymus degrading the RNA moiety of DNA-RNA Hybrids: effect on DNA-dependent RNA polymerase. *Science (New York, N.Y.)*, **166**, 393-395.
120. Lima, W.F., Rose, J.B., Nichols, J.G., Wu, H., Migawa, M.T., Wyrzykiewicz, T.K., Siwkowski, A.M. and Crooke, S.T. (2007) Human RNase H1 discriminates between subtle variations in the structure of the heteroduplex substrate. *Molecular pharmacology*, **71**, 83-91.
121. Cerritelli, S.M. and Crouch, R.J. (1998) Cloning, Expression, and Mapping of Ribonucleases H of Human and Mouse Related to Bacterial RNase HI. *Genomics*, **53**, 300-307.
122. Ho, M.H., De Vivo, M., Dal Peraro, M. and Klein, M.L. (2010) Understanding the effect of magnesium ion concentration on the catalytic activity of ribonuclease H through computation: does a third metal binding site modulate endonuclease catalysis? *J Am Chem Soc*, **132**, 13702-13712.
123. Fire, A., Xu, S., Montgomery, M.K., Kostas, S.A., Driver, S.E. and Mello, C.C. (1998) Potent and specific genetic interference by double-stranded RNA in *Caenorhabditis elegans*. *Nature*, **391**, 806-811.
124. Elbashir, S.M., Harborth, J., Lendeckel, W., Yalcin, A., Weber, K. and Tuschl, T. (2001) Duplexes of 21-nucleotide RNAs mediate RNA interference in cultured mammalian cells. *Nature*, **411**, 494-498.
125. Lewis, B.P., Burge, C.B. and Bartel, D.P. (2005) Conserved seed pairing, often flanked by adenosines, indicates that thousands of human genes are microRNA targets. *Cell*, **120**, 15-20.
126. Hutvagner, G. and Simard, M.J. (2008) Argonaute proteins: key players in RNA silencing. *Nat Rev Mol Cell Biol*, **9**, 22-32.
127. Jinek, M. and Doudna, J.A. (2009) A three-dimensional view of the molecular machinery of RNA interference. *Nature*, **457**, 405-412.
128. Filipowicz, W., Bhattacharyya, S.N. and Sonenberg, N. (2008) Mechanisms of post-transcriptional regulation by microRNAs: are the answers in sight? *Nat Rev Genet*, **9**, 102-114.
129. Kawamata, T. and Tomari, Y. (2010) Making RISC. *Trends in biochemical sciences*, **35**, 368-376.
130. Leuschner, P.J., Ameres, S.L., Kueng, S. and Martinez, J. (2006) Cleavage of the siRNA passenger strand during RISC assembly in human cells. *EMBO reports*, **7**, 314-320.
131. Matranga, C., Tomari, Y., Shin, C., Bartel, D.P. and Zamore, P.D. (2005) Passenger-strand cleavage facilitates assembly of siRNA into Ago2-containing RNAi enzyme complexes. *Cell*, **123**, 607-620.

132. Elbashir, S.M., Martinez, J., Patkaniowska, A., Lendeckel, W. and Tuschl, T. (2001) Functional anatomy of siRNAs for mediating efficient RNAi in *Drosophila melanogaster* embryo lysate. *The EMBO journal*, **20**, 6877-6888.
133. Nykanen, A., Haley, B. and Zamore, P.D. (2001) ATP requirements and small interfering RNA structure in the RNA interference pathway. *Cell*, **107**, 309-321.
134. Weitzer, S. and Martinez, J. (2007) The human RNA kinase hClp1 is active on 3[prime] transfer RNA exons and short interfering RNAs. *Nature*, **447**, 222-226.
135. Wang, Y., Juranek, S., Li, H., Sheng, G., Tuschl, T. and Patel, D.J. (2008) Structure of an argonaute silencing complex with a seed-containing guide DNA and target RNA duplex. *Nature*, **456**, 921-926.
136. Wang, Y., Sheng, G., Juranek, S., Tuschl, T. and Patel, D.J. (2008) Structure of the guide-strand-containing argonaute silencing complex. *Nature*, **456**, 209-213.
137. Wang, Y., Juranek, S., Li, H., Sheng, G., Wardle, G.S., Tuschl, T. and Patel, D.J. (2009) Nucleation, propagation and cleavage of target RNAs in Ago silencing complexes. *Nature*, **461**, 754-761.
138. Lee, H.Y., Zhou, K., Smith, A.M., Noland, C.L. and Doudna, J.A. (2013) Differential roles of human Dicer-binding proteins TRBP and PACT in small RNA processing. *Nucleic Acids Research*, **41**, 6568-6576.
139. Noland, Cameron L., Ma, E. and Doudna, Jennifer A. siRNA Repositioning for Guide Strand Selection by Human Dicer Complexes. *Molecular Cell*, **43**, 110-121.
140. Noland, C.L. and Doudna, J.A. (2013) Multiple sensors ensure guide strand selection in human RNAi pathways. *Rna*, **19**, 639-648.
141. Wang, H.-W., Noland, C., Siridechadilok, B., Taylor, D.W., Ma, E., Felderer, K., Doudna, J.A. and Nogales, E. (2009) Structural insights into RNA processing by the human RISC-loading complex. *Nat Struct Mol Biol*, **16**, 1148-1153.
142. Lee, H.Y., Zhou, K., Smith, A.M., Noland, C.L. and Doudna, J.A. (2013) Differential roles of human Dicer-binding proteins TRBP and PACT in small RNA processing. *Nucleic Acids Res*, **41**, 6568-6576.
143. Khvorova, A., Reynolds, A. and Jayasena, S.D. (2003) Functional siRNAs and miRNAs exhibit strand bias. *Cell*, **115**, 209-216.
144. Schwarz, D.S., Hutvagner, G., Du, T., Xu, Z., Aronin, N. and Zamore, P.D. (2003) Asymmetry in the assembly of the RNAi enzyme complex. *Cell*, **115**, 199-208.
145. Manoharan, M. (2002) Oligonucleotide conjugates as potential antisense drugs with improved uptake, biodistribution, targeted delivery, and mechanism of action. *Antisense & nucleic acid drug development*, **12**, 103-128.
146. Lonnberg, H. (2009) Solid-phase synthesis of oligonucleotide conjugates useful for delivery and targeting of potential nucleic acid therapeutics. *Bioconjug Chem*, **20**, 1065-1094.
147. Juliano, R.L., Ming, X. and Nakagawa, O. (2012) The chemistry and biology of oligonucleotide conjugates. *Acc Chem Res*, **45**, 1067-1076.
148. Yu, B., Zhao, X., Lee, L.J. and Lee, R. (2009) Targeted Delivery Systems for Oligonucleotide Therapeutics. *AAPS J*, **11**, 195-203.
149. Rettig, G.R. and Behlke, M.A. (2012) Progress toward in vivo use of siRNAs-II. *Molecular therapy : the journal of the American Society of Gene Therapy*, **20**, 483-512.

150. Yuan, X., Naguib, S. and Wu, Z. (2011) Recent advances of siRNA delivery by nanoparticles. *Expert opinion on drug delivery*, **8**, 521-536.
151. Jackson, A.L., Burchard, J., Leake, D., Reynolds, A., Schelter, J., Guo, J., Johnson, J.M., Lim, L., Karpilow, J., Nichols, K. *et al.* (2006) Position-specific chemical modification of siRNAs reduces “off-target” transcript silencing. *RNA*, **12**, 1197-1205.
152. Whitehead, K.A., Dahlman, J.E., Langer, R.S. and Anderson, D.G. (2011) Silencing or stimulation? siRNA delivery and the immune system. *Annual review of chemical and biomolecular engineering*, **2**, 77-96.
153. Turner, J.J., Jones, S.W., Moschos, S.A., Lindsay, M.A. and Gait, M.J. (2007) MALDI-TOF mass spectral analysis of siRNA degradation in serum confirms an RNase A-like activity. *Molecular bioSystems*, **3**, 43-50.
154. Gaynor, J.W., Campbell, B.J. and Cosstick, R. (2010) RNA interference: a chemist's perspective. *Chem Soc Rev*, **39**, 4169-4184.
155. Deleavey, Glen F. and Damha, Masad J. Designing Chemically Modified Oligonucleotides for Targeted Gene Silencing. *Chemistry & Biology*, **19**, 937-954.
156. Nielsen, P.E. (2010) Peptide Nucleic Acids (PNA) in Chemical Biology and Drug Discovery. *Chemistry & Biodiversity*, **7**, 786-804.
157. Eckstein, F. (2014) Phosphorothioates, Essential Components of Therapeutic Oligonucleotides. *Nucleic Acid Ther.*
158. Herdewijn, P. (2000) Heterocyclic Modifications of Oligonucleotides and Antisense Technology. *Antisense and Nucleic Acid Drug Development*, **10**, 297-310.
159. Peacock, H., Kannan, A., Beal, P.A. and Burrows, C.J. (2011) Chemical Modification of siRNA Bases To Probe and Enhance RNA Interference. *The Journal of Organic Chemistry*, **76**, 7295-7300.
160. Wojciechowski, F. and Hudson, R.H. (2007) Nucleobase modifications in peptide nucleic acids. *Current topics in medicinal chemistry*, **7**, 667-679.
161. Ostergaard, M.E., Dwight, T., Berdeja, A., Swayze, E.E., Jung, M.E. and Seth, P.P. (2014) Comparison of duplex stabilizing properties of 2'-fluorinated nucleic acid analogues with furanose and non-furanose sugar rings. *J Org Chem*, **79**, 8877-8881.
162. Prakash, T.P. (2011) An overview of sugar-modified oligonucleotides for antisense therapeutics. *Chem Biodivers*, **8**, 1616-1641.
163. Mangos, M.M. and Damha, M.J. (2002) Flexible and frozen sugar-modified nucleic acids - modulation of biological activity through furanose ring dynamics in the antisense strand. *Current topics in medicinal chemistry*, **2**, 1147-1171.
164. Sheehan, D., Lunstad, B., Yamada, C.M., Stell, B.G., Caruthers, M.H. and Dellinger, D.J. (2003) Biochemical properties of phosphonoacetate and thiophosphonoacetate oligodeoxyribonucleotides. *Nucleic Acids Res*, **31**, 4109-4118.
165. Damha, M.J., Wilds, C.J., Noronha, A., Brukner, I., Borkow, G., Arion, D. and Parniak, M.A. (1998) Hybrids of RNA and Arabinonucleic Acids (ANA and 2'-F-ANA) Are Substrates of Ribonuclease H. *Journal of the American Chemical Society*, **120**, 12976-12977.
166. Wilds, C.J. and Damha, M.J. (2000) 2'-Deoxy-2'-fluoro- β -d-arabinonucleosides and oligonucleotides (2'-F-ANA): synthesis and physicochemical studies. *Nucleic Acids Research*, **28**, 3625-3635.

167. Noronha, A.M., Wilds, C.J., Lok, C.-N., Viazovkina, K., Arion, D., Parniak, M.A. and Damha, M.J. (2000) Synthesis and Biophysical Properties of Arabinonucleic Acids (ANA): Circular Dichroic Spectra, Melting Temperatures, and Ribonuclease H Susceptibility of ANA-RNA Hybrid Duplexes. *Biochemistry*, **39**, 7050-7062.
168. Mangos, M.M., Min, K.-L., Viazovkina, E., Galarneau, A., Elzagheid, M.I., Parniak, M.A. and Damha, M.J. (2002) Efficient RNase H-Directed Cleavage of RNA Promoted by Antisense DNA or 2'-F-ANA Constructs Containing Acyclic Nucleotide Inserts. *Journal of the American Chemical Society*, **125**, 654-661.
169. Oda, Y., Iwa, S., Ohtsuka, E., Ishikawa, M., Ikehara, M. and Nakamura, H. (1993) Binding of nucleic acids to E.coli RNase HI observed by NMR and CD spectroscopy. *Nucleic Acids Research*, **21**, 4690-4695.
170. Nakamura, H., Oda, Y., Iwai, S., Inoue, H., Ohtsuka, E., Kanaya, S., Kimura, S., Katsuda, C., Katayanagi, K. and Morikawa, K. (1991) How does RNase H recognize a DNA.RNA hybrid? *Proceedings of the National Academy of Sciences*, **88**, 11535-11539.
171. Noy, A., Pérez, A., Márquez, M., Luque, F.J. and Orozco, M. (2005) Structure, Recognition Properties, and Flexibility of the DNA-RNA Hybrid. *Journal of the American Chemical Society*, **127**, 4910-4920.
172. Noy, A., Luque, F.J. and Orozco, M. (2008) Theoretical Analysis of Antisense Duplexes: Determinants of the RNase H Susceptibility. *Journal of the American Chemical Society*, **130**, 3486-3496.
173. Lima, W.F. and Crooke, S.T. (1997) Binding Affinity and Specificity of Escherichia coli RNase H1: Impact on the Kinetics of Catalysis of Antisense Oligonucleotide-RNA Hybrids. *Biochemistry*, **36**, 390-398.
174. Geary, R.S., Yu, R.Z. and Levin, A.A. (2001) Pharmacokinetics of phosphorothioate antisense oligodeoxynucleotides. *Current opinion in investigational drugs (London, England : 2000)*, **2**, 562-573.
175. Watanabe, T.A., Geary, R.S. and Levin, A.A. (2006) Plasma protein binding of an antisense oligonucleotide targeting human ICAM-1 (ISIS 2302). *Oligonucleotides*, **16**, 169-180.
176. Manoharan, M. (1999) 2'-carbohydrate modifications in antisense oligonucleotide therapy: importance of conformation, configuration and conjugation. *Biochimica et biophysica acta*, **1489**, 117-130.
177. Kalota, A., Karabon, L., Swider, C.R., Viazovkina, E., Elzagheid, M., Damha, M.J. and Gewirtz, A.M. (2006) 2'-Deoxy-2'-fluoro- β -d-arabinonucleic acid (2'-F-ANA) modified oligonucleotides (ON) effect highly efficient, and persistent, gene silencing. *Nucleic Acids Research*, **34**, 451-461.
178. Watts, J.K. and Damha, M.J. (2008) 2'-F-Arabinonucleic acids (2'-F-ANA) — History, properties, and new frontiers. *Canadian Journal of Chemistry*, **86**, 641-656.
179. Denisov, A.Y., Noronha, A.M., Wilds, C.J., Trempe, J.-F., Pon, R.T., Gehring, K. and Damha, M.J. (2001) Solution structure of an arabinonucleic acid (ANA)/RNA duplex in a chimeric hairpin: comparison with 2'-fluoro-ANA/RNA and DNA/RNA hybrids. *Nucleic Acids Research*, **29**, 4284-4293.
180. Chiu, Y.L. and Rana, T.M. (2003) siRNA function in RNAi: a chemical modification analysis. *Rna*, **9**, 1034-1048.

181. Muhonen, P., Holthofer, H. *RNA Interference: From Biology to Clinical Applications* (eds. Min, W.-P. & Ichim, T.). *Methods in Molecular Biology*, Volume 623, 93–107 (Humana Press).
182. Prakash, T.P., Allerson, C.R., Dande, P., Vickers, T.A., Sioufi, N., Jarres, R., Baker, B.F., Swayze, E.E., Griffey, R.H. and Bhat, B. (2005) Positional effect of chemical modifications on short interference RNA activity in mammalian cells. *J Med Chem*, **48**, 4247-4253.
183. Manoharan, M., Akinc, A., Pandey, R.K., Qin, J., Hadwiger, P., John, M., Mills, K., Charisse, K., Maier, M.A., Nechev, L. *et al.* (2011) Unique Gene-Silencing and Structural Properties of 2'-Fluoro-Modified siRNAs. *Angewandte Chemie International Edition*, **50**, 2284-2288.
184. Ikeda, H., Fernandez, R., Wilk, A., Barchi, J.J., Jr., Huang, X. and Marquez, V.E. (1998) The effect of two antipodal fluorine-induced sugar puckers on the conformation and stability of the Dickerson-Drew dodecamer duplex [d(CGCGAATTCGCG)]₂. *Nucleic Acids Res*, **26**, 2237-2244.
185. Deleavey, G.F., Watts, J.K., Alain, T., Robert, F., Kalota, A., Aishwarya, V., Pelletier, J., Gewirtz, A.M., Sonenberg, N. and Damha, M.J. (2010) Synergistic effects between analogs of DNA and RNA improve the potency of siRNA-mediated gene silencing. *Nucleic Acids Research*, **38**, 4547-4557.
186. Pallan, P.S., Greene, E.M., Jicman, P.A., Pandey, R.K., Manoharan, M., Rozners, E. and Egli, M. (2011) Unexpected origins of the enhanced pairing affinity of 2'-fluoro-modified RNA. *Nucleic Acids Research*, **39**, 3482-3495.
187. Patra, A., Paolillo, M., Charisse, K., Manoharan, M., Rozners, E. and Egli, M. (2012) 2'-Fluoro RNA Shows Increased Watson–Crick H-Bonding Strength and Stacking Relative to RNA: Evidence from NMR and Thermodynamic Data. *Angewandte Chemie International Edition*, **51**, 11863-11866.
188. Ma, J.B., Yuan, Y.R., Meister, G., Pei, Y., Tuschl, T. and Patel, D.J. (2005) Structural basis for 5'-end-specific recognition of guide RNA by the *A. fulgidus* Piwi protein. *Nature*, **434**, 666-670.
189. Rao, D.D., Vorhies, J.S., Senzer, N. and Nemunaitis, J. (2009) siRNA vs. shRNA: similarities and differences. *Advanced drug delivery reviews*, **61**, 746-759.
190. Kim, D.H., Behlke, M.A., Rose, S.D., Chang, M.S., Choi, S. and Rossi, J.J. (2005) Synthetic dsRNA Dicer substrates enhance RNAi potency and efficacy. *Nature biotechnology*, **23**, 222-226.
191. Amarzguioui, M., Lundberg, P., Cantin, E., Hagstrom, J., Behlke, M.A. and Rossi, J.J. (2006) Rational design and in vitro and in vivo delivery of Dicer substrate siRNA. *Nature protocols*, **1**, 508-517.
192. Amarzguioui, M. and Rossi, J.J. (2008) Principles of Dicer substrate (D-siRNA) design and function. *Methods in molecular biology (Clifton, N.J.)*, **442**, 3-10.
193. Abe, N., Abe, H., Nagai, C., Harada, M., Hatakeyama, H., Harashima, H., Ohshiro, T., Nishihara, M., Furukawa, K., Maeda, M. *et al.* (2011) Synthesis, structure, and biological activity of dumbbell-shaped nanocircular RNAs for RNA interference. *Bioconjug Chem*, **22**, 2082-2092.
194. Yu, D., Pendergraft, H., Liu, J., Kordasiewicz, H.B., Cleveland, Don W., Swayze, Eric E., Lima, Walt F., Crooke, Stanley T., Prakash, Thazha P. and Corey, David R. (2012) Single-

- Stranded RNAs Use RNAi to Potently and Allele-Selectively Inhibit Mutant Huntingtin Expression. *Cell*, **150**, 895-908.
195. Martinez, J., Patkaniowska, A., Urlaub, H., Luhrmann, R. and Tuschl, T. (2002) Single-stranded antisense siRNAs guide target RNA cleavage in RNAi. *Cell*, **110**, 563-574.
 196. Haringsma, H.J., Li, J.J., Soriano, F., Kenski, D.M., Flanagan, W.M. and Willingham, A.T. (2012) mRNA knockdown by single strand RNA is improved by chemical modifications. *Nucleic Acids Res*, **40**, 4125-4136.
 197. Puglisi, J.D. and Tinoco, I., Jr. (1989) Absorbance melting curves of RNA. *Methods in enzymology*, **180**, 304-325.
 198. Mergny, J.L. and Lacroix, L. (2003) Analysis of thermal melting curves. *Oligonucleotides*, **13**, 515-537.
 199. Mergny, J.L., Phan, A.T. and Lacroix, L. (1998) Following G-quartet formation by UV-spectroscopy. *FEBS Lett*, **435**, 74-78.
 200. Tinoco, I. (1960) Hypochromism in Polynucleotides1. *Journal of the American Chemical Society*, **82**, 4785-4790.
 201. Mergny, J.L. and Maurizot, J.C. (2001) Fluorescence resonance energy transfer as a probe for G-quartet formation by a telomeric repeat. *Chembiochem*, **2**, 124-132.
 202. Cahen, P., Luhmer, M., Fontaine, C., Morat, C., Reisse, J. and Bartik, K. (2000) Study by ²³Na-NMR, ¹H-NMR, and ultraviolet spectroscopy of the thermal stability of an 11-basepair oligonucleotide. *Biophysical Journal*, **78**, 1059-1069.
 203. Gray, D.M., Hung, S.H. and Johnson, K.H. (1995) Absorption and circular dichroism spectroscopy of nucleic acid duplexes and triplexes. *Methods in enzymology*, **246**, 19-34.
 204. Duguid, J.G., Bloomfield, V.A., Benevides, J.M. and Thomas, G.J., Jr. (1996) DNA melting investigated by differential scanning calorimetry and Raman spectroscopy. *Biophys J*, **71**, 3350-3360.
 205. Movileanu, L., Benevides, J.M. and Thomas, G.J. (2002) Determination of base and backbone contributions to the thermodynamics of premelting and melting transitions in B DNA. *Nucleic Acids Research*, **30**, 3767-3777.
 206. Mergny, J.-L., Lacroix, L., Han, X., Leroy, J.-L. and Helene, C. (1995) Intramolecular Folding of Pyrimidine Oligodeoxynucleotides into an i-DNA Motif. *Journal of the American Chemical Society*, **117**, 8887-8898.
 207. Mergny, J.L. and Lacroix, L. (1998) Kinetics and thermodynamics of i-DNA formation: phosphodiester versus modified oligodeoxynucleotides. *Nucleic Acids Res*, **26**, 4797-4803.
 208. Lane, A.N., Chaires, J.B., Gray, R.D. and Trent, J.O. (2008) Stability and kinetics of G-quadruplex structures. *Nucleic Acids Res*, **36**, 5482-5515.
 209. Marky, L.A. and Breslauer, K.J. (1987) Calculating thermodynamic data for transitions of any molecularity from equilibrium melting curves. *Biopolymers*, **26**, 1601-1620.
 210. Chiu, W.L.A.K., Sze, C.N., Ip, L.N., Chan, S.K. and Au-Yeung, S.C.F. (2001) NTDB: Thermodynamic Database for Nucleic Acids. *Nucleic Acids Research*, **29**, 230-233.
 211. Freier, S.M., Kierzek, R., Jaeger, J.A., Sugimoto, N., Caruthers, M.H., Neilson, T. and Turner, D.H. (1986) Improved free-energy parameters for predictions of RNA duplex stability. *Proceedings of the National Academy of Sciences of the United States of America*, **83**, 9373-9377.

212. Breslauer, K.J., Frank, R., Blöcker, H. and Marky, L.A. (1986) Predicting DNA duplex stability from the base sequence. *Proceedings of the National Academy of Sciences*, **83**, 3746-3750.
213. Jaeger, J.A., Turner, D.H. and Zuker, M. (1989) Improved predictions of secondary structures for RNA. *Proceedings of the National Academy of Sciences of the United States of America*, **86**, 7706-7710.
214. Mathews, D.H., Burkard, M.E., Freier, S.M., Wyatt, J.R. and Turner, D.H. (1999) Predicting oligonucleotide affinity to nucleic acid targets. *Rna*, **5**, 1458-1469.
215. Borer, P.N., Dengler, B., Tinoco, I., Jr. and Uhlenbeck, O.C. (1974) Stability of ribonucleic acid double-stranded helices. *J Mol Biol*, **86**, 843-853.
216. Fodor, S.P.A., Rava, R.P., Huang, X.C., Pease, A.C., Holmes, C.P. and Adams, C.L. (1993) Multiplexed biochemical assays with biological chips. *Nature*, **364**, 555-556.
217. Saiki, R.K., Gelfand, D.H., Stoffel, S., Scharf, S.J., Higuchi, R., Horn, G.T., Mullis, K.B. and Erlich, H.A. (1988) Primer-directed enzymatic amplification of DNA with a thermostable DNA polymerase. *Science (New York, N.Y.)*, **239**, 487-491.
218. Freier, S.M. (1993) in *Antisense Research and Applications* (Crooke, S. T., & Lebleu, B., Eds.) pp 67-82, CRC Press, Boca Raton, FL.
219. Crabbe, P. (1965) *Optical Rotatory Dispersion and Circular Dichroism in Organic Chemistry*. Holden-Day, San Francisco, Calif.
220. Woody, R.W. (1995) Circular dichroism. *Methods in enzymology*, **246**, 34-71.
221. Johnson, W.C.J. (2000) In *Circular Dichroism: Principles and Applications*. pp. 703-718. Wiley-VCH, New York.
222. Tinoco, I. and Cantor, C.R. (2006), *Methods of Biochemical Analysis*. John Wiley & Sons, Inc., pp. 81-203.
223. Johnson, W.C. (2006), *Methods of Biochemical Analysis*. John Wiley & Sons, Inc., pp. 61-163.
224. Gray, D.M., Ratliff, R.L. and Vaughan, M.R. (1992) Circular dichroism spectroscopy of DNA. *Methods in enzymology*, **211**, 389-406.
225. Vorlickova, M., Kejnovska, I., Bednarova, K., Renciuik, D. and Kypr, J. (2012) Circular dichroism spectroscopy of DNA: from duplexes to quadruplexes. *Chirality*, **24**, 691-698.
226. Kypr, J., Kejnovská, I., Renčiuik, D. and Vorlíčková, M. (2009) Circular dichroism and conformational polymorphism of DNA. *Nucleic Acids Research*, **37**, 1713-1725.
227. Gray, D.M., Wen, J.-D., Gray, C.W., Repges, R., Repges, C., Raabe, G. and Fleischhauer, J. (2008) Measured and calculated CD spectra of G-quartets stacked with the same or opposite polarities. *Chirality*, **20**, 431-440.
228. Bishop, G.R. and Chaires, J.B. (2001), *Current Protocols in Nucleic Acid Chemistry*. John Wiley & Sons, Inc.
229. Ratmeyer, L., Vinayak, R., Zhong, Y.Y., Zon, G. and Wilson, W.D. (1994) Sequence Specific Thermodynamic and Structural Properties for DNA.cntdot.RNA Duplexes. *Biochemistry*, **33**, 5298-5304.
230. Hung, S.-H., Yu, Q., Gray, D.M. and Ratliff, R.L. (1994) Evidence from CD spectra that d(purine)-r(pyrimidine) and r(purine)-d(pyrimidine) hybrids are in different structural classes. *Nucleic Acids Research*, **22**, 4326-4334.

231. Paramasivan, S., Rujan, I. and Bolton, P.H. (2007) Circular dichroism of quadruplex DNAs: applications to structure, cation effects and ligand binding. *Methods*, **43**, 324-331.
232. Vorlickova, M., Bednarova, K. and Kypr, J. (2006) Ethanol is a better inducer of DNA guanine tetraplexes than potassium cations. *Biopolymers*, **82**, 253-260.
233. Vorlíčková, M., Chládková, J., Kejnovská, I., Fialová, M. and Kypr, J. (2005) Guanine tetraplex topology of human telomere DNA is governed by the number of (TTAGGG) repeats. *Nucleic Acids Research*, **33**, 5851-5860.
234. Clore, G.M. and Gronenborn, A.M. (1989) Determination of Three-Dimensional Structures of Proteins and Nucleic Acids in Solution by Nuclear Magnetic Resonance Spectroscopy. *Critical reviews in biochemistry and molecular biology*, **24**, 479-564.
235. Wuthrich, K. (1986) *NMR of Proteins and Nucleic Acids*. Wiley, New York.
236. James, T.L. (2001), *Current Protocols in Nucleic Acid Chemistry*. John Wiley & Sons, Inc.
237. Feigon, J., Skelenář, V., Wang, E., Gilbert, D.E., Macaya, R.F. and Schultze, P. (1992) In David M.J. Lilley, J. E. D. (ed.), *Methods in enzymology*. Academic Press, Vol. Volume 211, pp. 235-253.
238. Feigon, J., Koshlap, K.M. and Smith, F.W. (1995) ¹H NMR spectroscopy of DNA triplexes and quadruplexes. *Methods in enzymology*, **261**, 225-255.
239. Radhakrishnan, I., de los Santos, C. and Patel, D.J. (1991) Nuclear magnetic resonance structural studies of intramolecular purine · purine · pyrimidine DNA triplexes in solution: Base triple pairing alignments and strand direction. *Journal of Molecular Biology*, **221**, 1403-1418.
240. Martín-Pintado, N., Yahyaee-Anzahaee, M., Deleavey, G.F., Portella, G., Orozco, M., Damha, M.J. and González, C. (2013) Dramatic Effect of Furanose C2' Substitution on Structure and Stability: Directing the Folding of the Human Telomeric Quadruplex with a Single Fluorine Atom. *Journal of the American Chemical Society*, **135**, 5344-5347.
241. Dai, J., Ambrus, A., Hurley, L.H. and Yang, D. (2009) A Direct and Nondestructive Approach To Determine the Folding Structure of the I-Motif DNA Secondary Structure by NMR. *Journal of the American Chemical Society*, **131**, 6102-6104.
242. Jardetzky, C.D. (1960) Proton Magnetic Resonance Studies on Purines, Pyrimidines, Ribose Nucleosides and Nucleotides. III. Ribose Conformation1. *Journal of the American Chemical Society*, **82**, 229-233.
243. Jardetzky, C.D. (1962) Proton magnetic resonance of nucleotides. IV. Ribose conformation. *Journal of the American Chemical Society*, **84**, 62-66.
244. Keeler, J. (2011) *Understanding NMR Spectroscopy, 2nd Edition*. Wiley, NYC.
245. Matthias Findeisen, S.B. (2013) *50 and More Essential NMR Experiments: A Detailed Guide*. Wiley, NYC.
246. Altona, C. and Sundaralingam, M. (1973) Conformational analysis of the sugar ring in nucleosides and nucleotides. Improved method for the interpretation of proton magnetic resonance coupling constants. *Journal of the American Chemical Society*, **95**, 2333-2344.
247. Damha, M.J. and Ogilvie, K.K. (1988) Conformational properties of branched RNA fragments in aqueous solution. *Biochemistry*, **27**, 6403-6416.
248. Evans, F.E. and Sarma, R.H. (1976) Nucleotide rigidity. *Nature*, **263**, 567-572.

249. Lee, C.-H., Ezra, F.S., Kondo, N.S., Sarma, R.H. and Danyluk, S.S. (1976) Conformational properties of dinucleoside monophosphates in solution: dipurines and dipyrimidines. *Biochemistry*, **15**, 3627-3639.
250. Cheng, D.M. and Sarma, R.H. (1977) Intimate details of the conformational characteristics of deoxyribodinucleoside monophosphates in aqueous solution. *Journal of the American Chemical Society*, **99**, 7333-7348.
251. Hare, D.R., Wemmer, D.E., Chou, S.H., Drobny, G. and Reid, B.R. (1983) Assignment of the non-exchangeable proton resonances of d(C-G-C-G-A-A-T-T-C-G-C-G) using two-dimensional nuclear magnetic resonance methods. *J Mol Biol*, **171**, 319-336.
252. Haasnoot, C.A., Westerink, H.P., van der Marel, G.A. and van Boom, J.H. (1984) Discrimination between A-type and B-type conformations of double helical nucleic acid fragments in solution by means of two-dimensional nuclear Overhauser experiments. *Journal of biomolecular structure & dynamics*, **2**, 345-360.
253. Nilsson, L., Clore, G.M., Gronenborn, A.M., Brünger, A.T. and Karplus, M. (1986) Structure refinement of oligonucleotides by molecular dynamics with nuclear Overhauser effect interproton distance restraints: application to 5' d(C-G-T-A-C-G)₂. *J Mol Biol*, **188**, 455-475.
254. Kearns, D.R., Patel, D.J. and Shulman, R.G. (1971) High Resolution Nuclear Magnetic Resonance Studies of Hydrogen Bonded Protons of tRNA in Water. *Nature*, **229**, 338-339.
255. Kessler, H., Gehrke, M. and Griesinger, C. (1988) Two-Dimensional NMR Spectroscopy: Background and Overview of the Experiments [New Analytical Methods (36)]. *Angewandte Chemie International Edition in English*, **27**, 490-536.
256. Hosur, R.V., Govil, G. and Miles, H.T. (1988) Application of two-dimensional NMR spectroscopy in the determination of solution conformation of nucleic acids. *Magnetic Resonance in Chemistry*, **26**, 927-944.
257. Clore, G.M. and Gronenborn, A.M. (1991) Two-, three-, and four-dimensional NMR methods for obtaining larger and more precise three-dimensional structures of proteins in solution. *Annual review of biophysics and biophysical chemistry*, **20**, 29-63.
258. Patel, D.J., Shapiro, L. and Hare, D. (1987) DNA and RNA: NMR studies of conformations and dynamics in solution. *Quarterly Reviews of Biophysics*, **20**, 35-112.
259. Neuhaus, D., Williamson, M. (2000) *The Nuclear Overhauser Effect in Structural and Conformational Analysis, 2nd Edition*. WILEY VCH.
260. Macomber, R. (1998) *A Complete Introduction to Modern NMR Spectroscopy*. Wiley, NYC.
261. Reid, B.R. (1987) Sequence-specific assignments and their use in NMR studies of DNA structure. *Q Rev Biophys*, **20**, 1-34.
262. Gorenstein, D.G. (1992) In David M.J. Lilley, J. E. D. (ed.), *Methods in enzymology*. Academic Press, Vol. Volume 211, pp. 254-286.
263. van de Ven, F.J. and Hilbers, C.W. (1988) Resonance assignments of non-exchangeable protons in B type DNA oligomers, an overview. *Nucleic Acids Research*, **16**, 5713-5726.
264. Cheng, D.M. (1987) *The studies of ³¹P NMR of nucleic acids and nucleic acid complexes, in Phosphorus NMR in Biology (Tyler, B. C., ed.), CRC Press, Boca Raton, pp. 135-151.*

265. Patel, D.J. (1976) Proton and phosphorus nmr studies of d-CpG(pCpG)_n duplexes in solution. Helix-coil transition and complex formation with actinomycin-D. *Biopolymers*, **15**, 533-558.
266. Rinaldi, P.L. (1983) Heteronuclear 2D-NOE spectroscopy. *Journal of the American Chemical Society*, **105**, 5167-5168.
267. Yu, C. and Levy, G.C. (1984) Two-dimensional heteronuclear NOE (HOESY) experiments: investigation of dipolar interactions between heteronuclei and nearby protons. *Journal of the American Chemical Society*, **106**, 6533-6537.
268. Karplus, M. (1963) Vicinal Proton Coupling in Nuclear Magnetic Resonance. *Journal of the American Chemical Society*, **85**, 2870-2871.
269. Minch, M.J. (1994) Orientational dependence of vicinal proton-proton NMR coupling constants: The Karplus relationship. *Concepts in Magnetic Resonance*, **6**, 41-56.
270. Karplus, M. (1959) Contact Electron-Spin Coupling of Nuclear Magnetic Moments. *The Journal of Chemical Physics*, **30**, 11-15.
271. Schmitz, U. and James, T.L. (1995) In Thomas, L. J. (ed.), *Methods in enzymology*. Academic Press, Vol. Volume 261, pp. 3-44.
272. Ulyanov, N.B. and James, T.L. (1995) In Thomas, L. J. (ed.), *Methods in enzymology*. Academic Press, Vol. Volume 261, pp. 90-120.

CHAPTER 2: ENERGETICALLY IMPORTANT C-H...2'F-C PSEUDOHYDROGEN BONDING IN WATER: ORIGIN OF DIFFERENTIAL STABILITY OF 2'F-ANA:RNA AND ANA:RNA HYBRID DUPLEXES

2.1 Differential Stability of 2'F-ANA:RNA and ANA:RNA Hybrid Duplexes

Our research group has had a longstanding interest in designing and defining the structural properties of synthetic nucleic acids for effective and selective gene regulation. The Damha lab has primarily concentrated its efforts in the development of oligonucleotides comprising arabino (ANA) (1-7) and 2'-deoxy-2'-fluoroarabinonucleotides (2'F-ANA; Figure 2.1) (8-14). Where ANA contains a hydroxyl group, 2'F-ANA contains fluorine at the C2' position (Figure 2.1).

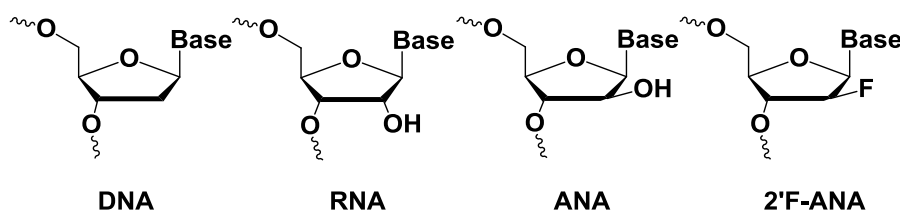


Figure 2.1 Chemical structures of ANA and 2'F-ANA in comparison with DNA and RNA.

Both 2'F-ANA and ANA have the rare ability to trigger the cleavage of their target mRNA by activating endogenous RNase H (1,9,15). This was an exciting finding since other changes at C2' of ribose (*e.g.* 2'-OMe-RNA, 2'F-RNA, LNA, etc), or alterations in the orientation of the sugar to the base (α vs. β glycosidic bonds), all completely abolish RNase H activation (16-20). Follow up NMR studies provided a rationale for the ability of RNase H to cleave the RNA strand of 2'F-ANA:RNA hybrids: the arabinose sugar (2'-OH or 2'-F) adopts a “DNA-like” South-East pucker and thus doesn't alter the overall helical structure of the AON:RNA hybrid when compared to the

native DNA:RNA substrate (3-5). These findings received significant attention by the antisense field for two reasons: Firstly, ANA and 2'F-ANA represented the very first examples of RNase H-competent oligonucleotides that lacked 2'-deoxy- β -D-ribofuranose. Secondly, these findings provided a very important advancement in understanding the catalytic mechanism and substrate selectivity of RNase H and how the oligonucleotide sugar stereochemistry impact on hybrid conformation. It also underscored the potential for using arabinose oligonucleotides as antisense molecules.

The 2'F-ANA modification displays substantial increases in thermal stability when hybridized with cognate DNA or RNA, with increases in melting temperatures of up to 2°C per modification relative to unmodified DNA of the same base composition (8). By contrast, ANA has relatively low affinity for RNA (2). This is a puzzle since as indicated above, ANA and 2'F-ANA hybrid duplexes with RNA display similar structure and flexibility patterns that make them both effective mimics of the DNA:RNA hybrid. Exploring the origin of this difference in binding affinity has been of significant interest to our research group.

Initial structural studies of ANA:RNA and 2'F-ANA:RNA duplexes, were performed on short hairpins with modified stems, which showed no major conformational differences between them—neither in sugar pucker nor in hydrogen bonding nor in steric effects (3,4). These studies were later followed up by Dr. Jonathan Watts during his PhD studies in the Damha lab, and resulted in the determination of the NMR structure of a fully modified 10-mer 2'F-ANA:RNA hybrid duplex with a sequence shown in Figure 2.2.A (5). Combined with detailed theoretical calculations and biophysical experiments, this study suggested that the surprisingly higher stability of 2'F-ANA:RNA hybrid relative to ANA:RNA hybrid is related to several subtle differences, most importantly to a favorable inter-residual pseudohydrogen bonding between F2'

and purine H8 of the 3'-proximal nucleotide in the 2'-F-ANA strand which contrasts with unfavorable 2'-OH–nucleobase steric interactions in the case of ANA (Figure 2.2.B) (5).

^{19}F – ^1H distance constraints were extracted from a qualitative analysis of HOESY experiments and strong sequential $^{19}\text{F}(\text{T})$ – $\text{H8}(\text{A/G})$ cross peaks (at TA and TG steps), along with three sequential ^{19}F –thymine methyl cross peaks, were observed in the HOESY spectrum which correlate well with short distances between F2' of T and aromatic H6/H8 protons of A and G (Figure 2.2.C) (5). Hence, the favorable 2'-F–H8 interactions in the 2'-F-ANA strand was optimal at 5'-pyrimidine-purine-3' steps, where the base stacking geometry could easily adjust.

This energetically important fluorine-mediated interaction is of particular interest since it constitutes one of the rare examples of hydrogen bonds of so-called “organic fluorine” in aqueous solutions. Occasional examples of such nonconventional interactions are briefly reviewed in the following section together with proposed follow up research that offers to further examine and exploit these interactions.

2.2 Nonconventional Hydrogen Bonding to Organic Fluorine

Organic fluorine does not generally act as a hydrogen bond acceptor (21,22). However, rare examples appear: researchers have observed short H–F distances in crystal structures (15,22–25), favorable interactions in molecular models (26,27), H...F scalar couplings in NMR spectra (4,8,28–30) and vibrational frequency shifts (31,32). Yet particularly in aqueous systems, where better hydrogen bond acceptors are abundant, it is rare to find examples of energetically important hydrogen bonds to fluorine.

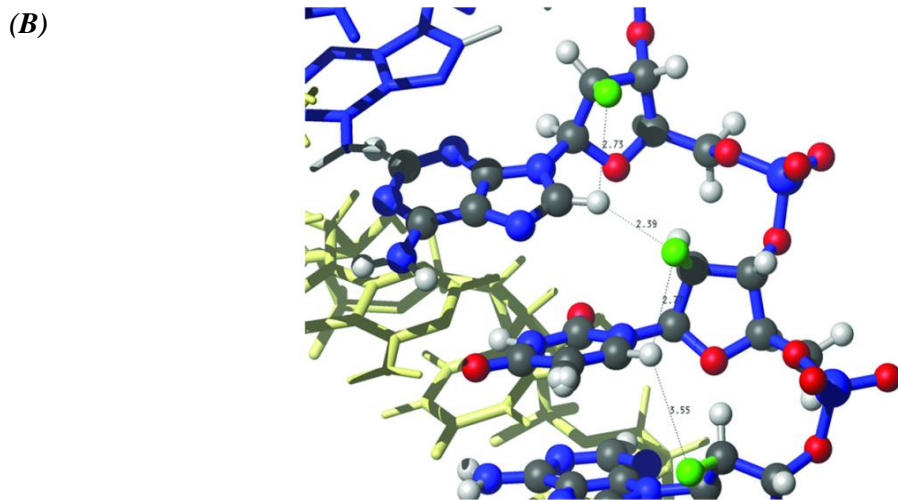
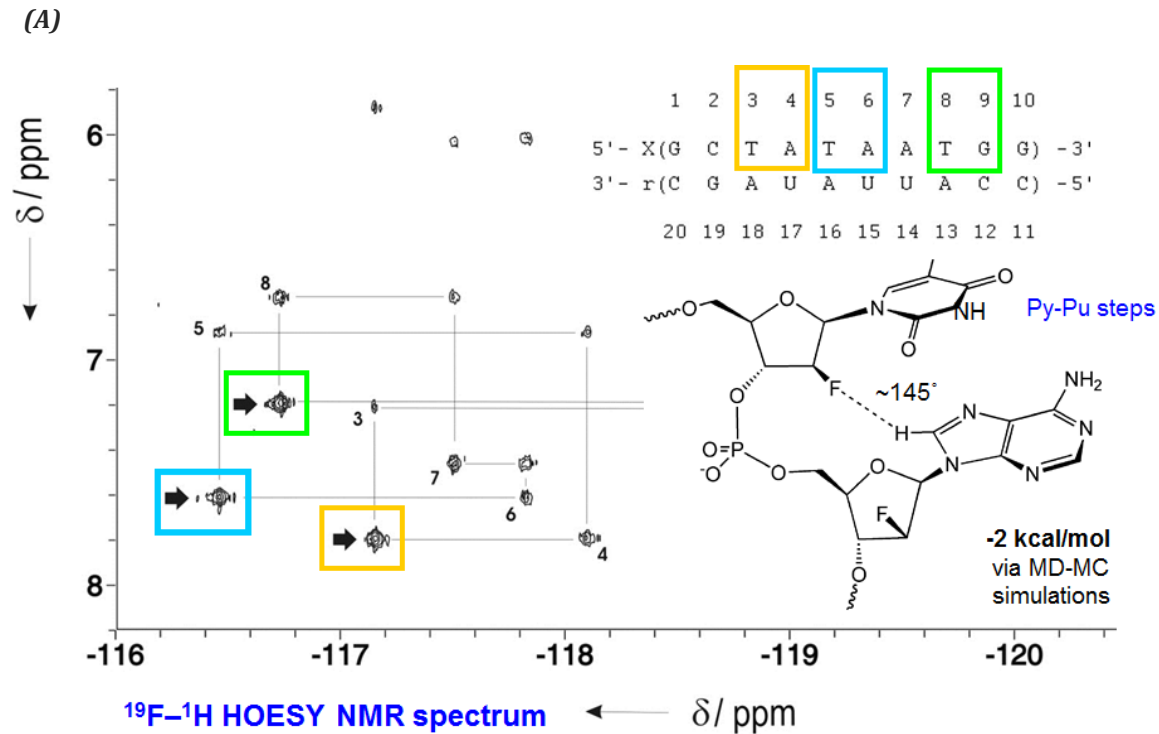


Figure 2.2 Selected results from structural analysis of 10-mer 2F-ANA:RNA hybrid in a previous study by the Damha lab (5). (A) Sequence (with numbering pattern of nucleotides) and Heteronuclear ^{19}F - ^1H HOESY spectrum of 2F-ANA:RNA in D_2O . Sequential assignment pathway between intra-residual and sequential ^{19}F - ^1H 6/ ^1H 8 cross peaks is shown. Strong sequential ^{19}F (T)-H8 (A/G) cross peaks (at TA and TG steps) are indicated with black arrows. (B) F2'-H8 interactions in 2F-ANA:RNA duplex, showing distances between F2' and aromatic H6/H8 protons. These distances correlate well with cross peak intensity of the ^{19}F - ^1H HOESY spectra.

The field of modified oligonucleotides has experienced a good deal of the controversy over whether fluorine-mediated hydrogen bonds are important. The highest profile example is the Kool group's difluorotoluene base (33,34). Developed as a nonhydrogen bonding isostere of thymine (35-37), controversy has raged for over a decade after its synthesis about whether it could in fact accept hydrogen bonds after all. A recent crystal structure showed a short N-H...F-C distance in a difluorotoluene-adenine base pair (25), but the weight of the evidence is that N-H...F-C interactions in difluorotoluene base pairs are of little energetic importance, especially in water where excellent hydrogen bond acceptors are abundant (33). Evidence for R-H...F-C interactions involving other modified nucleobases has come from crystallographic, computational and spectroscopic methods (24,27,32,38-41).

2.3 Sequence-Dependent C-2'F...H8-C Pseudohydrogen Bonding: A Testable Hypothesis

2.3.1 Background

As discussed earlier, our lab has previously argued that the unexpectedly high thermal stability of 2'F-ANA:RNA hybrids is largely due to an inter-residual pseudohydrogen bonding between F2' and purine H8 of the 3'-proximal nucleotide in the 2'F-ANA strand (5). It was hypothesized that this interaction was optimal at 5'-pyrimidine-purine-3' steps, where the base stacking geometry can adjust to afford a stable duplex structure. As discussed later in this chapter, Egli and co-workers have argued that additional polarization of the bases through inductive effects of the electronegative fluorine in 2'F-RNA:RNA duplexes, results in stronger Watson-Crick hydrogen bonding and base-base stacking interactions and hence a higher thermal stability for 2'F-RNA:RNA duplexes (42,43). Thus it is likely that these effects also operate in the stabilization of 2'F-ANA oligonucleotides when hybridized to a complementary RNA strand.

The sequence dependence of the C-2'F...H8-C pseudohydrogen bonds proposed by our group (5), suggested a testable hypothesis: if C-2'F...H8-C interactions at modified 5'-pyrimidine-purine-3' steps are of true energetic importance, then an oligonucleotide with more of these steps should have a greater increase in binding affinity upon modification with 2'F-ANA, as compared with a sequence of identical nucleotide composition and degree of 2'F-ANA modification, but fewer pyrimidine-purine steps. To test this hypothesis, herein we report on design and evaluation of several different 2'F-substituted duplexes with identical base composition but rearranged sequences, to lend further support that the energetically important pseudohydrogen bonding to fluorine –in a nonbase-pairing context– is indeed a major contributor to the high thermal stability of these duplexes.

2.3.2 Design and Evaluation of Thermal Stabilities of 2'F-ANA-Substituted Oligonucleotides Containing C-2'F...H8-C Pseudohydrogen Bonds

Two sequences of identical base composition were designed (Table 2.1). Sequence A contained four 5'-pyrimidine-purine-3' (i.e., TA) steps, while sequence B contained only one 5'-pyrimidine-purine-3' step.

The thermal stability of each sequence in A was compared to its corresponding control in B, which had the same nucleotide composition as A, but a rearranged sequence with fewer pyrimidine-purine steps.

Table 2.1. Sequences and T_m values of duplexes of A and B series

Name	Sequence (5'-3')	T_m^a	ΔT_m^b	ΔT_m /mod	ΔG^c
A1	ctatagtatac	27.5	-	-	-36.8
A2	c Ta Tag Ta Tac	31.0	3.5	0.9	-40.6
A3	ct At Agt At Ac	33.2	5.7	1.4	-43.2
A4	c TATAg TATA c	40.1	12.6	1.6	-50.2
B1	caattgaattc	27.7	-	-	-36.2
B2	caa TT gaa TT c	28.4	0.7	0.2	-37.2
B3	c A Attg A Attc	28.2	0.5	0.1	-37.1
B4	c AATTg AATT c	33.5	5.8	0.7	-43.1

Legend: **2'F-ANA**, dna. ^aIn °C, for a duplex of the strand with complementary RNA. ^bChange in T_m relative to A1 or B1, respectively. ^cIn kJ/mol at 298K, derived from the shape of the UV melting curves.

The unmodified hybrids (A1 and B1; Figure 2.3 and Table 2.1) have similar T_m values. Upon modification of all the dT and dA nucleotides to the corresponding 2'F-ANAs, T_m of sequence A increased by 12.6 °C while T_m of sequence B increased by less than 6 °C (Compare A4 with A1, and B4 with B1; Figure 2.3 and Table 2.1). This observation was in line with our original hypothesis: sequences that contain more 2'F-substituted pyrimidine-purine steps should show a greater increase in binding affinity upon modification with 2'F-ANAs, as compared to controls with identical nucleotide composition and degree of 2'F-ANA modifications but fewer modified pyrimidine-purine steps.

To further explore the nature of this change, we next modified only the dT or dA nucleotides to 2'F-ANAs (A2 and A3 vs. B2 and B3; Table 2.1). Modification of only the thymidines in A2 gave a hybrid with four modified pyrimidine-purine steps possibly forming inter-residual pseudohydrogen bonds, and led to stabilization of A2 as compared to B2 that had only one modified pyrimidine-purine step.

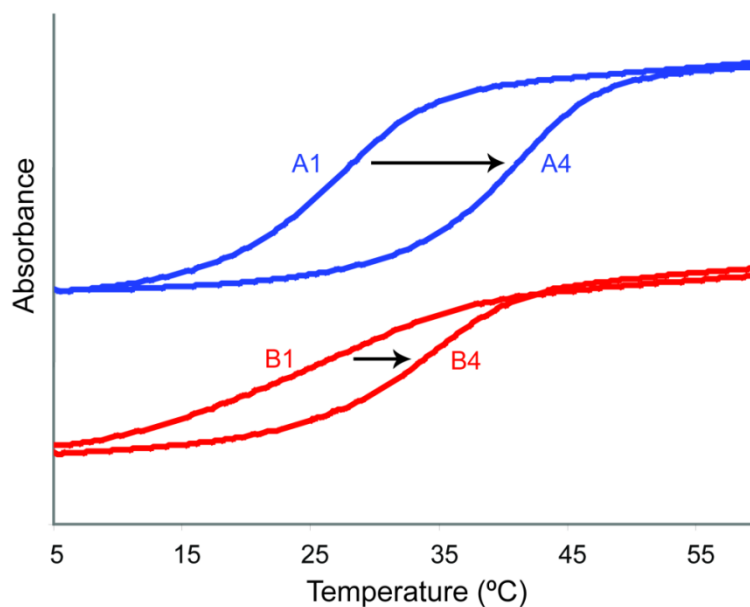


Figure 2.3 Thermal stability comparisons of duplexes of A and B series upon 2'F-ANA modification. Sequence A containing multiple py-pu steps is more heavily stabilized upon 2'F-ANA modification compared to sequence B with the same nucleotide composition but fewer py-pu steps.

Upon modification of only the adenines in hybrid A3, an unexpected substantial stabilization was observed: $\Delta T_m/\text{modification}$ was 1.4 °C, which was only about 15% lower than the 1.6 °C/modification observed for A4. This result was intriguing because in sequence A3, none of the pyrimidines were modified and therefore no inter-residual pseudohydrogen bonding would be present. We questioned whether this stabilization could be related to a C-2'F...H8-C intra-residue pseudohydrogen bonding between the top-face 2'-fluorine of the modified purine and its own nucleobase as shown in Figure 2.4.

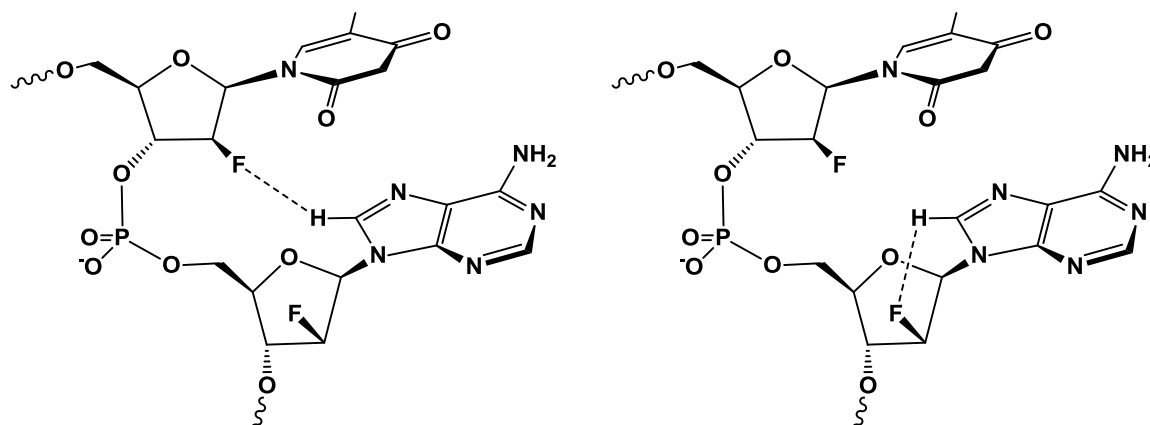


Figure 2.4 Schematic illustration of inter-residual (left) and intra-residual (right) C-2'F...H8-C pseudohydrogen bonds.

There is some evidence in the literature for pseudohydrogen bonding between a top-face 2'-fluorine and its own nucleobase as illustrated in Figure 2.4 (8,26,28,44). For a single 2'-F-ANA nucleoside, evidence for intramolecular C-H...F-C interactions has come from NMR splitting of purine H8 or pyrimidine H6 (4,8,26,28,44). Computational work has identified this interaction as a pseudohydrogen bond (i.e. having partial covalent character)(26).

2.4 Characterization of Intra-Residual C-H...2'F-C Interactions by NMR Experiments

We carried out three types of NMR experiments to further characterize this apparent C-H8...2'F-C pseudohydrogen bond in water.

2.4.1 Evaluation of Deuterium Exchange Rates of H8 of Adenosine in D₂O at 37°C

Upon dissolving purine nucleosides in D₂O, the acidic H8 proton undergoes deuterium exchange (45), and disappears from the NMR spectrum (pseudo-first order kinetics; Scheme 2.1). At neutral pH this exchange takes several days.

Scheme 2.1 Representation of the pseudo first-order kinetics for purine H8 exchange with deuterium in D₂O.

The kinetics of H8-deuterium exchange reaction is a pseudo first-order kinetic as shown in the following steps:



$$R_{\text{ex}} = -d[\text{Adenosine-H}]/dt = k'[\text{D}_2\text{O}][\text{Adenosine-H}]$$

Since D₂O is supplied in great excess, its concentration remains constant and can be absorbed within the rate constant:

$$k'[\text{D}_2\text{O}] = k$$

$$\text{Pseudofirst-order kinetics: } R_{\text{ex}} = -d[\text{Adenosine-H}]/dt = k[\text{Adenosine-H}]$$

The integrated rate law for pseudo first-order kinetic will be:

$$\ln [\text{Adenosine-H}] = -kt + \ln [\text{Adenosine-H}]_0,$$

Peak areas of H8 in the NMR spectra, at each time point, correspond to the concentration of Adenosine-H. Therefore:

$$\ln (\text{H8 peak area}) = -kt + \ln (\text{H8 peak area})_0,$$

A plot of $\ln(\text{H8 peak area})$ vs. time for each nucleoside, gives a straight line with a slope of $-k$, that is the rate constant of H8-deuterium exchange reaction for that nucleoside.

The integrated rate law could also be written in the form of the exponential decay equation as shown below:

$$(\text{H8 peak area}) = (\text{H8 peak area})_0 e^{-kt}$$

We dissolved adenine nucleosides dA, rA, 2'F-araA and 2'F-rA (Figure 2.5.A) in D₂O and monitored the gradual disappearance of the purine H8 peak as a result of exchange with deuterium at pH 7.4 on a 500-MHz-Varian NMR instrument. This process is shown for 2'F-riboadenosine nucleoside in Figure 2.5.B.

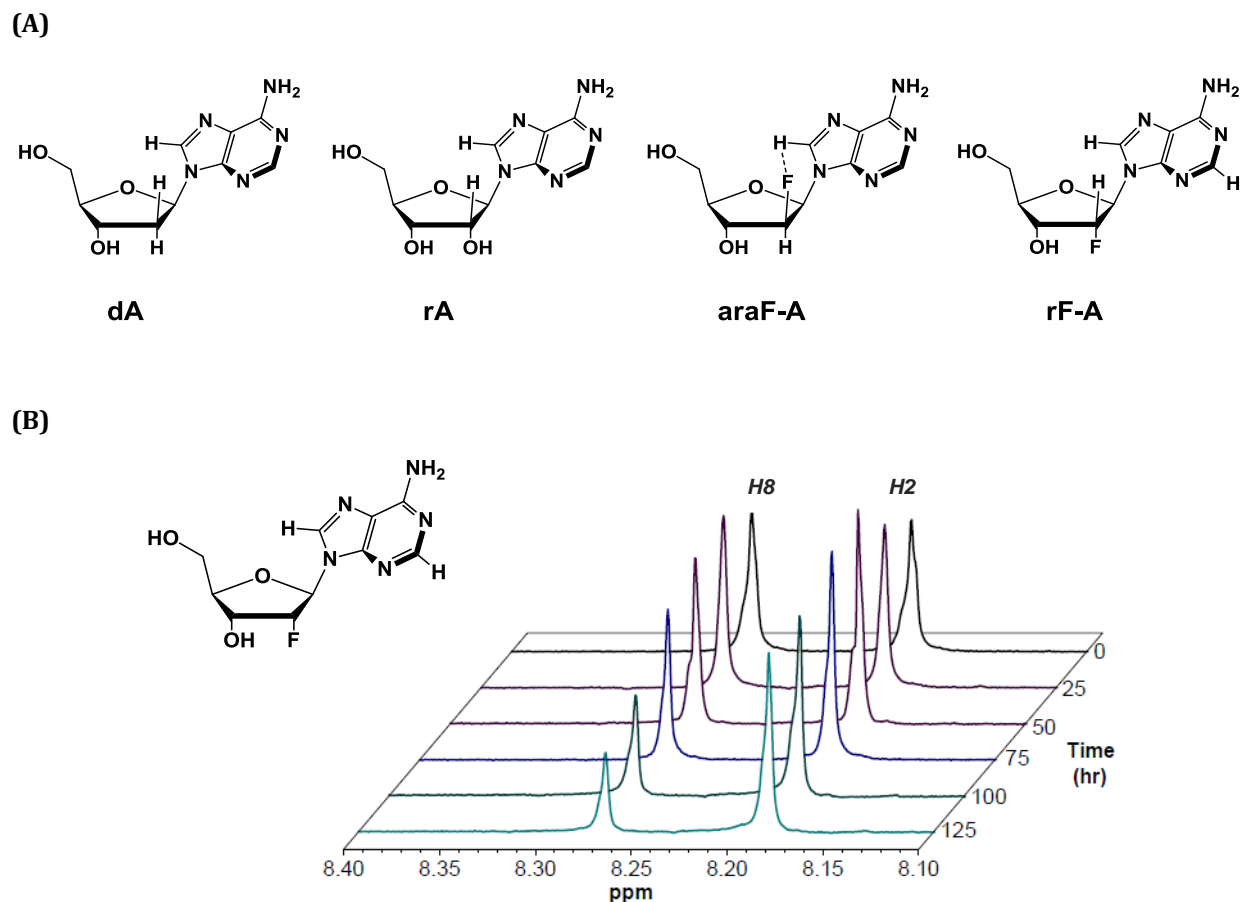


Figure 2.5 Evaluation of H8 exchange with deuterium in D₂O for different adenosine nucleosides at 37°C. **(A)** Structure of nucleosides dissolved in D₂O to monitor the purine's H8 exchange with deuterium. **(B)** Overlay of one-dimensional proton spectra of H2 and H8 protons for 2'F-riboadenosine at pH 7.4, showing the gradual exchange of acidic purine's H8 peak with deuterium.

We next plotted H8 peak areas of each of the four adenine nucleosides vs. time and calculated the rate constants for their exchange reactions (Figure 2.6) (See scheme 2.1 for equations).

The exchange rate for 2'F-araA was markedly lower than that of dA, rA, or 2'F-rA nucleosides ($k_{2'F-rA}/k_{2'F-araA} = 2.9$) (Figure 2.6). It has been reported in the literature that reduced hydrogen exchange rates with the solvent are among the NMR observables that provide indirect evidence for individual hydrogen bonds (46,47). Here, since there is no reason to expect that the 2'F-araA H8 is inherently less acidic than the other three analogues, we concluded that 2'F-araA H8 is likely stabilized from deuterium exchange by its engagement in a hydrogen bonding interaction as depicted in Figure 2.5A.

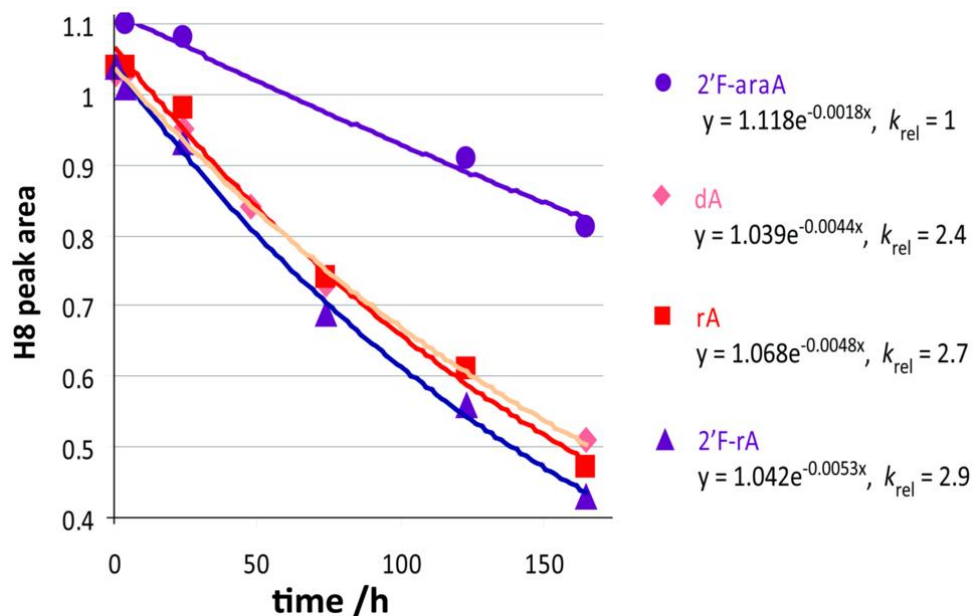


Figure 2.6 Rate constants for exchange reactions at H8 of DNA, RNA, 2'F-ANA and 2'F-RNA adenine nucleosides in D₂O.

2.4.2 Evaluation of Thermal Stability of C-H8...2'F-C Interaction in D₂O or DMSO at Various Temperatures

In the next set of experiments, we evaluated the thermal stability of the 2'F-modified purine's intra-residual C-H8...2'F-C interaction. A scalar coupling of 2 Hz was measured for 2'F-araA H8 doublet (Figure 2.7). This splitting of H8 peak to a doublet was only observed in the NMR spectra of 2'F-araA nucleoside, and not for the other three nucleosides, i.e., dA, rA, or 2'F-rA. We monitored the 2 Hz splitting in D₂O or DMSO at various temperatures, and it was shown to be stable even up to 100 °C (Figure 2.7). Most H-bonding interactions of relatively low energy disappear by this temperature, but this one remained unaffected and proved to be very stable. We reasoned that this extraordinary stability is, in part, due to the fact that the nucleobase is constrained in the anti orientation by steric effects from the top-face fluorine, and hence the nuclei on both sides of the hydrogen bonding bridge are forced to remain spatially close to each other (48,49).

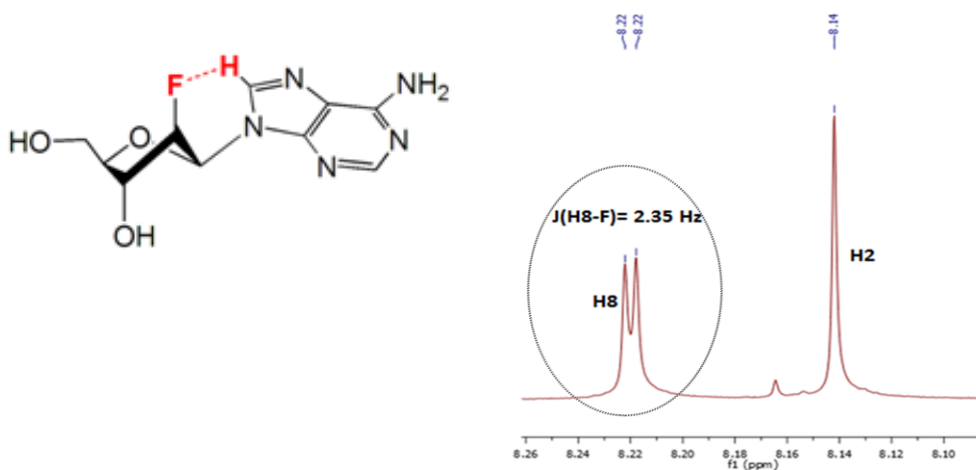


Figure 2.7 2Hz splitting of H8 peak to a doublet observed for 2'F-araA nucleoside.

2.4.3 Further Evaluation of H8/F2' Scalar Coupling Observed for 2'F-araA Nucleoside

To provide further evidence that the observed 2 Hz splitting at H8 peak of 2'F-araA, is in fact a result of scalar couplings between magnetically active nuclei on both sides of the pseudohydrogen bonding bridge, and not a through-bond coupling, we constrained the nucleoside to adopt a northern (N-type) conformation by connecting the 3' and 5' OH groups with the Markiewicz protecting group (50). This is in contrast to unconstrained 2'F-ANA nucleosides that generally adopt a southeast sugar pucker (51). Interestingly, as a result, the 2 Hz splitting disappeared and the disiloxane product showed no discernable H8/F2' splitting (Figure 2.8).

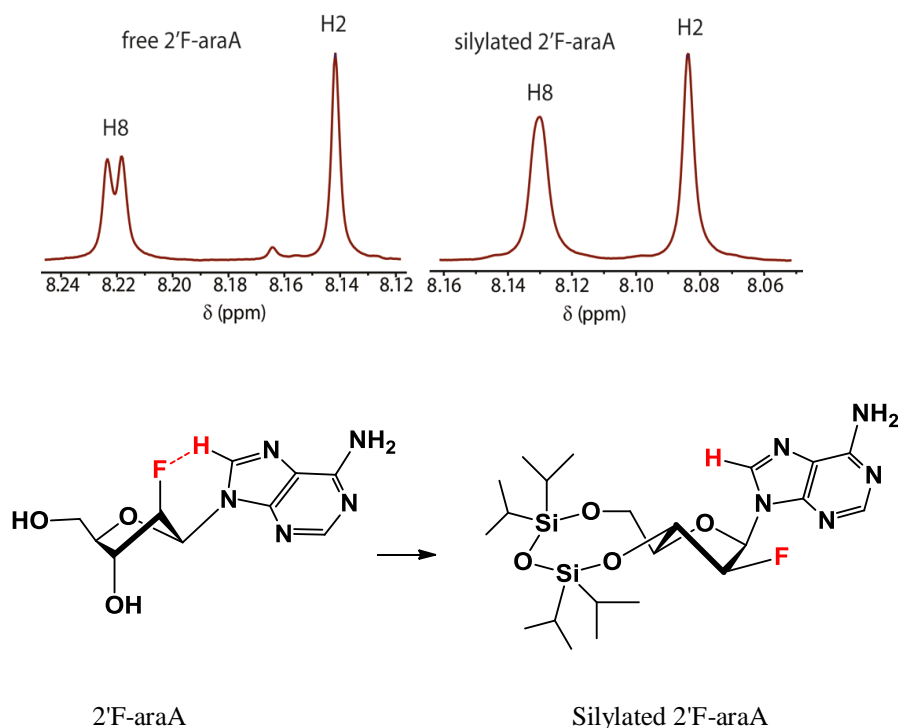


Figure 2.8 Inducing a northern conformation by connecting the 5' and 3' hydroxyl groups of 2'F-araA causes disruption of the otherwise stable H8/F2' coupling.

Taken together, our results from NMR experiments indicate the presence of a stable H8/F2' intra-residual interaction at the nucleoside level for 2'F-modified purine nucleosides.

2.5 “Cooperative” Inter- and Intra-Residual C-H...2'F-C Pseudohydrogen Bonding

It would not be surprising to find the same intra-residual C-H... F-C interaction described earlier for 2'F-modified purine nucleosides to be acting in oligonucleotide chains as well. If the base pairing geometry can adjust, such intra-molecular interactions could contribute to the pre-organization and presumably stability of 2'F-substituted nucleic acid duplexes.

In the initial structural study reported by Watts *et al.* (5), some short intra-residual C-H8... 2'F-C distances were observed in the fully modified 2'F-ANA strand (2.3 Å) but the geometry was more favorable for the inter-residual C-H8...2'F-C hydrogen bond formation, and therefore their analysis was focused on the latter.

In the current study, however, in a partially modified sequence like A3 (Table 2.1), the base-stacking geometry could readily adjust to optimize the intra-residual C-H8...2'F-C interactions. Thus, the relatively high stabilization observed for sequence A3 may be related at least in part to intra-residue pseudohydrogen bonding within the 2'F-substituted purines of the oligonucleotides. In contrast, for sequence B3 (Table 2.1), where the purines are adjacent, the base stacking geometry cannot adjust, and the stabilization is minimal (or if the base stacking does adjust, it imposes a steric penalty with an associated loss in binding affinity). Accordingly, sequence B3 showed an order of magnitude less stabilization than A3 as indicated by the T_m values of A3 versus B3 presented in Table 2.1.

Another interesting observation drawn from table 2.1 is that the inter-residual pseudohydrogen bonding at pyrimidine-purine steps is most favorable when both residues are replaced with 2'F-ANAs (compare the ΔT_m /modification values for A2 and A3). When only the thymidines of

sequence A2 were modified, substantially smaller stabilization was observed (0.9 °C/2'F-ANA vs. 1.4 °C/2'F-ANA). Two possible explanations emerge. Hydrogen bonding interactions are optimal when the donor is an acidic hydrogen. The presence of electronegative fluorine at nucleoside's 2'-position may render the corresponding purine H8 more acidic. For example, during the D₂O exchange experiment described above, 2'F-rA had a rate of exchange about 20% faster than that of dA at pH 7.4 (Figure 2.6). Besides the proton acidity, the exchange rate depends on conformation and other factors, so the relative acidity may in fact be smaller or larger. Alternatively, the pyrimidine-purine dimer may adopt a more favorable conformation for inter-residual pseudohydrogen bonding when both nucleotides are 2'F-ANA-modified.

It is not yet clear whether both intra- and inter-residual interactions can occur simultaneously at the same residues, since the base pairing geometry may need to adjust to optimize each independently. Thus while we provide strong evidence that pseudohydrogen bonding exists, it does appear to require cooperativity between several favorable circumstances. This too is consistent with previous work (38). Corey *et al.* coined the term “induced” or “cooperative” C-H...F hydrogen bonding for a related phenomenon (52). Likewise, Koller *et al.* showed that fluorine exerts both direct and indirect effects (through pseudohydrogen bonding and electronegativity) in stabilizing modified base pairs (41). Accordingly, we concluded that to obtain oligonucleotides displaying the highest affinity, both nucleotides of each pyrimidine-purine step should be modified with 2'F-ANA –one fluorine serves as H-bond acceptor and the other activates a suitable C-H donor.

2.6 Entropy and Enthalpy Contributions

In principle, intra-residual and inter-residual C2'-F...H8 pseudohydrogen bonds can occur in both the duplex and the single-stranded state. If these noncovalent interactions have an effect on pre-organizing the bases in the single-stranded state, by restricting conformational freedom, then the entropy penalty of duplex formation is reduced relative to a random coil. Furthermore, the favorable base-base geometry in the duplex would be re-inforced, as proposed by Egli, through enhanced π - π stacking interactions and tighter Watson-Crick pairing resulting from the inductive effects of the 2'-fluorine (42,43).

Follow up work on this topic centered on the structural analysis of several nonself-complementary short oligonucleotides presented in Table 2.2 in both the single-stranded state and the duplex state. Detailed comparison between the data acquired in the two states in water will help us learn more about the enthalpy and entropy contributions of pseudohydrogen bonds to fluorine.

Tet-F1 and Tet-F2 contain one and two 2'-F-ANA nucleotides in their sequence respectively (Table 2.2). As a result, tet-F1 has a 2'-F-ANA-DNA pyrimidine-purine step, while tet-F2 has a 2'-F-ANA-2'-F-ANA pyrimidine-purine step. These two dimers were subjected to high resolution NMR spectroscopy using a combination of NOESY, ^1H - ^{19}F HOESY, and correlation spectroscopy in order to verify whether the intra/inter-residual C-2'F...H8-C hydrogen bonds are present in the single-stranded state, and whether they can occur simultaneously.

Three other sequences were prepared and studied, namely tet-DNA, tet-RNA, and tet FR2 (Table 2.2). These control sequences have an equal number of purines and pyrimidines similar to tet-F1 and tet-F2; however, none is 2'-fluorinated, and thus no pseudohydrogen bonding interaction is possible.

Interestingly, our preliminary results from ^1H -

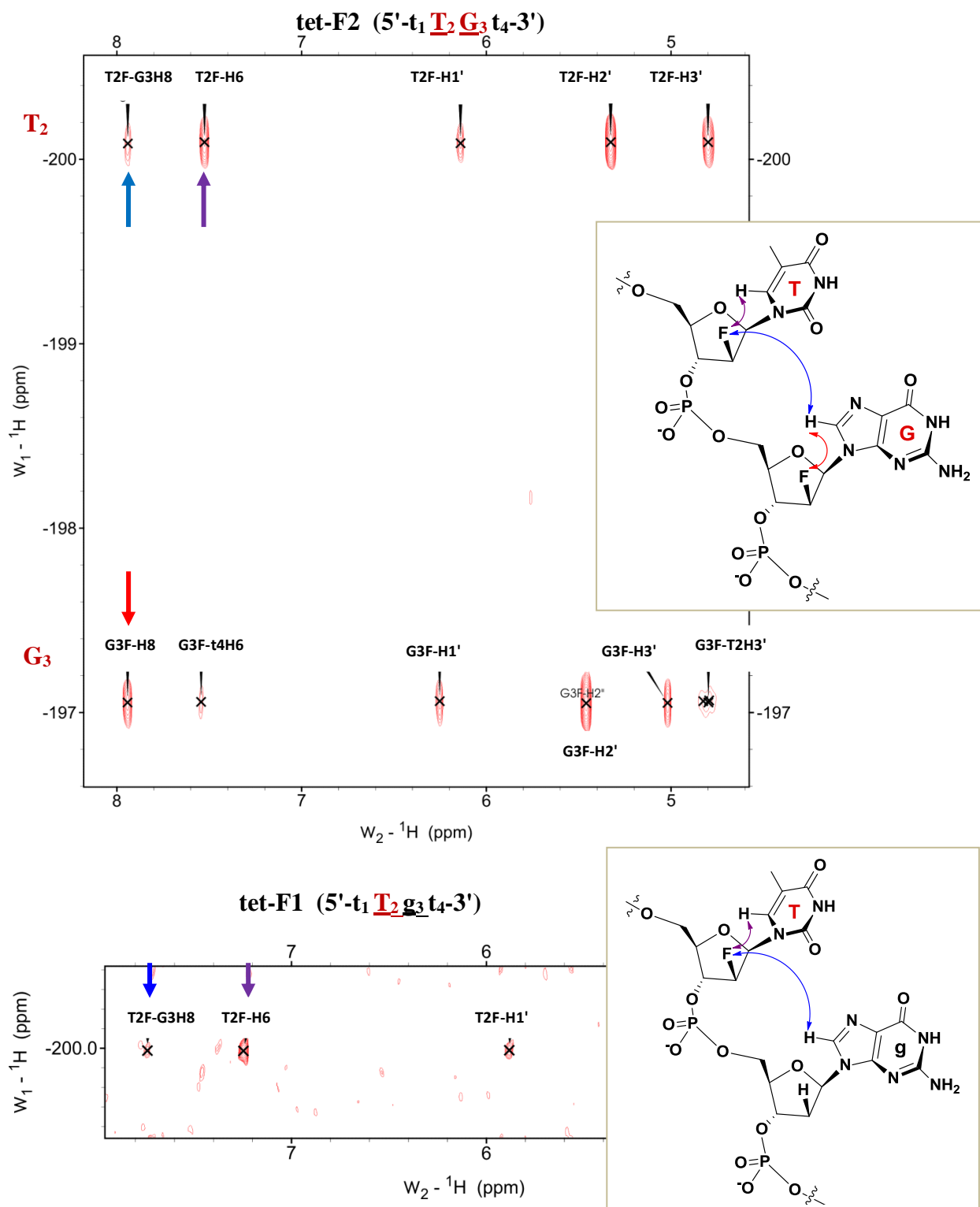
^{19}F HOESY spectra of tet-F2 indicate intense sequential $^{19}\text{F}(\text{T})$ - $^1\text{H}8(\text{G})$ cross peaks at 2'-F-ANA-2'-F-ANA pyrimidine-purine step (TG step; Figure 2.9), which correlates well with short distances between thymine's F2' and aromatic H8 proton of the proximal araF-G, and the possibility of formation of an inter-residual C-2'F...H8-C pseudohydrogen bond in the single-stranded state of tet-F2. Strong intra-nucleotide $^{19}\text{F}(\text{T})$ - $^1\text{H}6(\text{T})$ and $^{19}\text{F}(\text{G})$ - $^1\text{H}8(\text{G})$ cross peaks are also observed.

Sequential $^{19}\text{F}(\text{T})$ - $^1\text{H}8(\text{G})$ cross peak was also observed at the 2'-F-ANA-DNA pyrimidine-purine step for tet-F1 (Figure 2.9), which here is a direct result of short distances between thymine's F2' and aromatic H8 proton of sequential dG in tet-F1. Interestingly, the sequential $^{19}\text{F}(\text{T})$ - $^1\text{H}8(\text{G})$ cross peak observed for tet-F2 is more intense than the corresponding cross peak for tet-F1, which could suggest that the inter-nucleotide distances between F2' and aromatic H8 proton in tet-F2 are shorter than in tet-F1. Since shorter distances correlate with stronger bonds, one could conclude that the inter-nucleotide C-2'F...H8-C pseudohydrogen bond in tet-F2 is stronger than that in tet-F1, suggesting again that the inter-residual pseudohydrogen bonding is most favorable when both residues at pyrimidine-purine step are replaced with 2'-F-ANAs.

Table 2.2 Sequences of *ss*-tetramers.

Code	Sequence
tet-F1	5'-tTgt-3'
tet-F2	5'-tTGt-3'
tet-DNA	5'-ttgt-3'
tet-FR2	5'-tUGt-3'
tet-RNA	5'-tUGt-3'

Label: dna, 2'-F-ANA, RNA, 2'-F-RNA.



As expected, the indicative sequential $^{19}\text{F}(\text{U})\text{-}^1\text{H}8(\text{G})$ cross peak or the intra-nucleotide $^{19}\text{F}(\text{T})\text{-}^1\text{H}6(\text{T})$ and $^{19}\text{F}(\text{G})\text{-}^1\text{H}8(\text{G})$ cross peaks were not observed in the case of tet-FR2 single-stranded control (see Figure 2.10). As a result of a North sugar pucker for 2'F-RNA nucleotides, the F2' and aromatic protons are placed far from each other, making the formation of a pseudohydrogen bonding interaction to fluorine geometrically impossible. This observation reminds us of how changes in sugar pucker are important determinants of nucleic acid structure; changes in sugar pucker alters the orientation of C2', C3' and C4' substituents, resulting in major changes in backbone conformation and overall structure.

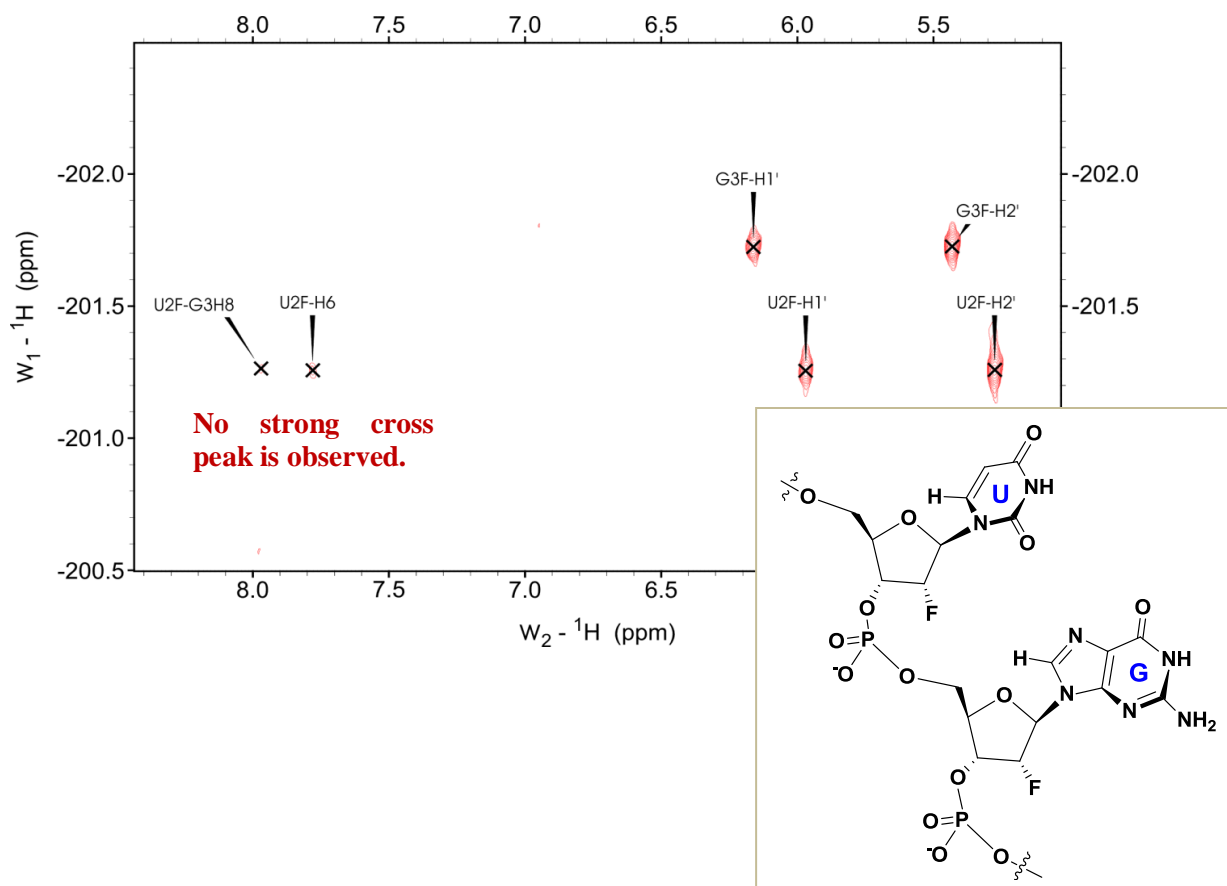


Figure 2.10 Heteronuclear $^{19}\text{F}\text{-}^1\text{H}$ HOESY spectra of tet-FR2 in D_2O . No strong intra-residual $^{19}\text{F}(\text{G})\text{-}^1\text{H}8/\text{H}6(\text{G}/\text{U})$ or sequential $^{19}\text{F}(\text{U})\text{-}^1\text{H}8(\text{G})$ cross peaks is observed for tet-FR2.

Future work will focus on NMR structure determination of the single-stranded tetramers paired to their complementary RNA strand (3'-AACAA- 5'). The duplex states of tet-F1 and tet-F2 will be compared carefully to duplex states of tet-DNA, tet-RNA and tet-FR2 controls. Specifically, measurement of one-bond scalar coupling constants of (G)N···H-N(C) Watson-Crick hydrogen bonds ($^1J(N,H)$, Figure 2.11) in these short duplexes will provide valuable data on their base pair strengths. Accordingly, measurement of $^1J(N,H)$ coupling constants at ^{15}N natural abundance has previously been used to demonstrate that N···H-N hydrogen bonds in RNA A:U base-pairs are stronger than those in DNA A:T base-pairs (53). Similar comparison between (G)N···H-N(C) hydrogen bonds of tet-F2:RNA vs. tet-DNA:RNA can help us assess their strengths and explore whether the WC hydrogen bonding in 2'F-ANA modified hybrids, that have electronegative fluorine atoms at C2' position, are truly more tightened than that of the DNA:RNA hybrids.

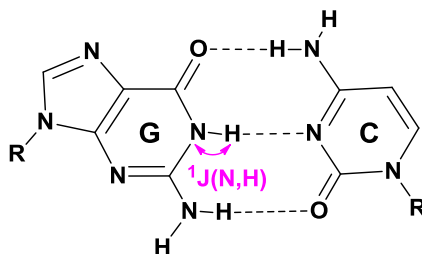


Figure 2.11 Schematic representation of $^1J(N,H)$ scalar coupling

2.7 Application of C-H...2'F-C Hydrogen Bonding to Rationally Design Oligonucleotide Based Therapeutics with High Binding Affinity

2.7.1 Overview

As discussed in chapter one, the appropriate chemical modification of oligonucleotides is among the most important efforts to develop effective antisense oligonucleotide-based therapeutics (AON) (54) as well as siRNAs (55).

Among the chemical modifications that have been introduced to date, 2'F-ANA has proven to be very useful modification in antisense applications (51). It is DNA-like in structure, and hence, 2'F-ANA modified oligonucleotides are able to activate RNase H-mediated mRNA cleavage. Moreover, 2'F-ANA improves nuclease resistance, and forms duplexes with RNA that have enhanced stability compared with unmodified DNA:RNA hybrids.

We demonstrated earlier that the origin of the higher binding affinity of 2'F-ANA toward RNA is due to the formation of energetically important fluorine-mediated pseudohydrogen bonds at 5'-pyrimidine-purine-3' steps. To expand upon these findings, we next sought to investigate whether these favorable interactions could be used in a rational way and serve us as an additional design rule for the creation of therapeutically relevant 2'F-ANA-based antisense oligonucleotides.

To find out, we chose a clinically relevant antisense oligonucleotide sequence (56), and applied the rules we learnt from our earlier studies to design new series of modified antisense oligonucleotides. We evaluated the thermal stabilities and rate of RNase H-mediated cleavage of the 2'F-ANA:RNA duplexes.

2.7.2 Design and Evaluation of Thermal Stabilities of Modified Antisense Oligonucleotides Containing C-H8...2'F-C Pseudoydrogen Bonding

Findings from a previous study have shown that a 2'F-ANA modified AON, directed towards selective inhibition of the phosphodiesterase (PDE) isoforms, is effective at reducing key inflammatory markers characterizing Chronic Obstructive Pulmonary Disease (COPD) (56).

We chose the same antisense sequence against COPD as a model system, and first regenerated the traditional unmodified AON (X-DNA; Table 2.3), as well as the 2'F-ANA substituted gapmer AON (X-gapmer, with 2'F-ANA wings and a central DNA section; Table 2.3). Following the design rules described in previous sections, we next selectively modified the pyrimidine-purine steps in the original gapmer sequence and designed four new altimer oligonucleotides containing 1, 2, 4 or 6 2'F-ANA-modified pyrimidine-purine steps (X-1, X-2, X-4 and X-6; Table 2.3). In all four altimers, an equal number of total nucleotides and an equal number of purines were modified with 2'F-ANA nucleotides. Furthermore, all four strands consisted of nine alternating segments –four regions of 2'F-ANA units and five regions of DNA units. The termini were native DNA in all cases. Thermal stabilities of the complexes of synthesized AONs with complementary RNA strands were measured in a Varian Cary 5000UV spectrophotometer. The T_m values are summarized in Table 2.3. As expected, the binding affinities of the four altimers to complementary RNA improved with the number of modified pyrimidine-purine steps. Thus the same number of 2'F-ANA nucleotides, including the same number of purines, can give higher binding affinity when pyrimidine-purine steps are selectively modified. This provides a rational means to increase the binding affinity of a given antisense oligonucleotide without increasing the degree of modification.

Table 2.3 Sequences, T_m values and RNase H cleavage velocities of designed antisense oligonucleotides

Name	Sequence (5'-3') ^a	T_m ^b	ΔT_m	V^c
X-DNA	tcatgagtggcagctgcaatt	64.9	-	1.00 ± 0.10
X-gap	TCATgagtggcagctgcAATT	68.0	3.1	0.80 ± 0.15
X-1	t <u>CAT</u> gAGTggcaGCTgcAATt	72.1	7.2	0.76 ± 0.03
X-2	tc <u>ATGA</u> gtgGCagCTg <u>CAAT</u> t	72.3	7.4	0.83 ± 0.12
X-4	t <u>CAT</u> gAGT <u>GgCagcTGCA</u> att	73.5	8.6	0.85 ± 0.05
X-6	t <u>CATGagTGgCAgcTGCA</u> att	74.2	9.3	0.59 ± 0.10

^aLegend: 2'-F-ANA, dna. Modified pyrimidine-purine steps are underlined in the altimers. ^bIn °C, for a duplex of the strand with complementary RNA. ^cRelative velocity for RNase H cleavage of the hybrid. By comparison, phosphorothioate X-DNA had a relative velocity of 0.27 ± 0.15 .

To ensure the therapeutic relevance of this strategy, we next carried out an RNase H assay on all of the modified oligonucleotides as described in the following section.

2.7.3 RNase H Cleavage Velocities of Designed Antisense Oligonucleotides

In collaboration with Dr. Allen Nicholson's laboratory at Temple University, all four altimers were hybridized to the RNA complement and tested for their susceptibility to cleavage by human RNase H1. The X-gap:RNA and phosphorothioate-DNA:RNA duplexes served as controls.

The four altimers had excellent RNase H activity and they were all superior to phosphorothioate DNA (Table 2.3 legend and Figure 2.12). Interestingly, altimer X-6, with the highest number of modified py-pu steps, exhibited lower cleavage rates relative to the gapmer design. The altimers X-1, X-2, X-4, and the gapmer trigger RNase H activity with similar rates (Figure 2.12 and Table 2.3). We reasoned that while the higher number of pseudohydrogen bonding enhances the binding affinity towards the complementary RNA, it may lead to higher duplex rigidity as well.

This could explain the slower cleavage rate observed for X-6, since it is known that more flexible (less rigid) antisense strands allow better malleability of the hybrid by RNase H, a structural requirement for efficient RNA cleavage (9,57,58).

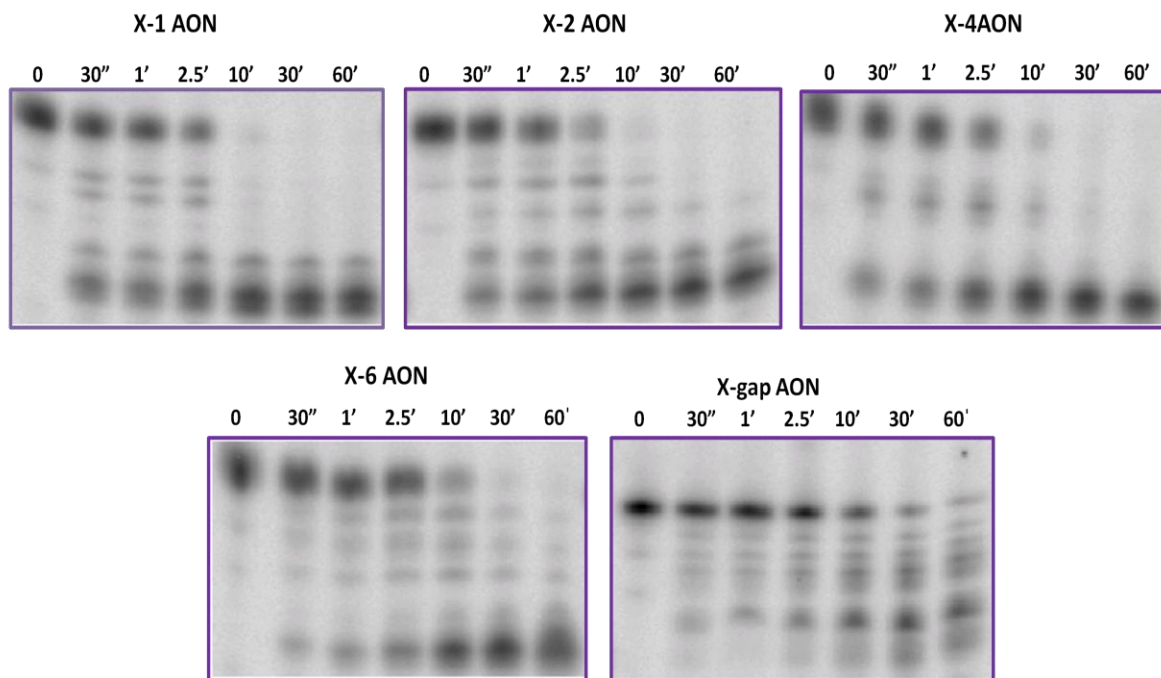


Figure 2.12 Cleavage of “X”-AON:RNA Hybrids by RNase H1 (A) Gel pictures of cleavage of “X”-AON:RNA Hybrids as well as the original X-gapmer sequence by RNase H1. Time points are: 0, 0.5, 1, 2.5, 10, 30, 60 minutes.

In conclusion, our data provide compelling evidence for C-H8...2'F-C pseudohydrogen bonding in double-stranded hybrids in water, and that this can be used to tune the binding affinity of nucleic acid duplexes in a rational way.

The principles described here may also be relevant to other fluorinated oligonucleotide structures. The following sections will briefly review our findings regarding the importance of

such nonconventional interactions in G-quadruplex stabilization and discuss how they modulate the folding of the two-repeat human telomeric G-quadruplex in K^+ Solution (59).

2.8 Directing the Folding of Human Telomeric Quadruplex with a Single Fluorine Atom: Evidence for C-H...2'F-C Pseudohydrogen Bonds in 2'F-Substituted Quadruplexes

2.8.1 Introduction

G-quadruplexes are nucleic acid structures occurring in human telomeres and oncogene-promoter regions, and they have garnered considerable attention due to their involvement in telomere maintenance and gene regulation (60,61). G-quadruplexes exhibit significant structural diversity (61-63) and different nucleoside modifications have been introduced to modulate G-quadruplex folding (64-66).

To expand upon the current knowledge and to investigate the structural basis of the effect of C2' modifications in G-quadruplex stability and conformation, we have evaluated the impact of several C2' modified guanosines, 2'F-ANA (AFtel), 2'F-RNA (RFtel), ANA (Atel), and RNA (Rtel), on the telomeric sequence, and found that arabinose and ribose substitutions can be used to stabilize the biologically relevant propeller parallel G-quadruplex form over other competing conformers (59). Interestingly, the 2'F-ANA modification in particular allowed for an exceptional stabilization of the parallel quadruplex. We wondered whether the origin of this great stabilization could be due to the formation of C-H...2'F-C pseudohydrogen bonding, similar to those observed for 2'F-ANA modified double-stranded hybrids as described earlier.

To find out, in collaboration with Prof. Carlos Gonzalez's lab at the CSIC in Spain, high resolution NMR experiments combined with state-of-the-art theoretical calculations were performed on modified G-quadruplexes. These studies demonstrated that the high stabilization

provided by 2'F-ANA substitution is indeed a result of 2'F...H8 pseudohydrogen bonding. Moreover, unique inter-residue F-CH...O4' electrostatic interactions were also characterized as an additional parameter in the stabilization of 2'F-ANA substituted G-quadruplexes.

2.8.2 Design and Thermal Stability Evaluation of Substituted Human Telomeric DNA Quadruplexes

We focused our studies on the two-repeat telomeric sequence, d(TAGGGTTAGGGT)(Dtel), which offers a convenient model for high-resolution studies by either NMR (67) or crystallography (68).

We replaced guanosine at position nine (d-G9) with several C2' modified nucleotides. Structures of the incorporated nucleotides are shown in Figure 2.10. Our rationale for modifying position nine stems from a previous observation that in antiparallel quadruplexes the guanine at the 3'-side of the first TTA loop, here d-G9, tends to adopt a syn glycosidic bond conformation (63). Thus, since the syn glycosidic conformation is highly disfavored in 2'F-arabinonucleosides, we hypothesized that modifying this residue will result in more dramatic changes.

G-quadruplex formation and melting were monitored by circular dichroism (CD) and NMR spectroscopy in the presence of K⁺ ions (Figure 2.13 and Table 2.4). Both arabinose modifications (AFtel and Atel) induce a strong stabilization, with the effect being more pronounced for AFtel ($\Delta T_m = +12$ and $+9$ °C, respectively, relative to the unmodified Dtel). In fact, AFtel exhibits the highest melting temperature (53 °C) of the entire series.

The rG substitution is also stabilizing ($\Delta T_m = +6$ °C), in contrast to the 2'F-rG modification which is destabilizing. The overall trend we observed is 2'F-araG > araG > rG > dG >> 2'F-rG.

Table 2.4 T_m Values for DNA Telomeric Sequence (Dtel) and for Singly Modified Sequences

Name	Sequence (5'-3')	T_m	ΔT_m
Dtel	TAGGGTTAGGGT	41	0
Rtel	TAGGGTTAGGGT	47	+6
Atel	TAGGGTTAGGGT	50	+9
AFtel	TAGGGTTAGGGT	53	+12
RFtel	TAGGGTTAGGGT	-	-

Legend: DNA, RNA, ANA, 2'-F-ANA, 2'-F-RNA. Buffer conditions: 15mM potassium phosphate, 5mM KCl, pH 7.0; strand concentration 75 μ M.

2.8.3 Structural Analysis of 2'-F-Substituted Human Telomeric DNA Quadruplex Reveals Pseudohydrogen Bonds Contribute to Structure and Stability

CD spectra of AFtel, Atel, and Rtel exhibit the distinctive features of a parallel quadruplex (a negative band at around 240nm, and a positive one at 265 nm), which contrast with the CD spectra of the unmodified sequence (Dtel, Figure 2.13). The CD spectrum of RFtel is clearly different from the others, displaying low-intensity bands, suggesting that it retains very little quadruplex structure, if at all, under the experimental conditions.

The one-dimensional proton spectra of the unmodified sequence, Dtel, were characteristic of a mixture of parallel and antiparallel topologies (Figure 2.13). By contrast, AFtel, Atel, and Rtel fold mainly into a single G-quadruplex form, as indicated by the number of proton resonances. Furthermore, the six sharp imino signals observed in the 10–12 ppm range, along with the data presented below are consistent with a symmetric, bimolecular G-quadruplex complex. In marked contrast, the imino region of RFtel shows very broad and weak signals, suggesting the presence of multiple species of very low stability (Figure 2.13).

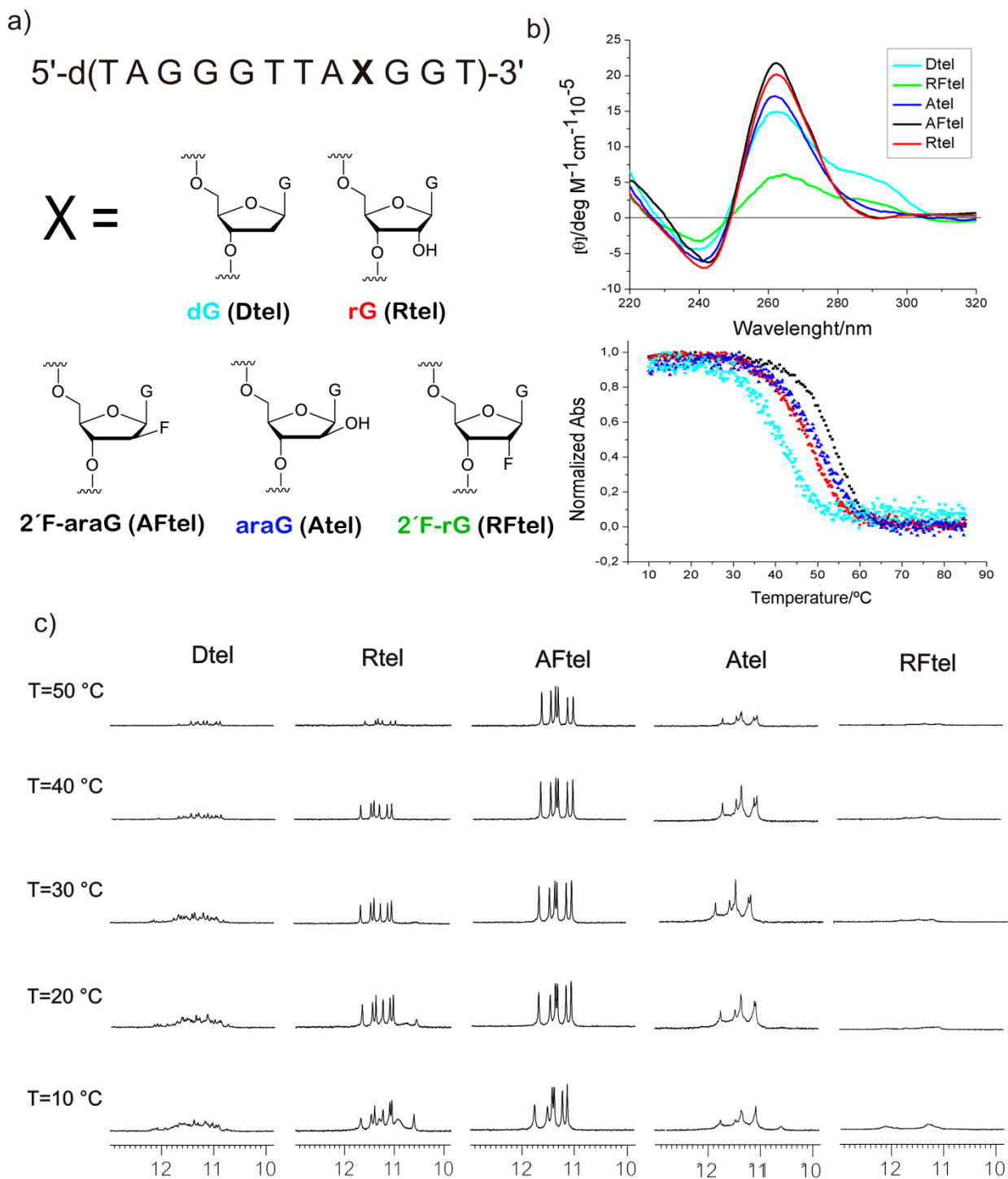


Figure 2.13 (a) Structures of the native guanosines (**DNA**, **RNA**) and chemically modified Gs (**2'F-ANA**, **ANA**, and **2'F-RNA**). (b) CD spectra and melting profiles. (c) Imino region of the $^1\text{H-NMR}$ spectra at different temperatures of all five G-rich telomeric sequences.

Careful NMR analysis of the fluorinated quadruplex (AFtel) and comparison of its structure to the crystallographic structure of d(BrUAGGGBrUTAGGGT) (PDB ID: 1K8P) as a model of the DNA telomeric sequence (68), revealed particularly interesting electrostatic interactions (Figure 2.14). These experiments were conducted by Dr. Carlos Gonzalez of the CSIC (Spain), and some brief highlights are presented here

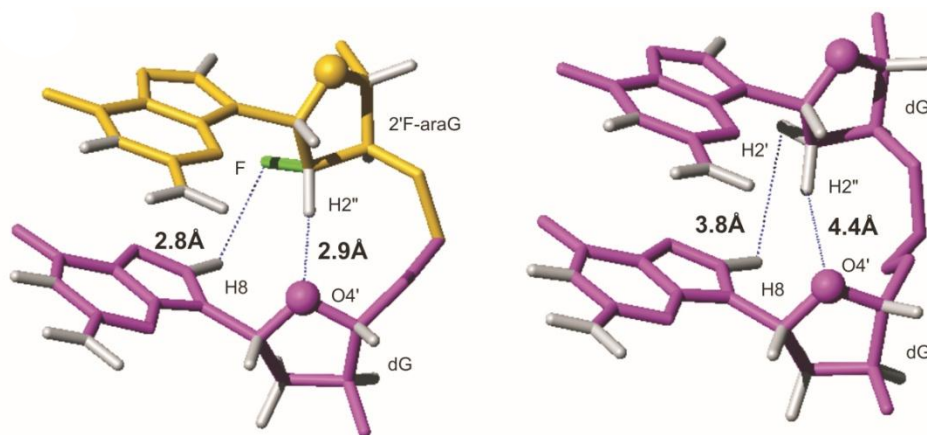


Figure 2.14 Distances between F_i-H8_{i+1} and $H2''_i-O4'_{i+1}$ in AFtel and $H2'_i-H8_{i+1}$ and $H2''_i-O4'_{i+1}$ in the crystallographic structure (PDB code: 1K8P). Guanines are shown in magenta for dG and yellow for 2'F-araG.

Superposition of the G-core residues in both structures indicates that the main differences reside around the 2'F-ANA modification. Specifically, the 2'F-ANA sugar residues (position 9 in each subunit) are displaced toward the minor groove and consequently toward their 3'-neighboring base (Figure 2.14 and Table 2.5). This effect provokes a substantial decrease in the distance between the 2'-fluorine and H8 of the adjacent base (3'-dG10) (Figure 2.14). The 2'F-H8 distance for AFtel is around 2.8 Å, compared to 3.8 Å for the crystallographic structure (Figure 2.14 and Table 2.5). The close 2'F...H8 contact here is similar to those found in 2'F-ANA:RNA hybrid duplexes described earlier in this chapter (5,69), and is indicative of a nonconventional pseudohydrogen bonding interaction. For AFtel, the 2'F...H8-C8 angle is around 140° (Table

2.6), which is 20° higher than that observed in the unmodified dG core. This value (140°) is also similar to that observed in the 2'F-ANA:RNA hybrids (145°), and it is considered optimum for formation of X–H...F (X = N, O, or C) pseudohydrogen bonds (70,71).

Table 2.5 Inter-residual 2'F...H8 and 2'H...H8 distances for **AFtel** and **1K8P** telomeric G-quadruplexes. Distances are in Å.

Nucleotide	inter 2'F _i -H8 _{i+1} /H2' _i -H8 _{i+1}	X-ray inter H2' _i -H8 _{i+1}
G3 _i -G4 _{i+1}	4.1 ± 0.6	3.3
G4 _i -G5 _{i+1}	4.3 ± 0.2	2.0
G9 _i -G10 _{i+1}	2.7 ± 0.2	3.8
G10 _i -G11 _{i+1}	3.6 ± 0.4	3.4

Table 2.6 Inter-residual 2'F...H8-C8 and H2'...H8-C8 angles for **AFtel** and **1K8P** telomeric G-quadruplexes. Angles are in degrees.

Nucleotide	inter 2'F _i – H8-C8 _{i+1} /H2' _i – H8-C8 _{i+1} (AFtel)	X...ray inter H2' _i – H8-C8 _{i+1} (1K8P)
G3 _i -G4 _{i+1}	117	128
G4 _i -G5 _{i+1}	112	116
G9 _i -G10 _{i+1}	137	124
G10 _i -G11 _{i+1}	121	121

Furthermore, the AFtel structure revealed an additional close contact between H2'' and O4' of the neighboring 3'-dG residue (2.9 Å in AFtel vs. 4.4 Å in the crystal structure), with a C2'-H2''...O4' angle of 150° (versus 120° for 1K8P). Stabilizing C-H...O interactions have previously been described for nucleic acid (72) and protein-protein interactions (73,74). All together, we conclude that the enhanced stability imparted by the 2'F-araG modification is due, at least in part, to C2'-F...H8 and FC2'-H2''...O4' interactions, both of which are lacking in the native structure. In contrast, 2'F-RNA substitution provokes a dramatic destabilization of the quadruplex structure due to unfavorable electrostatic repulsion between the phosphate and the 2'-F (Figure 2.15B).

For Atel, the top-side 2'-OH of the ANA-G nucleotide can easily be accommodated without incurring the steric penalty observed in duplex structures (2,6,75). Furthermore, ANA's 2'-OH in Atel is involved in favorable electrostatic interactions with the neighboring phosphates, as also seen for Rtel, but not for RFtel (Figure 2.15). This makes ANA modifications particularly useful for applications where additional stabilization of a quadruplex and concomitant destabilization of a competing duplex structure is desired. The impact of ANA modification on stability and hybridization properties of double-stranded nucleic acid structures will be discussed in Chapter 3 of the present thesis as well.

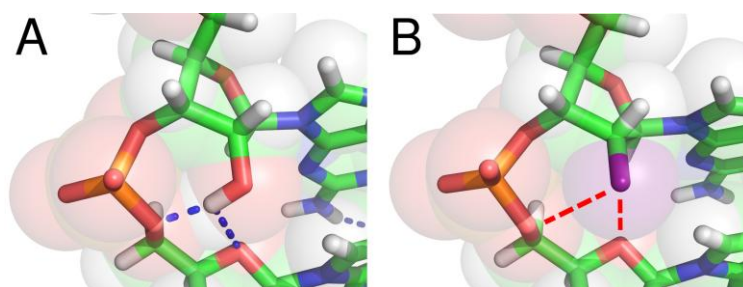


Figure 2.15 Snapshots of the most relevant configuration of the rG (A) and 2'F-rG (B) in the G-quadruplex as found in our molecular dynamics simulations. Note how the hydroxyl group favourably interacts with the oxygen atom of the neighbouring phosphate group, whereas this interaction is repulsive in the case of the fluorine substituent.

2.9 Concluding Remarks

In this study, we discussed the origin of the strikingly high binding affinity of 2'F-ANA toward RNA. Our data provides compelling evidence that the high thermal stability of 2'F-ANA:RNA duplexes is mainly due to formation of energetically important C2'-F...H8 pseudohydrogen bonding (inter-residual and/or intra-residual) at 5'-pyrimidine-purine-3' steps and in a nonbase-

pairing context. Such fluorine-mediated interactions were used as an additional design rule for the creation of therapeutically relevant 2'F-ANA-based oligonucleotides.

The principles described for formation of C2'-F...H8 pseudohydrogen bonds in 2'F-ANA:RNA double helices may be relevant to other fluorinated oligonucleotide structures as well. Our studies on 2'F-substituted human telomeric quadruplex demonstrated that the enhanced stability gained by the 2'F-ANA incorporation is due, at least in part, to the formation of C2'-F...H8 pseudohydrogen bonds along with FC2'-H2"...O4' electrostatic interactions; both of which are lacking in the native human telomeric quadruplex structure.

2.10 Experimental Methods

2.10.1 Oligonucleotide Synthesis and Purification

All oligonucleotides were synthesized using standard phosphoramidite chemistry on an Applied Biosystems 3400 DNA Synthesizer at a 1- μ mol scale using Unylink CPG support (ChemeGenes, Wilmington, MA) (76). All phosphoramidites were prepared as 0.15M solutions in acetonitrile (ACN), except DNA, which was prepared as 0.1M. 5-ethylthiotetrazole (0.25M in ACN) was used to activate phosphoramidites for coupling. Detritylations were accomplished with 3% trichloroacetic acid in dichloromethane for 110 seconds. Oxidation was done using 0.1M I₂ in 1:2:10 pyridine: water: THF. Coupling times were 600 seconds for RNA, and 2'F-ANA phosphoramidites, with the exception of their guanosine phosphoramidites which were allowed to couple for 900 seconds. For DNA, these coupling times were 100 seconds for A, C, and T and 270 seconds for G.

5'-phosphorylation of the chemically modified strands was achieved using bis-cyanoethyl-N,N-diisopropyl-2-cyanoethyl phosphoramidite at 0.15M (600 seconds coupling time). Deprotection

and cleavage from the solid support was accomplished with ammonia:ethanol (3:1 v/v) for 48 hours at room temperature (77). Oligonucleotides containing RNA were synthesized with standard 2'-TBDMS phosphoramidites, and desilylation was achieved with neat TEA.3HF for 48 hours at room temperature (78). Oligonucleotides were precipitated by adding 3M sodium acetate (25 μ L) followed by addition of cold butanol (1000 μ L) and then purified by reverse phase HPLC on an Agilent 1200 series using a Waters semipreparative C18 column. A stationary phase of 100mM triethylammonium acetate in water with 5% ACN (pH 7), and a mobile phase of HPLC grade ACN were used.

2.10.2 UV-Melting and Derivation of Thermodynamic Parameters of 2'F-Modified Duplexes

UV thermal denaturation data were obtained on a Varian Cary 5000 UV-VIS spectrophotometer equipped with a Peltier temperature controller. Duplex concentration was 2 μ M (4 μ M total concentration of strands) in buffer containing 140mM KCl, 1mM MgCl₂, and 5mM Na₂HPO₄, pH 7.2. Duplexes were annealed in the spectrophotometer by cooling from 65°C to 5°C for the 8mers (Table 2.1.) and from 93°C to 5°C for antisense oligonucleotides (Table 2.3). Samples were kept under flowing nitrogen when below 15°C. After an equilibration period, the temperature was increased at a rate of 0.4°C/min and absorbance values were recorded each minute. T_m values were calculated using the baseline method; assignment of baselines was very clear in all cases. Thermodynamic parameters were extracted from the melting curves using the Cary software. This method is based on Van't Hoff plots assuming a two-state model for a nonself-complementary bimolecular equilibrium.

2.10.3 RNase H Assays on 2'F-modified Antisense Oligonucleotides Targeting COPD

Purification of the Human RNase H1 and RNase H cleavage assays were performed by Nageswara R. Alla in the Nicholson lab in Temple University, Departments of Chemistry and Biology.

2.10.3.1 Purification of Human RNase H1

Human (Hs) RNase H1 was produced in the *E. coli* expression host, BL21 (DE3), carrying a recombinant pET-15b plasmid containing a cDNA for human RNase H1 (79). The cDNA lacked the N-terminal mitochondrial targeting sequence, therefore allowing production of the mature form of Hs-RNase H1, which also carries an N-terminal hexahistidine [(His)₆] affinity tag. The host strain also carried plasmid pLysS (Novagen, EMD Millipore), which provided additional control over Hs-RNase H1 expression. A freshly-transformed bacterial colony was introduced into LB broth (0.5 l) containing 100 µg/ml ampicillin. The culture was grown at 30°C with vigorous aeration to a density of ~ 0.5 (600nm). IPTG (1mM final concentration) was added, followed by further aeration at 30°C for 3 hours. Cells were collected by centrifugation and stored at -20°C until further use. The bacterial pellet was resuspended in buffer consisting of 400mM NaCl, 20mM HEPES, 10% glycerol, 5mM imidazole (pH 7.5) and protease inhibitor cocktail V (1X, EDTA free) (Novagen, EMD Millipore), and subjected to repeated sonication, with cooling between bursts. The sonicate was clarified by centrifugation, and subjected to Ni²⁺ affinity chromatography using a His Trap HP column (GE Healthcare; Mississauga, ON) on an AKTA FPLC Explorer system. The column was washed with 400mM NaCl, 30mM imidazole, 20mM HEPES (pH 7.5), 10% glycerol, then eluted with the same buffer containing 400mM imidazole. The sample was dialyzed against 300mM NaCl, 20mM HEPES (pH 7.5), and 10% glycerol, and stored at -20°C in 300mM NaCl, 20mM HEPES (pH7.5), 1mM DTT, 0.5mM

EDTA, and 50% glycerol. The protein was judged to be >90% pure, as determined by SDS-PAGE. Hs-RNase H1 exhibited similar catalytic behavior either with or without the (His)₆ tag (removable by thrombin treatment). The (His)₆ form of Hs-RNase H1 was used in these experiments.

2.10.3.2 RNase H1 Cleavage of Hybrids

Assays of RNase H1 cleavage of substrate used RNA:DNA hybrids containing 5'-³²P labeled RNA. Hybrids were formed by combining 25pmol of AON and 20pmol of RNA in 20mM Tris-HCl (pH 7.5), 50mM KCl, and 0.1mM DTT, then heating at 65°C for 2 minutes followed by cooling to room temperature. Cleavage reactions (10µL) involved 100nM hybrid and 30nM (His)₆-RNase H1 in buffer consisting of 150mM KCl, 10mM MgCl₂, 20mM Tris- HCl (pH 7.5) and 10mM DTT. Reactions that were otherwise complete except for MgCl₂ were first incubated at 30°C for 30 seconds, and then MgCl₂ was added to initiate the reaction. Reactions were incubated for the specified times at 30°C, then stopped by adding an equal volume of 95% formamide containing 20mM EDTA, 0.04% xylene cyanol and 0.04% bromophenol blue. Samples were heated at 95°C for 2 minutes, and aliquots electrophoresed in a 15% polyacrylamide gel containing TBE buffer and 7M urea. Bands were visualized by phosphorimaging. Reaction rates were analyzed using ImageQuant software by determining the fraction of substrate converted to product. For initial rate determinations, reaction times were used that limited substrate cleavage to ~<20%. Reactions were performed in duplicate, and average determined. Maximum error was generally <20%.

2.10.4 CD Spectroscopy and Derivation of Thermodynamic Parameters of DNA Human Telomeric Quadruplex and Modified Structures

CD spectra and thermal denaturation data for quadruplex structures (Table 2.4) were carried out on a JASCO J-810 circular dichroism spectrometer equipped with a Peltier temperature controller. Oligonucleotide concentration was 75 μ M in 15 mM potassium phosphate, 5 mM KCl, pH=7 buffer. After heating to 90°C, samples were slowly cooled (0.3°C/min) to room temperature and refrigerated overnight. Absorbance values were recorded after equilibration as the temperature was increased in 0.3°C steps at one minute intervals. T_m values were calculated using the base line method since assignment of baselines was clear in most cases. Despite the slow scan rate, some hysteresis was observed in all cases suggesting slow kinetics of formation/dissociation. This is a common effect in multimeric G-quadruplex structures, notifying that thermodynamic parameters should be considered with caution.

2.10.5 NMR experiments on DNA Human Telomeric Quadruplex Structures

NMR-based structural determination of G-quadruplexes was accomplished by Nerea Martin-Pintado in Prof. Carlos Gonzalez's lab at the CSIC in Spain. Very briefly, high-concentration samples (0.7mM) were suspended in 300 μ L of either D₂O or H₂O/D₂O 9:1 in 10mM potassium phosphate buffer, 5mM KCl (pH 7). NMR spectra were acquired in Bruker Advance spectrometers operating at 600, 700 or 800 MHz, and processed with Topspin software. ¹⁹F and ¹H ¹D melting experiments, DQF-COSY, TOCSY and NOESY experiments were recorded in D₂O and H₂O/D₂O 9:1. The NOESY spectra were acquired with mixing times of 100, 150 and 250 ms, and the TOCSY spectra were recorded with standard MLEV-17 spin-lock sequence, and 80 ms mixing time. High-concentration sample NOESY spectra in H₂O were acquired with 100

and 250 ms mixing times. In 2D experiments in H₂O, water suppression was achieved by including a WATERGATE (80) module in the pulse sequence prior to acquisition. Two-dimensional experiments in D₂O were carried out at 25°C, whereas spectra in H₂O were recorded at 5°C, to reduce the exchange with water, and 25°C. The spectral analysis program Sparky (81), was used for semiautomatic assignment of the NOESY cross peaks and quantitative evaluation of the NOE intensities.

2.11 References

1. Damha, M.J., Wilds, C.J., Noronha, A., Brukner, I., Borkow, G., Arion, D. and Parniak, M.A. (1998) Hybrids of RNA and Arabinonucleic Acids (ANA and 2'F-ANA) Are Substrates of Ribonuclease H. *Journal of the American Chemical Society*, **120**, 12976-12977.
2. Noronha, A.M., Wilds, C.J., Lok, C.-N., Viazovkina, K., Arion, D., Parniak, M.A. and Damha, M.J. (2000) Synthesis and Biophysical Properties of Arabinonucleic Acids (ANA): Circular Dichroic Spectra, Melting Temperatures, and Ribonuclease H Susceptibility of ANA-RNA Hybrid Duplexes. *Biochemistry*, **39**, 7050-7062.
3. Denisov, A.Y., Noronha, A.M., Wilds, C.J., Trempe, J.-F., Pon, R.T., Gehring, K. and Damha, M.J. (2001) Solution structure of an arabinonucleic acid (ANA)/RNA duplex in a chimeric hairpin: comparison with 2'-fluoro-ANA/RNA and DNA/RNA hybrids. *Nucleic Acids Research*, **29**, 4284-4293.
4. Trempe, J.-F., Wilds, C.J., Denisov, A.Y., Pon, R.T., Damha, M.J. and Gehring, K. (2001) NMR Solution Structure of an Oligonucleotide Hairpin with a 2'F-ANA/RNA Stem: Implications for RNase H Specificity toward DNA/RNA Hybrid Duplexes. *Journal of the American Chemical Society*, **123**, 4896-4903.
5. Watts, J.K., Martín-Pintado, N., Gómez-Pinto, I., Schwartzentruber, J., Portella, G., Orozco, M., González, C. and Damha, M.J. (2010) Differential stability of 2'F-ANA•RNA and ANA•RNA hybrid duplexes: roles of structure, pseudohydrogen bonding, hydration, ion uptake and flexibility. *Nucleic Acids Research*, **38**, 2498-2511.
6. Martín-Pintado, N., Yahyaee-Anzahae, M., Campos-Olivas, R., Noronha, A.M., Wilds, C.J., Damha, M.J. and González, C. (2012) The solution structure of double helical arabinonucleic acids (ANA and 2'F-ANA): effect of arabinoses in duplex-hairpin interconversion. *Nucleic Acids Research*, **40**, 9329-9339.
7. Anzahae, M.Y., Deleavey, G.F., Le, P.U., Fakhoury, J., Petrecca, K. and Damha, M.J. (2014) Arabinonucleic Acids: 2'-Stereoisomeric Modulators of siRNA Activity. *Nucleic Acid Ther*, **24**, 336-343.
8. Wilds, C.J. and Damha, M.J. (2000) 2'-Deoxy-2'-fluoro- β -d-arabinonucleosides and oligonucleotides (2'F-ANA): synthesis and physicochemical studies. *Nucleic Acids Research*, **28**, 3625-3635.
9. Mangos, M.M., Min, K.-L., Viazovkina, E., Galarneau, A., Elzagheid, M.I., Parniak, M.A. and Damha, M.J. (2002) Efficient RNase H-Directed Cleavage of RNA Promoted by Antisense DNA or 2'F-ANA Constructs Containing Acyclic Nucleotide Inserts. *Journal of the American Chemical Society*, **125**, 654-661.
10. Kalota, A., Karabon, L., Swider, C.R., Viazovkina, E., Elzagheid, M., Damha, M.J. and Gewirtz, A.M. (2006) 2'-Deoxy-2'-fluoro- β -d-arabinonucleic acid (2'F-ANA) modified oligonucleotides (ON) effect highly efficient, and persistent, gene silencing. *Nucleic Acids Research*, **34**, 451-461.

11. Dowler, T., Bergeron, D., Tedeschi, A.-L., Paquet, L., Ferrari, N. and Damha, M.J. (2006) Improvements in siRNA properties mediated by 2'-deoxy-2'-fluoro- β -d-arabinonucleic acid (FANA). *Nucleic Acids Research*, **34**, 1669-1675.
12. Deleavey, G.F., Watts, J.K., Alain, T., Robert, F., Kalota, A., Aishwarya, V., Pelletier, J., Gewirtz, A.M., Sonenberg, N. and Damha, M.J. (2010) Synergistic effects between analogs of DNA and RNA improve the potency of siRNA-mediated gene silencing. *Nucleic Acids Research*, **38**, 4547-4557.
13. Deleavey, G.F., Frank, F., Hassler, M., Wisnovsky, S., Nagar, B. and Damha, M.J. (2013) The 5' Binding MID Domain of Human Argonaute2 Tolerates Chemically Modified Nucleotide Analogues. *Nucleic Acid Therapeutics*, **23**, 81-87.
14. Martin-Pintado, N., Deleavey, G.F., Portella, G., Campos-Olivas, R., Orozco, M., Damha, M.J. and González, C. (2013) Backbone FCH...O Hydrogen Bonds in 2'-F-Substituted Nucleic Acids. *Angewandte Chemie International Edition*, **52**, 12065-12068.
15. Li, F., Sarkhel, S., Wilds, C.J., Wawrzak, Z., Prakash, T.P., Manoharan, M. and Egli, M. (2006) 2'-Fluoroarabino- and Arabinonucleic Acid Show Different Conformations, Resulting in Deviating RNA Affinities and Processing of Their Heteroduplexes with RNA by RNase H. *Biochemistry*, **45**, 4141-4152.
16. Manoharan, M. (1999) 2'-carbohydrate modifications in antisense oligonucleotide therapy: importance of conformation, configuration and conjugation. *Biochimica et biophysica acta*, **1489**, 117-130.
17. Prakash, T.P. (2011) An overview of sugar-modified oligonucleotides for antisense therapeutics. *Chem Biodivers*, **8**, 1616-1641.
18. Deleavey, G.F. and Damha, M.J. (2012) Designing chemically modified oligonucleotides for targeted gene silencing. *Chemistry and Biology*, **19**, 937-954.
19. Gagnor, C., Bertrand, J.R., Thenet, S., Lemaître, M., Morvan, F., Rayner, B., Malvy, C., Lebleu, B., Imbach, J.L. and Paoletti, C. (1987) alpha-DNA. VI: Comparative study of alpha- and beta-anomeric oligodeoxyribonucleotides in hybridization to mRNA and in cell free translation inhibition. *Nucleic Acids Research*, **15**, 10419-10436.
20. Zamaratski, E., Pradeepkumar, P.I. and Chattopadhyaya, J. (2001) A critical survey of the structure-function of the antisense oligo/RNA heteroduplex as substrate for RNase H. *Journal of biochemical and biophysical methods*, **48**, 189-208.
21. Dunitz, J.D. (2004) Organic Fluorine: Odd Man Out. *ChemBioChem*, **5**, 614-621.
22. Howard, J.A.K., Hoy, V.J., O'Hagan, D. and Smith, G.T. (1996) How good is fluorine as a hydrogen bond acceptor? *Tetrahedron*, **52**, 12613-12622.
23. Thalladi, V.R., Weiss, H.-C., Bläser, D., Boese, R., Nangia, A. and Desiraju, G.R. (1998) C-H...F Interactions in the Crystal Structures of Some Fluorobenzenes. *Journal of the American Chemical Society*, **120**, 8702-8710.
24. Bats, J.W., Parsch, J. and Engels, J.W. (2000) 1-Deoxy-1-(4-fluorophenyl)-[beta]-d-ribofuranose, its hemihydrate, and 1-deoxy-1-(2,4-difluorophenyl)-[beta]-d-ribofuranose: structural evidence for intermolecular C-H...F-C interactions. *Acta Crystallographica Section C*, **56**, 201-205.
25. Pallan, P.S. and Egli, M. (2009) Pairing Geometry of the Hydrophobic Thymine Analogue 2,4-Difluorotoluene in Duplex DNA as Analyzed by X-ray Crystallography. *Journal of the American Chemical Society*, **131**, 12548-12549.

26. Bergstrom, D.E., Swartling, D.J., Wisar, A. and Hoffmann, M.R. (1991) Evaluation of Thymidine, Dideoxythymidine and Fluorine Substituted Deoxyribonucleoside Geometry by the MINDO/3 Technique The Effect of Fluorine Substitution on Nucleoside Geometry and Biological Activity. *Nucleosides and Nucleotides*, **10**, 693-697.
27. Frey, J.A., Leist, R. and Leutwyler, S. (2006) Hydrogen Bonding of the Nucleobase Mimic 2-Pyridone to Fluorobenzenes: An ab Initio Investigation. *The Journal of Physical Chemistry A*, **110**, 4188-4195.
28. Wright, J.A., Taylor, N.F. and Fox, J.J. (1969) Nucleosides. LX. Fluorocarbohydrates. 22. Synthesis of 2-deoxy-2-fluoro-D-arabinose and 9-(2-deoxy-2-fluoro-.alpha. and .beta.-D-arabinofuranosyl)adenines. *The Journal of Organic Chemistry*, **34**, 2632-2636.
29. Barchi, J.J., Marquez, V.E., Driscoll, J.S., Ford, H., Mitsuya, H., Shirasaka, T., Aoki, S. and Kelley, J.A. (1991) Potential anti-AIDS drugs. Lipophilic, adenosine deaminase-activated prodrugs. *Journal of Medicinal Chemistry*, **34**, 1647-1655.
30. Biamonte, M.A. and Vasella, A. (1998) Glycosylidene Carbenes part 26. The intramolecular F...HO hydrogen bond of 1,3-diaxial 3-fluorocyclohexanols. *Helvetica Chimica Acta*, **81**, 695-717.
31. Barbarich, T.J., Rithner, C.D., Miller, S.M., Anderson, O.P. and Strauss, S.H. (1999) Significant Inter- and Intramolecular O-H...FC Hydrogen Bonding. *Journal of the American Chemical Society*, **121**, 4280-4281.
32. Leist, R., Frey, J.A. and Leutwyler, S. (2006) Fluorobenzene–Nucleobase Interactions: Hydrogen Bonding or π -Stacking? *The Journal of Physical Chemistry A*, **110**, 4180-4187.
33. Kool, E.T. and Sintim, H.O. (2006) The difluorotoluene debate-a decade later. *Chemical Communications*, 3665-3675.
34. A. Evans, T. and R. Seddon, K. (1997) Hydrogen bonding in DNA-a return to the status quo. *Chemical Communications*, 2023-2024.
35. Schweitzer, B.A. and Kool, E.T. (1994) Aromatic Nonpolar Nucleosides as Hydrophobic Isosteres of Pyrimidines and Purine Nucleosides. *The Journal of Organic Chemistry*, **59**, 7238-7242.
36. Moran, S., Ren, R.X.F., Rumney and Kool, E.T. (1997) Difluorotoluene, a Nonpolar Isostere for Thymine, Codes Specifically and Efficiently for Adenine in DNA Replication. *Journal of the American Chemical Society*, **119**, 2056-2057.
37. Moran, S., Ren, R.X.-F. and Kool, E.T. (1997) A thymidine triphosphate shape analog lacking Watson–Crick pairing ability is replicated with high sequence selectivity. *Proceedings of the National Academy of Sciences*, **94**, 10506-10511.
38. Parsch, J. and Engels, J.W. (2002) C–F...H–C Hydrogen Bonds in Ribonucleic Acids. *Journal of the American Chemical Society*, **124**, 5664-5672.
39. Parsch, J. and Engels, J.W. (2000) Synthesis of Fluorobenzene and Benzimidazole Nucleic-Acid Analogues and Their Influence on Stability of RNA Duplexes. *Helvetica Chimica Acta*, **83**, 1791-1808.
40. Sun, Z. and McLaughlin, L.W. (2007) Probing the Nature of Three-Centered Hydrogen Bonds in Minor-Groove Ligand–DNA Interactions: The Contribution of Fluorine Hydrogen Bonds to Complex Stability. *Journal of the American Chemical Society*, **129**, 12531-12536.

41. Koller, A.N., Božilović, J., Engels, J.W. and Gohlke, H. (2010) Aromatic N versus aromatic F: bioisosterism discovered in RNA base pairing interactions leads to a novel class of universal base analogs. *Nucleic Acids Research*, **38**, 3133-3146.
42. Pallan, P.S., Greene, E.M., Jicman, P.A., Pandey, R.K., Manoharan, M., Rozners, E. and Egli, M. (2011) Unexpected origins of the enhanced pairing affinity of 2'-fluoro-modified RNA. *Nucleic Acids Research*, **39**, 3482-3495.
43. Patra, A., Paolillo, M., Charisse, K., Manoharan, M., Rozners, E. and Egli, M. (2012) 2'-Fluoro RNA Shows Increased Watson–Crick H-Bonding Strength and Stacking Relative to RNA: Evidence from NMR and Thermodynamic Data. *Angewandte Chemie International Edition*, **51**, 11863-11866.
44. Herdewijn, P., Aerschot, A.V. and Kerremans, L. (1989) Synthesis of Nucleosides Fluorinated in the Sugar Moiety. The Application of Diethylaminosulfur Trifluoride to the Synthesis of Fluorinated Nucleosides. *Nucleosides and Nucleotides*, **8**, 65-96.
45. Thomas, G.J. and Livramento, J. (1975) Kinetics of hydrogen-deuterium exchange in adenosine 5'-monophosphate, adenosine 3':5'-monophosphate, and poly(riboadenylic acid) determined by laser-Raman spectroscopy. *Biochemistry*, **14**, 5210-5218.
46. Dingley, A.J., Cordier, F. and Grzesiek, S. (2001) An introduction to hydrogen bond scalar couplings. *Concepts in Magnetic Resonance*, **13**, 103-127.
47. Dingley, A.J. and Grzesiek, S. (1998) Direct Observation of Hydrogen Bonds in Nucleic Acid Base Pairs by Internucleotide 2JNN Couplings. *Journal of the American Chemical Society*, **120**, 8293-8297.
48. Sapse, A.M. and Snyder, G. (1985) Ab initio studies of the antiviral drug 1-(2-fluoro-2-deoxy-beta-D-arabinofuranosyl) thymine. *Cancer Invest.*, **3**, 115-121.
49. Peng, C.G. and Damha, M.J. (2007) G-quadruplex induced stabilization by 2'-deoxy-2'-fluoro-D-arabinonucleic acids (2'F-ANA). *Nucl. Acids Res.*, **35**, 4977-4988.
50. Markiewicz, W.T. and Wiewiórowski, M. (1978) A new type of silyl protecting groups in nucleoside chemistry. *Nucl. Acids Res.*, **5**, **Suppl.1** s185-s190.
51. Watts, J.K. and Damha, M.J. (2008) 2'F-Arabinonucleic acids (2'F-ANA) — History, properties, and new frontiers. *Canadian Journal of Chemistry*, **86**, 641-656.
52. Corey, E.J. and Lee, T.W. (2001) The formyl C-HO hydrogen bond as a critical factor in enantioselective Lewis-acid catalyzed reactions of aldehydes. *Chemical Communications*, 1321-1329.
53. Manalo, M.N., Kong, X. and LiWang, A. (2005) 1JNH Values Show that N1···N3 Hydrogen Bonds Are Stronger in dsRNA A:U than dsDNA A:T Base Pairs. *Journal of the American Chemical Society*, **127**, 17974-17975.
54. Egli, M. (1996) Structural Aspects of Nucleic Acid Analogs and Antisense Oligonucleotides. *Angewandte Chemie International Edition in English*, **35**, 1894-1909.
55. Deleavey, Glen F. and Damha, Masad J. Designing Chemically Modified Oligonucleotides for Targeted Gene Silencing. *Chemistry & Biology*, **19**, 937-954.
56. Fortin, M., D'Anjou, H., Higgins, M.-E., Gougeon, J., Aube, P., Moktefi, K., Mouissi, S., Seguin, S., Seguin, R., Renzi, P. *et al.* (2009) A multi-target antisense approach against PDE4 and PDE7 reduces smoke-induced lung inflammation in mice. *Respiratory Research*, **10**, 39.

57. Oda, Y., Iwa, S., Ohtsuka, E., Ishikawa, M., Ikehara, M. and Nakamura, H. (1993) Binding of nucleic acids to E.coli RNase HI observed by NMR and CD spectroscopy. *Nucleic Acids Research*, **21**, 4690-4695.
58. Nakamura, H., Oda, Y., Iwai, S., Inoue, H., Ohtsuka, E., Kanaya, S., Kimura, S., Katsuda, C., Katayanagi, K. and Morikawa, K. (1991) How does RNase H recognize a DNA.RNA hybrid? *Proceedings of the National Academy of Sciences*, **88**, 11535-11539.
59. Martín-Pintado, N., Yahyaee-Anzahaee, M., Deleavey, G.F., Portella, G., Orozco, M., Damha, M.J. and González, C. (2013) Dramatic Effect of Furanose C2' Substitution on Structure and Stability: Directing the Folding of the Human Telomeric Quadruplex with a Single Fluorine Atom. *Journal of the American Chemical Society*, **135**, 5344-5347.
60. Sandell, L.L. and Zakian, V.A. Loss of a yeast telomere: Arrest, recovery, and chromosome loss. *Cell*, **75**, 729-739.
61. Paeschke, K., Simonsson, T., Postberg, J., Rhodes, D. and Lipps, H.J. (2005) Telomere end-binding proteins control the formation of G-quadruplex DNA structures in vivo. *Nat Struct Mol Biol*, **12**, 847-854.
62. Burge, S., Parkinson, G.N., Hazel, P., Todd, A.K. and Neidle, S. (2006) Quadruplex DNA: sequence, topology and structure. *Nucleic Acids Research*, **34**, 5402-5415.
63. Phan, A.T. (2010) Human telomeric G-quadruplex: structures of DNA and RNA sequences. *FEBS Journal*, **277**, 1107-1117.
64. Peng, C.G. and Damha, M.J. (2007) G-quadruplex induced stabilization by 2'-deoxy-2'-fluoro-d-arabinonucleic acids (2'F-ANA). *Nucleic Acids Research*, **35**, 4977-4988.
65. Lech, C.J., Li, Z., Heddi, B. and Phan, A.T. (2012) 2[prime or minute]-F-ANA-guanosine and 2[prime or minute]-F-guanosine as powerful tools for structural manipulation of G-quadruplexes. *Chemical Communications*, **48**, 11425-11427.
66. Doluca, O., Withers, J.M. and Filichev, V.V. (2013) Molecular Engineering of Guanine-Rich Sequences: Z-DNA, DNA Triplexes, and G-Quadruplexes. *Chemical Reviews*, **113**, 3044-3083.
67. Phan, A.T. and Patel, D.J. (2003) Two-Repeat Human Telomeric d(TAGGGTTAGGGT) Sequence Forms Interconverting Parallel and Antiparallel G-Quadruplexes in Solution: Distinct Topologies, Thermodynamic Properties, and Folding/Unfolding Kinetics. *Journal of the American Chemical Society*, **125**, 15021-15027.
68. Parkinson, G.N., Lee, M.P.H. and Neidle, S. (2002) Crystal structure of parallel quadruplexes from human telomeric DNA. *Nature*, **417**, 876-880.
69. Anzahaee, M.Y., Watts, J.K., Alla, N.R., Nicholson, A.W. and Damha, M.J. (2010) Energetically Important C-H...F-C Pseudohydrogen Bonding in Water: Evidence and Application to Rational Design of Oligonucleotides with High Binding Affinity. *Journal of the American Chemical Society*, **133**, 728-731.
70. Mehta, G. and Sen, S. (2010) Probing Fluorine Interactions in a Polyhydroxylated Environment: Conservation of a C-F...H-C Recognition Motif in Presence of O-H...O Hydrogen Bonds. *European Journal of Organic Chemistry*, **2010**, 3387-3394.
71. Dalvit, C. and Vulpetti, A. (2012) Intermolecular and Intramolecular Hydrogen Bonds Involving Fluorine Atoms: Implications for Recognition, Selectivity, and Chemical Properties. *ChemMedChem*, **7**, 262-272.

72. Berger, I., Egli, M. and Rich, A. (1996) Inter-strand C-H...O hydrogen bonds stabilizing four-stranded intercalated molecules: stereoelectronic effects of O4' in cytosine-rich DNA. *Proceedings of the National Academy of Sciences*, **93**, 12116-12121.
73. Jiang, L. and Lai, L. (2002) CH...O Hydrogen Bonds at Protein-Protein Interfaces. *J. Biol. Chem.*, **277**, 37732-37740.
74. Horowitz, S., Yesselman, J.D., Al-Hashimi, H.M. and Trievel, R.C. (2011) Direct Evidence for Methyl Group Coordination by Carbon-Oxygen Hydrogen Bonds in the Lysine Methyltransferase SET7/9. *J. Biol. Chem.*, **286**, 18658-18663.
75. Giannaris, P.A. and Damha, M.J. (1994) Hybridization properties of oligoarabinonucleotides. *Canadian Journal of Chemistry*, **72**, 909-918.
76. Damha, M. and Ogilvie, K. (1993) In Agrawal, S. (ed.), *Protocols for Oligonucleotides and Analogs*. Humana Press, Vol. 20, pp. 81-114.
77. Bellon, L. (2001) Oligoribonucleotides with 2'-O-(tert-Butyldimethylsilyl) Groups. *Current protocols in nucleic acid chemistry*, **Unit 3.6.1-3.6.13**.
78. Westman, E. and Stromberg, R. (1994) Removal of t-butyldimethylsilyl protection in RNA-synthesis. Triethylamine trihydrofluoride (TEA, 3HF) is a more reliable alternative to tetrabutylammonium fluoride (TBAF). *Nucleic Acids Research*, **22**, 2430-2431.
79. Cerritelli, S.M. and Crouch, R.J. (1998) Cloning, Expression, and Mapping of Ribonucleases H of Human and Mouse Related to Bacterial RNase HI. *Genomics*, **53**, 300-307.
80. Piotto, M., Saudek, V. and Sklenář, V. (1992) Gradient-tailored excitation for single-quantum NMR spectroscopy of aqueous solutions. *J Biomol NMR*, **2**, 661-665.
81. Goddard, D.T.a.K., D.G. . SPARKY, 3rd ed. University of California, San Francisco.

CHAPTER 3: THE SOLUTION STRUCTURE OF DOUBLE HELICAL ARABINO NUCLEIC ACIDS: EFFECT OF ARABINOSES IN DUPLEX-HAIRPIN INTERCONVERSION

3.1 ANA versus 2'F-ANA: An Overview

The increasing number of promising applications for chemically modified nucleic acids range from new antisense/siRNA therapies to the design of DNA-based nanodevices, diagnostics, high-throughput genomics and target validation. For this reason, investigations directed towards gaining a better understanding on structural effects of chemical modifications on nucleic acid function is a field of significant importance.

Among the many modified nucleic acids, and specifically those with modifications in their sugar moiety, arabino nucleic acid and its 2'-fluorinated derivative (ANA and 2'F-ANA respectively; Figure 3.1) are particularly interesting (1-4).

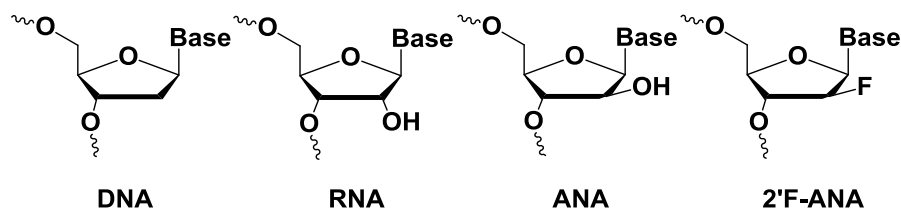


Figure 3.1 Chemical structures of ANA and 2'F-ANA in comparison with DNA and RNA.

The attractiveness of arabinose modified oligonucleotides was first based on their nuclease resistance and their ability to bind to target mRNA and elicit enzymatic degradation of target mRNA (5-8). Since then, many other applications for ANA have been reported in the literature.

For instance, arabinose nucleotide derivatives have been used as *in vivo* cellular DNA labels (9). ANA has also found its way into the realm of synthetic biology and has become an attractive system for studying the evolution of functional biopolymers using *in vitro* selection (10,11). Recent work on ANA, 2'F-ANA and other nucleic acid analogues has been inspired by the desire to construct genetic systems based on alternative chemical platforms (12).

As discussed in chapter two of the present thesis, despite the close similarity between ANA and 2'F-ANA, their binding affinities for RNA are strikingly different (7,8,13-15). ANA binds to RNA with relatively low affinity, whereas 2'F-ANA forms thermally stable hybrids with RNA. The solution structure of 2'F-ANA:RNA and ANA:RNA hybrid duplexes, as determined in a previous study (15), reveals that the different binding affinity between these two derivatives is related to several factors, among them a favourable inter-residual pseudohydrogen bond (2'F...purine H8) that contrasts with unfavourable inter 2'-OH...nucleobase steric clash in the case of ANA:RNA hybrid duplexes. In 2'F-ANA:RNA hybrids, noncovalent pseudohydrogen bonding interactions occur between consecutive residues (15,16). Although the structures of these hybrids retain many features of the A-form family of double-stranded helices, 2'F-arabinoses adopt a south/east sugar pucker instead of a north pucker. This contrasts the common north sugar pucker of pure A-form duplexes. This particular south/east sugar pucker conformation provokes the close proximity between F2' and H8 atoms of pyrimidine–purine steps as well as a favourable geometry for sequential pseudohydrogen bond formation (co-linearity of C8-H8-2'F) (16).

Besides its high binding affinity toward RNA, 2'F-ANA also binds to itself to form very stable 2'F-ANA:2'F-ANA B-like duplexes (4). ANA, unlike its C2'-epimer (RNA) or its F2' cousin

(2'F-ANA), forms ANA:ANA duplexes of very poor thermal stability. The origin of such difference in thermal stability between 2'F-ANA:2'F-ANA and ANA:ANA duplexes, as well as the structural analysis of pure 2'F-ANA and pure ANA duplexes have remained largely unexplored. Thus, in an extension to our research on properties and structural analysis of arabino-based oligonucleotides, and in a collaboration with Prof. Carlos Gonzalez lab at the CSIC in Spain, we aimed to study the stability and structure of 2'F-ANA:2'F-ANA and ANA:ANA duplexes.

In the work discussed in chapter two, we studied hybrids of ANA and 2'F-ANA with RNA. This chapter will investigate the structural features of pure 2'F-ANA:2'F-ANA and ANA:ANA duplexes. We have focused on analysis of arabino modified chimeric dodecamer shown in Figure 3.2, and via combining thermal denaturation experiments, high resolution NMR and restrained molecular dynamics, we have shown that while ANA:ANA duplexes are too unstable to be detected under normal conditions, an appropriate combination of 2'F-ANA and ANA nucleotides can be used to force ANA to bind to a complementary ANA strand with sufficient stability that permitted the structural characterization of an ANA:ANA duplex for the first time.

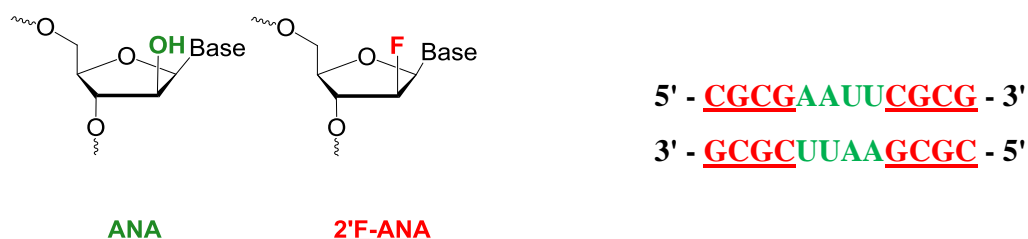


Figure 3.2 Self-complementary duplex designed to study the differential stabilities of ANA:ANA and 2'F-ANA:2'F-ANA base pairs.

3.2 Sequence Design and Thermal Melting of Arabinose Modified Chimeric Dodecamers

Self-complementary oligonucleotide duplexes (AA), gap(FA), and alt (AF) were designed based on the Dickerson-Drew dodecamer sequence (17) (Table 3.1). As well, self-complementary RNA:RNA (RR), DNA:DNA (DD), 2'FANA:2'F-ANA (FF), gap(FD), and alt (DF) control duplexes were included in this study. Melting temperatures (T_m) are given in Table 3.1. Corresponding normalized melting curves are presented in Figure 3.12.

Table 3.1 T_m values for the self-complementary chimeric duplexes

Name	Sequence (5'-3')	T_m (°C)
DD	5'-CGCGAATTCGCG-3'	58.4
RR	5'-CGCGAAUUCGCG-3'	65.1
FF	5'-CGCGAATTCGCG-3'	76.1
AA	5'-CGCGAAUUCGCG-3'	–
alt (AF)	5'-CGCGAAUUCGCG-3'	35.9
alt (DF)	5'-CGCGAATTCGCG-3'	59.9
gap (FA)	5'-CGCGAAUUCGCG-3'	55.0
gap (FD)	5'-CGCGAATTCGCG-3'	57.8

Buffer conditions: 140mM KCl, 1mM MgCl₂ and 5mM Na₂HPO₄, pH 7.2). Legend: **2'F-ANA**, **RNA**, **DNA** and **ANA**. Duplex concentration is 2μM.

The FF duplex, containing only 2'F-ANA nucleotides, exhibits the highest thermal stability. AA with only ANA nucleotides does not form a duplex of measurable thermal stability. Comparison between the 1–1 altimer (alt(AF)) or gapmer (gap(FA)) designs with the all 2'F-ANA modified duplex (FF) shows that insertion of ANA nucleotides in the sequence is destabilizing. However, gap(FA) is especially interesting. Its T_m value is somewhat comparable to the T_m value of gap(FD) control duplex that contains DNA and 2'F-ANA nucleotides and has no destabilizing ANA modification (Table 3.1). This suggest that although gap(FA) contains a continuous tract of ANA units, the insertion of 2'F-ANA nucleotides on the flanks and around the ANA units

counterbalances the destabilizing effect of ANAs to the extent that now enables duplex formation.

To verify this, we conducted a combination of 2D correlation and NOE NMR experiments at different oligonucleotide concentrations. Interestingly, the NMR experiments recorded at low oligonucleotide concentrations were indicative of duplex-hairpin equilibrium as illustrated in Figure 3.3a. Since the equilibrium between the duplex and hairpin species was a kinetically slow process on the NMR time scale, we were able to determine the 3D solution structures of both gap(FA) species independently. The results of these experiments are the focus of the following sections.

3.3 Duplex-Hairpin Equilibrium

3.3.1 Evidence of Unimolecular Hairpin Structure

Evidence of unimolecular hairpin structure came from NMR experiments. One of the simplest ways to detect Watson–Crick A:T, A:U, and G:C base pairs is via 1D ^1H -NMR spectrum recorded at lower temperatures (5–15°C) in $\text{H}_2\text{O}/\text{D}_2\text{O}$ solution and in a slightly acidic buffer (~pH 6) in order to slow down the rapid exchange of labile base protons with the surrounding solvent.

There are several classes of labile (exchangeable) protons in natural oligonucleotides, i.e., imino protons, amino protons, and hydroxyl protons. The imino and amino protons are the -NH and - NH_2 protons of the heterocyclic nucleobases that are involved in the formation of inter-chain Watson-Crick hydrogen bonds (Figure 3.3b). The imino protons resonance far downfield from other protons (12-14.5ppm) and only one imino resonance is contributed by each base pair.

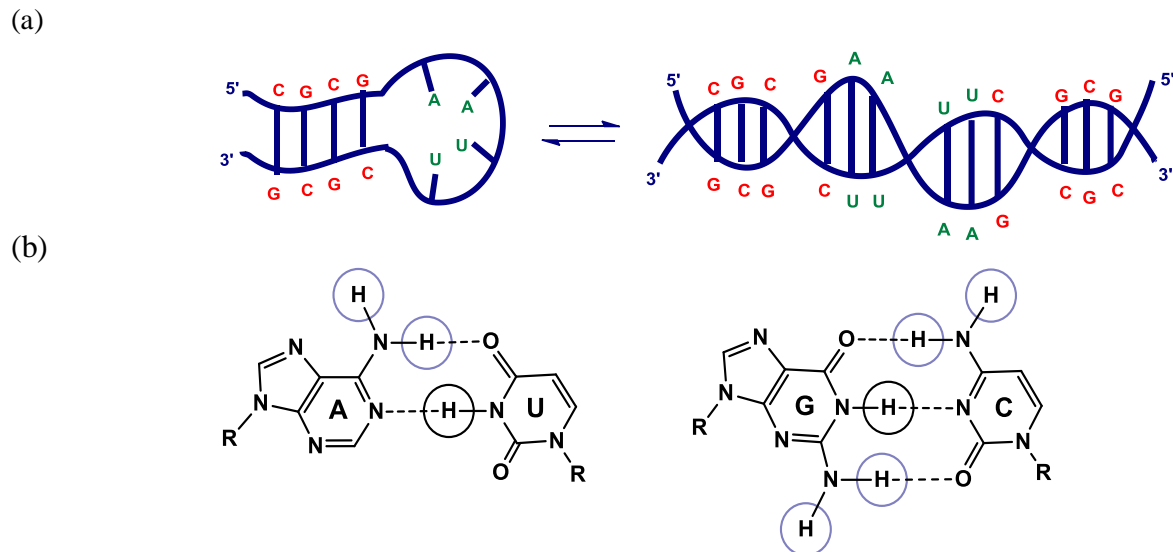


Figure 3.3 (a) Schematic illustration of dissociation of hairpin (left) and duplex (right) structures of gap(FA); (b) Representation of the exchangeable protons, imino (-NH proton highlighted with black circles) and amino (-NH₂ protons highlighted with blue circles), which are involved in formation of Watson-Crick hydrogen bonds.

The imino region of the 1D proton NMR spectra of gap(FA) is particularly informative (Figure 3.3). At low concentrations, only signals corresponding to imino protons of C:G base pairs are observed and no signal corresponding to imino proton of a A:U pair is detected. This observation clearly suggests the formation of a hairpin structure in which the stems contain 2'F-ANA C:G pairs and the loop consists of four unpaired ANA nucleotides. At high oligonucleotide concentrations, however, the imino region reflects the formation of a double-stranded duplex structure. We observed five out of six exchangeable imino resonances for the self-complementary Dickerson-Drew sequence which is consistent with the formation of a twelve WC base-paired duplex with 2-fold symmetry in solution (Figure 3.4).

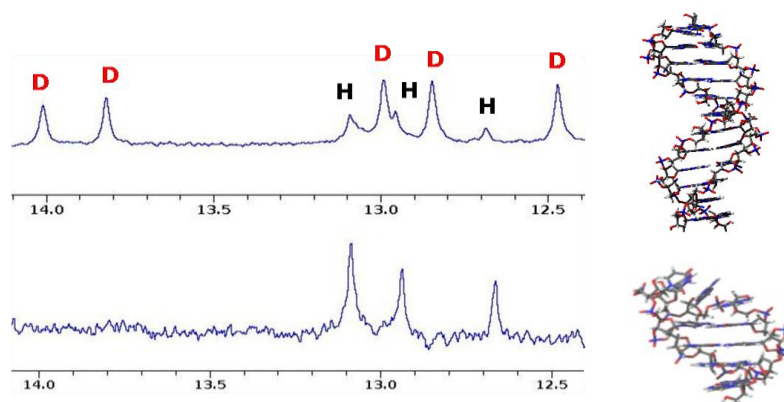


Figure 3.4 Imino region of the ^1H -NMR spectra of 5'-CGCGAAUUCGCG-3' at two different oligonucleotide concentrations: top: 0.9mM and bottom: 0.2mM (phosphate buffer 100mM NaCl,pH=7). **D** labels on the figure stand for duplex and **H** labels for hairpin. Legend: 2F-ANA, ANA.

3.3.2 NMR Melting Experiments

NMR and UV thermal denaturation experiments provide equivalent means for determining T_m values for cooperative transitions only if they are run at comparable duplex and salt concentrations. Thus, the observation of a hairpin species at low NMR concentrations suggests that the monophasic UV melting curve ($T_m = 55^\circ\text{C}$; Table 3.1) recorded for gap(FA) at low duplex concentrations corresponds, in fact, to the unimolecular hairpin denaturation and not to duplex dissociation. Since the equilibrium between duplex and hairpin species exhibits a slow kinetics on the NMR time scale— the exchange process is slow compared with the chemical shift difference between the two resonances of the same proton— their melting processes and stabilities relative to each other could be studied independently by temperature-dependent ^1H or ^{19}F NMR spectroscopy (Figure 3.5). Both ^1H -NMR and ^{19}F -NMR spectroscopy are particularly useful techniques to monitor and investigate the dynamics and thermodynamics of order-disorder transitions in nucleic acid double helices over a range of temperatures (18-20). The chemical

shifts and widths of signals in duplex state can be different from those in single strands, and thus the unwinding of a duplex can be monitored using these changes.

As shown in Figure 3.5, at high gap(FA) concentrations both ^1H -NMR spectra of imino protons and ^{19}F -NMR spectra recorded at different temperatures indicate that hairpin and duplex species have similar melting temperatures and thus are of similar thermal stabilities.

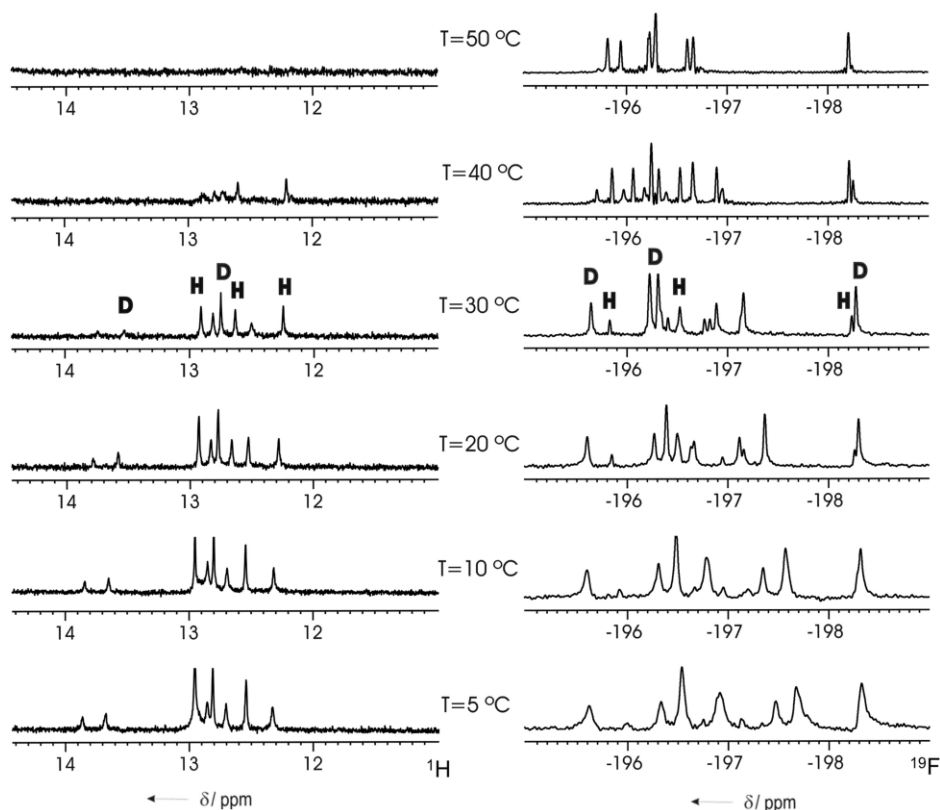


Figure 3.5 Temperature-dependent 1D NMR experiments. (left) Imino region (12-14 ppm) of the ^1H -NMR; and (right) complete ^{19}F -NMR spectra of gap(FA) at different temperatures. **D** labels on the figure stand for duplex and **H** labels stand for hairpin. Oligonucleotide concentration is 0.8mM in the same buffer conditions as in Figure 3.4).

We also compared the temperature-dependent ^1H -NMR spectra of gap(FA) with that of the unmodified DNA (DD) control. All the imino proton signals of the DNA control duplex started to disappear together at the same temperature, with the only exception being the imino protons of

the terminal base pairs (Figure 3.6). However, for the gap(FA) sequence, ANA imino protons located in the central region of the duplex disappeared more readily and at much lower temperatures compared with imino protons of the 2'F-ANA flanks in gap(FA). Such behaviour indicates that ANA:ANA segment is less stable than both the DNA:DNA pairs in DD and the 2'F-ANA:2'F-ANA segment in gap(FA).

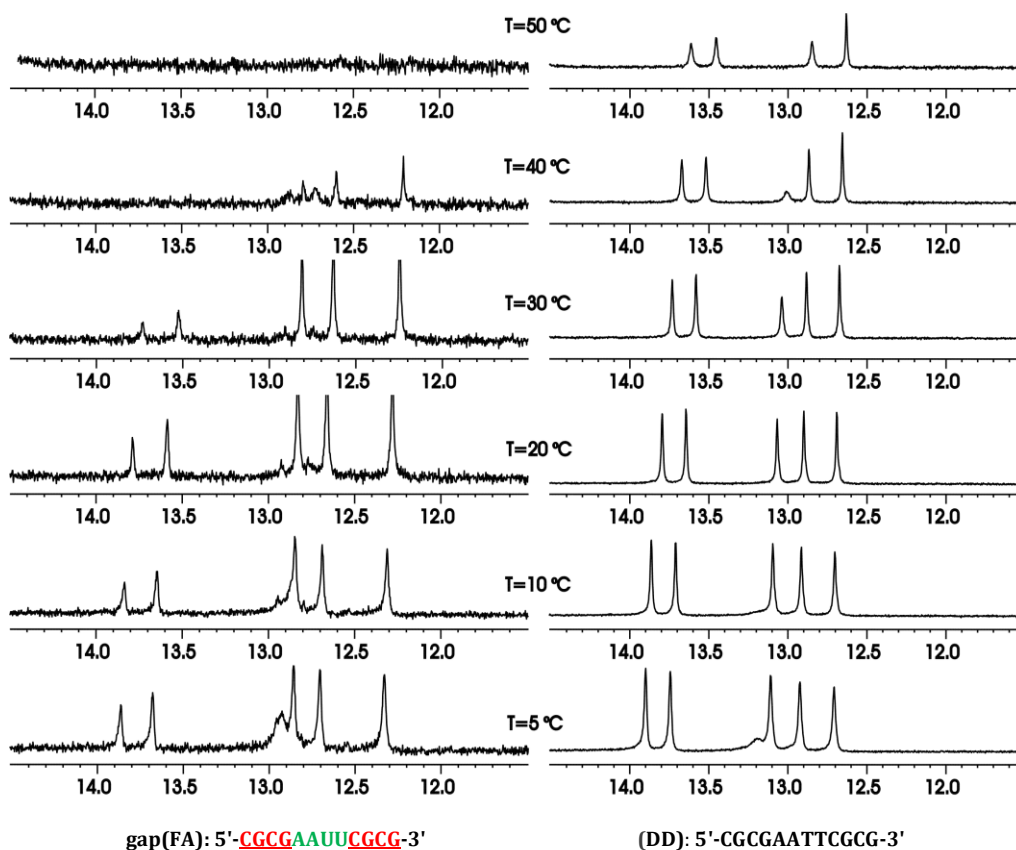


Figure 3.6 Comparison between the ^1H -NMR spectra of gap(FA) (left) and control DNA sequence (DD) (right) at different temperatures. Oligonucleotide concentration is 0.9mM, in the same buffer conditions as in Figure 3.4. Legend: DNA, 2'F-ANA, ANA.

3.3.3 Thermodynamic Parameters for the Hairpin to Duplex Equilibrium

Since the equilibrium between the duplex and the hairpin is slow on the NMR time scale, we could observe the resonances from both hairpin and duplex species simultaneously under appropriate conditions, and determine the equilibrium constant (K_{eq}) based on the ratio of the areas of equivalent peaks. The thermodynamic parameters for the hairpin-to-duplex equilibrium were then estimated from the van't Hoff analysis of the equilibrium constants:

$$\ln(K_{eq}) = -\Delta H^\circ/RT + \Delta S^\circ/R$$

We determined the equilibrium constant from the relative intensities of equivalent fluorine signals in the ^{19}F -NMR spectra recorded over a variety of temperatures, assuming that at each specific temperature, the ^{19}F peak areas represent the concentration of the corresponding duplex or hairpin structure at that temperature. We carried out our analysis at temperatures somewhat below the T_m of both species, where the two-state approximation is valid. Next, the equilibrium constants were plotted on a graph with $\ln(K_{eq})$ on the Y-axis and $1/T$ on the X-axis, and linear regression of the experimental data yielded a line with a slope of $-\Delta H^\circ/R$ and an intercept of $\Delta S^\circ/R$ (Figure 3.7).

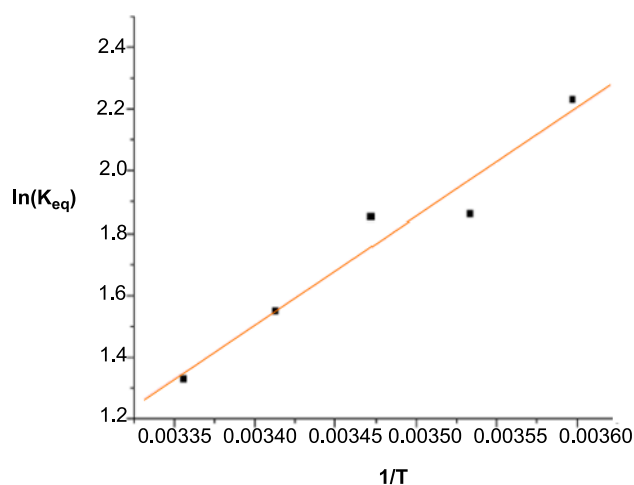


Figure 3.7 van't Hoff plot of $\ln(K_{eq})$ vs. $1/T$ for gap(FA). The positive slope of the van't Hoff plot implies that the hairpin-to-duplex conversion is an exothermic process, in which energy is released.

The resulting values for $\Delta G^\circ_{(\text{hairpin-to-duplex})}$, ΔH° and $T\Delta S^\circ$ at 25°C are -0.7 kcal/mol, -6.6 kcal/mol and -5.9 kcal/mol·K, respectively. The negative and somewhat small value of ΔG° indicates that the duplex is “slightly” more stable than the hairpin under these experimental conditions. As expected for a hairpin to duplex conversion, the ΔS is negative. However, its value is surprisingly small, which could be attributed to better hydration of the hairpin structure. The arabinose 2'-OH groups are more solvent exposed in the loop than in the duplex, which yields in a more ordered solvent network around the loop. Dehydration of 2'-OH groups and interruption of this ordered solvent network around the hairpin is required for its conversion to duplex. This effect may, in part, explain the small entropy difference between the two conformations (states).

The small negative enthalpy change between duplex and hairpin forms suggests that the contribution of ANA:ANA base pairs to the stability of the duplex is only marginal.

3.4 NMR-Based Structure Determination of gap(FA)

All NMR experiments and structure determination calculations described below were accomplished in collaboration with Prof. Gonzalez at the CSIC in Spain. Thanks to a Research Mobility Grant (Department of Chemistry, McGill University), I had the opportunity to spend two months in the Gonzalez lab and learn NMR techniques through performing the required experiments under the direction of Prof. Gonzalez, and with close help of Dr. Nerea Martin Pintado, a former member of the Gonzalez lab.

3.4.1 Introduction

NMR, in conjunction with appropriate computational searching algorithms, has become the method of choice for determining solution structure of nucleic acids (21-23). The general

procedure to characterize the nucleic acid structure by NMR is summarized in scheme 3.2. Briefly, the resonances have to be assigned first and then structural constraints have to be collected (24-30). Inter-proton distances are established from individual 2D NOE cross peak intensities ($\text{NOE} \sim 1/r^6$) (31-33). Because base protons and sugar protons are separated by a minimum of four bonds, spin couplings are not usually observed between these units and NOE measurements are used alternatively to determine the sugar and base sequential connectivities. Bond torsion angles can be determined using Karplus-type relation (34-36) and vicinal coupling constants (3J), which are obtained from various correlation spectroscopic techniques— e.g. COSY, TOCSY. In principal, these should make it possible to determine the sugar ring pucker conformations.

Heteronuclear coupling between ^1H and ^{31}P can also be used to draw sequential connectivities between residues (27,37). This is possible because there is a continuous array of homonuclear and heteronuclear couplings along the oligonucleotide backbone.

The NMR-derived structural constraints are then used to search conformational space for a single energetically feasible model that is most compatible with all restraints. A variety of search tools is available, including restrained molecular dynamics (rMD) (38) (e.g. AMBER, GROMOS, XPLOR), and distance geometry (DG) in conjunction with back calculations.

Indeed, the ability to determine the solution structures by NMR is limited by the quantity, accuracy, and distribution of structural restraints that can be extracted from the NMR data. The accuracy of the derived NMR structure can be assessed by back-calculating the NOE intensities and torsion angles and comparing them with the observed experimental values, analogous to that used in crystallography

I. Sample Preparation

Preparation of mM quantities
Monitor imino protons in 1D Spectra
Establish appropriate solution conditions:
e.g., pH, salts, detergents (stable, not aggregated)

Non-exchangeable Protons

Exchangeable Protons

II. NMR-Data Accumulation

Resonance Assignments

D_2O

experiments
that can be
done without
labelling

$^1H, ^1H$ -NOESY
 $^1H, ^1H$ -COSY/TOCSY
 $^1H, ^{31}P$ -Correlations
 $^1H, ^{13}C$ -Correlations

$^1H, ^{13}C$ -Ribose Correlations
 $^1H, ^{13}C, ^{15}N$ -Ribose/Base Correlations
 $^1H, ^{13}C, ^{31}P$ -Backbone Correlations

Collecting Structural Restraints

NOEs, Torsion Angles,
Dipolar Couplings, Cross-Correlated Relation Rates

H_2O

$^1H, ^1H$ -NOESY

$^1H, ^{15}N$ -Correlations
 $^1H, ^{15}N$ H-bond Correlations
 $^1H, ^{13}C, ^{15}N$ -Base Correlations

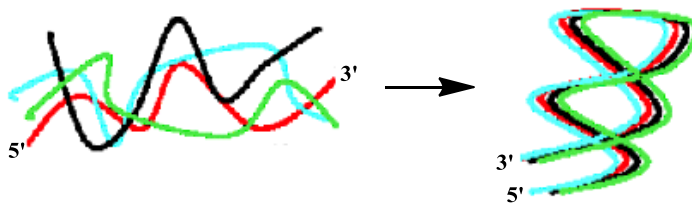
III. Structure Calculations

Generation of the Restraint File

Bond Distances, Bond Angles, J-couplings, Dipolar couplings,
Cross-Correlated Relation Rates

Molecular Dynamics Calculations

Structural Statistics



-AMBER (Assisted Model building and Energy Refinement); Available from
<http://www.igc.ethz.ch/gromos/>

-GROMOS (Groningen Molecular Simulation); Available from <http://www.igc.ethz.ch/gromos/>

-CHARMM (Chemistry at Harvard Macromolecular Mechanics). The fore-runner of n X-PLOR
and CNS; the latter is available from <http://cns.csb.yale.edu/v1.1/>

Scheme 3.1 Description of general approach for 3D structure determination of oligonucleotides using NMR in conjunction with conformational searching procedures.

3.4.2 Description of the Duplex and Hairpin Structures Associated with gap(FA) Sequence

Herein, employing the same methodology as shown in scheme 3.1, first the sequential assignments of nonexchangeable proton resonances of gap(FA) were performed following standard methods for right-handed double-stranded nucleic acids (24-27). Structural constraints were extracted from analysis of DQF-COSY, TOCSY and 2D NOESY and then used to calculate 3D structures of both species associated with the gap(FA) sequence by restrained molecular dynamics (rMD) (see experimental method sections 3.9.4 to 3.9.6).

The 2D NMR experiments and rMD calculations were accomplished in collaboration with the Gonzalez lab at the CSIC in Spain, and only some brief highlights of these experiments are discussed here. More details can be found in [Martín-Pintado, N., Yahyaee Anzahae, M. *et al.* (2012) *Nucleic Acids Research*, 40, 9329-9339].

At high oligonucleotide concentrations, the complete assignment of ^1H and ^{19}F resonances of both species was carried out by the analysis of experiments recorded at different temperatures and different oligonucleotide concentrations. The assignment pathways of the low-concentration species could not be followed between loop residues A6 to C9 because of the loss of sequential connectivities. The observed NOESY cross peak patterns confirmed that all bases in the double-stranded duplex and in the stems of the hairpin structure are forming Watson–Crick hydrogen bonds. Some typical NOE cross peak patterns observable in Watson-Crick hydrogen bonding of antiparallel duplexes are highlighted in Figure 3.8.

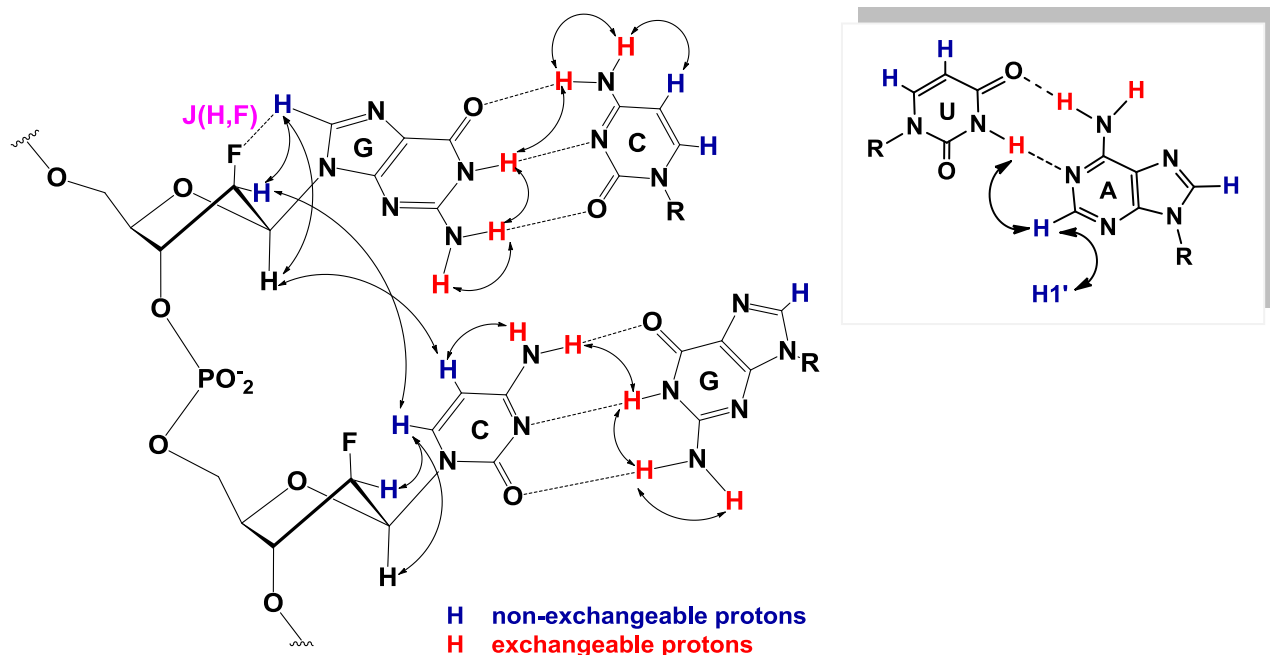
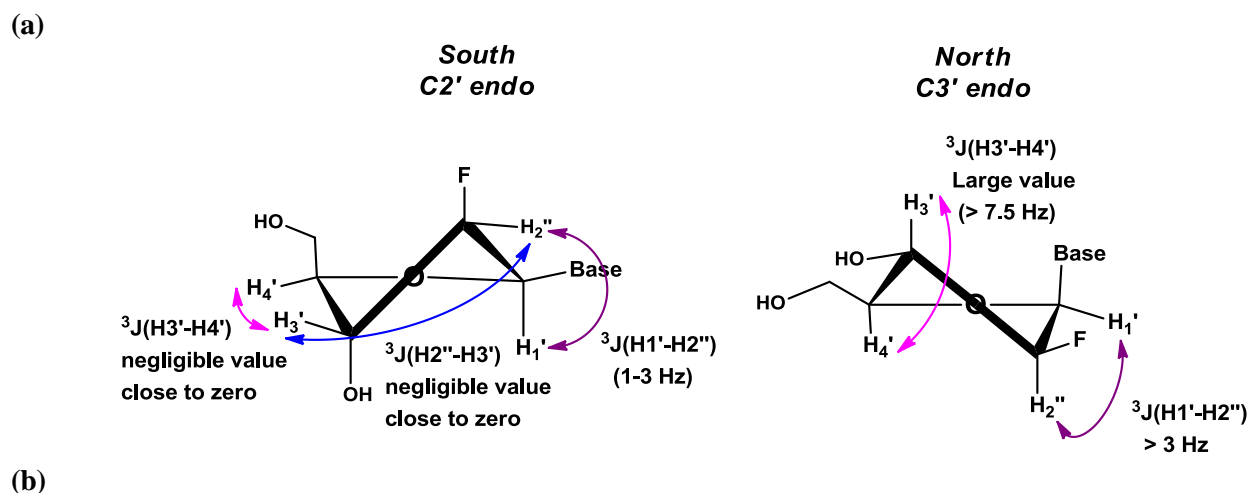


Figure 3.8 Schematic illustration of intra-nucleotide and sequential base-sugar NOEs in 2'F-ANA modified B-type duplex, along with some NOEs observed over canonical Watson-Crick hydrogen bonds. Arrows indicate the through-space connectivities.

In addition to the NOE-derived information, semi-quantitative analysis of the J-coupling constants obtained from DQF-COSY spectra was carried out. For 2'F-ANA nucleotides, $J(\text{H1}',\text{H2}'')$ values are between 1 and 3 Hz and $J(\text{H3}',\text{H2}'')$ values are almost zero, whereas $J(\text{H1}',\text{H2}'')$ and $J(\text{H3}',\text{H2}'')$ values are both negligible for ANA nucleotides (Figure 3.9). $J(\text{F}-\text{H1}')$ and $J(\text{F}-\text{H3}')$ were estimated from the splitting in the NOESY cross peaks.

Both heteronuclear and homonuclear J-couplings are consistent with a south puckering in all arabinose nucleotides (39). Accordingly, for structure calculations, sugar torsion angles were constrained to avoid north conformations, allowing east and south. Backbone dihedral angles were not constrained.



Residue	F-H1'	F-H2''	F-H3'	F-H4'	H2''-H1'	H2''-H3'	H3'-H4'	F-H8/H6
1 Cyt	19	52	-	0	1-3	0	n.a.	0
2 Gua	22	49	16	0	1-3	0	n.a.	7
3 Cyt	21	51	25	0	1-3	0	n.a.	0
4 Gua	25	51	22	0	1-3	0	n.a.	5
5 Ade	-	-	-	-	1-2	0	n.a.	-
6 Ade	-	-	-	-	1-2	0	n.a.	-
7 Ura	-	-	-	-	1-2	0	n.a.	-
8 Ura	-	-	-	-	1-2	0	n.a.	-
9 Cyt	24	51	n.a.	n.a.	1-3	0	n.a.	0
10 Gua	22	50	22	0	1-3	0	n.a.	5
11 Cyt	24	50	n.a.	n.a.	1-3	0	n.a.	0
12 Gua	16	52	24	0	1-3	0	n.a.	4

Figure 3.9 (a) Schematic representation of South 2'F-ANA and North 2'F-ANA and comparison between some of the 3J -couplings by which the sugar pucker can be determined. These three-bond 1H - 1H scalar couplings are indicated by arrows (b) J-coupling constants in Hz for gap(FA) sequence (100mM NaCl, T=25°C, pH=7, D₂O).

The duplex structure of gap(FA) sequence belongs to the B-form family. The root-mean-square deviation (RMSD) between the average structure of gap(FA) and the canonical A-form structure of the same Dickerson dodecamer sequence was larger than the RMSD between gap(FA) and a canonical B-form (5.4Å vs. 1.8Å, respectively). In addition, helical parameters were characteristics of B-form helices, with an average rise of 3.3Å and twist angles around 34°. The geometry of arabinoses and 2'F-arabinoses were similar; most sugar pseudorotation phase angles

ranged from -120° to -170° and glycosidic angles from -110° to -135° (excluding terminal residues). Backbone torsion angles were well defined and within the usual range for double helical structures.

The gap(FA) hairpin structure is predominant only at low oligonucleotide concentrations, where conditions for obtaining structural constraints from NMR data are not optimal. Although most of the signals could be assigned, the number of distance constraints derived from NOESY experiments was low, impeding the determination of a high resolution structure. However, some features of this interesting unimolecular hairpin structure were deduced from the NMR data.

The sequential sugar-base NOE connectivity could be traced for all 2'F-ANA residues and also for A5 residue in the 2'F-ANA-ANA interface but not for other ANA residues, which suggests the presence of a hairpin structure comprising of 2'F-ANA modified C:G base-paired stems and a four-residue loop formed by ANA nucleotides.

Furthermore, strong sequential sugar-base NOEs (H2"-H6/8 NOEs) are indicative of a B-like conformation for the 2'F-ANA stem, which is similar to the corresponding segment of the duplex structure (Figure 3.8). In case of ANA nucleotides, the lack of NOE connectivities involving aromatic protons suggests that the bases are somewhat disordered. This is also supported by the chemical shifts of ANA H6/H8 protons, which exhibited similar values as those of the fully denatured oligonucleotide at high temperatures.

3.4.3 Structural Analysis of gap(FA) Reveals Electrostatic Interactions Contributing to Thermal Stability

Assignment of ^{19}F resonances was carried out through their heteronuclear correlations with the adjacent H2", H3', H4' and H1' protons of the sugar ring. Sequential and intra-residual ^{19}F -

$^1\text{H}_6/^1\text{H}_8$ cross peaks were observed in the heteronuclear NOE (HOESY) spectrum. An interesting observation was the splitting of the H8 proton signals because of heteronuclear $^{19}\text{F}-^1\text{H}$ J-couplings as depicted in Figure 3.8 (also see values reported in Figure 3.9b). These couplings likely reflect pseudohydrogen bonds between 2'-fluorine and purine H8 of the same nucleotide (15,16), as the intra-residual distances between the 2'-F and H8 protons are short ($<2.7\text{\AA}$). The intra-residual distances between the arabinose 2'-OH group and H8 protons were also short ($<2.6\text{\AA}$). We hypothesized that in the latter case, because of the larger size of the hydroxyl group, the 2'-OH/H8 close contact would lead to an unfavourable steric clash between 2'-OH and H8, which outweighs a favourable C2'-O...H8-C electrostatic interaction. In line with this hypothesis, we observed for arabinose nucleotides that their glycosidic angles were shifted toward high anti values (-135°) (40). Expectedly, these distortions in glycosidic angles of arabinose nucleotides would affect the geometry of the WC hydrogen bonds. In fact, as shown by some base:base helical parameters, the co-planarity of ANA:ANA base pairs (A:U base pairs) was partially hindered (41).

3.5 Comparison of ANA and 2'F-ANA Modified Dodecamers with the Unmodified DNA

The Dickerson dodecamer is probably the most studied DNA duplex in the literature (17,42,43). Among the different structures that have been deposited in the protein data bank (PDB), the structure obtained by Tjandra *et al.* (PDB: 1DUF) was the most appropriate model to use for comparison, as it was also determined by high resolution NMR methods like ours (43).

Tjandra *et al.*'s structure is similar to that of the duplex conformation of gap(FA), with a few differences that should be noted. The RMSD between average structure of gap(FA) duplex and Tjandra's average structure is 1.3\AA for heavy atoms and 0.9\AA for the bases. RMSD between

ANA bases is 0.5\AA and between 2'F-ANA bases is $\sim 0.6\text{\AA}$. The pseudorotation phase angles of ANA and 2'F-ANA sugars are more south relative to the DNA sugars. These results suggest that arabinose sugars are more rigid compared to deoxyribose sugars, which are in dynamic equilibrium between the northern and southern conformations (44-46). In fact, observed J (H1',H2'') coupling values (Figure 3.9b), convinced us that such north-south conformational transitions do not occur in ANA and 2'F-ANA nucleotides, since even a small population of north conformation would give rise to a larger value for J (H1',H2'') couplings. Our findings were consistent with results from previous NMR studies conducted on ANA:RNA (PDB: 2KP3) and 2'F-ANA:RNA (PDB: 2KP4) hybrids, which also demonstrate rigid arabinose conformations (15).

Differences in glycosidic angles between gap(FA) and Tjandra *et al.*'s structures were limited to the ANA residues. On the other hand, backbone dihedral angles were found similar, with the exception of the zeta torsion angles (ζ) which were smaller than those of the solution structures of unmodified DNA Dickerson dodecamer (43). This is caused by the repulsion between the 2'-substituent and the adjacent phosphate groups. Thus, sequential P-H2' distances in Tjandra's structure are smaller than 4\AA , whereas in gap(FA) these distances (sequential P-F2' and P-O2') are around 5\AA . Another structural difference is the minor groove width which is narrower than in canonical B-form helices in solution (Figure 3.10). Interestingly, a minor groove narrowing was observed in the central part of the sequence.

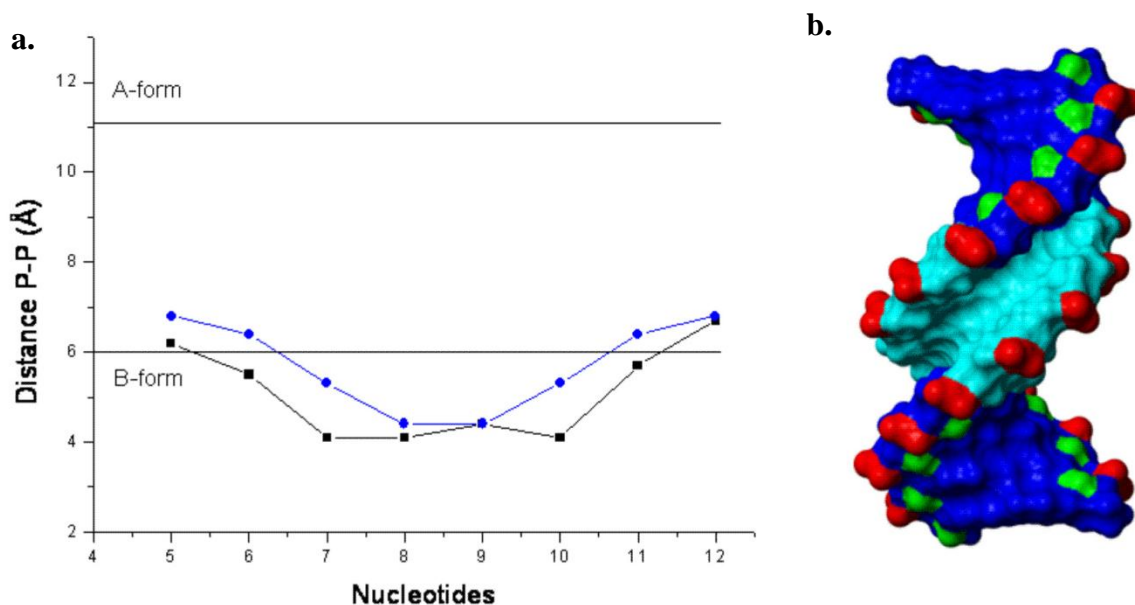


Figure 3.10 Comparison between gap(FA) and Tjandra *et al.*'s DNA structures **(a)** Minor groove width vs. nucleotide positions in the sequence; **(b)** accessible surface showing the minor groove narrowing observed in the central part of the molecule. In **(a)**, gap(FA) parameters are shown in black and DNA values in blue. In **(b)**, Surface corresponding to ANA residues is shown in cyan, 2'F-ANA residues in blue, phosphates in red and fluorine atoms in green.

3.6 ANA Stabilizes Stem-Loop Structures

All palindromic sequences can, in principle, form stem-loop hairpin structures at low salt and oligonucleotide concentrations. Early spectroscopic studies on Dickerson DNA sequence suggested the formation of alternative conformations such as hairpins (47,48). However, they only occur at much lower concentrations than those required for structural studies. In the concentrations required for running high resolution NMR and crystallographic studies, the unmodified DNA Dickerson dodecamer has been found as a double-stranded helix rather than a unimolecular hairpin structure (49). Most DNA analogues studied with the Dickerson sequence also adopt a predominant duplex structure. Same is observed with unmodified RNA; the pure Dickerson RNA sequence adopts a duplex structure in solution (50). However, several

modifications in the RNA sequence have been reported that induce hairpin formation instead of the duplex (51-53).

In the present work, with the ANA modified Dickerson sequence, we observed that the unfavourable steric interactions in the duplex form of gap(FA), induced by the short 2'-OH to base proton distances, become partially alleviated in the loop structure. Such a reduction of unfavourable steric clash led to the energetic balance between the duplex and the hairpin forms, and is partially responsible for the similar stability of the two forms (see section 3.3.3 for duplex versus hairpin stability comparisons). We also observed several intra-residual hydrogen bonds between 2'-OH and phosphate oxygens in the arabinose loop residues during the rMD calculations that do not exist in the duplex (Figure 3.11). The intra O2'-H2'...O5' hydrogen bonds have been previously observed in ANA nucleosides and were shown to stabilize the south sugar conformation (40,54). Such interactions are not feasible in B-type double helices.

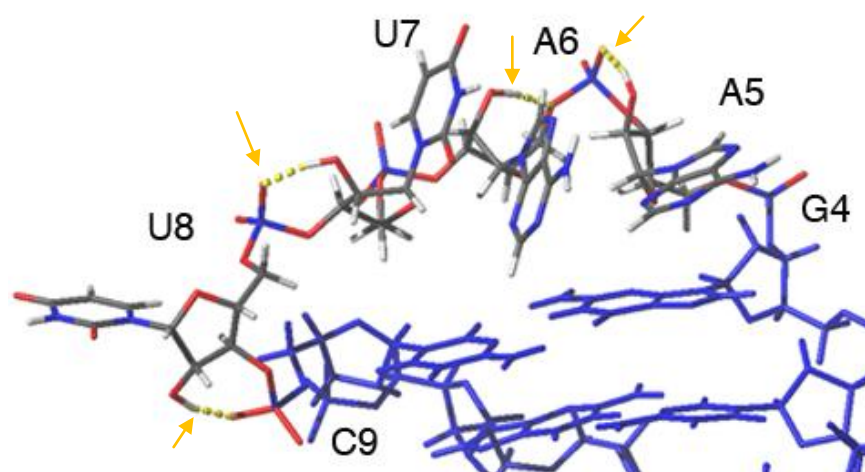


Figure 3.11 Model of the hairpin structure of gap(FA) and detail of the ANA residues in the loop, showing hydrogen bonds between the 2'-OH and phosphate oxygen.

Stem-loop hairpin structures are more common in RNA than in DNA (55); and solvation of 2'-OH groups has been shown to be a key contributor to the higher stability of hairpins for RNA. Thereby, we asked ourselves whether ANA is a DNA mimic or an RNA mimic. In the context of double helical structures, ANA is clearly a DNA analogue (i.e. C2'-endo sugar conformations, B-type duplex). However, ANA promotes formation of stem-loop structures, and thus in this sense, behaves as an RNA analogue. This tendency of ANA nucleotide tracts to form loop structures offers a range of new applications for this modification. For instance, in the rational design of nucleic acid hairpin structures, or in applications where a duplex/hairpin conformational switch is desirable, e.g. mimicking a biological process. It is common in biological systems that short oligoribonucleotides adopt duplex and hairpin structures of comparable stabilities, and the transition between the two states is a direct consequence of a biological process (56).

3.7 Alternative Genetic Systems Based on Arabinonucleic Acids?

Some of the work on nucleic acid analogues has been inspired by the desire for labelled RNAs and proteins, which requires alternative base pairing topologies capable of expanding the existing genetic code (57,58). The use of such artificial bases in various methodologies for protein- and nucleic acid-directed evolution requires polymerases that are able to recognize and incorporate them.

Interestingly, it has been reported that DNA polymerases can catalyze DNA synthesis on a 2'-F-ANA template strand (10-12). As well, the DNA polymerases were able to synthesize ANA (12), 2'-F-ANA or chimeric 2'-F-ANA-DNA strands on the template DNA strand (10,11). This ability of ANA and 2'-F-ANA oligonucleotides to be “copied to” and “copied from” DNA with good

fidelity (10-12) is in principle sufficient to carry out the directed evolution of functional ANA and 2'F-ANA molecules.

It is generally assumed that stable duplex formation is a crucial aspect of directed evolution of functional biopolymers based on a synthetic nucleic acid system. However, there is ample evidence in the literature that polymerases are in fact able to analyze oligonucleotide synthesis in the absence of a stable product-template duplex (59). Thus, the poor stability of ANA duplexes would perhaps not restrict their use in the storage or the propagation of information. In line with this statement, an engineered D4K polymerase was found to be able to carry out template-dependent DNA synthesis on an ANA template (12). As for 2'F-ANA modification, it has been copied to its own complement (12), but this process is less efficient than copying information between 2'F-ANA “to” and “from” DNA (10-12), which indicates subtle structural differences between DNA and 2'F-ANA duplexes (e.g., rigidity of fluorinated sugar) that have been revealed in this study.

3.8 Conclusions

This chapter describes the first report on NMR-based structural determination of a pure ANA:ANA duplex. It also presents the first structural characterization of a pure 2'F-ANA:2'F-ANA duplex.

The analysis of the thermal stability of chimeric dodecamers given in Table 3.1 demonstrated that a 2'F-ANA strand binds to itself to form 2'F-ANA:2'F-ANA duplexes that are substantially more stable than DNA:DNA and RNA:RNA duplexes of the same sequence, whereas ANA:ANA duplexes are weak at best if they form. Duplex thermal stability increases from ANA:ANA < DNA:DNA < RNA:RNA < 2'F-ANA:2'F-ANA (see Table 3.1). While stable pure

ANA duplexes do not form on their own, with appropriate combinations of 2'-F-ANA and ANA nucleotides we were able to increase the stability of the ANA:ANA internal segment of the gap(FA) sequence, thus making the characterization of the bound ANA:ANA segment by NMR feasible.

It was demonstrated that both arabinose (ANA) and its fluorine-substituted analogue, 2'-fluoroarabinose (2'-F-ANA) adopt pure C2'-endo conformations, with little variation along the sequence. Interestingly, encompassing the destabilizing ANA nucleotides with stabilizing 2'-F-ANA flanks, led to an oligonucleotide which adopted a duplex and a hairpin structure of surprisingly similar thermal stabilities. The co-existence of arabinose-containing duplex and hairpin species, as observed independently by NMR methods for gap(FA) would be a particularly promising tool in applications where a duplex/hairpin conformational switch is desirable.

The analysis of the 2'-F-ANA:2'-F-ANA and ANA:ANA segments of gap(FA) sequence also revealed that while sugar and glycosidic angle conformations induce a systematic steric clash between the 2'-OH and their own H6/H8 base protons in the ANA:ANA segment of gap(FA) duplex, the same conformational configuration also leads to favourable electrostatic interactions between the 2'-F and H6/H8 base protons in the 2'-F-ANA:2'-F-ANA segment, which is due to the smaller radius of fluorine and its higher electronegativity compared to a hydroxyl group. Similar interactions have been previously observed by us for 2'-F-ANA:RNA and ANA:RNA hybrids (15,16) and were discussed earlier in Chapter 2 of the present thesis work. We hypothesized that these stabilizing intra-residue interactions to fluorine contribute greatly to the higher stability of 2'-F-ANA:2'-F-ANA duplexes.

3.9 Experimental Methods

3.9.1 Oligonucleotide Synthesis and Purification

Oligonucleotides were synthesized from phosphoramidite precursors, using standard solid-phase methods on an Applied Biosystems 3400 DNA Synthesizer at a 1- μ mol scale using Unylink CPG support (ChemeGenes, Wilmington, MA) (60). All phosphoramidites were prepared as 0.15M solutions in acetonitrile (ACN), except DNA, which was prepared as 0.1M. Coupling times were 600 seconds for ANA, 2'F-ANA, and RNA phosphoramidites, and 100 seconds for DNA, with the exception of their guanosine phosphoramidites which were allowed to couple for 900 seconds for ANA, 2'F-ANA, and RNA, and 270 seconds for DNA. Deprotection and cleavage from the solid support was accomplished with ammonia:ethanol (3:1 v/v) for 48 hours at room temperature (61). Oligonucleotides containing RNA were synthesized with standard 2'-TBDMS phosphoramidites, and desilylation was achieved with neat TEA.3HF for 48 hours at room temperature (62). Purification of crude oligonucleotides was done by preparative denaturing polyacrylamide gel electrophoresis (PAGE) using 24% acrylamide gels. Gel bands were extracted overnight in DEPC-treated autoclaved Millipore water, and lyophilized to dryness. Purified oligonucleotides were desalted with Nap-25 Sephadex columns (GE Healthcare, Mississauga, ON). Sequences were verified by analytical denaturing PAGE and ESI-LCMS (Table 3.2).

Table 3.2 MS characterization of self-complementary chimeric dodecamer duplexes

Name	Sequence (5'-3')	Calculated Mass (g/mol)	Experimental Mass (g/mol)
DD	5'-CGCGAATTCGCG-3'	3644.647	3645.6
RR	5'-CGCGAAUUCGCG-3'	3808.5545	3809.9
FF	5'-CGCGAATTCGCG-3'	3860.5338	n.d.
AA	5'-CGCGAAUUCGCG-3'	3808.5545	3809.5
alt (AF)	5'-CGCGAAUUCGCG-3'	3834.5442	3836.4
alt (DF)	5'-CGCGAATTCGCG-3'	3752.5904	n.d.
gap (FA)	5'-CGCGAAUUCGCG-3'	3824.5198	3822, and 3844.4 (+Na ⁺)
gap (FD)	5'-CGCGAATTCGCG-3'	3788.5714	n.d.

Legend: RNA, DNA, ANA, 2F-ANA

3.9.2 UV Melting Experiments and Derivation of Thermodynamic Parameters

UV thermal denaturation data were obtained on a Varian Cary 5000 UV-visible spectrophotometer equipped with a Peltier temperature controller. Duplex concentration was 2 μ M (total concentration of strands: 4 μ M). After heating, samples were cooled to room temperature at a rate of 0.3°C/min and were then refrigerated overnight. Samples were transferred into cold cuvettes in the spectrophotometer and were kept under flowing nitrogen when below 15°C. Absorbance values were recorded after equilibration as the temperature was increased in 0.5°C steps at 1-minute intervals (buffer: 140mM KCl, 1mM MgCl₂, and 5mM Na₂HPO₄, pH 7.2). The optimal melting temperature (T_m) values were calculated using the baseline method, as assignment of baselines was clear in most cases. T_m values are given in Table 3.1 and normalized T_m curves are shown in Figure 3.12.

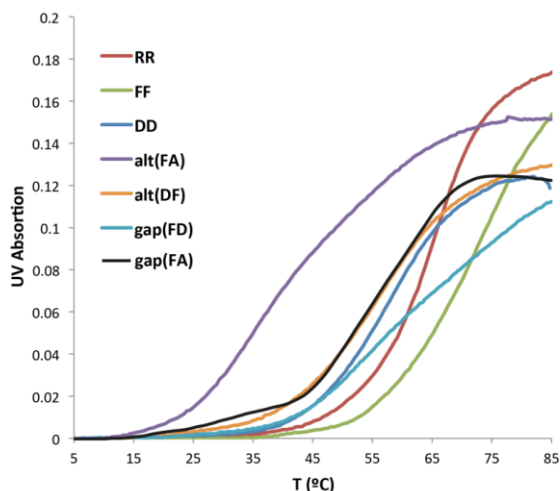


Figure 3.12 UV melting curves of DD, RR, FF, alt(AF), alt(DF), gap(FD) and gap(FA), as followed by observing the change in A_{260} of samples upon heating from 5°C to 85°C. Sequences are as shown in Table 3.1.

3.9.3 NMR Experiments

Sample gap(FA) (Table 3.1) was suspended in 500 mL of either D₂O or H₂O/D₂O 9:1 in 25mM phosphate buffer, 100mM NaCl (pH 7). NMR spectra were acquired in Bruker spectrometers operating at 600, 700 or 800MHz and were processed with Topspin software. ¹⁹F and ¹H ¹D melting experiments, double quantum filtered correlation spectroscopy (DQF-COSY), total correlation spectroscopy (TOCSY) and nuclear overhauser effect spectroscopy (NOESY) were recorded in D₂O and H₂O/ D₂O 9:1. The NOESY spectra were acquired with mixing times of 50, 100, 150, 250 and 300ms, and the total correlation spectroscopy spectra (TOCSY) were recorded with standard MLEV-17 spin-lock sequence at 80ms mixing time. For highly concentrated samples, NOESY spectra in H₂O were acquired with 50 and 100ms mixing times.

For 2D experiments in H₂O, water suppression was achieved by including a WATERGATE (63) module in the pulse sequence before acquisition. 2D experiments in D₂O were carried out at temperatures ranging from 5°C to 35°C, whereas spectra in H₂O were recorded at 5°C to reduce the exchange with water. ¹⁹F resonances were assigned from ¹⁹F detected using heteronuclear

overhauser effect spectroscopy spectra (HOESY) ($t_m=200\text{ms}$) (64). The spectral analysis program Sparky (65), was used for semiautomatic assignment of the NOESY cross peaks and quantitative evaluation of the nuclear overhauser effect (NOE) intensities.

3.9.4 Experimental Constraints

Quantitative distance constraints were obtained from NOESY experiments by using a complete relaxation matrix analysis with the program MARDIGRAS (66). Error bounds in the inter-proton distances were estimated by carrying out several MARDIGRAS calculations with different initial models, mixing times and correlation times. Standard A- and B-form duplexes were used as initial models, and three correlation times (1.0, 2.0 and 4.0ns) were employed, assuming an isotropic motion for the molecule. Experimental intensities were recorded at three different mixing times (100, 150 and 250ms) for non-exchangeable protons. Final constraints were obtained by averaging the upper and lower distance bounds in all the MARDIGRAS runs. Qualitative limits of 1.8Å and 5Å were set in those distances where no quantitative analysis could be carried out because of overlapping cross peaks or peaks with weak intensities. In addition to these experimentally derived constraints, Watson–Crick hydrogen bond restraints were used as well. Target values for distances and angles related to hydrogen bonds were set as described from the crystallographic data. ^{19}F - ^1H distance constraints from qualitative analysis of HOESY experiments were not used in these calculations. No backbone angle constraints were applied. Distance constraints with their corresponding error bounds were incorporated into the AMBER potential energy by defining a flat-well potential term. ^1H - ^1H J-coupling constants could not be accurately measured because of the relatively broad line-widths of the sugar proton signals. However, sum of the J-coupling constants were roughly estimated from DQF-COSY

cross peaks, and some ^1H - ^{19}F J-coupling constants could be measured using NOESY and DQF-COSY spectra. Loose values were set for the sugar dihedral angles δ , ν_1 and ν_2 to constrain 2'F-arabinose and arabinose conformations to the east or south domain.

3.9.5 Structure Determination of the Duplex

Structures were calculated with the SANDER module of the MD package AMBER 7.0 (67). Starting models of the arabino duplexes were built in the A- and B- canonical structures using SYBYL. These structures were taken as starting points for the AMBER refinement, which started with a short run in vacuo (using hexahydrated Na^+ counter-ions placed near the phosphates to neutralize the system). The resulting structures from in vacuo calculations were refined; including explicit solvent, periodic boundary conditions and the particle-mesh Ewald method, to evaluate long-range electrostatic interactions (68). Thus, the structures obtained in the previous step were placed in the center of a water-box with around 4000 water molecules and 20 sodium counter-ions to obtain electroneutral systems. We used the parmbsc0 (69) revision of the parm99 force field (70,71), including suitable parameters for the arabino and 2'F-arabino derivatives extracted from Noy *et al.* (72). The TIP3P model was used to describe water molecules (73). The protocol for the MD refinement consisted of an equilibration period of 160ps using a standard equilibration process (74), followed by 10 independent 500ps runs. Final structures were obtained by averaging the last ps of individual trajectories and further relaxation of the structure. A number of tools are available to calculate structural parameters for individual final rMD structures; they are also used to calculate averaged and energy-minimized coordinates and even used to analyze structural ensembles obtained by sampling conformational space around the otherwise static final structure. Herein, the analysis of the representative structures

and the rMD trajectories was carried out with the programs MOLMOL (75), CURVES V5.1 (76), the analysis tools of AMBER and SYBYL and additional ‘in-house’ programs.

3.9.6 Molecular Modeling of the Hairpin Structure

Initial structural models of the hairpin species were built with the program SYBYL on the basis of qualitative NMR information. Conformation of 2'F-ANA residues in the stem was set according to standard B-form parameters. Initial models were submitted to a MD calculation following the same protocols described previously. Only hydrogen bonds restraints for the Watson–Crick G:C base pairs in the stem were used.

3.10 References

1. Watts, J.K. and Damha, M.J. (2008) 2'F-Arabinonucleic acids (2'F-ANA) — History, properties, and new frontiers. *Canadian Journal of Chemistry*, **86**, 641-656.
2. Anzahaee, M.Y., Deleavey, G.F., Le, P.U., Fakhoury, J., Petrecca, K. and Damha, M.J. (2014) Arabinonucleic Acids: 2'-Stereoisomeric Modulators of siRNA Activity. *Nucleic Acid Ther*, **24**, 336-343.
3. Martín-Pintado, N., Yahyaee-Anzahaee, M., Deleavey, G.F., Portella, G., Orozco, M., Damha, M.J. and González, C. (2013) Dramatic Effect of Furanose C2' Substitution on Structure and Stability: Directing the Folding of the Human Telomeric Quadruplex with a Single Fluorine Atom. *Journal of the American Chemical Society*, **135**, 5344-5347.
4. Deleavey, G.F., Watts, J.K., Alain, T., Robert, F., Kalota, A., Aishwarya, V., Pelletier, J., Gewirtz, A.M., Sonenberg, N. and Damha, M.J. (2010) Synergistic effects between analogs of DNA and RNA improve the potency of siRNA-mediated gene silencing. *Nucleic Acids Research*, **38**, 4547-4557.
5. Damha, M.J., Wilds, C.J., Noronha, A., Brukner, I., Borkow, G., Arion, D. and Parniak, M.A. (1998) Hybrids of RNA and Arabinonucleic Acids (ANA and 2'F-ANA) Are Substrates of Ribonuclease H. *Journal of the American Chemical Society*, **120**, 12976-12977.
6. Mangos, M.M., Min, K.-L., Viazovkina, E., Galarneau, A., Elzagheid, M.I., Parniak, M.A. and Damha, M.J. (2002) Efficient RNase H-Directed Cleavage of RNA Promoted by

- Antisense DNA or 2'-F-ANA Constructs Containing Acyclic Nucleotide Inserts. *Journal of the American Chemical Society*, **125**, 654-661.
7. Noronha, A.M., Wilds, C.J., Lok, C.-N., Viazovkina, K., Arion, D., Parniak, M.A. and Damha, M.J. (2000) Synthesis and Biophysical Properties of Arabinonucleic Acids (ANA): Circular Dichroic Spectra, Melting Temperatures, and Ribonuclease H Susceptibility of ANA-RNA Hybrid Duplexes. *Biochemistry*, **39**, 7050-7062.
 8. Li, F., Sarkhel, S., Wilds, C.J., Wawrzak, Z., Prakash, T.P., Manoharan, M. and Egli, M. (2006) 2'-Fluoroarabino- and Arabinonucleic Acid Show Different Conformations, Resulting in Deviating RNA Affinities and Processing of Their Heteroduplexes with RNA by RNase H. *Biochemistry*, **45**, 4141-4152.
 9. Neef, A.B. and Luedtke, N.W. (2011) Dynamic metabolic labeling of DNA in vivo with arabinosyl nucleosides. *Proceedings of the National Academy of Sciences*, **108**, 20404-20409.
 10. Peng, C.G. and Damha, M.J. (2008) Probing DNA polymerase activity with stereoisomeric 2'-fluoro- β -D-arabinose (2'-F-araNTPs) and 2'-fluoro- β -D-ribose (2'-F-rNTPs) nucleoside 5'-triphosphates. *Canadian Journal of Chemistry*, **86**, 881-891.
 11. Peng, C.G. and Damha, M.J. (2007) Polymerase-Directed Synthesis of 2'-Deoxy-2'-fluoro- β -D-arabinonucleic Acids. *Journal of the American Chemical Society*, **129**, 5310-5311.
 12. Pinheiro, V.B., Taylor, A.I., Cozens, C., Abramov, M., Renders, M., Zhang, S., Chaput, J.C., Wengel, J., Peak-Chew, S.-Y., McLaughlin, S.H. *et al.* (2012) Synthetic Genetic Polymers Capable of Heredity and Evolution. *Science (New York, N.Y.)*, **336**, 341-344.
 13. Wilds, C.J. and Damha, M.J. (2000) 2'-Deoxy-2'-fluoro- β -d-arabinonucleosides and oligonucleotides (2'-F-ANA): synthesis and physicochemical studies. *Nucleic Acids Research*, **28**, 3625-3635.
 14. Gao, Y.G., Van der Marel, G.A., Van Boom, J.H. and Wang, A.H.J. (1991) Molecular structure of a DNA decamer containing an anticancer nucleoside arabinosylcytosine: conformational perturbation by arabinosylcytosine in B-DNA. *Biochemistry*, **30**, 9922-9931.
 15. Watts, J.K., Martín-Pintado, N., Gómez-Pinto, I., Schwartzenruber, J., Portella, G., Orozco, M., González, C. and Damha, M.J. (2010) Differential stability of 2'-F-ANA•RNA and ANA•RNA hybrid duplexes: roles of structure, pseudohydrogen bonding, hydration, ion uptake and flexibility. *Nucleic Acids Research*, **38**, 2498-2511.
 16. Anzahae, M.Y., Watts, J.K., Alla, N.R., Nicholson, A.W. and Damha, M.J. (2010) Energetically Important C-H...F-C Pseudohydrogen Bonding in Water: Evidence and Application to Rational Design of Oligonucleotides with High Binding Affinity. *Journal of the American Chemical Society*, **133**, 728-731.
 17. Drew, H.R., Wing, R.M., Takano, T., Broka, C., Tanaka, S., Itakura, K. and Dickerson, R.E. (1981) Structure of a B-DNA dodecamer: conformation and dynamics. *Proceedings of the National Academy of Sciences*, **78**, 2179-2183.
 18. Graber, D., Moroder, H. and Micura, R. (2008) 19F NMR Spectroscopy for the Analysis of RNA Secondary Structure Populations. *Journal of the American Chemical Society*, **130**, 17230-17231.

19. Kreutz, C., Kählig, H., Konrat, R. and Micura, R. (2005) Ribose 2'-F Labeling: A Simple Tool for the Characterization of RNA Secondary Structure Equilibria by ¹⁹F NMR Spectroscopy. *Journal of the American Chemical Society*, **127**, 11558-11559.
20. Patel, D.J., Kozlowski, S.A., Marky, L.A., Broka, C., Rice, J.A., Itakura, K. and Breslauer, K.J. (1982) Premelting and melting transitions in the d(CGCGAATTCGCG) self-complementary duplex in solution. *Biochemistry*, **21**, 428-436.
21. James, T.L. (2001), *Current Protocols in Nucleic Acid Chemistry*. John Wiley & Sons, Inc.
22. Schmitz, U. and James, T.L. (1995) In Thomas, L. J. (ed.), *Methods in enzymology*. Academic Press, Vol. Volume 261, pp. 3-44.
23. Ulyanov, N.B. and James, T.L. (1995) In Thomas, L. J. (ed.), *Methods in enzymology*. Academic Press, Vol. Volume 261, pp. 90-120.
24. Reid, B.R. (1987) Sequence-specific assignments and their use in NMR studies of DNA structure. *Q Rev Biophys*, **20**, 1-34.
25. Patel, D.J., Shapiro, L. and Hare, D. (1987) DNA and RNA: NMR studies of conformations and dynamics in solution. *Quarterly Reviews of Biophysics*, **20**, 35-112.
26. Feigon, J., Skelenář, V., Wang, E., Gilbert, D.E., Macaya, R.F. and Schultze, P. (1992) In David M.J. Lilley, J. E. D. (ed.), *Methods in enzymology*. Academic Press, Vol. Volume 211, pp. 235-253.
27. Gorenstein, D.G. (1992) In David M.J. Lilley, J. E. D. (ed.), *Methods in enzymology*. Academic Press, Vol. Volume 211, pp. 254-286.
28. Wuthrich, K. (1986) *NMR of Proteins and Nucleic Acids*. Wiley, New York.
29. Kessler, H., Gehrke, M. and Griesinger, C. (1988) Two-Dimensional NMR Spectroscopy: Background and Overview of the Experiments [New Analytical Methods (36)]. *Angewandte Chemie International Edition in English*, **27**, 490-536.
30. van de Ven, F.J. and Hilbers, C.W. (1988) Resonance assignments of non-exchangeable protons in B type DNA oligomers, an overview. *Nucleic Acids Research*, **16**, 5713-5726.
31. Nilsson, L., Clore, G.M., Gronenborn, A.M., Brunger, A.T. and Karplus, M. (1986) Structure refinement of oligonucleotides by molecular dynamics with nuclear Overhauser effect interproton distance restraints: application to 5' d(C-G-T-A-C-G)₂. *J Mol Biol*, **188**, 455-475.
32. Neuhaus, D., Williamson, M. (2000) *The Nuclear Overhauser Effect in Structural and Conformational Analysis, 2nd Edition*. WILEY VCH.
33. Keepers, J.W. and James, T.L. (1984) A theoretical study of distance determinations from NMR. Two-dimensional nuclear overhauser effect spectra. *Journal of Magnetic Resonance (1969)*, **57**, 404-426.
34. Karplus, M. (1963) Vicinal Proton Coupling in Nuclear Magnetic Resonance. *Journal of the American Chemical Society*, **85**, 2870-2871.
35. Minch, M.J. (1994) Orientational dependence of vicinal proton-proton NMR coupling constants: The Karplus relationship. *Concepts in Magnetic Resonance*, **6**, 41-56.
36. Karplus, M. (1959) Contact Electron-Spin Coupling of Nuclear Magnetic Moments. *The Journal of Chemical Physics*, **30**, 11-15.
37. Cheng, D.M. (1987) *The studies of ³¹P NMR of nucleic acids and nucleic acid complexes, in Phosphorus NMR in Biology (Tyler, B. C., ed.), CRC Press, Boca Raton, pp. 135-151.*

38. Bruenger, A.T. and Karplus, M. (1991) Molecular dynamics simulations with experimental restraints. *Accounts of Chemical Research*, **24**, 54-61.
39. Thibaudeau, C., Plavec, J. and Chattopadhyaya, J. (1998) A New Generalized Karplus-Type Equation Relating Vicinal Proton-Fluorine Coupling Constants to H-C-C-F Torsion Angles. *The Journal of Organic Chemistry*, **63**, 4967-4984.
40. Gao, Y.G., van der Marel, G.A., van Boom, J.H. and Wang, A.H. (1991) Molecular structure of a DNA dodecamer containing an anticancer nucleoside arabinosylcytosine: conformational perturbation by arabinosylcytosine in B-DNA. *Biochemistry*, **30**, 9922-9931.
41. Martín-Pintado, N., Yahyaee-Anzahaee, M., Campos-Olivas, R., Noronha, A.M., Wilds, C.J., Damha, M.J. and González, C. (2012) The solution structure of double helical arabino nucleic acids (ANA and 2'F-ANA): effect of arabinoses in duplex-hairpin interconversion. *Nucleic Acids Research*, **40**, 9329-9339.
42. Tereshko, V., Minasov, G. and Egli, M. (1998) The Dickerson-Drew B-DNA Dodecamer Revisited at Atomic Resolution. *Journal of the American Chemical Society*, **121**, 470-471.
43. Tjandra, N., Tate, S.-i., Ono, A., Kainosho, M. and Bax, A. (2000) The NMR Structure of a DNA Dodecamer in an Aqueous Dilute Liquid Crystalline Phase. *Journal of the American Chemical Society*, **122**, 6190-6200.
44. Gyi, J.I., Lane, A.N., Conn, G.L. and Brown, T. (1998) Solution Structures of DNA-RNA Hybrids with Purine-Rich and Pyrimidine-Rich Strands: Comparison with the Homologous DNA and RNA Duplexes. *Biochemistry*, **37**, 73-80.
45. Bachelin, M., Hessler, G., Kurz, G., Hacia, J.G., Dervan, P.B. and Kessler, H. (1998) Structure of a stereoregular phosphorothioate DNA/RNA duplex. *Nat Struct Mol Biol*, **5**, 271-276.
46. Gonzalez, C., Stec, W., Reynolds, M.A. and James, T.L. (1995) Structure and Dynamics of a DNA.cntdot.RNA Hybrid Duplex with a Chiral Phosphorothioate Moiety: NMR and Molecular Dynamics with Conventional and Time-Averaged Restraints. *Biochemistry*, **34**, 4969-4982.
47. Marky, L.A., Blumenfeld, K.S., Kozlowski, S. and Breslauer, K.J. (1983) Salt-dependent conformational transitions in the self-complementary deoxydodecanucleotide d(CGCAATTCGCG): Evidence for hairpin formation. *Biopolymers*, **22**, 1247-1257.
48. Miller, M., Kirchoff, W., Schwarz, F., Appella, E., Chiu, Y.Y., Cohen, J.S. and Sussman, J.L. (1987) Conformational transitions of synthetic DNA sequences with inserted bases, related to the dodecamer d(CGCGAATTCGCG). *Nucleic Acids Res*, **15**, 3877-3890.
49. Hald, M., Pedersen, J.B., Stein, P.C., Kirpekar, F. and Jacobsen, J.P. (1995) A comparison of the hairpin stability of the palindromic d(CGCG(A/T)4CGCG) oligonucleotides. *Nucleic Acids Research*, **23**, 4576-4582.
50. Chou, S.H., Flynn, P. and Reid, B. (1989) Solid-phase synthesis and high-resolution NMR studies of two synthetic double-helical RNA dodecamers: r(CGCGAAUUCGCG) and r(CGCGUAUACGCG). *Biochemistry*, **28**, 2422-2435.
51. Micura, R., Pils, W., Höbartner, C., Grubmayr, K., Ebert, M.-O. and Jaun, B. (2001) Methylation of the nucleobases in RNA oligonucleotides mediates duplex-hairpin conversion. *Nucleic Acids Research*, **29**, 3997-4005.

52. Plevnik, M., Gdaniec, Z. and Plavec, J. (2005) Solution structure of a modified 2',5'-linked RNA hairpin involved in an equilibrium with duplex. *Nucleic Acids Research*, **33**, 1749-1759.
53. Höbartner, C., Ebert, M.-O., Jaun, B. and Micura, R. (2002) RNA Two-State Conformation Equilibria and the Effect of Nucleobase Methylation. *Angewandte Chemie International Edition*, **41**, 605-609.
54. Venkateswarlu, D. and Ferguson, D.M. (1999) Effects of C2'-Substitution on Arabinonucleic Acid Structure and Conformation. *Journal of the American Chemical Society*, **121**, 5609-5610.
55. Varani, G. (1995) Exceptionally stable nucleic acid hairpins. *Annual review of biophysics and biomolecular structure*, **24**, 379-404.
56. Bernacchi, S., Ennifar, E., Tóth, K., Walter, P., Langowski, J. and Dumas, P. (2005) Mechanism of Hairpin-Duplex Conversion for the HIV-1 Dimerization Initiation Site. *J. Biol. Chem.*, **280**, 40112-40121.
57. Wojciechowski, F. and Leumann, C.J. (2011) Alternative DNA base-pairs: from efforts to expand the genetic code to potential material applications. *Chemical Society Reviews*, **40**, 5669-5679.
58. Hirao, I., Kimoto, M. and Yamashige, R. (2012) Natural versus Artificial Creation of Base Pairs in DNA: Origin of Nucleobases from the Perspectives of Unnatural Base Pair Studies. *Accounts of Chemical Research*, **45**, 2055-2065.
59. Tsai, C.-H., Chen, J. and Szostak, J.W. (2007) Enzymatic synthesis of DNA on glycerol nucleic acid templates without stable duplex formation between product and template. *Proceedings of the National Academy of Sciences*, **104**, 14598-14603.
60. Damha, M. and Ogilvie, K. (1993) In Agrawal, S. (ed.), *Protocols for Oligonucleotides and Analogs*. Humana Press, Vol. 20, pp. 81-114.
61. Bellon, L. (2001) Oligoribonucleotides with 2'-O-(tert-Butyldimethylsilyl) Groups. *Current protocols in nucleic acid chemistry*, **Unit 3.6.1-3.6.13**.
62. Westmanu, E. and Stromberg, R. (1994) Removal of t-butyldimethylsilyl protection in RNA-synthesis. Triethylamine trihydrofluoride (TEA, 3HF) is a more reliable alternative to tetrabutylammonium fluoride (TBAF). *Nucleic Acids Research*, **22**, 2430-2431.
63. Piotto, M., Saudek, V. and Sklenar, V. (1992) Gradient-tailored excitation for single-quantum NMR spectroscopy of aqueous solutions. *J Biomol NMR*, **2**, 661-665.
64. Yu, C. and Levy, G.C. (1984) Two-dimensional heteronuclear NOE (HOESY) experiments: investigation of dipolar interactions between heteronuclei and nearby protons. *Journal of the American Chemical Society*, **106**, 6533-6537.
65. Goddard, D.T.a.K., D.G. . SPARKY, 3rd ed. University of California, San Francisco.
66. Borgias, B.A. and James, T.L. (1990) MARDIGRAS-A procedure for matrix analysis of relaxation for discerning geometry of an aqueous structure. *Journal of Magnetic Resonance (1969)*, **87**, 475-487.
67. Case, D.A., Pearlman, D.A., Caldwell, J.W. III et al. (2007). AMBER7. University of California, San Francisco.
68. Darden, T., York, D. and Pedersen, L. (1993) Particle mesh Ewald: An N·log(N) method for Ewald sums in large systems. *The Journal of Chemical Physics*, **98**, 10089-10092.

69. Perez, A., Marchan, I., Svozil, D., Sponer, J., Cheatham, T.E., 3rd, Laughton, C.A. and Orozco, M. (2007) Refinement of the AMBER force field for nucleic acids: improving the description of alpha/gamma conformers. *Biophys J*, **92**, 3817-3829.
70. Cheatham, T.E., 3rd, Cieplak, P. and Kollman, P.A. (1999) A modified version of the Cornell et al. force field with improved sugar pucker phases and helical repeat. *Journal of biomolecular structure & dynamics*, **16**, 845-862.
71. Cornell, W.D., Cieplak, P., Bayly, C.I., Gould, I.R., Merz, K.M., Ferguson, D.M., Spellmeyer, D.C., Fox, T., Caldwell, J.W. and Kollman, P.A. (1995) A Second Generation Force Field for the Simulation of Proteins, Nucleic Acids, and Organic Molecules. *Journal of the American Chemical Society*, **117**, 5179-5197.
72. Noy, A., Luque, F.J. and Orozco, M. (2008) Theoretical Analysis of Antisense Duplexes: Determinants of the RNase H Susceptibility. *Journal of the American Chemical Society*, **130**, 3486-3496.
73. Jorgensen, W.L., Chandrasekhar, J., Madura, J.D., Impey, R.W. and Klein, M.L. (1983) Comparison of simple potential functions for simulating liquid water. *The Journal of Chemical Physics*, **79**, 926-935.
74. Shields, G.C., Laughton, C.A. and Orozco, M. (1997) Molecular Dynamics Simulations of the d(T·A·T) Triple Helix. *Journal of the American Chemical Society*, **119**, 7463-7469.
75. Koradi, R., Billeter, M. and Wüthrich, K. (1996) MOLMOL: A program for display and analysis of macromolecular structures. *Journal of Molecular Graphics*, **14**, 51-55.
76. Lavery, R., Sklenar, H. (1990) CURVES, helical analysis of irregular nucleic acids. Laboratory of Theoretical Biochemistry CNRS, Paris.

CHAPTER 4: ARABINONUCLEIC ACIDS AS 2'-STEREoisomeric Modulators of siRNA Activity

4.1 Overview

RNA interference (RNAi) is an oligonucleotide (ON) based therapeutic approach utilizing small interfering RNAs (siRNAs) to silence a target gene through mRNA knockdown (1,2). Despite their immense therapeutic potential, siRNAs suffer from poor nuclease stability, poor cellular uptake, and off-target effects arising from partial complementarities to unintended genes and nonspecific immune responses (3,4). Our perspective is that many of these shortcomings can be solved through chemical modification of the oligonucleotide sugar backbone (5-13).

Among the wide variety of nucleotide modifications available, arabinonucleic acid (ANA) and its 2'-fluorinated derivative (2'F-ANA) are particularly interesting (Figure 4.1) (14-18). As mentioned in previous chapters of the present thesis work, ANA and 2'F-ANA both closely mimic DNA with respect to duplex structure (19,20) and their hybrid duplexes with RNA display structure and flexibility patterns that make them effective mimics of the DNA:RNA hybrids with increased nuclease resistance. 2'F-ANA and ANA can also mimic DNA in their ability to trigger RNase H mediated mRNA degradation and have been shown to have applications in antisense technology (21-24).

Interestingly, although a DNA-mimic, 2'F-ANA is also compatible and often stabilizing within a double-stranded RNA (*ds*-RNA) context and therefore it has been successfully incorporated into siRNAs. In siRNA, 2'F-ANA enhances nuclease stability (25,26), is readily tolerated in the passenger strand (25,26), and can be combined with 2'F-ribonucleic acid (2'F-RNA; Figure 4.1), to fully modify siRNAs for improved potency (25). Moreover, the combination of these

modifications reduces immunostimulation and provides a thermodynamic bias for antisense strand RISC loading (25,26).

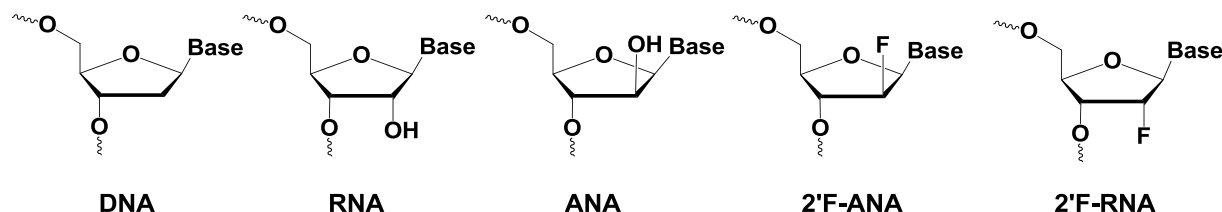


Figure 4.1 Chemical structures of 2'F-ANA, ANA, and 2'F-RNA in comparison with DNA and RNA.

ANA, on the other hand, despite its high resistance towards nucleases, has never been incorporated to siRNAs, partly because this modification, unlike 2'F-ANA, leads to duplex destabilization when introduced within *ds*-RNA constructs (20,23). However, given the important role of siRNA duplex thermal bias in determining siRNA activity and off-target effects (12,27-32), we hypothesized that ANA (alone or in combination with other modifications) may be of significant use in the development of chemically modified siRNAs. We took advantage of ANA's destabilizing effect to rationally design modified siRNAs that had altered thermal bias; and the results of these investigations are the focus of the present chapter.

As a first step, we carried out a widely used cell-based firefly luciferase assay (25,33-36), to verify the gene silencing activity of our siRNA designs. We examined the properties of modified siRNA duplexes containing ANA in the passenger strand, alone or in combination with 2'F-ANAs and/or RNAs. By judiciously altering the location of ANA, 2'F-ANA, and RNA nucleotides along the passenger strand, duplexes with potency comparable to native siRNA were identified. The active modification design motifs that emerged from this screen were

subsequently used to target the protein *DownRegulated in Renal cell carcinoma (DRR)*, a novel and clinically tractable target for the treatment of glioblastoma (GBM) (37,38). DRR expression is seen in cancerous GBM cells of all subtypes and positively correlates with the invasiveness of GBM *in vitro* and *in vivo* (37,38). As demonstrated in the following sections, DRR-targeting si-duplexes containing ANA and 2'F-ANA modified sense strands gave potency only slightly reduced from that of the unmodified siRNAs.

4.2 RISC's Thermodynamic Bias

Exogenous triggers for the RNAi pathway, small interfering RNAs (siRNAs) (39) are 21-nt long *ds*-RNA duplexes with 2-nt 3' overhangs. siRNAs are designed to share full sequence complementarity with a single target mRNA. During RISC loading with siRNA, one of the two siRNA strands (guide strand) is loaded into RISC, while the other (passenger strand) is cleaved, unwound from the guide strand and discarded (40,41), although cleavage is not obligatory (41).

When designing chemically modified siRNAs, a detailed understanding of the mechanism of RNAi and the enzymes involved in this process is invaluable. Chapter 1 provides a discussion of the current model for the RNAi mechanism, guide strand selection and loading (see section 1.4.2). Briefly, it is suggested that Argonaute2 (Ago2) acts in concert with Dicer/double-stranded RNA binding proteins (*ds*-RBPs) “thermodynamic asymmetry sensors” to ensure proper strand selection and that Ago2 does not function exclusively in siRNA guide strand selection (42). In this model Dicer interacts with the siRNA on the less stable end of the duplex and one of the *ds*-RBPs on the more stable end, spatially orienting the duplex for a subsequent Ago2 loading step in which *ds*-RBP may “hand off” the more stable end of the duplex to the PAZ domain (the guide strand 3'-binding domain) of Ago2 (31). This model suggests a mechanism through which

guide strand selection can occur based on siRNA duplex thermodynamic asymmetry, correlating with observations that the siRNA strand with the least tightly bound 5' end frequently becomes the RISC guide (27,28).

Given these structural insights on siRNA guide (antisense) strand selection and RISC loading, and the role of siRNA duplex thermal bias in determining siRNA activity, a goal of our studies was set to explore whether the thermal destabilization of a siRNA duplex through ANA incorporation, alone or in combination with 2'F-ANA and RNA nucleotides, could be beneficial to siRNA activity. Results of these investigations are the focus of the following sections.

4.3 Targeting Firefly Luciferase by ANA-modified si-Duplexes

4.3.1 Sequence Design

We first used cell-based firefly luciferase gene silencing assays to verify siRNA activity and evaluate potency. ANA nucleotides, alone or in combination with 2'F-ANA and RNA, were introduced into the passenger (sense) strand, as this strand is known to better tolerate chemical modifications (Figure 4.2A) (25,43,44). These strands were then hybridized to RNA or a 5'-phosphorylated 2'F-RNA antisense strand (25,45). The modified sense strands were not chemically phosphorylated, potentially inhibiting sense strand loading into RISC. T_m values of all combinations are summarized in Figures 4.2A and 4.3A and normalized UV melting profiles are given in Figures 4.5 in experimental section 4.6.3.

Replacing either strand of the native siRNA duplex with ANA decreased the duplex T_m value with respect to the native duplex, as previously observed (compare A1:RNA and CTRL:ANA with CTRL:RNA in Figures 4.2A and 4.3A) (20,23,46). The same was observed when A1 (all-

ANA) and CTRL (all-RNA) were hybridized to fully modified 2'F-RNA antisense strands (A1: 2'F-RNA vs. CTRL: 2'F-RNA, Figure 4.2C).

As expected, in line with our previous observations, including 2'F-ANA modifications on the sense strand improved the thermal stability of the modified si-duplexes (Figure 4.2A) (20,47).

4.3.2 Luciferase Gene Silencing

Gene silencing assays based on firefly luciferase are excellent reporter systems for evaluating RNAi activity (33), and have been widely used in the field (25,33,34,48). In these assays, cells are modified to stably express the firefly luciferase. Following treatment with siRNAs targeting the luciferase mRNA, luciferase levels can be quickly quantified using commercially available kits and through the addition of a luciferase substrate, luciferin, which is oxidized to produce light that can be measured using a luminometer. Since firefly luciferase is the protein that catalyzes the luciferin oxidation to the product molecule, oxyluciferin, the luminometer readings correspond to cellular levels of the luciferase. Overall, with proper controls, the luciferase gene silencing assay system is a very useful and convenient tool in RNAi research.

The luciferase assays described in this chapter were conducted by Dr. Johans Fakhoury in the Sleiman research group in the Department of Chemistry at McGill University. Cells were transfected with our chemically modified siRNAs at various siRNA concentrations and luciferase activity was measured 24 hours following transfection. Firefly luciferase levels are shown in Figures 4.2B/C, and 4.3B. For dose-response curves, see Figure 4.7 presented in experimental section 4.6.4. Calculated EC_{50} values of the modified and native control siRNA

duplexes are given in Figure 4.2A and 4.3A. EC_{50} values were calculated by setting the negative scramble control as 0% and the lipofectamine control as 100%.

As shown in Figure 4.2B, despite the significantly lower T_m value of A1:RNA relative to the unmodified siRNA (CTRL:RNA), its potency is comparable to that of the unmodified duplex, with EC_{50} values in the low nanomolar range. A similar trend was observed when A1 and CTRL were hybridized to fully modified 2'F-RNA antisense strands. A1:2'F-RNA potency is only slightly reduced from that of the CTRL:2'F-RNA duplex, with EC_{50} values in the low nanomolar range (Figure 4.2C). Except for the unmodified CTRL:2'F-RNA duplex, hybrids with native RNA antisense strands were generally more potent or had comparable activities to those with fully modified 2'F-RNA antisense strands (Figure 4.2B vs. 4.2C). Thus, one could conclude that for this particular sequence, heavy modification of both the sense and antisense strand, and all through the siRNA, is not very well tolerated.

It has been established that a fully modified 2'F-ANA strand works better as the sense strand than as the antisense strand when incorporated to siRNAs (26,49). We made a similar observation with the arabinonucleic acid (ANA) modification: a fully modified ANA sense strand works better than a fully modified ANA antisense strand (compare A1:RNA vs. CTRL:ANA in Figure 4.3B and Figure 4.7).

Given the better affinity of 2'F-ANA relative to ANA for RNA, and the important role of thermal bias in determining siRNA activity, we introduced a string of 2'F-ANA residues at the 5'-end of A1 to create A4 (Figure 4.2A). Since A4 has stabilizing 2'F-ANA residues on its 5'-end, we hypothesized that duplexes derived from A4 would exhibit more favorable RISC loading and potency than those derived from A1. As an additional control to test thermal bias, we also

prepared A3 in which the 2'F-ANA units are inter-dispersed within the ANA strand and less accumulated on the 5' end of the sense strand (Figure 4.2A).

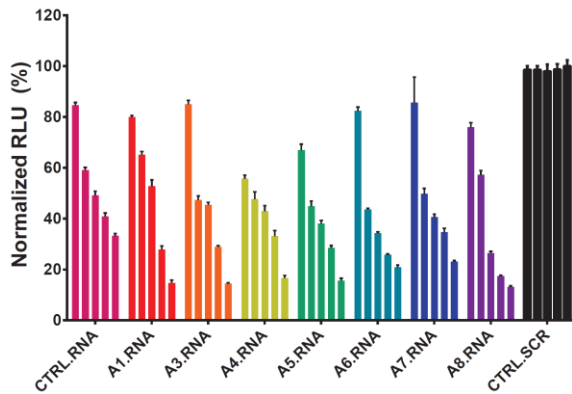
Despite the same number of 2'F-ANA modifications in A3 and A4, a modest improvement in potency was observed when the stabilising 2'F-ANA nucleotides were all accumulated at the 5' end of the sense strand (e.g., A4:RNA or A4:2'F-RNA), compared to when they were inter-dispersed along sense strand (e.g., A3:RNA or A3:2'F-RNA).

Next, other duplex designs with potential enhanced asymmetry in thermal stability were examined. Keeping the stabilizing 7-nt 2'F-ANA segment at the 5'-end of the sense strand (as in A4), we replaced six internal ANA units with better binding native RNA units to create A5 (Figure 4.2A). As a control strand, we synthesized A6 which was expected to yield a duplex with opposite thermodynamic bias and hence lower gene silencing activity. The results were somewhat consistent with expectations. Duplexes A4:2'F-RNA and A5:2'F-RNA were at least 10 fold more potent relative to A6:2'F-RNA (Figure 4.2C); however, activities of the resulting duplexes were comparable when A4, A5 and A6 were paired with native RNA strands (Figure 4.2B).

A)

Code	Sense (Passenger) Strand	RNA Antisense Strand 3'-ttCGAACUUCAGAAAUAUU-5'		2'F-RNA Antisense Strand 3'-ttCGAACUUCAGAAAUAUU ^p -5'	
		T _m (°C)	EC ₅₀ (nM)	T _m (°C)	EC ₅₀ (nM)
CTRL	5'-GCUUGAAGUCUUUAAUUAAtt-3'	60.2	6.1	68.2	0.8
A1	5'-GCUUGAAGUCUUUAAUUAAtt-3'	41.0	3.4	48.2	1.4
A3	5'-GCUUGAAAGUCUUUAAUUAAtt-3'	48.1	2.0	59.8	1.6
A4	5'-GCUUGAAGUCUUUAAUUAAtt-3'	48.9	0.6	59.0	0.36
A5	5'-GCUUGAAGUCUUUAAUUAAtt-3'	49.2	0.8	61.1	1.5
A6	5'-GCUUGAAGUCUUUAAUUAAtt-3'	48.8	1.3	59.9	17
A7	5'-GCUUGAAGUCUUUAAUUAAtt-3'	52.5	2.4	53.8	3.8
A8	5'-GCUUGAAGUCUUUAAUUAAtt-3'	49.8	1.1	51.0	6.1

B)



C)

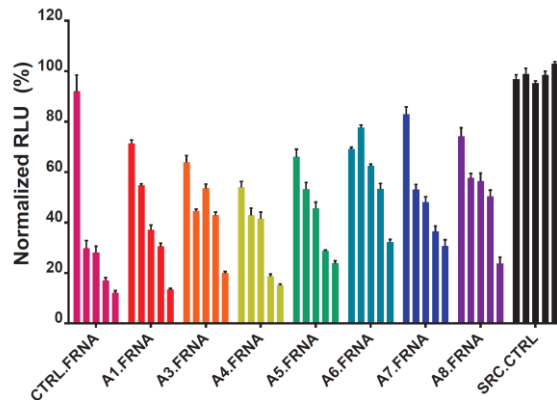


Figure 4.2 (A) Sequences, thermal denaturation studies, and EC₅₀ values of siRNAs targeting firefly luciferase mRNA in HeLa X1/5 cells. (B) Activity of duplexes that have RNA as their antisense strand (R-series) and (C) Activity of duplexes that have 2'F-RNA as their antisense strand (FR-series). Luciferase levels were normalized to total cellular protein and luciferase counts of mock treated cells. Bars indicate standard deviation. Experiments were conducted at 5 concentrations (100nM, 20nM, 4nM, 0.8nM and 0.16nM). Legend: RNA, 2'F-RNA, ANA, 2'F-ANA, dna.

A)

Code	Sequence (5'-3')	T _m (°C)	EC50 (nM)
CTRL.RNA	5'-GCUUGAAGUCUUUAAUAA tt -3' 3'- tt CGAACUUCAGAAAUAAUU-5'	60.2	6.1
A1.RNA	5'-GCUUGAAGUCUUUAAUAA tt -3' 3'- tt CGAACUUCAGAAAUAAUU-5'	41.0	3.4
CTRL.ANA	5'-GCUUGAAGUCUUUAAUAA tt -3' 3'- tt CGAACUUCAGAAAUAAUU-5'	42.9	17

B)

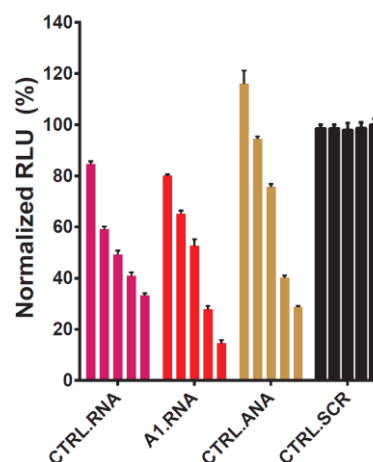


Figure 4.3 (A) Sequences and thermal denaturation studies of firefly luciferase mRNA targeting siRNAs that contain fully ANA-modified sense or antisense strands. (B) Assays demonstrating activity of modified siRNAs. Luciferase levels were normalized to total cellular protein and luciferase counts of mock treated cells. Bars indicate standard deviation. Experiments were conducted at 5 concentrations (100nM, 20nM, 4nM, 0.8nM and 0.16nM). None of the strands were 5'-phosphorylated. Legend: RNA, ANA, dna.

Architectures A7 and A8 (Figure 4.2A) were designed to take advantage of previous observations by the Damha lab, showing that combination of ‘DNA-like’ (2’F-ANA) with the ‘RNA-like’ (2’F-RNA) nucleotides in the 1–1 alternating configuration decreases the duplex stability, while the 3–3 alternating configuration does not (25). In fact, this design (“FFC-611”) was among the most potent siRNAs in this particular data set, suggesting that a rational design strategy could improve siRNA activity. In the present work, inspired by the FFC-611 model and by placing a 1–1 altimer stretch (2’F-RNA-ANA) at the 3'-end of the sense strand, we hoped to destabilize the duplex at the 5'-end of the antisense strand and thus favor loading of the antisense strand into RISC (25,50,51). A8 is analogous to A7 but contains fewer number of ANA substitutions (Figure 4.2A). The gene silencing activities observed for A7 and A8 (Figure

4.2A/B) suggest that these patterns are well tolerated in this particular sequence as well, with EC₅₀'s of duplexes falling in the 1-6 nM range.

4.4 Targeting Down-Regulated in Renal Cell Carcinoma by ANA-modified si-Duplexes

siRNA research is focused on developing tools for targeting therapeutically relevant cellular genes, and hence we sought to apply our siRNA optimizations (with altered thermal bias) to a therapeutically relevant endogenous gene, namely the *Down-Regulated in Renal cell carcinoma (DRR)* gene. DRR is a highly interesting target for the development of anticancer drugs for malignant gliomas which are highly invasive forms of brain cancer. The failure of present treatments for malignant gliomas is, in large part, due to the cancer cells' ability to rapidly invade the surrounding brain tissue and give rise to recurrent tumors.

Recently, Petrecca and co-workers at the Montreal Neurological Institute & Hospital (McGill University) found that, unlike normal glial cells, malignant gliomas overexpress DRR (37,38). Through regulation of cell movement, specifically through regulation of focal adhesion dynamics and AKT activation, DRR is the primary driver of the highly invasive nature of these malignant gliomas (37,38). Thus knockdown of DRR expression provides a promising approach for treatment of malignant glioma in brain cancer.

DRR expression triggers cells to adopt an elongated spindle-shaped phenotype associated with invasion (37). When DRR expression is reduced, focal adhesion turnover, AKT activation, and cancer cell invasion decreases (37). Since DRR inhibition causes marked changes in cell morphology and phenotype, alongside standard Western blotting methods, visualization of the treated cells is also a very useful in monitoring DRR expression (37).

Because of the therapeutic relevance of DRR and the multiple methods available to monitor DRR levels, we chose DRR as an endogenous target for testing our chemically modified constructs, applying the design rules we established with the firefly luciferase system. The results of these experiments are presented in the following sections.

4.4.1 siRNA Sequence Design and Knockdown of DRR Gene

The DRR-targeting siRNA sequence was originally designed by Dr. Glen Deleavey from our laboratory (52), using the mRNA sequence for this gene (DRR: NM_007177.2). This siRNA sequence has less than 15% identity with other cellular mRNAs to minimize off-target effects, and targets both known isoforms of DRR (transcript variants 1 and 2).

The siRNA DRR1 (unmodified native RNA) and the ANA-based duplexes (DRR-A1 through A7) were used to target DRR in malignant glioma cells. Si-duplex sequences of the DRR series and T_m values are presented in Table 4.1 (see Figure 4.6 in experimental section 4.6.3 for normalized T_m curves). We also included two other modified targeting siRNAs in our study: DRR2 (with 2'F-ANA modified sense strand, and 2'F-RNA modified antisense strand; Table 4.1), and DRR3 (designed based on the FFC-611 pattern previously described by our group (25); Table 4.1). DRR2 and DRR3 were used in the present work as positive controls to the activity of ANA-modified si-duplexes targeting DRR. A non-targeting siRNA duplex (\emptyset , Figure 4.4) was used as a negative control.

Table 4.1. Sequences and T_m values of siRNAs targeting DRR

Code	Duplexes targeting DRR	T_m (°C)
DRR-A1	5'-GGA ACC AGC UCA UCA AGA Att-3' 3'-ttC CUU GGU CGA GUA GUU CUU-5'	54.6
DRR-A2	5'-GGA ACC AGC TCA TCA AGA Att-3' 3'-ttC CUU GGU CGA GUA GUU CUU-5'	72.6
DRR-A3	5'-GGA ACC AGC UCA UCA AGA Att-3' 3'-ttC CUU GGU CGA GUA GUU CUU-5'	67.0
DRR-A4	5'-GGA ACC AGC UCA UCA AGA Att-3' 3'-ttC CUU GGU CGA GUA GUU CUU-5'	61.3
DRR-A5	5'-GGA ACC AGC UCA UCA AGA Att-3' 3'-ttC CUU GGU CGA GUA GUU CUU-5'	63.7
DRR-A6	5'-GGA ACC AGC UCA UCA AGA Att-3' 3'-ttC CUU GGU CGA GUA GUU CUU-5'	63.1
DRR-A7	5'-GGA ACC AGC UCA UCA AGA Att-3' 3'-ttC CUU GGU CGA GUA GUU CUU-5'	47.9
DRR1	5'-GGA ACC AGC UCA UCA AGA Att-3' 3'-ttC CUU GGU CGA GUA GUU CUU-5'	70.4
DRR2	5'-GGA ACC AGC UCA UCA AGA AUU-3' 3'-UUC CUU GGU CGA GUA GUU CUU-5'	n.d.
DRR2-Cy5	Cy5-5'-GGA ACC AGC UCA UCA AGA AUU-3' 3'-UUC CUU GGU CGA GUA GUU CUU-5'	n.d.
DRR3	5'-GGA ACC AGC UCA UCA AGA AUU-3' 3'-UUC CUU GGU CGA GUA GUU CUU-5'	n.d.

Legend: RNA, 2F-RNA, 2F-ANA, ANA, dna; n.d.: not measured.

Levels of DRR expression after treating cells with siRNA (transfection with Lipofectamine 2000) are shown in Figure 4.4., and the corresponding densitometry plot is given in Figure 4.8 in the experimental section 4.6.5 of the present chapter.

Several trends emerged from this set of duplex designs. For example, in line with our observations on preferences of ANA for the sense strand and RNA for the antisense strand in the luciferase series, DRR-A1 had good gene silencing activity, while DRR-A7 was ineffective (Figure 4.4C and Figure 4.8). As expected, the non-targeting negative control siRNA (\emptyset) did not produce DRR downregulation.

At 40nM concentration, DRR-A1 and DRR-A4 compositions produced significant knockdown (40-70%; Figure 4.4C), demonstrating the utility of our modification patterns for both the DRR sequence and the luciferase sequence. However, with DRR, contrary to luciferase, the chemically modified compositions did not exceed the activity of the native siRNA (DRR1). DRR1 was the most efficient (90%), followed by DRR2 \approx DRR-A4 (70%), and DRR3 (50%).

Following treatment with these DRR targeting siRNAs, malignant glioma cells underwent phenotypic changes, indicative of DRR downregulation (Figure 4.4A and 4.4B). Phenotypic changes and focal adhesion dynamics were visualized by staining with vinculin (37).

Untreated cells remained spindle-shaped, with small focal adhesions. However, cells treated with DRR1 and Cy5-labelled DRR2 targeting siRNAs adopted round-shaped and large focal adhesions. The same was true for cells treated with DRR-A4, and somewhat with DRR-A1, but not with DRR-A7 (Figure 4.4B), consistent with the ability of these duplexes to knockdown DRR expression (Figure 4.4C). The Cy5-labelled DRR2 siRNA allowed the visualization of siRNA within cells, indicating that Cy5-labelled siRNAs are localized within cells, and thus demonstrating this non-invasive phenotype (DRR2-Cy5 lane; Figure 4.4A).

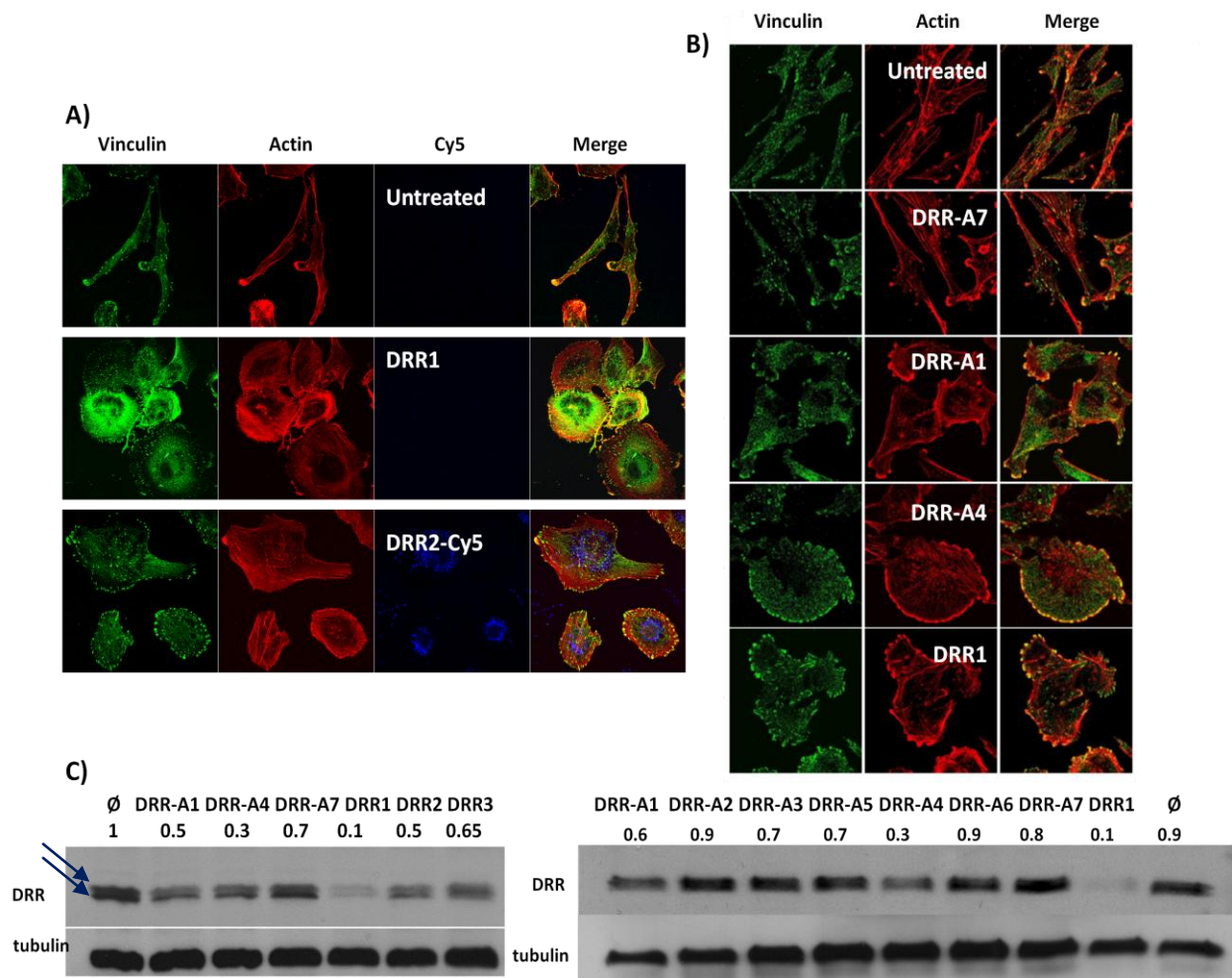


Figure 4.4. Gene silencing produced by siRNAs targeting DRR in invasive glioma cells. (A) & (B) Phenotypic outcome following DRR silencing. The green channel shows Vinculin staining (stains focal adhesions), red shows Actin staining, and blue shows Cy5 (only present in the DRR2-Cy5 siRNA). Untreated cells are shown in top row, DRR1-treated cells in middle row, and DRR2-Cy5-treated cells in bottom row. DRR expression promotes focal adhesion disassembly, whereas DRR deficiency leads to more stable focal adhesions. (C) Western blots comparing the gene silencing activity of DRR-targeting duplexes from Table 4.1. Western blot analyses were performed on samples with final duplex concentrations of 50nM (left) and 40nM (right). Top two bands indicated are the two DRR isoforms of interest; these are better resolved on left gel in Panel (C).

4.5 Conclusions

In summary, we have investigated, for the first time, short interfering duplexes containing arabinonucleotides (ANA; the 2'-stereoisomer of RNA), as well as combinations of ANA with RNA, and their 2'-fluorinated derivatives 2'F-ANA and/or 2'F-RNA. We took advantage of ANA's destabilizing effect to rationally design modified siRNAs that had altered thermal bias. We showed that ANA in combination with other modifications allowed siRNA duplex thermodynamics to be finely tuned to produce heavily-modified active siRNA duplexes against a reporter (firefly luciferase) and endogenous gene (DRR) relevant to brain cancer cell invasion.

Luciferase assays showed that si-duplexes with ANAs at the 3'-end of the sense strand (A4 and A5) were the most active; in fact, somewhat more active than the unmodified standard siRNA. Some of these patterns of modification were also useful for DRR downregulation, resulting in observable changes in cell phenotype properties. Chemically modified siRNA duplexes yielded a consistent DRR downregulation as well as the desired anti-invasive phenotype. DRR2 (with a fully 2'F-ANA sense strand and an all-2'F-RNA antisense strand), and DDR-A4 (with a fully ANA/2'F-ANA sense and all-RNA antisense strand), were the most active modified siRNA constructs tested against DRR, with potencies only slightly reduced from that of the unmodified siRNA duplex. Hence, arabinonucleic acid (ANA) modification has a place among chemically modified oligonucleotides known to be compatible with siRNA-mediated gene silencing in mammalian cells.

4.6 Experimental Methods

4.6.1 Oligonucleotide Synthesis and Purification

All oligonucleotides were synthesized using standard phosphoramidite chemistry on an Applied Biosystems 3400 DNA Synthesizer at a 1- μ mol scale using Unylink CPG support (ChemeGenes, Wilmington, MA) (53). All phosphoramidites were prepared as 0.15M solutions in acetonitrile (ACN), except DNA, which was prepared as 0.1M. 5-ethylthiotetrazole (0.25M in ACN) was used to activate phosphoramidites for coupling. Detritylations were accomplished with 3% trichloroacetic acid in dichloromethane for 110 seconds. Oxidation was done using 0.1M I₂ in 1:2:10 pyridine: water: THF. Coupling times were 600 seconds for ANA, 2'F-ANA, RNA, and 2'F-RNA phosphoramidites, with the exception of their guanosine phosphoramidites which were allowed to couple for 900 seconds. 5'-phosphorylation of the chemically modified strands was achieved using bis-cyanoethyl-N,N-diisopropyl-2-cyanoethyl phosphoramidite at 0.15M (600 seconds coupling time). Deprotection and cleavage from the solid support was accomplished with ammonia/ethanol (3:1 v/v) for 48 hours at room temperature (54). Oligonucleotides containing RNA were synthesized with standard 2'-TBDMS phosphoramidites, and desilylation was achieved with neat TEA.3HF for 48 hours at room temperature (55). Oligonucleotides were precipitated by adding of 3M sodium acetate (25 μ L) followed by addition of cold butanol (1000 μ L) and then purified by reverse phase HPLC on an Agilent 1200 series using a Waters semipreparative C18 column. For reverse phase purifications, a stationary phase of 100mM triethylammonium acetate in water with 5% ACN (pH7) and a mobile phase of HPLC-grade ACN were used (with a gradient of 0%-35% over 30 minutes). Purified oligonucleotides were then lyophilized to dryness, and were characterized by ESI-mass spectrometry. All oligonucleotides were quantitated by UV (extinction coefficients were calculated using the

online IDT OligoAnalyzer tool (www.idtdna.com/analyzer/Applications/OligoAnalyzer); ANA and 2'F-ANA extinction coefficients were calculated using DNA values and 2'F-RNA extinction coefficients were calculated using RNA values. Oligonucleotides were characterized by LC-MS. The MS data for all oligonucleotides used in this work are given in Tables 4.2 (luciferase series) and 4.3 (DRR series).

Table 4.2 MS characterization of si-duplexes targeting luciferase mRNA

Code	Sequence	Calculated mass (g/mole)	Experimental mass (g/mole)
CTRL (SS)	5'-GCUUGAAGUCUUUAAUUAAtt-3'	6613.8	6638.9 (+Na)
A1 (SS)	5'-GCUUGAAGUCUUUAAUUAAtt-3'	6613.8	6615.9
A3 (SS)	5'-GCUUGAAGUCUUUAAUUAAtt-3'	6657.8	6659.9
A4 (SS)	5'-GCUUGAAGUCUUUAAUUAAtt-3'	6655.8	6657.9
A5 (SS)	5'-GCUUGAAGUCUUUAAUUAAtt-3'	6655.8	6680.2 (+Na)
A6 (SS)	5'-GCUUGAAGUCUUUAAUUAAtt-3'	6653.8	6653.89
A7 (SS)	5'-GCUUGAAGUCUUUAAUUAAtt-3'	6671.8	n.d.
A8 (SS)	5'-GCUUGAAGUCUUUAAUUAAtt-3'	6631.8	6638.9
RNA (AS)	3'-ttCGAACUUCAGAAAUAAUU-5'	6619.9	6623.75
2'F-RNA (AS)	3'-ttCGAACUUCAGAAAUAAUUp-5'	6736.8	n.d.
ANA (AS)	3'-ttCGAACUUCAGAAAUAAUU-5'	6619.9	6619.9

Legend: RNA, 2'F-RNA, 2'F-ANA, ANA, dna; n.d. not measured, (SS): Sense Strand, (AS): Antisense Strand.

Table 4.3. MS characterization of si-duplexes targeting DRR mRNA

Code	Sequence	Calculated mass (g/mole)	Experimental mass(g/mole)
DRR-A1(SS)	5'-GGA ACC AGC UCA UCA AGA Att-3'	6696.0	6699.0
DRR-A2 (SS)	5'-GGA ACC AGC TCA TCA AGA Att-3'	6762.0	6765.2
DRR-A3 (SS)	5'-GGA ACC AGC UCA UCA AGA Att-3'	6712.0	6714.9
DRR-A4 (SS)	5'-GGA ACC AGC UCA UCA AGA Att-3'	6710.0	6712.9
DRR-A5 (SS)	5'-GGA ACC AGC UCA UCA AGA Att-3'	6710.0	6713.3
DRR-A6 (SS)	5'-GGA ACC AGC UCA UCA AGA Att-3'	6708.0	6713.2
DRR1& -A7(SS)	5'-GGA ACC AGC UCA UCA AGA Att-3'	6696.0	6699.1
RNA (AS)	3'-ttC CUU GGU CGA GUA GUU CUU-5'	6597.8	6600.0
ANA (AS)	3'-ttC CUU GGU CGA GUA GUU CUU-5'	6597.8	6601.0

Legend: RNA, 2'F-RNA, 2'F-ANA, ANA, dna; (SS): Sense Strand, (AS): Antisense Strand

4.6.2 siRNA Duplex Formation

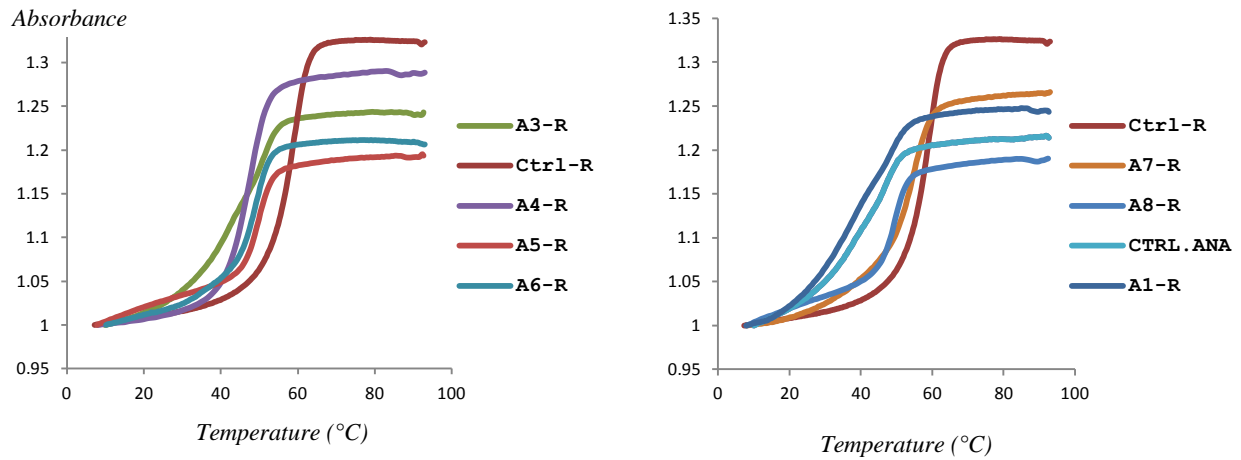
Hybridization to form siRNA duplexes was accomplished by combining equal amounts of purified passenger and guide strands to a final concentration of 2 μ M in siRNA buffer (100mM KOAc, 30mM HEPES-KOH, 2mM Mg(OAc)₂, pH 7.2). The samples were heated to 93°C for 2 minutes followed by cooling to room temperature over a period of approximately 6 hours. Samples were then placed in a 4°C fridge overnight to ensure perfect annealing.

4.6.3 Thermal Denaturation Experiments

UV thermal denaturation data were obtained on a Varian Cary 500 UV-VIS spectrophotometer equipped with a Peltier temperature controller. Equimolar amounts of the sense and antisense complement strands of each oligonucleotide duplex were combined in annealing buffer (140 mM KCl, 1mM MgCl₂, 5 mM NaHPO₄, pH 7.2) for a final duplex concentration of 2 μ M (4 μ M total concentration of single strands).

The temperature was increased at a rate of 0.4°C/min from 7°C to 93°C and absorbance values were recorded each 30 seconds. Samples were kept under flowing nitrogen when below 15°C. T_m values were calculated using the baseline method as assignment of baselines was clear in all cases. Normalized T_m curves for all si-duplexes used in this work are given in Figures 4.5 for luciferase series and Figure 4.6 for DRR series.

(A)



(B)

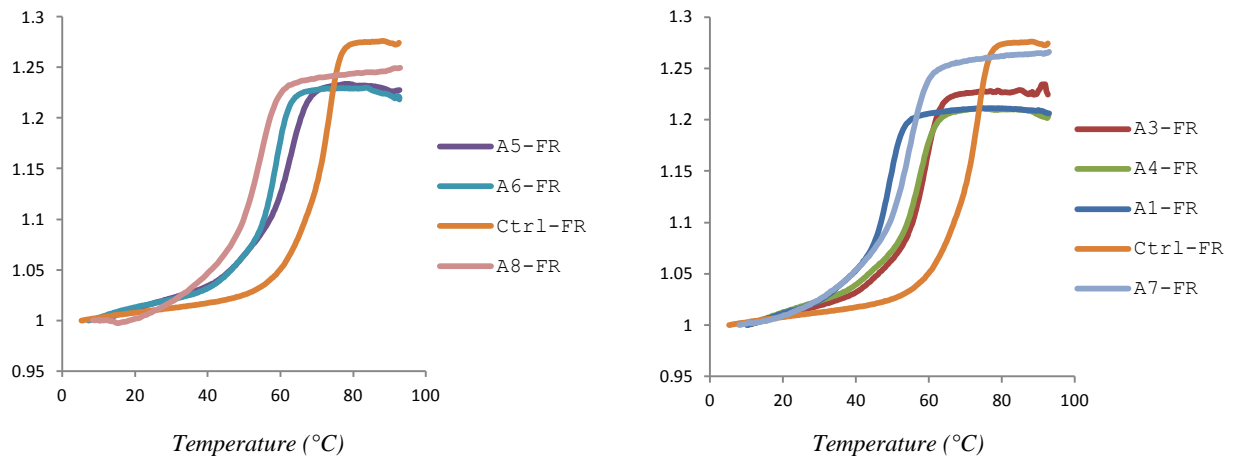


Figure 4.5. Melting profiles of si-duplexes targeting luciferase (A) with a native RNA antisense strand, and (B) with a 2'F-RNA modified antisense strand, as followed by observing the change in absorbance at 260 nm (A_{260}) of duplex samples upon heating from 7°C to 93°C. Duplexes were 2 μ M (4 μ M total concentration of strands) in phosphate buffer (140mM KCl, 5mM Na₂HPO₄, 1mM MgCl₂, pH 7.2). si-duplex sequences are as shown in Fig. 4.2A.

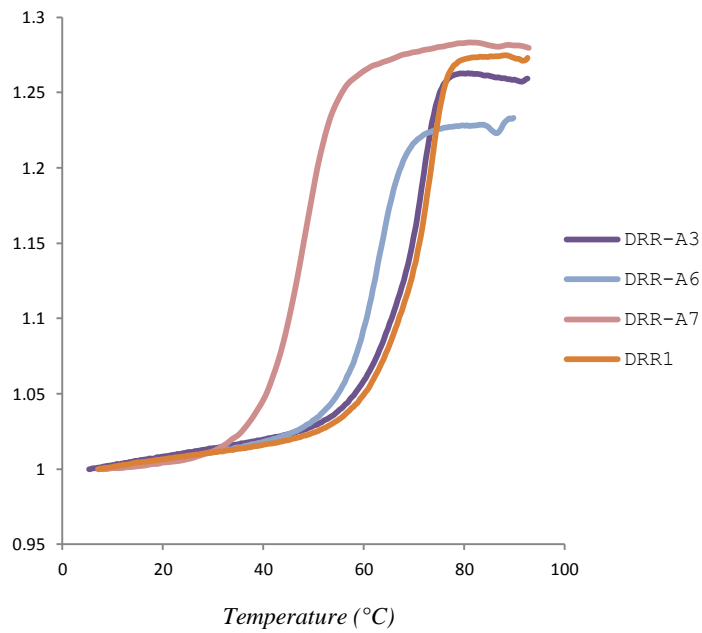
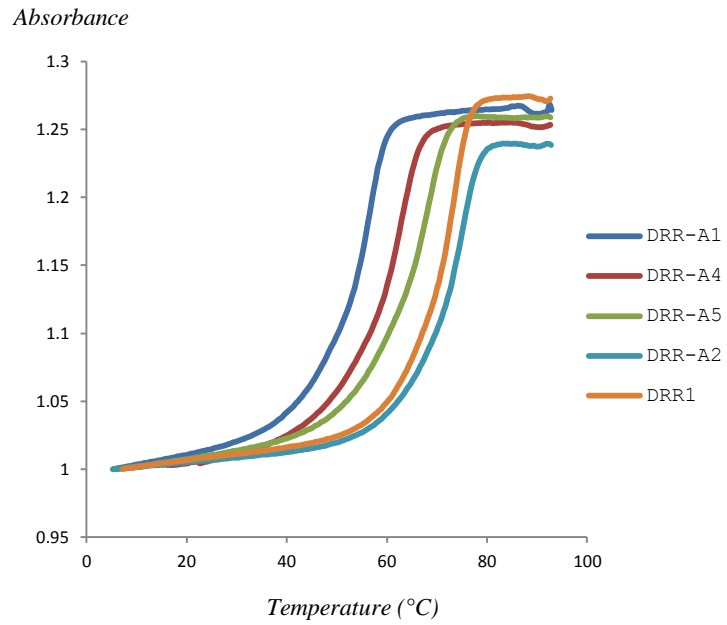


Figure 4.6. Melting profiles of si-duplexes targeting down-regulated in renal cell carcinoma (DRR) as followed by observing the change in absorbance at 260nm (A_{260}) of duplex samples upon heating from 7°C to 93°C. Duplexes were 2 μ M (4 μ M total concentration of strands) in phosphate buffer (140mM KCl, 5mM Na_2HPO_4 , 1mM MgCl_2 , pH 7.2). si-duplex sequences are as shown in Table 4.1.

4.6.4 Luciferase Assays

All luciferase knockdown assays were performed by Dr. Johans Fakhoury in the Sleiman lab at McGill University, Department of Chemistry. The procedure was as described by Deleavey *et al.* (25), with a few modifications. Typically, HeLa cells were counted and seeded at a density of 10,000 cells/well in a 96-well plate. Cells were allowed to recover for 24 hours at 37°C with 5% CO₂. Subsequently, cells were washed once with serum-free Dulbecco's Modified Eagle Medium (DMEM) and then 80µL of serum-free DMEM media was added. siRNA and control nucleic acid preparations were diluted up to 20µL with serum-free media and transfection reagent (Oligofectamine purchased from Invitrogen, Carlsbad, CA) and added to the appropriate well (for a total of 100µL) at increasing concentrations (0.16, 0.8, 4, 20, and 100nM). Cells were incubated for 4 hours; at that point each well was supplemented with 50µL of serum-enriched DMEM media. Cells were further incubated overnight (for a total of 24 hours post-DNA addition). Then 50µL of ONE-Glo luciferase reagent (Promega, Madison, WI) was added to each well and luminescence was measured and normalized to protein levels using a Biotek Synergy HT plate reader. Data was acquired with the Gen5 software suite and data was processed and plotted using Graphpad Prism software suite. The corresponding dose-response curves for all the si-duplexes used in this work are given in Figures 4.7.

Figure 4.7 (A)

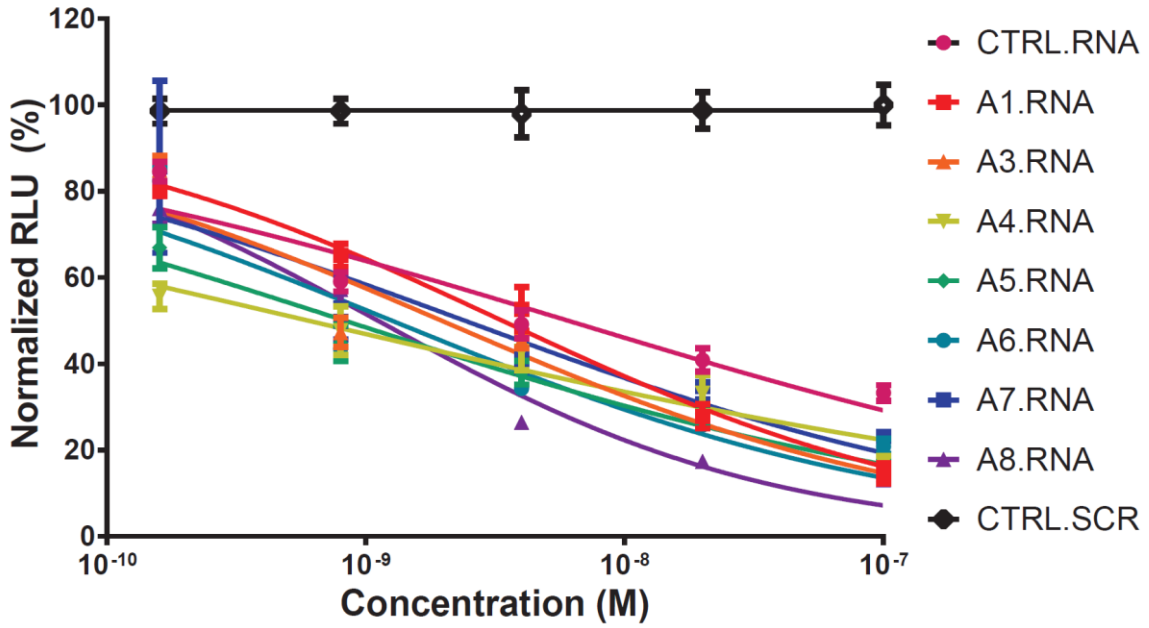
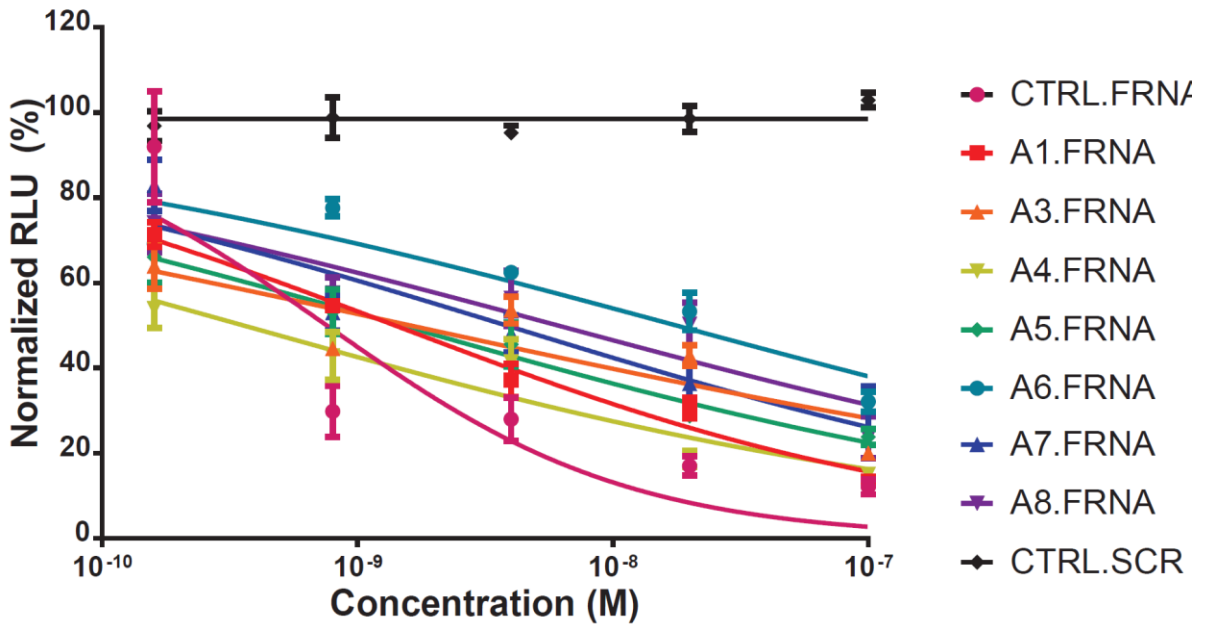


Figure 4.7 (B)



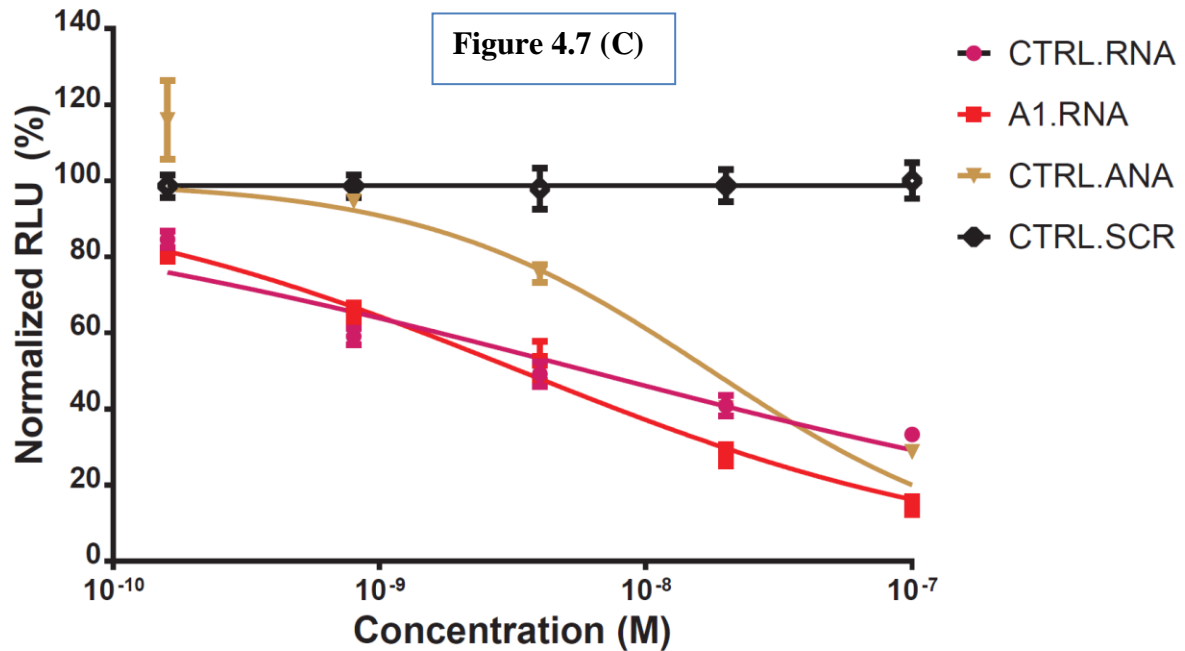


Figure 4.7 Dose-response curves for firefly luciferase targeting si-duplexes that have (A) native RNA antisense strand; (B) 2'F-RNA fully modified antisense strand; (C) all-ANA modified sense or antisense strand. Experiments were conducted at 5 concentrations (100nM, 20nM, 4nM, 0.8nM and 0.16nM) and luciferase levels were normalized to total cellular protein and luciferase counts of mock treated cells. si-duplex sequences can be found in Figures 4.2A and 4.3A.

4.6.5 DRR Assays

All DRR knockdown assays and cell imaging experiments were performed by Dr. Phuong Le in Petrecca's lab at the Montreal Neurological Institute and Hospital, Department of Neurology and Neurosurgery, McGill University.

4.6.5.1 Cell culture and transfection. Human glioblastoma, DRR⁺ cell line were cultured as previously described (37). One day before transfection, DRR⁺ cells were plated in 24 well or 6 well plates such that they reach 75% confluency at the time of transfection. All transfections were done using lipofectamine 2000 reagent according to the manufacturer indications. Briefly, lipofectamine was gently mixed in opti-MEM and left at room temperature for 5 minutes. DRR duplexes were first mixed with opti-MEM such that the final concentration added to the cells were 40nM and then gently mixed with lipofectamine. Lipofectamine-DRR duplexes were incubated at room temperature for 20 minutes before being added to the cells. The day after transfection, fresh cell media was added to the transfected cells. Cells were lysed or fixed following 72 hours post-transfection.

4.6.5.2 Western blot analysis. Cells were washed with Phosphate-Buffered Saline (PBS), and then lysed with 2% hot sodium dodecyl sulfate (SDS); equal cell lysates were separated by 12% SDS-polyacrylamide gel electrophoresis and transferred on to nitrocellulose membrane. Then, the membrane was blocked for 30 minutes with 2.5% condensed milk before being incubated overnight at 4°C with rabbit anti-DRR antibody or mouse anti-tubulin (Sigma, Oakville, ON) for loading control. Immuno-reactive bands were detected by a goat anti-rabbit or anti-mouse antibody linked to horseradish peroxidase (Jackson ImmunoResearch, West Grove, PA), and

visualized by chemiluminescence (Pierce ECL substrate purchased from Thermo Scientific, Rockford, IL).

Densitometry analysis of four different western blots of DRR expression is illustrated in Figure 4.8. Intensity of protein bands was quantified using ImageJ (NIH). DRR protein expression level was normalized against tubulin and represented as mean \pm s.e.m with values measured relative to the control (\emptyset) condition. siRNA sequences are as shown in Table 4.1.

4.6.5.3 Immunofluorescence. Cells were washed with PBS, then fixed with 4% Paraformaldehyde (PFA) in PBS and permeabilized with 0.5% TritonX-100 before being processed for immuno-staining. Cells were labelled for 30 minutes with mouse anti-vinculin to visualize focal adhesions and rhodamine-phalloidin was used to stain actin. Alexa 488 anti-mouse was used to detect vinculin. Fluorescently labelled cells were visualized with a Zeiss LSM700 confocal microscope using 63x objectives.

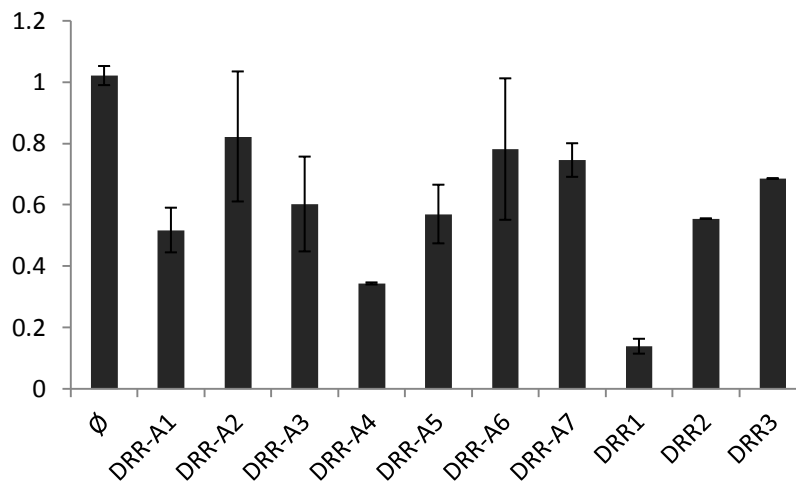


Figure 4.8 Densitometry analyses of four different western blots of DRR expression after treatment with designed siRNAs.

4.7 References

1. Kubo, T., Takamori, K., Kanno, K.-i., Rumiana, B., Ohba, H., Matsukisono, M., Akebiyama, Y. and Fujii, M. (2005) Efficient cleavage of RNA, enhanced cellular uptake, and controlled intracellular localization of conjugate DNAzymes. *Bioorganic & Medicinal Chemistry Letters*, **15**, 167-170.
2. Kubo, T., Morikawa, M., Ohba, H. and Fujii, M. (2003) Synthesis of DNA–Peptide Conjugates by Solid-Phase Fragment Condensation. *Organic Letters*, **5**, 2623-2626.
3. Jackson, A.L., Burchard, J., Leake, D., Reynolds, A., Schelter, J., Guo, J., Johnson, J.M., Lim, L., Karpilow, J., Nichols, K. *et al.* (2006) Position-specific chemical modification of siRNAs reduces “off-target” transcript silencing. *RNA*, **12**, 1197-1205.
4. Whitehead, K.A., Dahlman, J.E., Langer, R.S. and Anderson, D.G. (2011) Silencing or stimulation? siRNA delivery and the immune system. *Annual review of chemical and biomolecular engineering*, **2**, 77-96.
5. Czauderna, F., Fechtner, M., Dames, S., Aygün, H., Klippel, A., Pronk, G.J., Giese, K. and Kaufmann, J. (2003) Structural variations and stabilising modifications of synthetic siRNAs in mammalian cells. *Nucleic Acids Research*, **31**, 2705-2716.
6. Amarzguioui, M., Holen, T., Babaie, E. and Prydz, H. (2003) Tolerance for mutations and chemical modifications in a siRNA. *Nucleic Acids Research*, **31**, 589-595.
7. Braasch, D.A., Jensen, S., Liu, Y., Kaur, K., Arar, K., White, M.A. and Corey, D.R. (2003) RNA Interference in Mammalian Cells by Chemically-Modified RNA[†]. *Biochemistry*, **42**, 7967-7975.
8. Kenski, D.M., Cooper, A.J., Li, J.J., Willingham, A.T., Haringsma, H.J., Young, T.A., Kuklin, N.A., Jones, J.J., Cancilla, M.T., McMasters, D.R. *et al.* (2010) Analysis of acyclic nucleoside modifications in siRNAs finds sensitivity at position 1 that is restored by 5'-terminal phosphorylation both in vitro and in vivo. *Nucleic Acids Research*, **38**, 660-671.
9. Hall, A.H.S., Wan, J., Spesock, A., Sergueeva, Z., Shaw, B.R. and Alexander, K.A. (2006) High potency silencing by single-stranded boranophosphate siRNA. *Nucleic Acids Research*, **34**, 2773-2781.
10. Watts, J.K., Deleavey, G.F. and Damha, M.J. (2008) Chemically modified siRNA: tools and applications. *Drug Discovery Today*, **13**, 842-855.
11. Deleavey, G.F., Watts, J.K. and Damha, M.J. (2001), *Current Protocols in Nucleic Acid Chemistry*. John Wiley & Sons, Inc.
12. Deleavey, G.F. and Damha, M.J. (2012) Designing chemically modified oligonucleotides for targeted gene silencing. *Chemistry and Biology*, **19**, 937-954.
13. Watts, J.K. and Corey, D.R. (2012) Silencing disease genes in the laboratory and the clinic. *The Journal of Pathology*, **226**, 365-379.
14. Wilds, C.J. and Damha, M.J. (2000) 2'-Deoxy-2'-fluoro-β-d-arabinonucleosides and oligonucleotides (2'F-ANA): synthesis and physicochemical studies. *Nucleic Acids Research*, **28**, 3625-3635.
15. Damha, M.J., Wilds, C.J., Noronha, A., Brukner, I., Borkow, G., Arion, D. and Parniak, M.A. (1998) Hybrids of RNA and Arabinonucleic Acids (ANA and 2'F-ANA) Are Substrates of Ribonuclease H. *Journal of the American Chemical Society*, **120**, 12976-12977.

16. Rosenberg, I., Soler, J.F., Tocik, Z., Ren, W.-Y., Ciszewski, L.A., Kois, P., Pankiewicz, K.W., Spassova, M. and Watanabe, K.A. (1993) Synthesis of Oligodeoxynucleotides Containing the C-Nucleoside and 2'-Deoxy-2'-Fluoro-ara-Nucleoside Moieties by the H-Phosphonate Method.1,2. *Nucleosides and Nucleotides*, **12**, 381-401.
17. Kois, P., Tocik, Z., Spassova, M., Ren, W.-Y., Rosenberg, I., Soler, J.F. and Watanabe, K.A. (1993) Synthesis and Some Properties of Modified Oligonucleotides. II. Oligonucleotides Containing 2'-Deoxy-2'-fluoro- β -D-arabinofuranosyl Pyrimidine Nucleosides. *Nucleosides and Nucleotides*, **12**, 1093-1109.
18. Watts, J.K. and Damha, M.J. (2008) 2'-F-Arabinonucleic acids (2'-F-ANA) — History, properties, and new frontiers. *Canadian Journal of Chemistry*, **86**, 641-656.
19. Watts, J.K. and Damha, M.J. (2008) ChemInform Abstract: 2'-F-Arabinonucleic Acids (2'-F-ANA) — History, Properties, and New Frontiers. *ChemInform*, **39**, no-no.
20. Watts, J.K., Martín-Pintado, N., Gómez-Pinto, I., Schwartzentruber, J., Portella, G., Orozco, M., González, C. and Damha, M.J. (2010) Differential stability of 2'-F-ANA•RNA and ANA•RNA hybrid duplexes: roles of structure, pseudohydrogen bonding, hydration, ion uptake and flexibility. *Nucleic Acids Research*, **38**, 2498-2511.
21. Kalota, A., Karabon, L., Swider, C.R., Viazovkina, E., Elzagheid, M., Damha, M.J. and Gewirtz, A.M. (2006) 2'-Deoxy-2'-fluoro- β -d-arabinonucleic acid (2'-F-ANA) modified oligonucleotides (ON) effect highly efficient, and persistent, gene silencing. *Nucleic Acids Research*, **34**, 451-461.
22. Denisov, A.Y., Noronha, A.M., Wilds, C.J., Trempe, J.-F., Pon, R.T., Gehring, K. and Damha, M.J. (2001) Solution structure of an arabinonucleic acid (ANA)/RNA duplex in a chimeric hairpin: comparison with 2'-fluoro-ANA/RNA and DNA/RNA hybrids. *Nucleic Acids Research*, **29**, 4284-4293.
23. Noronha, A.M., Wilds, C.J., Lok, C.-N., Viazovkina, K., Arion, D., Parniak, M.A. and Damha, M.J. (2000) Synthesis and Biophysical Properties of Arabinonucleic Acids (ANA): Circular Dichroic Spectra, Melting Temperatures, and Ribonuclease H Susceptibility of ANA•RNA Hybrid Duplexes. *Biochemistry*, **39**, 7050-7062.
24. Mangos, M.M., Min, K.-L., Viazovkina, E., Galarneau, A., Elzagheid, M.I., Parniak, M.A. and Damha, M.J. (2002) Efficient RNase H-Directed Cleavage of RNA Promoted by Antisense DNA or 2'-F-ANA Constructs Containing Acyclic Nucleotide Inserts. *Journal of the American Chemical Society*, **125**, 654-661.
25. Deleavey, G.F., Watts, J.K., Alain, T., Robert, F., Kalota, A., Aishwarya, V., Pelletier, J., Gewirtz, A.M., Sonenberg, N. and Damha, M.J. (2010) Synergistic effects between analogs of DNA and RNA improve the potency of siRNA-mediated gene silencing. *Nucleic Acids Research*, **38**, 4547-4557.
26. Dowler, T., Bergeron, D., Tedeschi, A.-L., Paquet, L., Ferrari, N. and Damha, M.J. (2006) Improvements in siRNA properties mediated by 2'-deoxy-2'-fluoro- β -d-arabinonucleic acid (FANA). *Nucleic Acids Research*, **34**, 1669-1675.
27. Khvorova, A., Reynolds, A. and Jayasena, S.D. (2003) Functional siRNAs and miRNAs exhibit strand bias. *Cell*, **115**, 209-216.
28. Schwarz, D.S., Hutvagner, G., Du, T., Xu, Z., Aronin, N. and Zamore, P.D. (2003) Asymmetry in the assembly of the RNAi enzyme complex. *Cell*, **115**, 199-208.

29. Jinek, M. and Doudna, J.A. (2009) A three-dimensional view of the molecular machinery of RNA interference. *Nature*, **457**, 405-412.
30. Wang, H.-W., Noland, C., Siridechadilok, B., Taylor, D.W., Ma, E., Felderer, K., Doudna, J.A. and Nogales, E. (2009) Structural insights into RNA processing by the human RISC-loading complex. *Nat Struct Mol Biol*, **16**, 1148-1153.
31. Noland, Cameron L., Ma, E. and Doudna, Jennifer A. siRNA Repositioning for Guide Strand Selection by Human Dicer Complexes. *Molecular Cell*, **43**, 110-121.
32. Noland, C.L. and Doudna, J.A. (2013) Multiple sensors ensure guide strand selection in human RNAi pathways. *Rna*, **19**, 639-648.
33. Iijima, A., Hachisu, R., Kobayashi, H., Hashimoto, K., Asano, D. and Kikuchi, H. (2007) Establishment of Evaluation Method for siRNA Delivery Using Stable Cell Line Carrying the Luciferase Reporter Gene. *Biological and Pharmaceutical Bulletin*, **30**, 1844-1850.
34. Lee, H., Lytton-Jean, A.K.R., Chen, Y., Love, K.T., Park, A.I., Karagiannis, E.D., Sehgal, A., Querbes, W., Zurenko, C.S., Jayaraman, M. *et al.* (2012) Molecularly self-assembled nucleic acid nanoparticles for targeted in vivo siRNA delivery. *Nat Nano*, **7**, 389-393.
35. Lavergne, T., Baraguey, C., Dupouy, C., Parey, N., Wuensche, W., Sczakiel, G., Vasseur, J.-J. and Debart, F.o. (2011) Synthesis and Preliminary Evaluation of pro-RNA 2'-O-Masked with Biolabile Pivaloyloxymethyl Groups in an RNA Interference Assay. *The Journal of Organic Chemistry*, **76**, 5719-5731.
36. Giljohann, D.A., Seferos, D.S., Prigodich, A.E., Patel, P.C. and Mirkin, C.A. (2009) Gene Regulation with Polyvalent siRNA–Nanoparticle Conjugates. *Journal of the American Chemical Society*, **131**, 2072-2073.
37. Le, P.U., Angers-Loustau, A., Oliveira, R.M.W.d., Ajlan, A., Brassard, C.L., Dudley, A., Brent, H., Siu, V., Trinh, G., Mölenkamp, G. *et al.* (2010) DRR drives brain cancer invasion by regulating cytoskeletal-focal adhesion dynamics. *Oncogene*, **29**, 4636-4647.
38. Dudley, A., Sater, M., Le, P.U., Trinh, G., Sadr, M.S., Bergeron, J., Deleavey, G.F., Bedell, B., Damha, M.J. and Petrecca, K. (2013) DRR regulates AKT activation to drive brain cancer invasion. *Oncogene*.
39. Elbashir, S.M., Harborth, J., Lendeckel, W., Yalcin, A., Weber, K. and Tuschl, T. (2001) Duplexes of 21-nucleotide RNAs mediate RNA interference in cultured mammalian cells. *Nature*, **411**, 494-498.
40. Leuschner, P.J., Ameres, S.L., Kueng, S. and Martinez, J. (2006) Cleavage of the siRNA passenger strand during RISC assembly in human cells. *EMBO reports*, **7**, 314-320.
41. Matranga, C., Tomari, Y., Shin, C., Bartel, D.P. and Zamore, P.D. (2005) Passenger-strand cleavage facilitates assembly of siRNA into Ago2-containing RNAi enzyme complexes. *Cell*, **123**, 607-620.
42. Lee, H.Y., Zhou, K., Smith, A.M., Noland, C.L. and Doudna, J.A. (2013) Differential roles of human Dicer-binding proteins TRBP and PACT in small RNA processing. *Nucleic Acids Res*, **41**, 6568-6576.
43. Gong, W. and Desaulniers, J.-P. (2012) Gene-silencing properties of siRNAs that contain internal amide-bond linkages. *Bioorganic & Medicinal Chemistry Letters*, **22**, 6934-6937.
44. Hall, A.H.S., Wan, J., Shaughnessy, E.E., Ramsay Shaw, B. and Alexander, K.A. (2004) RNA interference using boranophosphate siRNAs: structure–activity relationships. *Nucleic Acids Research*, **32**, 5991-6000.

45. Blidner, R.A., Hammer, R.P., Lopez, M.J., Robinson, S.O. and Monroe, W.T. (2007) Fully 2'-Deoxy-2'-Fluoro Substituted Nucleic Acids Induce RNA Interference in Mammalian Cell Culture. *Chemical Biology & Drug Design*, **70**, 113-122.
46. Martín-Pintado, N., Yahyaee-Anzahae, M., Campos-Olivas, R., Noronha, A.M., Wilds, C.J., Damha, M.J. and González, C. (2012) The solution structure of double helical arabino nucleic acids (ANA and 2'-F-ANA): effect of arabinoses in duplex-hairpin interconversion. *Nucleic Acids Research*, **40**, 9329-9339.
47. Anzahae, M.Y., Watts, J.K., Alla, N.R., Nicholson, A.W. and Damha, M.J. (2010) Energetically Important C-H...F-C Pseudohydrogen Bonding in Water: Evidence and Application to Rational Design of Oligonucleotides with High Binding Affinity. *Journal of the American Chemical Society*, **133**, 728-731.
48. Lavergne, T., Baraguey, C., Dupouy, C., Parey, N., Wuensche, W., Sczakiel, G., Vasseur, J.J. and Debart, F. (2011) Synthesis and preliminary evaluation of pro-RNA 2'-O-masked with biolabile pivaloyloxymethyl groups in an RNA interference assay. *J Org Chem*, **76**, 5719-5731.
49. Watts, J.K., Choubdar, N., Sadalapure, K., Robert, F., Wahba, A.S., Pelletier, J., Mario Pinto, B. and Damha, M.J. (2007) 2'-Fluoro-4'-thioarabino-modified oligonucleotides: conformational switches linked to siRNA activity. *Nucleic Acids Research*, **35**, 1441-1451.
50. Deleavey, G.F., Frank, F., Hassler, M., Wisnovsky, S., Nagar, B. and Damha, M.J. (2013) The 5' Binding MID Domain of Human Argonaute2 Tolerates Chemically Modified Nucleotide Analogues. *Nucleic Acid Therapeutics*, **23**, 81-87.
51. Martín-Pintado, N., Deleavey, G.F., Portella, G., Campos-Olivas, R., Orozco, M., Damha, M.J. and González, C. (2013) Backbone FCH...O Hydrogen Bonds in 2'-F-Substituted Nucleic Acids. *Angewandte Chemie International Edition*, **52**, 12065-12068.
52. Deleavey, G.F. (2013) *2' and 4' Fluorinated Nucleosides: Developing Modified Nucleic Acids for the Regulation of Gene Expression*. PhD Thesis, McGill University, Department of Chemistry.
53. Damha, M. and Ogilvie, K. (1993) In Agrawal, S. (ed.), *Protocols for Oligonucleotides and Analogs*. Humana Press, Vol. 20, pp. 81-114.
54. Bellon, L. (2001) Oligoribonucleotides with 2'-O-(tert-Butyldimethylsilyl) Groups. *Current protocols in nucleic acid chemistry*, **Unit 3.6.1-3.6.13**.
55. Westman, E. and Stromberg, R. (1994) Removal of t-butylidimethylsilyl protection in RNA-synthesis. Triethylamine trihydrofluoride (TEA, 3HF) is a more reliable alternative to tetrabutylammonium fluoride (TBAF). *Nucleic Acids Research*, **22**, 2430-2431.

CHAPTER 5: STRUCTURAL PROPERTIES AND GENE SILENCING ACTIVITY OF PARALLEL-STRANDED NUCLEIC ACID DUPLEXES AT PHYSIOLOGICAL CONDITIONS

5.1 Parallel-Stranded DNA and RNA

Nucleic acid double helices adopt an antiparallel-stranded (*aps*) conformation with one strand in 5'-3' and the other in 3'-5' orientation (1). However, they have the capacity to adopt the less common parallel-stranded (*ps*) arrangement as well (2-7) (Figure 5.1). Parallel hybridization is also observed in higher-ordered nucleic acid structures like in triplexes (8-12), G-quadruplexes (13-17) and i-motifs (18,19) as well.



Figure 5.1 Illustration of antiparallel (left) and parallel (right) chain orientation in double helices.

The feasibility of parallel hybridization was a question to researchers for a long time. In 1986, Pattabiraman for the first time demonstrated the possibility of formation of a *ps*-DNA duplex, $dA_6:dT_6$, via quantum mechanics calculations (20). A characteristic feature of the calculated parallel duplex was the equal size of the grooves. Also, each individual strand in such complex essentially maintained a conformation that was similar to B-DNA, with anti-orientation of the bases and C2'-*endo* sugar puckering (20). The theoretical study by Pattabiraman triggered an interest for further investigation on parallel hybridization. Soon after, the first structural and thermodynamic study was performed by Van de Sande in 1988 and on hairpin sequences that contained either a 3'-p-3' or a 5'-p-5' linkage on the loop, and as a result their two arms were

forced to run parallel to each other (5). Since then, immense progress has been made in the synthesis as well as the theoretical and experimental evaluation of parallel double helical structures (21-33).

In general, the construction of parallel double helices is difficult and requires sequences that are perfectly complementary in parallel orientation and poorly matched towards the function of all competitive antiparallel hybridization possibilities. Moreover, it requires a selection of unnatural chemical or environmental conditions. For instance, it has been established that parallel orientation of the strands and nonWatson-Crick base pairing can be achieved via chemical modification of the nucleobases (34-38), as a consequence of polarity strand reversal by introducing a 3'/3' or 5'/5' linkage (5,39,40), or by changing the stereochemistry of the glycosidic bonds e.g. parallel hybrids are observed with α -anomeric oligodeoxynucleotides and complementary β -oligodeoxynucleotides (41,42). Parallel hybridization can also be achieved at pHs lower than the neutral pH and mainly through formation of Hoogsteen or C:C⁺ base pairs (7,33,43-45). As expected, spectroscopic properties, enzymatic recognition as well as ligand-binding (drug or protein) properties of noncanonical *ps* duplexes are different from that of the antiparallel duplexes (46-52).

5.2 Noncanonical Base Pairing Patterns in Parallel-Stranded Duplexes

As mentioned in Chapter 1, formation of parallel double helices like many other noncanonical nucleic acid structures arises from the fact that nucleobases have different sites (edges) for base pairing (53). These are (i) Watson- Crick (WC) edge, (ii) Hoogsteen (H) edge (purines)/ C-H edge (pyrimidines), and (iii) Sugar edge (SE), which involves the ribose where the 2'-hydroxyl group is capable of forming efficient H-bonds, in contrast to deoxyribose in DNA (see Figure 1.6

in Chapter 1). The canonical hydrogen bonding motif is a WC edge-to-WC edge interaction, with the glycosidic bonds oriented cis relative to the axis of interaction (Figure 5.2a).

For parallel duplexes of mixed base composition, one major type of hetero-base pairing pattern (purine-pyrimidine hydrogen bonding) is the reverse Watson Crick (rWC) base pairing (Figure 5.2b). In rWC base pairs, the nucleobases are interacting through their Watson-Crick edges as in canonical WC base pairs; however, the glycosidic bonds of the nucleotides are oriented trans relative to the axis of interaction (4). Specifically, A/T rich oligonucleotides, either those that contain blocks of A and T stretches (32), or those that contain alternating A-T residues (25), can form stable reverse rWC parallel-stranded duplexes. That is because thymine is symmetrical about the central thymine-N3-adenine-N1 axis of an A:T pair. This symmetry allows adenine-thymine pair to form two hydrogen bonds not only in the antiparallel orientation, but also in the parallel arrangement. In comparison to canonical B-DNA duplexes, such parallel constructs contain grooves of about equal size (5,20); and hence, their molecular recognition by proteins and intercalating drugs or dyes is expected to be different from that of duplexes with antiparallel chain orientation (25,49).

Reverse Watson-Crick parallel sequences can also tolerate the presence of G:C pairs, albeit with reduced stability, which is characterized by low-cooperative melting profiles (4,31,54,55). That is because unlike T (U), cytosine is not symmetrical with regard to the axis of interaction. Therefore, in order for guanine and cytosine to pair in rWC arrangement, the bases might need to shift relative to one another which causes stability loss as compared to canonical G:C pair (see the “sheared” reverse Watson-Crick G:C pair in Figure 5.2b).

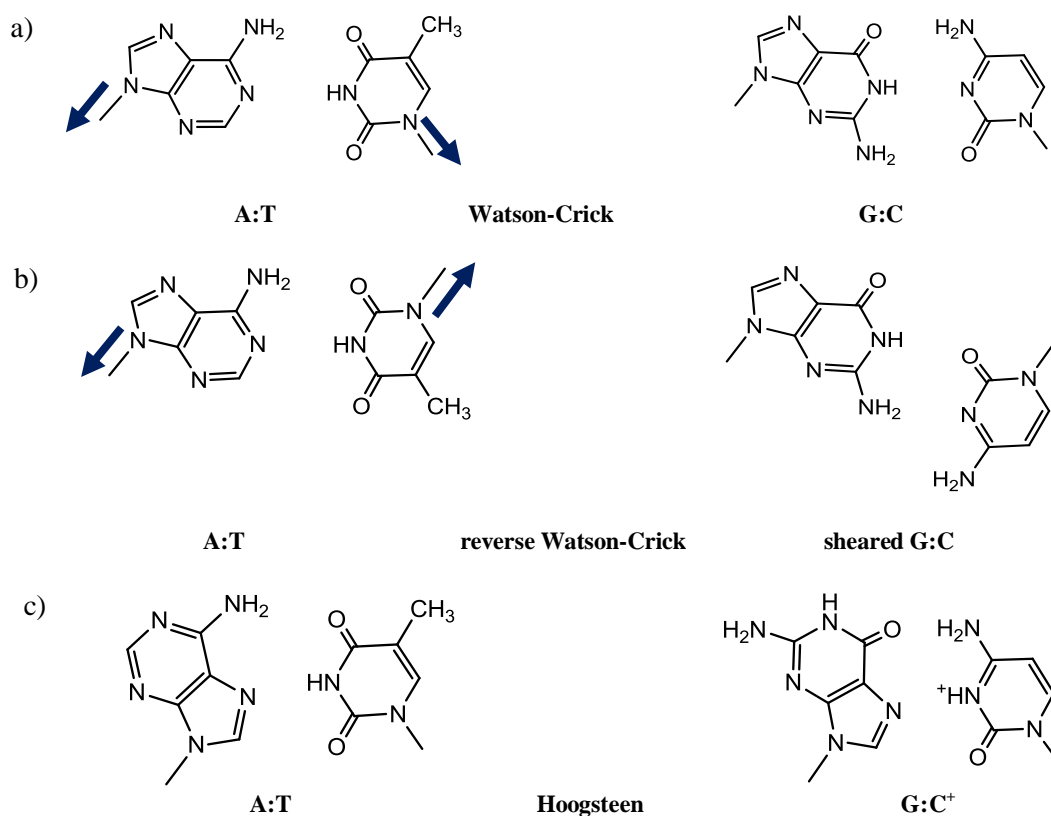


Figure 5.2 Common base pairing schemes in antiparallel and parallel *ds*-DNA containing canonical nucleobases. Arrows indicate the geometry of glycosidic bonds in WC and rWC duplexes. Note that in (a) and (b), the nucleobases adopt anti conformation while in (c) purines adopt syn conformation.

The most plausible explanation for the energy loss is perhaps the distortion of the sugar-phosphate backbone at the A:T/G:C stacking contact in parallel orientation, as the “sheared” trans G:C pair is not isomorphous to the trans AT pair (4,51). In order to compensate for this energy loss when designing rWC parallel duplexes of mixed-base composition and to improve the hybridization properties of trans G:C base pairs, the use of chemically modified nucleobases is one solution. The existence of stable parallel duplexes of mixed-base composition containing adenine-thymine, isoguanine-cytosine, and isocytosine-guanine reverse Watson-Crick (rWC) pairs has been reported in which the complete hydrogen bond pairing is restored (Figure 5.3) (36-38,56,57).

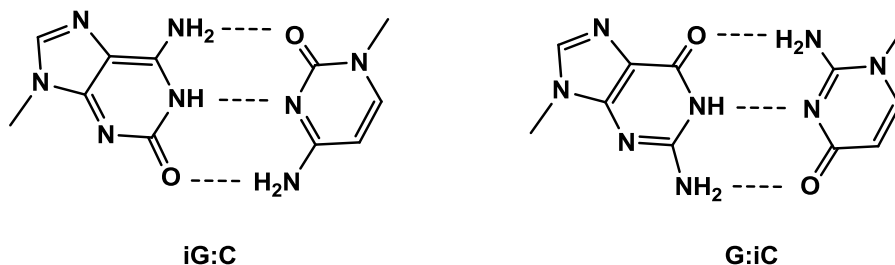


Figure 5.3 Representation of three hydrogen bonds associated with isoguanine-cytosine pair (iG:C) and guanine-isocytosine pair (G:iC) in reverse Watson-Crick geometry.

The formation of parallel-stranded duplexes is not restricted to reverse Watson-Crick pairing. The Hoogsteen hydrogen bonds are another class of hetero-base pairs observed for parallel hybridization, which match the Hoogsteen edge of “syn” purines to the Watson-Crick edge of “anti” pyrimidines (Figure 5.2c). This pairing mode is favored in acidic conditions where the cytosine N3 is protonated, and hence additional stabilization is achieved via C⁺:G Hoogsteen hydrogen bonding (Figure 5.2c) (7,45,58). Acidic conditions also efficiently stabilize purine-purine and pyrimidine-pyrimidine self-pairing in parallel orientation (33,59-64).

5.3 Objectives

The interest in nucleic acid parallel double helices has grown significantly in the recent years, mainly because of their possible roles in biological function (65,66), their potential to be used as an entirely new base pairing system in synthetic biology (67), for the development of DNA nanostructures (68), and for designing novel oligonucleotide hybridization probes and oligonucleotide-based therapeutics (63,69). Despite the emerging interest in employing parallel hybridization for different applications, the research conducted in the field is restricted to *ps*-

DNA, and our understanding on the formation of other types of parallel duplexes such as *ps*-RNA or *ps*-RNA:DNA is extremely limited and remains mostly at the level of stability from T_m measurements (36,38,43,70,71). Their biological significance, if any, also remains to be established.

To expand upon our current knowledge of parallel-stranded duplexes, we aimed to study the impact of several sugar and nucleobase substitutions on the formation of parallel duplexes at neutral pH. Our study is the first to incorporate ribo isoguanine and ribo isocytosine (r-iG and r-iC; Figure 5.4) into an RNA strand, investigating whether formation of a stable *ps*-RNA or *ps*-DNA:RNA hybrid is possible under physiological-like conditions. We also examine the impact of sugar modification (2'-fluorinated sugars; Figure 5.4) on duplex strength and assess whether similar stabilizing effects as in 2'-fluorinated *aps*-duplexes are observed (72-75). Previous efforts undertaken towards the stabilization of a parallel motif have mainly focused on modifying the isoguanine and isocytosine nucleobases of *ps*-DNA (76,77).

We first examined the structure and stability of several parallel 12-bp hybrids incorporating a combination of different base and sugar modifications. Next, in an extension of our work, stable patterns of modification identified with parallel 12-bp hybrids were used to synthesize longer-chain parallel oligonucleotides (21-mers) and produce, for the first time, parallel-stranded duplexes that inhibit the expression of the oncoprotein Bcl-2 via the RNA interference pathway.

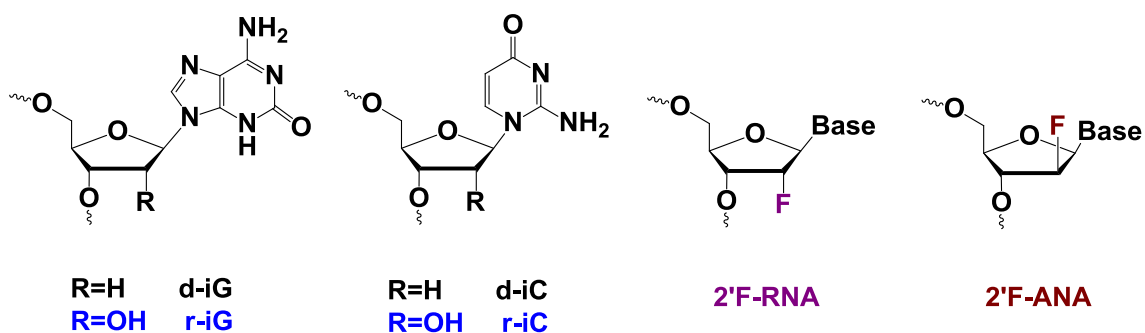


Figure 5.4 Structures of chemically modified nucleotides incorporated to the parallel arrangement.

5.4 Parallel 12-bp Oligonucleotides

5.4.1 Design of 12-bp Parallel Hybrids and Thermal Denaturation Analysis

The thermal stability of the *ps*-DNA dodecamer shown in Figure 5.5A was previously reported (38). We started our studies using the same model sequence and incorporated deoxy isocytosine (d-iC) and deoxy isoguanine (d-iG) nucleotides to regenerate the iso-modified DNA strand (iDD, Strand 1, Figure 5.5B). In order to explore whether 2'F-arabinose modification could stabilize this duplex, as observed for antiparallel duplexes, we also prepared iD-aF (Strand 1, Figure 5.5B). To determine whether RNA can form parallel duplexes, we prepared the corresponding r-iC/r-iG RNA strand (iR, Strand 1, Figure 5.5B). Control oligomers containing rC/rG and no r-iC/r-iG were prepared to assess the requirement of the iso modification in parallel duplex formation (D1 and R1 controls, Strand 1, Figure 5.5B). All of these sequences were then hybridized to series of complementary strands designed to form either parallel (D2, R2, aF2, rF2, Strand 2) or antiparallel (D3, R3, Strand 3) duplexes of the same base sequence (Figure 5.5B). As shown in Figure 5.5, a variety of strand pairing is possible, producing a rather large library of duplex combinations.

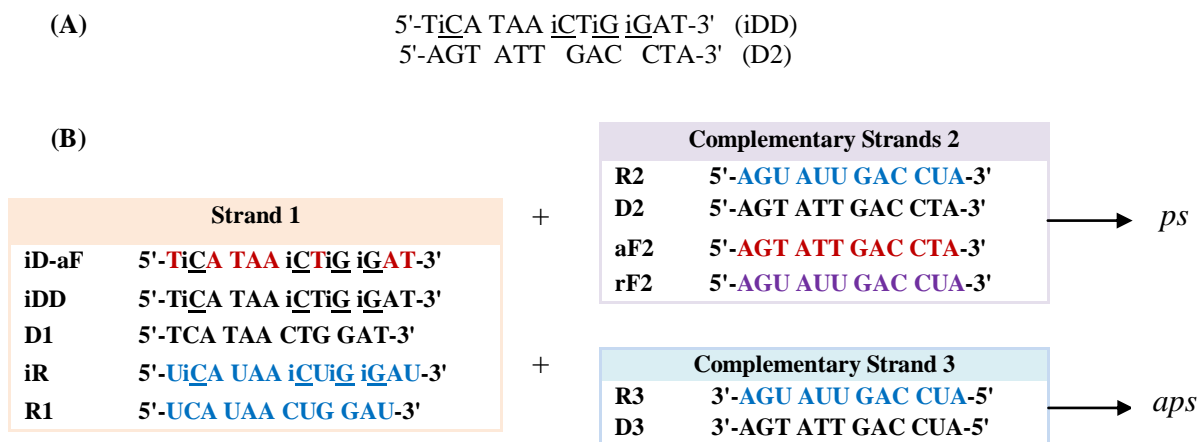


Figure 5.5 (A) Sequence of previously studied parallel DNA dodecamer.(38) (B) Representation of parallel and antiparallel strand pairings for synthesized dodecamers. Legend: RNA, DNA, 2F-ANA, iso-RNA, iso-DNA, 2F-RNA.

Duplex formation in each case was monitored by UV thermal melting experiments, NMR, and circular dichroism (CD) spectroscopy. T_m values are summarized in Table 5.1 and normalized UV melting profiles are presented in Figure 5.16 in the experimental section. Several trends emerged: As shown previously, iso-modified DNA strand (iDD) and D2 yielded a complex (T_m 32.9°C, %H 15.7) previously characterized as a parallel duplex (38). iDD also paired with RNA (R2), providing a complex of slightly lower stability ($\Delta T_m = -2^\circ\text{C}$, with respect to the iDD:D2 duplex). Furthermore, iDD paired with the corresponding fluorinated RNA strand (rF2) to afford iDD:rF2, which exhibited a T_m that was 6 degrees higher than that of iDD:R2 (Table 5.1). As expected, the unmodified D1 + D2 and R1 + D2 did not show any thermally induced transitions, implying that the incorporations of isoguanine and isocytosine are necessary for parallel duplex formation. Interestingly, our results indicate that replacing either strand of a parallel DNA:RNA hybrid with the corresponding iC/iG modified strand will yield a stable parallel hybrid (iDD:R2 and iR:D2 are both stable and have comparable T_m values). Substitution of the DNA residues in iDD with 2F-ANA was stabilizing since it afforded a duplex (iD-aF:D2) with higher T_m (+3°C)

and hyperchromicity compared to iDD:D2 (Table 5.1). The opposite effect was observed when the target was RNA (R2); hence iD-aF:R2 had lower T_m and %H values than iDD:R2. This is not in agreement with what has been observed with antiparallel duplexes, where in most cases DNA to 2'F-ANA substitutions stabilize the *aps*-DNA:RNA hybrids (72,73,78). All attempts to form a parallel RNA:RNA duplexes failed, e.g., iR + R2, R1 + R2, or iR + rF2 did not yield any clear UV melting transition, in contrast to R1 + R3 (*aps*-RNA) which gave the expected high temperature transition.

Table 5.1 Melting temperatures (T_m) and percent hyperchromicity (%H) for parallel and antiparallel 12-nt hybrids

Strand 1 (5'-3')		<i>ps</i> target: Strand 2								<i>aps</i> target: Strand 3			
		R2		D2		rF2		aF2		R3		D3	
		T_m	H%	T_m	H%	T_m	H%	T_m	H%	T_m	H%	T_m	H%
iDD	TiCATAAAiCTiGiGAT	28.0	18.2	32.9	15.7	34.0	13.3	30.1	11.3	30	14.1	-	-
iD-aF	TiCATAAAiCTiGiGAT	25.1	13.4	35.9	17.4	n.d.	13.8	28.1	12	n.d.	12.3	-	-
D1	TCATAACTGGAT	n.d.	8.9	n.d.	5.7	n.d.	9.8	n.d.	11.8	36.9	24.2	41.0	21.1
iR	UiCAUAAiCUiGiGAU	n.d.	15.9	29.0	16.5	n.d.	13.3	25	12.2	34.1	27.8	-	-
R1	UCAUAACUGGAU	n.d.	16.7	n.d.	12.1	n.d.	13.0	n.d.	13.0	64.1	29.0	37.1	24.0

Legend: RNA, DNA, 2'F-ANA, isoRNA, isoDNA. 2'F-RNA. %H: $[A(f)-A(0)]/A(0)$. Buffer: 140mM KCl, 1mMMgCl₂ and 5mM NaHPO₄. n.d.: curves that did not show measurable transitions, and thus their T_m could not be determined. In D3 column, only the hybridization of *aps*-D1:D3 and *aps*-R1:D3 controls were monitored.

5.4.2 Circular Dichroism Studies of 12-bp Parallel Hybrids

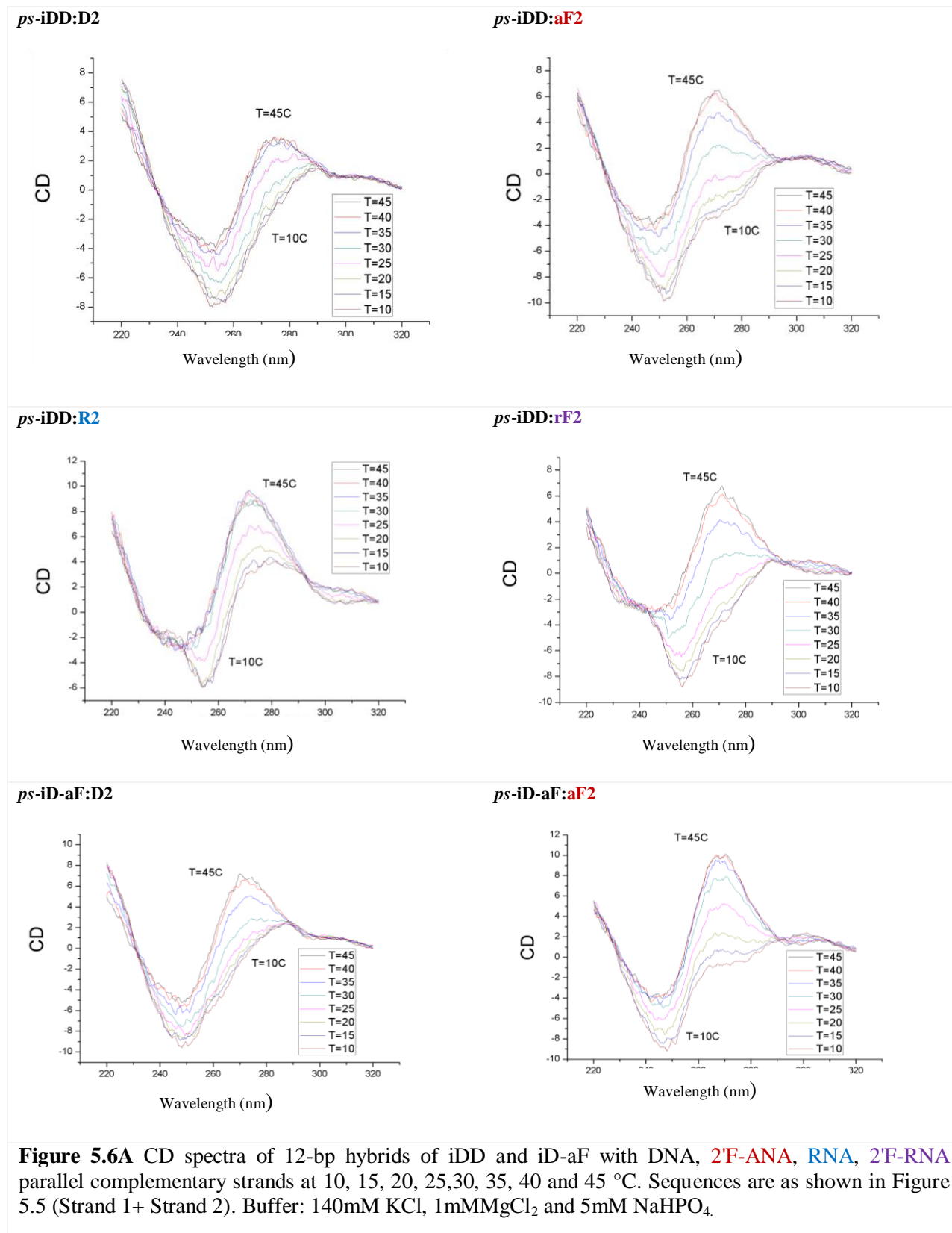
Circular dichroism (CD) is a powerful technique for studying nucleic acid structure, particularly the helical arrangement of double helices (79-81). The spectrum of the antiparallel DNA duplex D1:D3 is characteristic of a B-form helix, with a positive band centered near 275-280nm, a negative band near 245-250nm, and a crossover signature at around 260nm. Native A-form RNA duplexes exhibit a strong positive band centered at around 260nm and a weak negative band

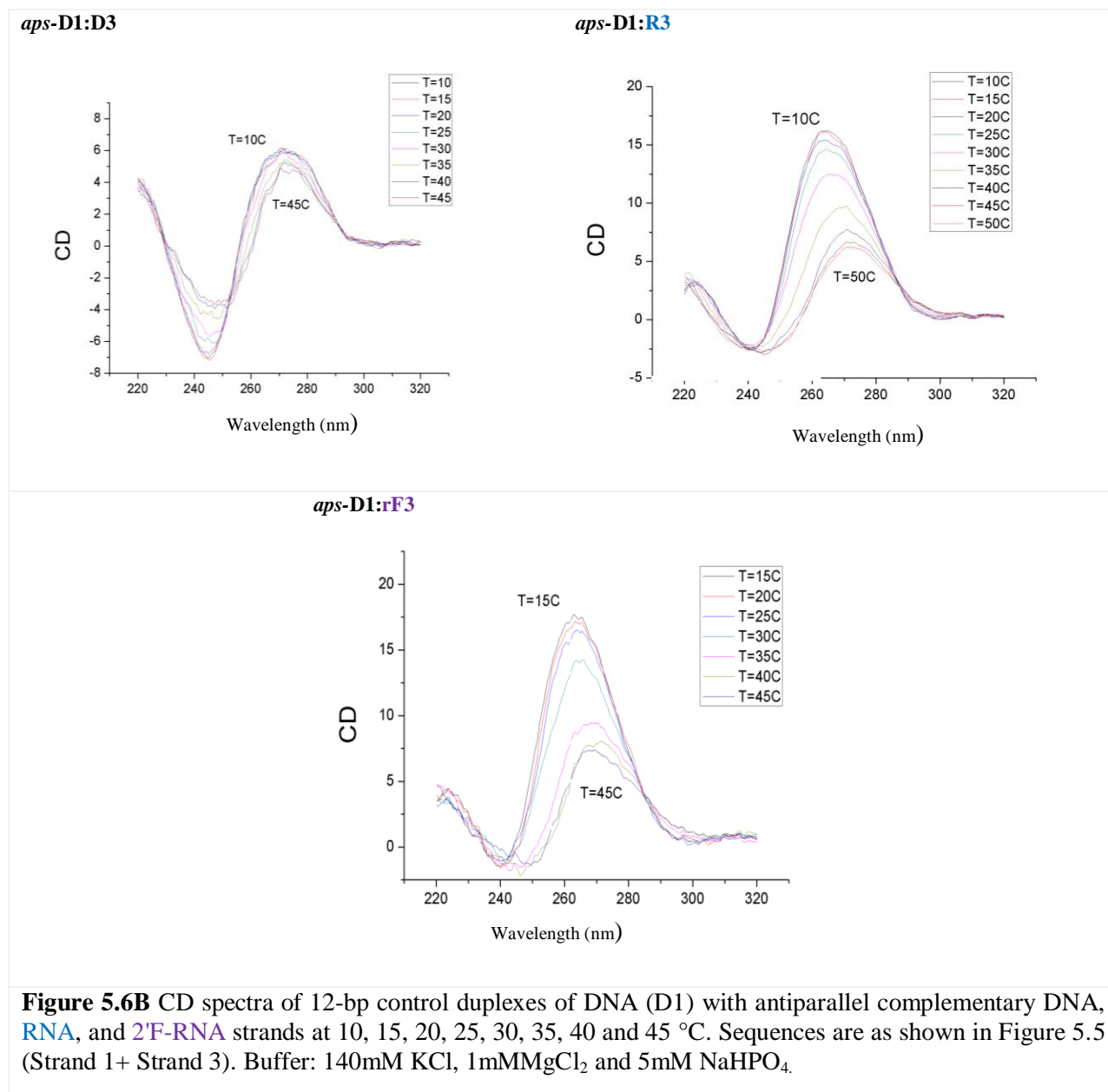
centered at around 240nm. Native DNA/RNA hybrids adopt a more sequence-dependent structure that generally resembles the A-helical structure (79-81). Figure 5.6 compares the CD profiles of 12-bp *ps*- and *aps*-duplexes. The traces are reminiscent of right-handed helical structures (79-81) in all cases. However, the parallel duplexes exhibit positive and negative peaks (and crossover points) that are red-shifted relative to the antiparallel duplexes. An interesting feature in the CD spectra of parallel duplexes is that the magnitude of their positive CD increases upon raising the temperature, whereas an opposite (hypochromic) effect is seen for the corresponding antiparallel duplexes (Figure 5.6). These differences are not surprising given the nature of the duplexes and the altered spectroscopic properties of the iC/iG nucleobases.

5.4.3 ¹H-NMR of 12-bp Parallel Hybrids

Previous NMR studies on *ps*-DNA with rWC base pairs demonstrated that their proton resonances roughly fall in the same chemical shift ranges as those of the same type of protons in *aps*-DNA (82,83). We made a similar observation: the chemical shifts of the imino exchangeable protons in parallel hybrids were generally comparable to those observed in antiparallel control duplexes, which confirms the reverse Watson-Crick base pairing pattern in 12-bp *ps*-hybrids (Figure 5.17). This observation could also, in part, suggest that a similar base stacking geometry exists in the parallel and antiparallel-stranded structures, thus reinforcing the idea of a right-handed *ps*-helix.

For further evaluation of the conformational parameters of these parallel double-stranded hybrids with good accuracy and determination of their structures, future work will focus on performing high resolution NMR spectroscopy experiments. These experiments are ongoing and we are currently characterizing the d-iG:rC and d-iC:rG base pairs of the *ps*-iDD:R2 parallel construct.





5.5 Parallel si-Duplexes

5.5.1 Design and Evaluation of Thermal Stabilities of Parallel si-Duplexes

Short interfering RNAs (siRNAs) are typically 21-nt in length, and are used as exogenous triggers of the RNA interference gene regulation pathway (84-86). In classical antiparallel

siRNA designs, guide (antisense) strand shares full Watson-Crick complementarity with the target mRNA while the other strand (passenger or sense strand) has the same sequence as the region on the target mRNA (Figure 5.7).

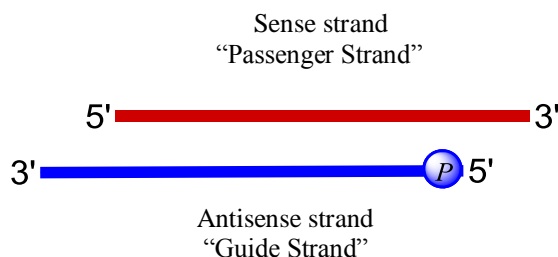


Figure 5.7 Schematic representation of classical siRNA duplex (WC antiparallel duplex).

A goal of our study was to exploit rWC parallel hybridization as an alternative to the classical WC antiparallel hybridization in the RNAi pathway. While our efforts to form parallel RNA:RNA duplexes failed, the formation of stable parallel DNA:RNA and DNA:2'F-RNA hybrids motivated us to test these duplexes in our gene silencing experiments, particularly because modified *aps*-siRNAs with DNA or 2'F-RNA modifications are effective triggers of RNAi (87-90). The potential anticancer applications of Bcl-2 targeting siRNAs (91), encouraged us to choose Bcl-2 as an endogenous target for testing our parallel-stranded siRNAs. At first glance, three strategies might appear for designing parallel si-duplexes for gene silencing (Figure 5.8). The first strategy involves the incorporation of d-iG and d-iC nucleotides into the sense strand of a *ps*-DNA:RNA duplex, with its native RNA antisense strand designed to bind to the target mRNA in an antiparallel fashion, producing a standard A-form antisense:mRNA duplex (Figure 5.8a). The second and third strategies involve constructing *ps*-DNA/RNA si-duplexes with r-iG and r-iC incorporations in the antisense strand (Figures 5.8b & c).

Given that RNA was unable to form stable 12-nt parallel RNA:RNA duplexes, and that incorporation of iG:C/iC:G is destabilizing in the antiparallel fashion, we only pursued the first strategy (Figure 5.8a). This strategy has the added advantage of using native RNA or 2'-fluoro RNA (87,88,90,92,93) which is a desirable property given the fact that normally very few modifications are tolerated in the antisense (guide) strand. Moreover, since the sense strand is heavily modified, the likelihood of this strand to act as guide (antisense) strand may be reduced, a feature that would in principle minimize off-target effects.



Figure 5.8 Strategies to design rWC parallel si-duplexes incorporating iG and iC. Note that in all three cases, the si-duplex itself is parallel. Codes: DNA, iso-DNA, RNA, iso-RNA.

The thermal stabilities of various parallel and antiparallel control si-duplexes were evaluated in a buffer containing 140mM KCl, 1mM MgCl₂, and 5mMNa₂HPO₄, pH 7.2, which is representative of intracellular conditions. Several siRNA controls were also prepared for this study (Table 5.2). The measured T_m values for parallel hybrids incorporating d-iG/d-iC modifications, and in particular for iDD:rF3 (2'F-RNA antisense strand), were remarkably high and their melting profiles adopted clear sigmoidal transitions (Figure 5.9).

Table 5.2 Melting temperatures of 21-nt parallel and antiparallel si-duplexes targeting Bcl-2.

Code	Sequence	T _m (°C)
iDD:R3	3'-iGiCATiGiCiGiGiCiCTiCTiGTTTiGATT-5' 3'-UUCGUACGCCGGAGACAAACU-5'	48.1
iDD:rF3	3'-iGiCATiGiCiGiGiCiCTiCTiGTTTiGATT-5' 3'-UUCGUACGCCGGAGACAAACU-5'	57.9
D1:R3	3'-GCATGCGGCCTCTGTTTGATT-5' 3'-UUCGUACGCCGGAGACAAACU-5'	32.1
D1:rF3	3'-GCATGCGGCCTCTGTTTGATT-5' 3'-UUCGUACGCCGGAGACAAACU-5'	44.1
D2:R3	5'- GCATGCGGCCTCTGTTTGATT-3' 3'-UUCGUACGCCGGAGACAAACU-5'	69.1
D2:rF3	5'- GCATGCGGCCTCTGTTTGATT-3' 3'-UUCGUACGCCGGAGACAAACU-5'	71.3
R2:R3	5'- GCAUGC GGCCUCUGUUUGATT-3' 3'-UUCGUACGCCGGAGACAAACU-5'	79.0
R2:rF3	5'- GCAUGC GGCCUCUGUUUGATT-3' 3'-UUCGUACGCCGGAGACAAACU-5'	84

Legend: RNA, DNA, isoDNA, 2'F-RNA. R2:R3 is the *aps* native siRNA that has been shown to demonstrate gene silencing activity (91).

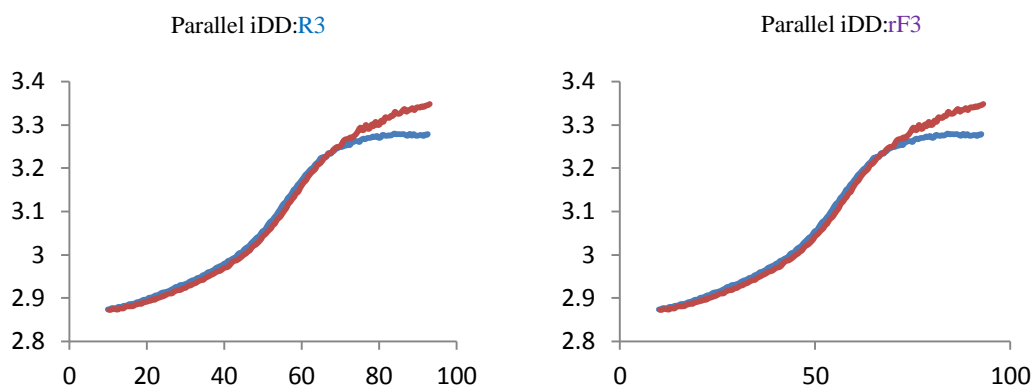


Figure 5.9 UV melting profiles of parallel si-duplexes targeting Bcl-2. (left) iDD:R3 and (right) iDD:rF3. The A₂₆₀ was monitored from 7 to 85°C with a heating rate of 0.4 °C/min. Legend: RNA, 2'F-RNA, DNA.

5.5.2 Native Gel Electrophoretic Analysis

Parallel si-duplexes were also analyzed by gel electrophoresis under native conditions. Parallel si-duplexes incorporating d-iG and d-iC (iDD:R3 and iDD:rF3; Figure 5.10) eluted as a single band reminiscent of a duplex species, and no bands due to *ss*-multimers or bands with

unexpected mobilities were found for them. Antiparallel control duplexes also appeared as a single species on the gel, as indicated in figure 5.10. Both the *ps* and *aps* complexes migrated somewhat slower than the single-stranded DNA and RNA controls, which was expected since the longer and heavier oligonucleotides normally move more slowly when loaded on electrophoretic gel. However, surprisingly, the fully-modified 2'F-RNA single-stranded control, rF3, had the slowest mobility on the gel, migrating even slower than the complexes. We wondered whether this slow migration could be a result of rF3 self-association. No bands indicative of parallel intermolecular hybridization was observed for *ps*-D1:R3 and *ps*-D1:rF3 control duplexes under native conditions.

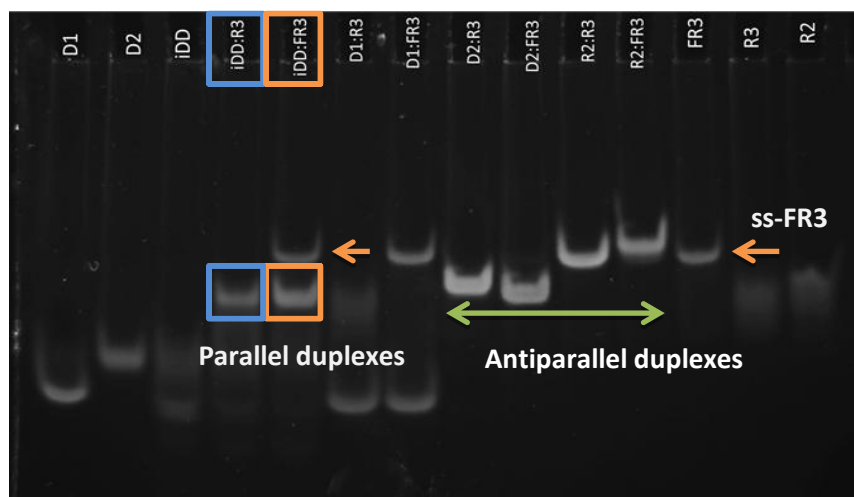


Figure 5.10 Native gel electrophoretic analysis of parallel and antiparallel 21-nt si-duplexes targeting Bcl-2 (0.1 μg duplexes/ well and 0.2 μg single strands/ well). Sequences are as shown in Table 5.2.

5.5.3 Determination of si-Duplex Parallel Chain Orientation by FRET Measurements

Fluorescence Resonance Energy Transfer (FRET) has been used in previous studies to characterize the similar chain orientation of strands in *ps*-DNA duplexes (94). Employing cyanine fluorophores (Cy3 and Cy5), we used FRET-based studies as a detection method to

further ensure the parallel chain orientation of si-duplex targeting Bcl-2. The properties of Cy3-Cy5 FRET pair are summarized in Figure 5.11. Cy3 is the donor molecule and Cy5 is the acceptor molecule.

The underlying principals of Förster Resonance Energy Transfer can be found elsewhere (95-97). Briefly, if the donor and the acceptor molecules are in close proximity and in appropriate orientation relative to each other, the energy is transferred from the (excited) donor to the acceptor via nonradiative dipole-dipole interactions, and subsequently, FRET can be detected by the appearance of fluorescence of the acceptor, or by quenching of donor fluorescence, or both if the acceptor and donor are both fluorescent dyes. The efficiency of energy transfer from donor to acceptor is inversely proportional to the sixth power of the distance between the donor and acceptor which makes FRET extremely sensitive to small changes in distance between the dyes (95-97). The distance at which 50% of the energy is transferred is called the Förster distance (R_0). R_0 is dependent on a number of factors including the fluorescence quantum yield of the donor in the absence of acceptor, and the spectral overlap integral of the donor and acceptor.

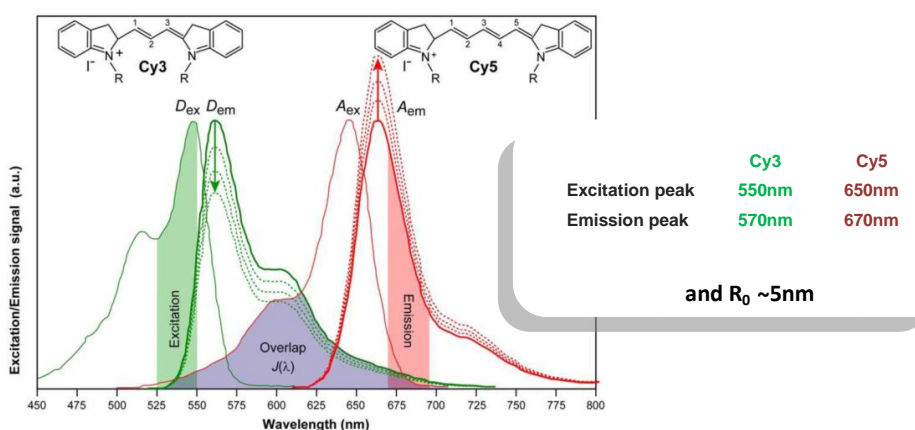


Figure 5.11 Schematic representation of the spectral overlap integral of Cy3-Cy5 FRET pair. Diagram is adapted from reference (98).

To confirm the mutual chain orientation in Bcl-2 parallel oligomer, the 5'-ends of the sense and antisense strands were covalently labeled to afford the parallel probe shown in Table 5.3. Two antiparallel control systems were also included in this study: the positive *aps* control was designed to have Cy3 and Cy5 dyes in close proximity and hence resemble the parallel probe. In the other *aps* control, however, the dyes were placed at the very far ends (negative control; Table 5.3). We expected the FRET efficiency of labeled parallel probe to be similar to that of the positive *aps* control and significantly higher than FRET efficiency of the negative control.

Fluorescence energy transfer spectra were recorded using a PTI QuantaMaster spectrofluorimeter. We performed the experiments at three different temperatures (Table 5.3). At each temperature, the donor Cy3 was excited with a 500nm laser line and emission fluorescence of both fluorophores was recorded from 520 to 800nm. At 500nm, no direct excitation of the Cy5 dye is expected, since there is no or very little spectral overlap between excitation peaks of Cy3 and Cy5 close to 500nm. Nonetheless, we included an acceptor-only control (Cy5-only, Table 5.3) to carefully correct the possible leakage from direct excitation of Cy5 at 500nm.

Table 5.3 Probes for parallel chain verification employing Cy3-Cy5 FRET pair

Probe	Duplex	Sequence	Cy3-Cy5 distance	FRET Efficiencies		
				7°C	37°C	80°C
parallel	iDD:R3	3'-iG <i>C</i> ATiG <i>C</i> iG <i>C</i> iG <i>C</i> iC <i>T</i> iC <i>T</i> iGTTT <i>G</i> ATT-5'-Cy3 3'-UU CGU ACG CCG GAG ACA AACU-5'-Cy5	A:U rWC pair ~0.3nm	0.88	0.81	0.15
Positive ctrl	D2:R3	5'-GCA TGC GGC CTC TGT TTG ATT-3'-Cy3 3'-UU CGU ACG CCG GAG ACA AACU-5'-Cy5	A:U WC pair ~0.3nm	0.95	0.95	0.17
Negative ctrl	D2:R3	Cy3-5'-GCA TGC GGC CTC TGT TTG ATT-3' 3'-UU CGU ACG CCG GAG ACA AACU-5'-Cy5	3Å *21nt ~6nm	0.50	0.26	0.12
Cy5-only ctrl	D2:R3	5'- GCA TGC GGC CTC TGT TTG ATT-3' 3'-UU CGU ACG CCG GAG ACA AACU-5'-Cy5	-	-	-	-

Legend: RNA, DNA, isoDNA; Buffer: 140mM KCl, 1mM MgCl₂ and 5mM NaHPO₄; Duplex concentration is 2μM (4μM total concentration of single strands). FRET efficiencies are given by $(I_A - I_{Cy5\text{-only}})/I_D + (I_A - I_{Cy5\text{-only}})$, where I_A and I_D are the intensities of acceptor and donor, respectively, measured at their peaks.

In line with our expectations, at 7°C and much below the melting temperatures of duplexes, the close proximity of the Cy3-Cy5 dyes in the *aps* positive probe as well as in the parallel probe allowed for energy transfer to occur with very high efficiency and resulted in strong emission from Cy5 at 670nm. This observation demonstrates that the dyes are held in close proximity in both probes at 7°C, and thus confirming the mutual orientation of strands in the parallel si-duplex (Figure 5.12). As for the antiparallel negative control at 7°C, a significant portion of Cy3 excitation energy at 500nm is not transferred and therefore FRET-based emissions at 670nm are much lower (Figure 5.12). This was expected because of the longer distances between the Cy3 and Cy5 dyes (~ 6nm).

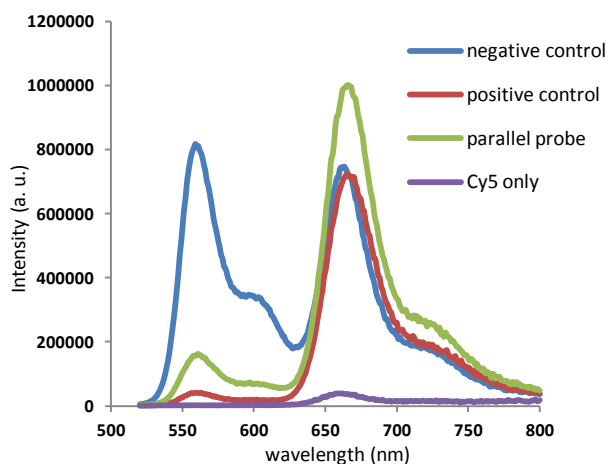


Figure 5.12 Emission signals of parallel probe and control systems at 7°C. Sequences are as shown in Table 5.3.

At 37 °C, strong Cy5 emission signals and high FRET efficiencies were again observed in both the parallel probe and *aps* positive control which confirms that the strands are still closely paired at 37°C. At 80°C however, when the labeled molecules are no longer annealed and strands are

free in solution, excitation of Cy3 resulted in only the emission of light by Cy3 itself at 570 nm and no emission from Cy5 was detected. FRET signals for all three experimental temperatures are shown in Figure 5.13.

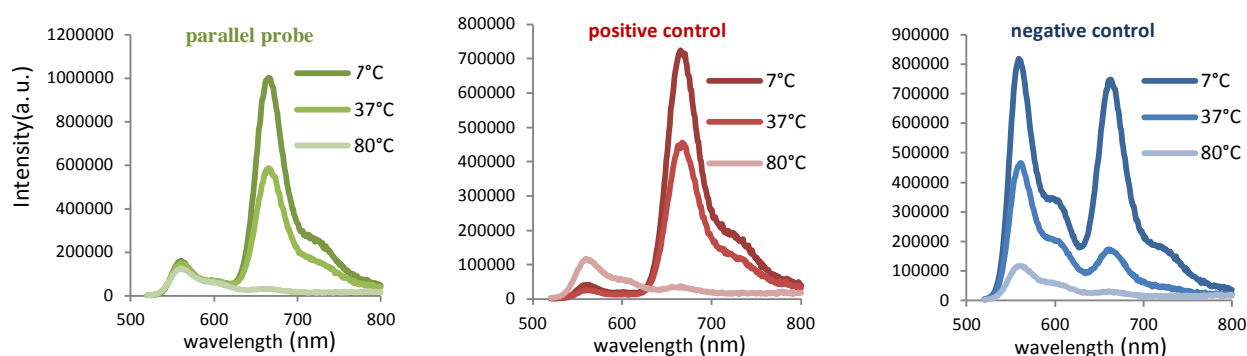


Figure 5.13 Emission peaks of each labeled probe at all three experimental temperatures. Sequences are as shown in Table 5.3.

5.5.4 Induction of RNAi Activity by Parallel Hybrids

To assess the ability of Bcl-2 parallel oligomers to stimulate RNAi activity, we first examined the susceptibility of iso-modified *ps*-iDD:R3, along with the corresponding single-stranded (*ss*) antisense-only control (*ss*-R3), the unmodified *ps*-D1:R3 control, and the antiparallel control duplexes (*aps*-D2:R3, *aps*-R2:R3). The dose-response diagram and the calculated half maximal effective concentration (EC_{50}) values of all tested duplexes are presented in Figure 5.14. These gene silencing biological assays were conducted by Elena Moroz in the laboratory of Dr. Jean-Christophe Leroux at ETH, Zurich.

The native classical siRNA (R2:R3; Figure 5.14) greatly reduced the Bcl-2 mRNA levels in Caco-2 cells ($EC_{50}=15nM$). Parallel iDD:R3 si-duplex reduced mRNA levels better than the *aps*-D2:R3 control, with EC_{50} values in the low nanomolar range (Figure 5.14); however, it did not exceed the activity of native R2:R3 siRNA. The lack of optimal activity observed with the

parallel si-duplex at 37 °C may reflect the lower thermal stability of this particular complex as compared to the native siRNA which is highly stable ($T_m=79.0^\circ\text{C}$). At 37 °C, the temperature at which the biological assays are performed, ~35% of molecules of *ps*-iDD:R3 ($T_m=48.1^\circ\text{C}$) are estimated to be present as single strands i.e. as free sense and antisense strands instead of the duplex form. We wondered whether these single strands might produce gene silencing activity. The sense strand alone is not complementary to mRNA, and thus, no activity is expected for that. The antisense strand, however, is a complement of mRNA. Thereby, we also included a single-stranded antisense control (*ss*-R3) in our study. Our results demonstrate that *ss*-R3 is not much efficient at silencing Bcl-2 gene expression (Figure 5.14). This is also reflected in the low activity observed for *ps*-D1:R3 sample ($T_m=32.1^\circ\text{C}$). Taken together, we concluded that the activity observed with iso-modified *ps*-iDD:R3 is primarily coming from the parallel duplex structure present in the medium at 37°C.

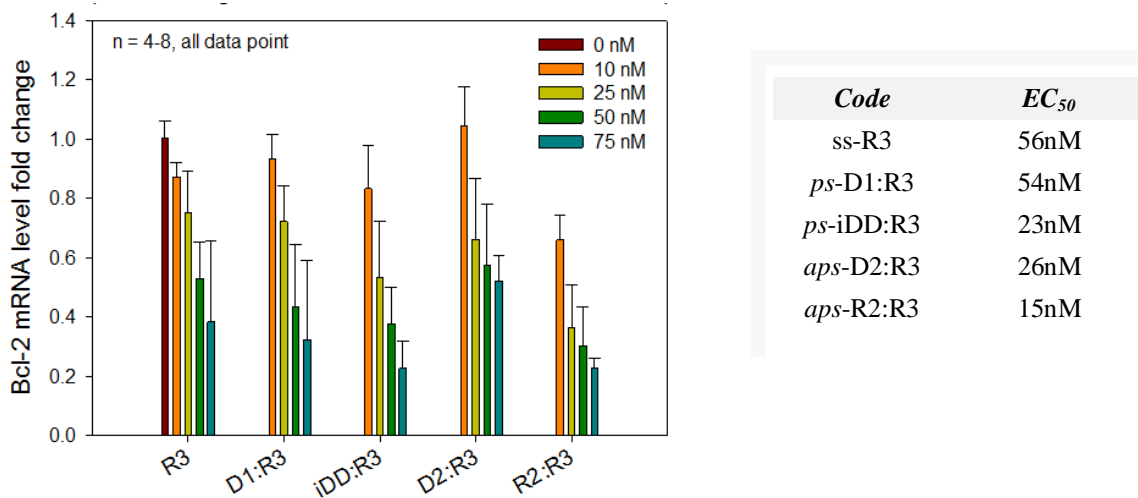


Figure 5.14 Knockdown of Bcl-2 mRNA in Caco-2 cells. Activity and half maximal effective concentration (EC_{50}) values of duplexes that have native RNA as their antisense strand. Duplex sequences and their thermal stability values are as presented in Table 5.2.

Next, we assessed the activity of *ps*-iDD:rF3 with a fully modified 2'F-RNA antisense strand (sequence shown in Table 5.2). Previous studies have shown that classical *aps*-siRNAs with fully modified 2'F-RNA antisense strands function well in RNAi (87,90). Interestingly, our preliminary results on *ps*-iDD:rF3 ($T_m=57.9^\circ\text{C}$) also shows that this chemically modified parallel si-duplex is very active against Bcl-2 gene expression, and in fact reduces the mRNA level with a comparable potency to that of the antiparallel R2:rF3 control siRNA. Our preliminary results on this series also indicate that the fully modified single-stranded antisense control (*ss*-rF3) is able to silence Bcl-2 gene expression. This observation is in agreement with previous reports demonstrating that 2'F-RNA modified *ss*-antisense functions well through the RNAi pathway (99,100). More experiments are currently underway to complete these sets of biological assays.

5.5.5 Can Parallel Hybridization Enhance the siRNA Properties?

Despite their immense therapeutic potential, siRNAs are disadvantaged by poor nuclease stability, poor cellular uptake, and off-target effects arising from partial complementarities to unintended genes and nonspecific immune responses (101,102). Up to now, the typical strategy employed to overcome these problems and to enhance the gene silencing properties of siRNA molecules has mostly focused on the use of alternatives to the native ribose and/or phosphate backbone of antiparallel siRNAs (103-112). For the first time, we utilized parallel hybridization as an alternative to classical modification approaches, and questioned whether such “global” modification of the siRNA structure could improve the siRNA properties.

As mentioned earlier, when the sense strand of a parallel si-duplex is heavily modified, the likelihood of its sense (passenger) strand to act as guide strand might be decreased. This is a feature that can be beneficial for minimizing off-target effects. Besides the possibility of

minimizing off-target effects, it may be possible to improve the nuclease stability, mainly due to the fact that helical structure of rWC parallel double helices differ from WC antiparallel duplexes. In antiparallel duplexes, the major and minor grooves differ in polarity, hydrogen bonding, steric effects, and hydration. Based on these differences, certain proteins (and ligands) bind to the major groove, while some other recognize and bind to the minor groove. With rWC parallel duplexes that have grooves of equal size (5), however, the nature of molecular recognition by intercalating molecules and proteins like nucleases is expected to be different (47). In fact, previous findings indicate that *ps*-DNA duplexes show resistance against certain nucleases and restriction endonucleases as compared to *aps*-DNA (48). We assume that the same could apply to other parallel hybrids like *ps*-DNA:RNA. It is also plausible to assume that these structural differences might modulate siRNA interactions with off-target proteins. For example, the RNA-dependent protein kinase (PKR), a cellular *ds*-RNA binding protein that participates in sequence-independent binding to siRNAs and off-target effects, interacts with siRNAs through minor groove contacts. Thus it is plausible to assume that duplexes with grooves of equal size could be exploited as a means to decrease the off-target effects via the manipulation of the binding of siRNA to PKR, while still allowing correct RISC loading. To examine these hypotheses, future work will evaluate multiple iDD:R3 and iDD:rF3 parallel si-duplexes with regards to RNAi gene silencing, serum stability and immunostimulation assays.

5.6 Concluding Remarks and Future Work

The results obtained from structural analysis and thermal stability measurements of parallel hybrids at physiological conditions prompted us to assess the ability of these oligomers for stimulation of RNAi activity. We introduced parallel hybridization as a completely different base pairing system to design a new class of siRNAs. Our preliminary results from gene silencing assays against the expression of the oncoprotein Bcl-2 indicated that a parallel si-duplex is capable of RNA activation and eliciting gene silencing activity. Our preliminary conclusion drawn from this observation is that, since the parallel si-duplex is capable of silencing the Bcl-2 gene expression, the helical conformation of the si-duplex and its groove dimensions are not the critical determinants in activation of RNAi and duplexes that do not closely resemble the A-form standard siRNAs are still recognized by RISC.

Our results open up new perspectives for the development of parallel-stranded double helices at natural pH and ion conditions. We demonstrate here, for the first time, that rWC parallel hybridization incorporating iC/iG nucleobases occurs not only in *ps*-DNA:DNA, but also in *ps*-DNA:RNA, *ps*-DNA:2'F-RNA, and *ps*-DNA:2'F-ANA hybrids. This observation is of importance for potential future applications of parallel hybridization, and in particular in the design of novel oligonucleotide hybridization probes or oligonucleotide-based therapeutics.

5.7 Experimental Methods

5.7.1 Synthesis and Purification of Oligonucleotides Containing Isoguanine and Isocytosine

Isoguanosine and isocytidine phosphoramidites (both ribose and deoxy ribose) were purchased from ChemeGenes Inc. (Wilmington, MA). The oligonucleotide synthesis was performed on an Applied Biosystems 3400 DNA Synthesizer at a 1- μ mol scale using Unylink CPG support

(ChemeGenes, Wilmington, MA)(113). Iso-phosphoramidites were prepared as 0.15M solutions in acetonitrile (ACN). 5-ethylthiotetrazole (0.25M in ACN) was used to activate phosphoramidites for coupling. For detritylation 3% dichloroacetic acid in toluene was used. Oxidation was done using 0.1M I₂ in 1:2:10 pyridine: water: THF. Coupling times were 600 seconds for isocytidine phosphoramidites (d-iC and r-iC) and 900 seconds for the isoguanosine phosphoramidites (d-iG and r-iG). The removal of CPG support, base protecting groups and the cyanoethyl protecting groups occurred best with moisture-free ethanolic ammonia, which has been saturated at 0°C. This anhydrous solution is added to the CPG containing bound oligo and the tightly sealed solution is kept at 37°C for 36 hours.

Oligonucleotides containing ribo-isoguanine and ribo-isocytosine were synthesized with standard 2'-TBDMS phosphoramidites, and desilylation was achieved with neat TEA.3HF for 48 hours at room temperature (114). Oligonucleotides were precipitated by adding of 3M sodium acetate (25µL) followed by addition of cold butanol (1000µL).

Oligonucleotides were purified by reverse phase HPLC on an Agilent 1200 series using a Waters semipreparative C18 column. A stationary phase of 100mM triethylammonium acetate in water with 5% ACN (pH 7), and a mobile phase of HPLC grade ACN were used. Purified oligonucleotides were then lyophilized to dryness, and were characterized by ESI-mass spectrometry (Table 5.4 and Table 5.5).

Table 5.4 MS characterization of 12-nt oligonucleotides

Code	Sequence	Calculated Mass (g/mol)	Experimental Mass (g/mol)
iDD	5'-Ti <u>CA</u> TAA i <u>CTiG</u> i <u>GAT</u> -3'	3642.6	3642.65
iD-aF	5'-Ti <u>CA</u> TAA i <u>CTiG</u> i <u>GAT</u> -3'	3786.6	n.d.
D1	5'-TCA TAA CTG GAT-3'	3642.6	3642.68
iR	5'-Ui <u>CA</u> UAA i <u>CUiG</u> i <u>GAU</u> -3'	3778.5	3778.57
R1	5'-UCA UAA CUG GAU-3'	3778.5	3778.57
D2	5'-AGT ATT GAC CTA-3'	3642.6	3642.68
R2	5'-AGU AUU GAC CUA-3'	3778.5	3778.57
rF2	5'-AGU AUU GAC CUA-3'	3802.5	3802.46
aF2	5'-AGT ATT GAC CTA-3'	3858.5	3858.55

Designation: isoDNA, DNA, isoRNA, RNA, 2F-ANA, 2F-RNA; n.d. not measured.

Table 5.5 MS characterization of 21-nt oligonucleotides used to construct Bcl-2 si-duplexes

Code	Sequence	Exact Mass (g/mol)	Experimental Mass (g/mol)
iDD	3'-iGi <u>CA</u> Ti <u>GiC</u> iGi <u>GiC</u> i <u>CTiC</u> Ti <u>GT</u> TTi <u>G</u>	6416.1	6416.09
D1	3'-GCA TGC GGC CTC TGT TTG ATT-5'	6416.1	6418.15
R2	5'-GCA UGC GGC CUC UGU UUG AUU-3'	6639.8	6641.8
D2	5'- GCA TGC GGC CTC TGT TTG ATT-3'	6416.1	6416.1
R3	3'-UUC GUA CGC CGG AGA CAA ACU-5'	6691.9	6695.0
rF3	3'-UUC GUA CGC CGG AGA CAA ACUp-5'	6812.8	6815.9

Designation: isoDNA, DNA, isoRNA, RNA, 2F-ANA, 2F-RNA

5.7.2 Synthesis and Purification of Oligonucleotides Labeled with Cyanine Dyes

Oligonucleotides containing Cyanine-3 phosphoramidites (Glen Research, Sterling, VA) were synthesized using standard phosphoramidite solid-phase synthesis conditions (113), with the exception that a 0.02M oxidation solution was used in place of the regular 0.1M solution. Syntheses were performed on an Applied Biosystems (ABI) 3400 DNA Synthesizer at a 1 μ mol scale using Unylink CPG as the solid support (ChemeGenes Wilmington, MA). The removal of CPG support, base protecting groups and the cyanoethyl protecting groups occur with standard

deprotection methods in the presence of Cy3 dye. The oligonucleotides containing Cyanine-5 phosphoramidites (Glen Research, Sterling, VA), however, need very mild deprotection conditions (30% NH_4OH , 2 hours at room temperature); which is sufficient to deprotect monomers with PAC base protecting groups. Thus, rC(PAC), rA(PAC) and rG(PAC) and U (Glen Research, Sterling, VA) were used to synthesize the RNA strand labeled with Cy5. Amidites (U, rC(PAC), rA(PAC) and rG(PAC) were dissolved in ACN to a concentration of 0.15M, and ethylthiotetrazole (0.25 M) was used as activator. A, C and U monomers were coupled for 600 seconds; G was coupled for 900 seconds. Detritylation was carried out for 110 seconds using 3% TCA in CH_2Cl_2 . After the synthesis was completed, the support was transferred to an eppendorf tube and 30% NH_4OH (1mL) was added and the mixture was shaken at room temperature for 2 hours. The mixture was decanted and the solid support was washed with EtOH:MeCN (3:1 v:v) twice and then dried down. TREAT-HF (150 μL) was added and the mixture was shaken at room temperature for 48 hours (114). Oligonucleotides were precipitated by adding of 3M sodium acetate (25 μL) followed by addition of cold butanol (1000 μL).

Both series, oligonucleotides labeled either with Cy3 or Cy5, were purified by reverse phase HPLC using a Waters semipreparative C18 column. A stationary phase of 100mM triethylammonium acetate in water with 5% ACN (pH 7), and a mobile phase of HPLC grade ACN were used.

5.7.3 Thermal Denaturation Experiments and Circular Dichroism Studies

UV thermal denaturation data were obtained on a Varian Cary 5000 UV-VIS spectrophotometer equipped with a Peltier temperature controller. Duplex concentration, for both series (12-mers and 21-mers), was 2 μM (4 μM total concentration of single strands) in 100mM KOAc, 30mM HEPES-KOH, 2mM $\text{Mg}(\text{OAc})_2$ buffer (pH 7.2). The temperature was increased at a rate of

0.4°C/min from 7°C to 75°C for 12-bp samples and from 7°C to 85°C for Bcl-2 21-mers. Absorbance values were recorded each minute. Samples were kept under flowing nitrogen when below 15°C. T_m values were calculated using the baseline method. Normalized T_m curves are shown in Figure 5.15.

CD spectra were obtained on a JASCO J-810 circular dichroism spectrometer equipped with a Peltier temperature controller, and by using samples annealed in the same buffer and under the same conditions as for the thermal denaturation studies. Spectra were baseline-corrected with respect to a blank containing the buffer but no duplex. Smoothing and adjustment for duplex concentration were affected using the Spectra-Manager program (Jasco).

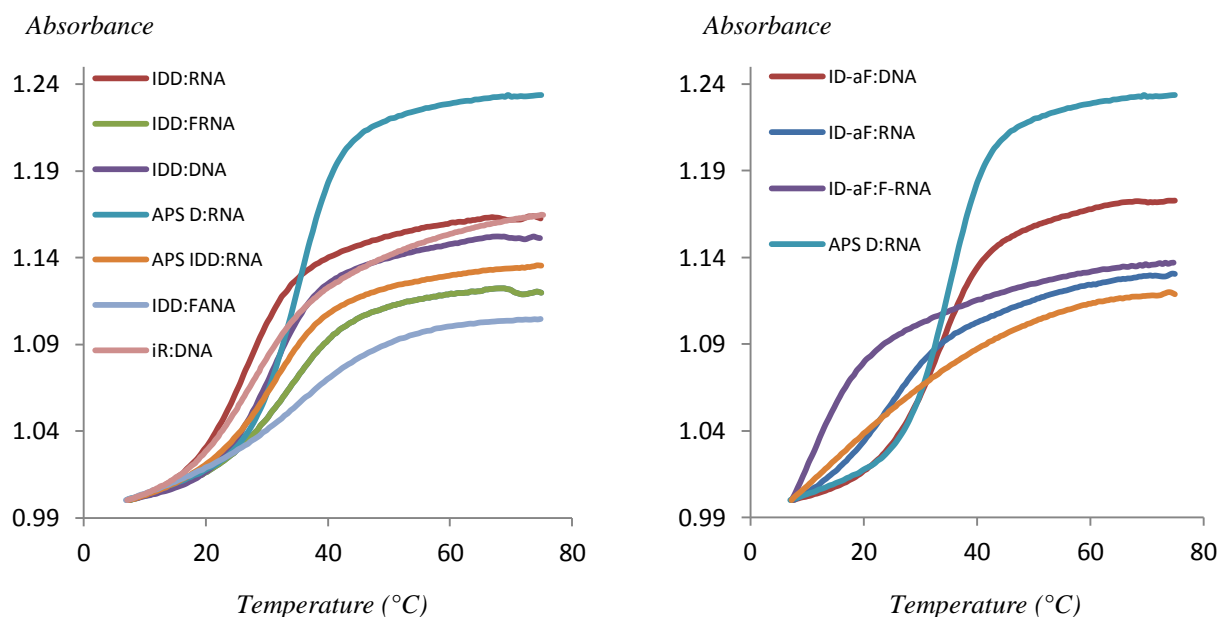


Figure 5.15 Normalized UV melting profiles of parallel hybrids iDD (left), and iD-aF (right). A_{260} was monitored from 7°C to 75°C with a heating rate of 0.4°C per minute.

5.7.4 NMR Experiments

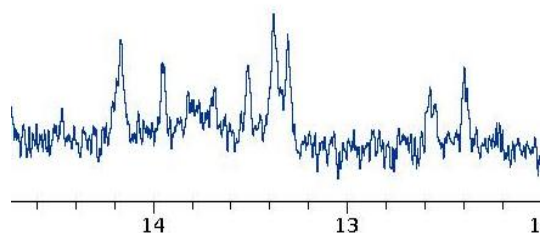
Samples of duplexes (40 μ M samples) were suspended in 300 μ L of H₂O/D₂O 9:1 in sodium buffer, 250mM Na₂HPO₄, 1M NaCl and 1mM EDTA (pH 7). NMR spectra were acquired in a Bruker Avance spectrometers operating at 700 MHz and processed with Topspin software (Figure 5.16).

5.7.5 Characterization of Duplex Formation by Gel Electrophoresis

To confirm formation of parallel si-duplexes, acrylamide gel electrophoresis of duplexes and single strands was performed. Samples were prepared to contain 7.5pmol of oligonucleotides in 10 μ L of PBS (Invitrogen, Carlsbad, CA) and mixed with 1 μ L of DNA loading dye (Thermo Fisher Scientific, Waltham, MA). Samples were then loaded onto 20% (w/v) acrylamide running gel prepared in a Tris-acetate-EDTA buffer (TAE buffer: 40 mM Tris-acetate, 1 mM EDTA, pH 8.0). Gel was then immersed in TAE buffer and electrophoresed at constant voltage of 60V for 15 minutes, followed by 60 minutes at 150V. Oligonucleotides were revealed following manufacture's protocol for SYBR Gold nucleic acid gel stain (Invitrogen, Carlsbad, CA) and fluorescence was recorded on a ChemiDoc XRS (Bio-Rad, Gladesville NSW).

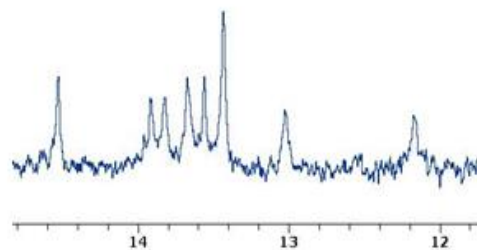
ps-iDD:D2

5'-TiCA TAA iCTiG iGAT-3'
5'-AGT ATT GAC CTA-3'



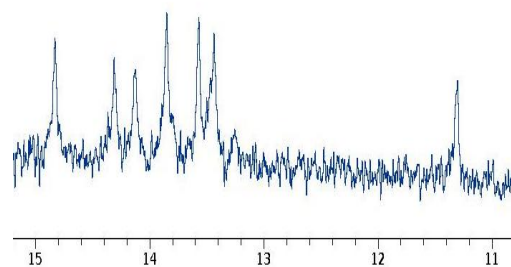
ps-iDD:aF2

5'-TiCA TAA iCTiG iGAT-3'
5'-AGT ATT **GAC CTA**-3'



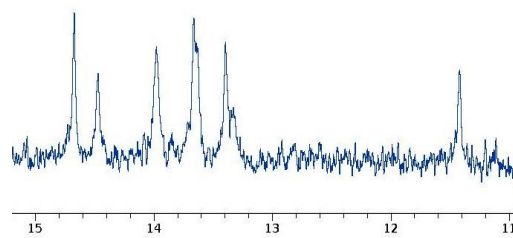
ps-iDD:R2

5'-TiCA TAA iCTiG iGAT-3'
5'-AGU AUU **GAC CUA**-3'



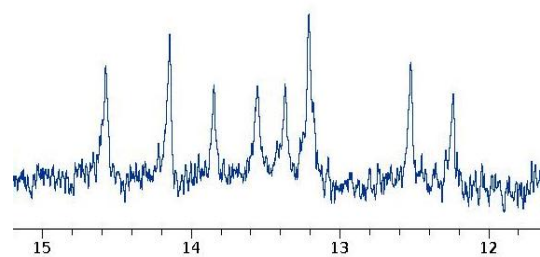
ps-iDD:rF2

5'-TiCA TAA iCTiG iGAT-3'
5'-AGU AUU **GAC CUA**-3'



ps-iD-aF:D2

5'-TiCA **TAA** iCTiG iGAT-3'
5'-AGT ATT GAC CTA-3'



ps-iD-aF:aF2

5'-TiCA **TAA** iCTiG iGAT-3'
5'-AGT ATT **GAC CTA**-3'

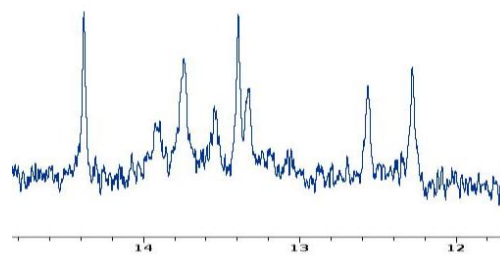
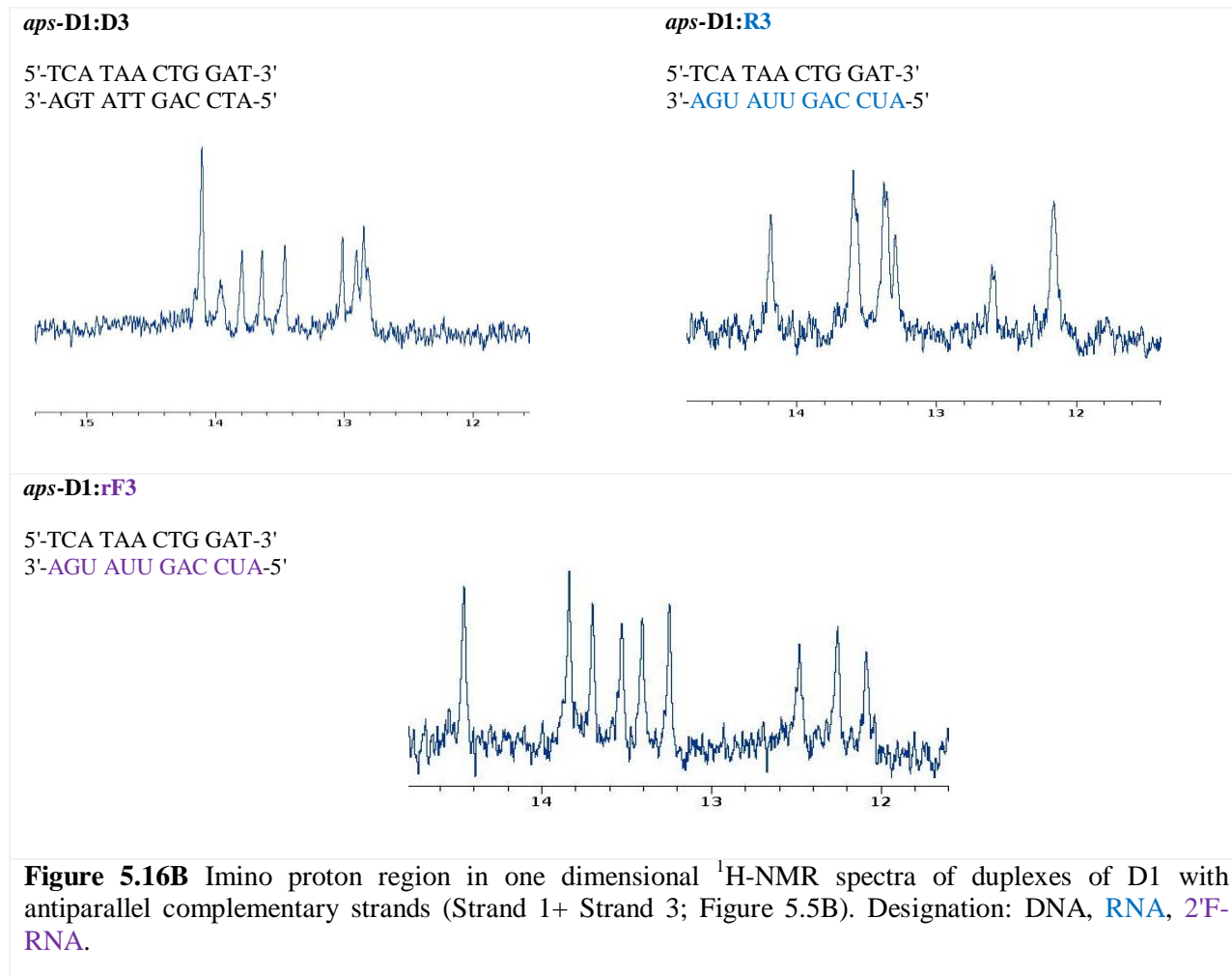


Figure 5.16A Imino region of 1D $^1\text{H-NMR}$ spectra of hybrids of iDD and iD-Af with various parallel complementary strands (Strand 1 + Strand 2; Figure 5.5B). Designation: DNA, iso-DNA, **2'F-ANA**, RNA, **2'F-RNA**.



5.7.6 FRET Assays

Hybridization of Cy3 and Cy5 labeled strands was accomplished by combining equal amounts of labeled strands to a final concentration of $2\mu\text{M}$ in siRNA buffer (100mM KOAc, 30mM HEPES-KOH, 2mM $\text{Mg}(\text{OAc})_2$, pH 7.2). The mixtures were then heated to 93°C for 2 minutes followed by cooling to room temperature over a period of approximately 6 hours. Samples were then placed in a 4°C fridge overnight.

Luminescence spectra were recorded using a PTI QuantaMaster spectrofluorimeter using 1cm × 1cm quartz cuvettes and corrected for detector sensitivity. Slits were set at 2nm. At each experimental temperature, samples were excited at 500nm and emission was detected from 520 to 800nm.

5.7.7 Bcl-2 si-Duplex Formation and *in Vitro* Bcl-2 Assays

5.7.7.1 Bcl-2 si-duplex formation

Si-duplexes were obtained by annealing equimolar ratios of the sense and antisense strands in buffer (100 mM Potassium Acetate, 30 mM HEPES, pH 7.5, IDT, Coralville, IA) to a final concentration of 10 μ M. Samples were heated at 93 °C for 1 minute and slowly cooled at 4 °C overnight and left in fridge over night.

5.7.7.2 Cell Culture

Caco-2 cells were maintained in Dulbecco's modified Eagle's medium (DMEM; Invitrogen, Carlsbad, CA) supplemented with 4.5 g/L glucose, 10% fetal bovine serum (FBS; Invitrogen, Carlsbad, CA), 1% nonessential amino acids (Invitrogen, Carlsbad, CA) and a 1% antibiotic solution (100 units/mL penicillin, 100 μ g/mL streptomycin; Invitrogen, Carlsbad, CA) at 37⁰C in a 5% CO₂ humidified atmosphere. The cells were seeded one day prior to the experiment in a 12-multiwell plate at a density of 7 × 10⁴ cells/well in complete DMEM containing 10% FBS.

5.7.7.3 Lipofectamine™ 2000 -Mediated Oligonucleotide Delivery

For the assessment of the knockdown efficacies, the duplexes or single-stranded oligonucleotides were complexed with Lipofectamine™ 2000 (Invitrogen, Carlsbad, CA) in DMEM as recommended by the manufacturer. Samples were then diluted 10 times with 10% FBS DMEM

medium, and incubated with the cells for 5 hours in a total volume of 500 μ L. Subsequently, the transfection medium was changed to complete DMEM containing 10% FBS. Medium containing no oligonucleotides was used as a control. After a 72 hour total incubation time, cells were harvested and RNA was isolated using RNeasy Mini kit (QIAGEN, Valencia, CA). Purified RNA ($OD_{260}/OD_{230} > 1.6$) was used as a template to assess the gene expression level of B-cl2 via a two-step quantitative reverse-transcription PCR (qRT-PCR) (115). Briefly, reverse-transcription reaction was carried out using high capacity cDNA reverse transcriptase kit (Applied Biosystems, Carlsbad, MA). Following the cDNA synthesis, the qPCR was done using Power SYBR Green PCR Master Mix (Applied Biosystems) with a 7900HT Fast Real Time PCR system (Applied Biosystems). The data were normalized to the internal control; β - actin. The primers for B-cl2 and β -actin were purchased from QIAGEN. All procedures followed the manufacturer's protocol. Relative gene expression levels were calculated using the delta Ct method ($2^{-\Delta\Delta Ct}$). Results are expressed as the B-cl2 mRNA level fold change between treated and non-treated samples. Potency (EC_{50}) was calculated using a four-parameter logistic function to fit the dose-response data and SigmaPlot software.

5.8 References

1. Watson, J.D. and Crick, F.H.C. (1953) Molecular Structure of Nucleic Acids: A Structure for Deoxyribose Nucleic Acid. *Nature*, **171**, 737-738.
2. Rippe, K. and Jovin, T.M. (1992) In David M.J. Lilley, J. E. D. (ed.), *Methods in enzymology*. Academic Press, Vol. Volume 211, pp. 199-220.
3. Ramsing, N.B., Rippe, K. and Jovin, T.M. (1989) Helix-coil transition of parallel-stranded DNA. Thermodynamics of hairpin and linear duplex oligonucleotides. *Biochemistry*, **28**, 9528-9535.
4. Rippe, K., Ramsing, N.B., Klement, R. and Jovin, T.M. (1990) A Parallel Stranded Linear DNA Duplex Incorporating dG · dC Base Pairs. *Journal of Biomolecular Structure and Dynamics*, **7**, 1199-1209.

5. van de Sande, J., Ramsing, N., Germann, M., Elhorst, W., Kalisch, B., von Kitzing, E., Pon, R., Clegg, R. and Jovin, T. (1988) Parallel stranded DNA. *Science (New York, N.Y.)*, **241**, 551-557.
6. Shchyolkina, A.K., Lysov Yu, P., Il'ichova, I.A., Chernyi, A.A., Golova Yu, B., Chernov, B.K., Gottikh, B.P. and Florentiev, V.L. (1989) Parallel stranded DNA with AT base pairing. *FEBS Lett*, **244**, 39-42.
7. Raghunathan, G., Miles, H.T. and Sasisekharan, V. (1994) Parallel nucleic acid helices with Hoogsteen base pairing: Symmetry and structure. *Biopolymers*, **34**, 1573-1581.
8. Frank-Kamenetskii, M.D. and Mirkin, S.M. (1995) Triplex DNA Structures. *Annual Review of Biochemistry*, **64**, 65-95.
9. Lavelle, L. and Fresco, J.R. (1995) UV spectroscopic identification and thermodynamic analysis of protonated third strand deoxycytidine residues at neutrality in the triplex d(C⁺-T)₆:[d(A-G)₆d(C⁻-T)₆]; evidence for a proton switch. *Nucleic Acids Research*, **23**, 2692-2705.
10. Marfurt, J. and Leumann, C. (1998) Evidence for C-H...O Hydrogen Bond Assisted Recognition of a Pyrimidine Base in the Parallel DNA Triple-Helical Motif. *Angewandte Chemie International Edition*, **37**, 175-177.
11. Marfurt, J., Parel, S.P. and Leumann, C.J. (1997) Strong, specific, monodentate G-C base pair recognition by N7-inosine derivatives in the pyrimidine•purine-pyrimidine triple-helical binding motif. *Nucleic Acids Research*, **25**, 1875-1882.
12. Sun, J.-s., Carestier, T. and Hélène, C. (1996) Oligonucleotide directed triple helix formation. *Current Opinion in Structural Biology*, **6**, 327-333.
13. Burge, S., Parkinson, G.N., Hazel, P., Todd, A.K. and Neidle, S. (2006) Quadruplex DNA: sequence, topology and structure. *Nucleic Acids Research*, **34**, 5402-5415.
14. Blackburn, E.H. and Szostak, J.W. (1984) The Molecular Structure of Centromeres and Telomeres. *Annual Review of Biochemistry*, **53**, 163-194.
15. Hurley, L.H. (2002) DNA and its associated processes as targets for cancer therapy. *Nat Rev Cancer*, **2**, 188-200.
16. Sundquist, W.I. and Klug, A. (1989) Telomeric DNA dimerizes by formation of guanine tetrads between hairpin loops. *Nature*, **342**, 825-829.
17. Sen, D. and Gilbert, W. (1988) Formation of parallel four-stranded complexes by guanine-rich motifs in DNA and its implications for meiosis. *Nature*, **334**, 364-366.
18. Guéron, M. and Leroy, J.-L. (2000) The i-motif in nucleic acids. *Current Opinion in Structural Biology*, **10**, 326-331.
19. Völker, J., Klump, H.H. and Breslauer, K.J. (2007) The energetics of i-DNA tetraplex structures formed intermolecularly by d(TC5) and intramolecularly by d[(C5T3)3C5]. *Biopolymers*, **86**, 136-147.
20. Pattabiraman, N. (1986) Can the double helix be parallel? *Biopolymers*, **25**, 1603-1606.
21. Shchyolkina, A.K., Borisova, O.F. and Jovin, T.M. (1999) Parallel-Stranded Oligonucleotides with Alternating d(A-isoG)/d(T-C) and d(A-G)/d(T-m5isoC) Sequences. *Nucleosides and Nucleotides*, **18**, 1555-1562.
22. Parvathy, V.R., Bhaumik, S.R., Chary, K.V.R., Govil, G., Liu, K., Howard, F.B. and Miles, H.T. (2002) NMR structure of a parallel-stranded DNA duplex at atomic resolution. *Nucleic Acids Research*, **30**, 1500-1511.

23. Germann, M.W., Zhou, N., van de Sande, J.H. and Vogel, H.J. (1995) Parallel-stranded duplex DNA: an NMR perspective. *Methods in enzymology*, **261**, 207-225.
24. Germann, M.W., Kalisch, B.W. and van de Sande, J.H. (1998) Structure of d(GT)_n.d(GA)_n sequences: formation of parallel stranded duplex DNA. *Biochemistry*, **37**, 12962-12970.
25. Germann, M.W., Kalisch, B.W. and van de Sande, J.H. (1988) Relative stability of parallel- and anti-parallel-stranded duplex DNA. *Biochemistry*, **27**, 8302-8306.
26. Barsky, D. and Colvin, M.E. (2000) Guanine–Cytosine Base Pairs in Parallel-Stranded DNA: An ab Initio Study of the Keto–Amino Wobble Pair versus the Enol–Imino Minor Tautomer Pair. *The Journal of Physical Chemistry A*, **104**, 8570-8576.
27. Sunami, T., Kondo, J., Kobuna, T., Hirao, I., Watanabe, K., Miura, K.i. and Takénaka, A. (2002) Crystal structure of d(GCGAAAGCT) containing a parallel-stranded duplex with homo base pairs and an anti-parallel duplex with Watson–Crick base pairs. *Nucleic Acids Research*, **30**, 5253-5260.
28. Cubero, E., Aviñó, A., de la Torre, B.G., Frieden, M., Eritja, R., Luque, F.J., González, C. and Orozco, M. (2002) Hoogsteen-Based Parallel-Stranded Duplexes of DNA. Effect of 8-Amino-purine Derivatives. *Journal of the American Chemical Society*, **124**, 3133-3142.
29. Garcia, A.E., Soumpasis, D.M. and Jovin, T.M. (1994) Dynamics and relative stabilities of parallel- and antiparallel-stranded DNA duplexes. *Biophysical Journal*, **66**, 1742-1755.
30. Rippe, K., Ramsing, N.B. and Jovin, T.M. (1989) Spectroscopic properties and helical stabilities of 25-nt parallel-stranded linear DNA duplexes. *Biochemistry*, **28**, 9536-9541.
31. Rentzeperis, D., Rippe, K., Jovin, T.M. and Marky, L.A. (1992) Calorimetric characterization of parallel-stranded DNA: stability, conformational flexibility, and ion binding. *Journal of the American Chemical Society*, **114**, 5926-5928.
32. Ramsing, N.B. and Jovin, T.M. (1988) Parallel stranded duplex DNA. *Nucleic Acids Res*, **16**, 6659-6676.
33. Luo, J., Sarma, M.H., Yuan, R.-d. and Sarma, R.H. (1992) NMR study of self-paired parallel duplex of d(AAAAACCCCC) in solution. *FEBS Letters*, **306**, 223-228.
34. Ishikawa, F., Frazier, J., Howard, F.B. and Miles, H.T. (1972) Polyadenylate polyuridylate helices with non-Watson-Crick hydrogen bonding. *Journal of Molecular Biology*, **70**, 475-490.
35. Seela, F., Melenewski, A. and Wei, C. (1997) Parallel-stranded duplex DNA formed by a new base pair between guanine and 5-aza-7-deazaguanine. *Bioorganic & Medicinal Chemistry Letters*, **7**, 2173-2176.
36. Sugiyama, H., Ikeda, S. and Saito, I. (1996) Remarkably Stable Parallel-Stranded Oligonucleotides Containing 5-Methylisocytosine and Isoguanine. *Journal of the American Chemical Society*, **118**, 9994-9995.
37. Seela, F., Wei, C., Melenewski, A., He, Y., Kröschel, R. and Feiling, E. (1999) Parallel-Stranded DNA Formed by New Base Pairs Related to the Isoguanine-Cytosine or Isocytosine-Guanine Motifs. *Nucleosides and Nucleotides*, **18**, 1543-1548.
38. Seela, F., He, Y. and Wei, C. (1999) Parallel-stranded oligonucleotide duplexes containing 5-methylisocytosine-guanine and isoguanine-cytosine base pairs. *Tetrahedron*, **55**, 9481-9500.
39. Lancelot, G., Guesnet, J.L. and Vovelle, F. (1989) Solution structure of the parallel-stranded duplex oligonucleotide .alpha.-d(TCTAAAC)-.beta.-(AGATTTG) via complete

- relaxation matrix analysis of the NOE effects and molecular mechanics calculations. *Biochemistry*, **28**, 7871-7878.
40. Thuong, N.T., Asseline, U., Roig, V., Takasugi, M. and Hélène, C. (1987) Oligo(alpha-deoxynucleotide)s covalently linked to intercalating agents: differential binding to ribo- and deoxyribopolynucleotides and stability towards nuclease digestion. *Proceedings of the National Academy of Sciences*, **84**, 5129-5133.
 41. Praseuth, D., Chassignol, M., Takasugi, M., Le Doan, T., Thuong, N.T. and Hélène, C. (1987) Double helices with parallel strands are formed by nuclease-resistant oligo-[α]-deoxynucleotides and oligo-[α]-deoxynucleotides covalently linked to an intercalating agent with complementary oligo-[β]-deoxynucleotides. *Journal of Molecular Biology*, **196**, 939-942.
 42. Aramini, J.M., Kalisch, B.W., Pon, R.T., van de Sande, J.H. and Germann, M.W. (1996) Structure of a DNA duplex that contains alpha-anomeric nucleotides and 3'-3' and 5'-5' phosphodiester linkages: coexistence of parallel and antiparallel DNA. *Biochemistry*, **35**, 9355-9365.
 43. Rich, A., Davies, D.R., Crick, F.H.C. and Watson, J.D. (1961) The molecular structure of polyadenylic acid. *Journal of Molecular Biology*, **3**, 71-119.
 44. Coll, M., Solans, X., Font-Altaba, M. and Subirana, J.A. (1987) Crystal and Molecular Structure of the Sodium Salt of the Dinucleotide Duplex d(CpG). *Journal of Biomolecular Structure and Dynamics*, **4**, 797-811.
 45. Liu, K., Miles, H.T., Frazier, J. and Sasisekharan, V. (1993) A novel DNA duplex. A parallel-stranded DNA helix with Hoogsteen base pairing. *Biochemistry*, **32**, 11802-11809.
 46. Jain, A.K. and Bhattacharya, S. (2010) Groove Binding Ligands for the Interaction with Parallel-Stranded ps-Duplex DNA and Triplex DNA. *Bioconjugate Chemistry*, **21**, 1389-1403.
 47. Li, H., Peng, X., Leonard, P. and Seela, F. (2006) Binding of actinomycin C1 (D) and actinomycin to base-modified oligonucleotide duplexes with parallel chain orientation. *Bioorganic & Medicinal Chemistry*, **14**, 4089-4100.
 48. Rippe, K. and Jovin, T.M. (1989) Substrate properties of 25-nt parallel-stranded linear DNA duplexes. *Biochemistry*, **28**, 9542-9549.
 49. Förtsch, I., Birch-Hirschfeld, E., Jovin, T.M., Stelzner, A. and Zimmer, C. (1998) Studies on the Interaction of Dna-Ligands with Modified Parallel-Stranded Duplex-Dna Oligomers. *Nucleosides and Nucleotides*, **17**, 1539-1545.
 50. Klysik, J., Rippe, K. and Jovin, T.M. (1990) Reactivity of parallel-stranded DNA to chemical modification reagents. *Biochemistry*, **29**, 9831-9839.
 51. Mohammadi, S., Klement, R., Shchylkina, A.K., Liquier, J., Jovin, T.M. and Taillandier, E. (1998) FTIR and UV Spectroscopy of Parallel-Stranded DNAs with Mixed A•T/G•C Sequences and Their A•T/I•C Analogues. *Biochemistry*, **37**, 16529-16537.
 52. Otto, C., Thomas, G.A., Rippe, K., Jovin, T.M. and Peticolas, W.L. (1991) The hydrogen-bonding structure in parallel-stranded duplex DNA is reverse Watson-Crick. *Biochemistry*, **30**, 3062-3069.
 53. Leontis, N.B., Stombaugh, J. and Westhof, E. (2002) The non-Watson-Crick base pairs and their associated isostericity matrices. *Nucleic Acids Research*, **30**, 3497-3531.

54. Tchurikov, N.A., Chernov, B.K., Golova, Y.B. and Nechipurenko, Y.D. (1989) Parallel DNA: generation of a duplex between two *Drosophila* sequences in vitro. *FEBS Lett*, **257**, 415-418.
55. Borisova, O.F., Shchvolkina, A.K., Chernov, B.K. and Tchurikov, N.A. (1993) Relative stability of AT and GC pairs in parallel DNA duplex formed by a natural sequence. *FEBS Lett*, **322**, 304-306.
56. Yang, X.-L., Sugiyama, H., Ikeda, S., Saito, I. and Wang, A.H.J. (1998) Structural Studies of a Stable Parallel-Stranded DNA Duplex Incorporating Isoguanine:Cytosine and Isocytosine:Guanine Basepairs by Nuclear Magnetic Resonance Spectroscopy. *Biophysical Journal*, **75**, 1163-1171.
57. Geinguenaud, F., Mondragon-Sanchez, J.A., Liquier, J., Shchvolkina, A.K., Klement, R., Arndt-Jovin, D.J., Jovin, T.M. and Taillandier, E. (2005) Parallel DNA double helices incorporating isoG or m5isoC bases studied by FTIR, CD and molecular modeling. *Spectrochimica Acta Part A: Molecular and Biomolecular Spectroscopy*, **61**, 579-587.
58. Escudé, C., Mohammadi, S., Sun, J.-S., Nguyen, C.-H., Bisagni, E., Liquier, J., Taillandier, E., Garestier, T. and Hélène, C. (1996) Ligand-induced formation of Hoogsteen-paired parallel DNA. *Chemistry & Biology*, **3**, 57-65.
59. Suda, T., Mishima, Y., Asakura, H. and Kominami, R. (1995) Formation of a parallel-stranded DNA homoduplex by d(GGA) repeat oligonucleotides. *Nucleic Acids Research*, **23**, 3771-3777.
60. Wang, Y. and Patel, D.J. (1994) Solution Structure of the d(T-C-G-A) Duplex at Acidic pH: A Parallel-Stranded Helix Containing C⁺ · C, G · G and A · A Pairs. *Journal of Molecular Biology*, **242**, 508-526.
61. Robinson, H. and Wang, A.H. (1993) 5'-CGA sequence is a strong motif for homo base-paired parallel-stranded DNA duplex as revealed by NMR analysis. *Proceedings of the National Academy of Sciences*, **90**, 5224-5228.
62. Robinson, H., Van der Marel, G.A., Van Boom, J.H. and Wang, A.H.J. (1992) Unusual DNA conformation at low pH revealed by NMR: parallel-stranded DNA duplex with homo base pairs. *Biochemistry*, **31**, 10510-10517.
63. Rippe, K., Fritsch, V., Westhof, E. and Jovin, T.M. (1992) Alternating d(G-A) sequences form a parallel-stranded DNA homoduplex. *The EMBO journal*, **11**, 3777-3786.
64. Dolinnaya, N.G., Ulku, A. and Fresco, J.R. (1997) Parallel-Stranded Linear Homoduplexes of d(A⁺-G)/n > 10 and d(A-G)n > 10 Manifesting the Contrasting Ionic Strength Sensitivities of Poly(A⁺-A⁺) and DNA. *Nucleic Acids Research*, **25**, 1100-1107.
65. Tchurikov, N.A., Chistyakova, L.G., Zavilgelsky, G.B., Manukhov, I.V., Chernov, B.K. and Golova, Y.B. (2000) Gene-specific Silencing by Expression of Parallel Complementary RNA in *Escherichia coli*. *J. Biol. Chem.*, **275**, 26523-26529.
66. Liu, Y., Zhang, Y., Yang, L., Yao, T. and Xiao, C. (2009) Gene-specific silencing induced by parallel complementary RNA in *Pseudomonas aeruginosa*. *Biotechnol Lett*, **31**, 1571-1575.
67. Tchurikov, N.A. (1992) Natural DNA sequences complementary in the same direction: evidence for parallel biosynthesis? *Genetica*, **87**, 113-117.
68. Soyfer, V. and Potaman, V. (1996), *Triple-Helical Nucleic Acids*. Springer New York, pp. 1-46.

69. Fritzsche, H., Akhebat, A., Taillandier, E., Rippe, K. and Jovin, T.M. (1993) Structure and Drug interaction of parallel-stranded DNA studies by infrared spectroscopy and fluorescence. *Nucleic Acids Research*, **21**, 5085-5091.
70. Tchurikov, N.A., Ponomarenko, N.A., Golova, Y.B. and Chernov, B.K. (1995) The formation of parallel RNA-RNA duplexes in vitro. *Journal of biomolecular structure & dynamics*, **13**, 507-513.
71. Safaee, N., Noronha, A.M., Rodionov, D., Kozlov, G., Wilds, C.J., Sheldrick, G.M. and Gehring, K. (2013) Structure of the Parallel Duplex of Poly(A) RNA: Evaluation of a 50 Year-Old Prediction. *Angewandte Chemie International Edition*, **52**, 10370-10373.
72. Watts, J.K., Martín-Pintado, N., Gómez-Pinto, I., Schwartzentruber, J., Portella, G., Orozco, M., González, C. and Damha, M.J. (2010) Differential stability of 2'-F-ANA•RNA and ANA•RNA hybrid duplexes: roles of structure, pseudohydrogen bonding, hydration, ion uptake and flexibility. *Nucleic Acids Research*, **38**, 2498-2511.
73. Anzahaee, M.Y., Watts, J.K., Alla, N.R., Nicholson, A.W. and Damha, M.J. (2010) Energetically Important C-H...F-C Pseudohydrogen Bonding in Water: Evidence and Application to Rational Design of Oligonucleotides with High Binding Affinity. *Journal of the American Chemical Society*, **133**, 728-731.
74. Pallan, P.S., Greene, E.M., Jicman, P.A., Pandey, R.K., Manoharan, M., Rozners, E. and Egli, M. (2011) Unexpected origins of the enhanced pairing affinity of 2'-fluoro-modified RNA. *Nucleic Acids Research*, **39**, 3482-3495.
75. Patra, A., Paolillo, M., Charisse, K., Manoharan, M., Rozners, E. and Egli, M. (2012) 2'-Fluoro RNA Shows Increased Watson-Crick H-Bonding Strength and Stacking Relative to RNA: Evidence from NMR and Thermodynamic Data. *Angewandte Chemie International Edition*, **51**, 11863-11866.
76. Seela, F., Wei, C., Becher, G., Zulauf, M. and Leonard, P. (2000) The influence of modified purine bases on the stability of parallel DNA. *Bioorganic & Medicinal Chemistry Letters*, **10**, 289-292.
77. Seela, F., Peng, X. and Li, H. (2005) Base-Pairing, Tautomerism, and Mismatch Discrimination of 7-Halogenated 7-Deaza-2'-deoxyisoguanosine: Oligonucleotide Duplexes with Parallel and Antiparallel Chain Orientation. *Journal of the American Chemical Society*, **127**, 7739-7751.
78. Wilds, C.J. and Damha, M.J. (2000) 2'-Deoxy-2'-fluoro- β -D-arabinonucleosides and oligonucleotides (2'-F-ANA): synthesis and physicochemical studies. *Nucleic Acids Research*, **28**, 3625-3635.
79. Gray, D.M., Ratliff, R.L. and Vaughan, M.R. (1992) Circular dichroism spectroscopy of DNA. *Methods in enzymology*, **211**, 389-406.
80. Ratmeyer, L., Vinayak, R., Zhong, Y.Y., Zon, G. and Wilson, W.D. (1994) Sequence Specific Thermodynamic and Structural Properties for DNA•RNA Duplexes. *Biochemistry*, **33**, 5298-5304.
81. Hung, S.-H., Yu, Q., Gray, D.M. and Ratliff, R.L. (1994) Evidence from CD spectra that d(purine)-r(pyrimidine) and r(purine)-d(pyrimidine) hybrids are in different structural classes. *Nucleic Acids Research*, **22**, 4326-4334.

82. Zhou, N., Germann, M.W., van de Sande, J.H., Pattabiraman, N. and Vogel, H.J. (1993) Solution structure of the parallel-stranded hairpin d(T8.ltbbbrac..rtbbbrac.C4A8) as determined by two-dimensional NMR. *Biochemistry*, **32**, 646-656.
83. Germann, M.W., Zhou, N., van de Sande, J.H. and Vogel, H.J. (1995) In Thomas, L. J. (ed.), *Methods in enzymology*. Academic Press, Vol. Volume 261, pp. 207-225.
84. Kubo, T., Zhelev, Z., Rumiana, B., Ohba, H., Doi, K. and Fujii, M. (2005) Controlled intracellular localization and enhanced antisense effect of oligonucleotides by chemical conjugation. *Organic & Biomolecular Chemistry*, **3**, 3257-3259.
85. Kubo, T., Takamori, K., Kanno, K.-i., Rumiana, B., Ohba, H., Matsukisono, M., Akebiyama, Y. and Fujii, M. (2005) Efficient cleavage of RNA, enhanced cellular uptake, and controlled intracellular localization of conjugate DNAzymes. *Bioorganic & Medicinal Chemistry Letters*, **15**, 167-170.
86. Kubo, T., Morikawa, M., Ohba, H. and Fujii, M. (2003) Synthesis of DNA–Peptide Conjugates by Solid-Phase Fragment Condensation. *Organic Letters*, **5**, 2623-2626.
87. Deleavey, G.F., Watts, J.K., Alain, T., Robert, F., Kalota, A., Aishwarya, V., Pelletier, J., Gewirtz, A.M., Sonenberg, N. and Damha, M.J. (2010) Synergistic effects between analogs of DNA and RNA improve the potency of siRNA-mediated gene silencing. *Nucleic Acids Research*, **38**, 4547-4557.
88. Manoharan, M., Akinc, A., Pandey, R.K., Qin, J., Hadwiger, P., John, M., Mills, K., Charisse, K., Maier, M.A., Nechev, L. *et al.* (2011) Unique Gene-Silencing and Structural Properties of 2'-Fluoro-Modified siRNAs. *Angewandte Chemie International Edition*, **50**, 2284-2288.
89. Ui-Tei, K., Naito, Y., Zenno, S., Nishi, K., Yamato, K., Takahashi, F., Juni, A. and Saigo, K. (2008) Functional dissection of siRNA sequence by systematic DNA substitution: modified siRNA with a DNA seed arm is a powerful tool for mammalian gene silencing with significantly reduced off-target effect. *Nucleic Acids Research*, **36**, 2136-2151.
90. Anzahaee, M.Y., Deleavey, G.F., Le, P.U., Fakhoury, J., Petrecca, K. and Damha, M.J. (2014) Arabinonucleic Acids: 2'-Stereoisomeric Modulators of siRNA Activity. *Nucleic Acid Ther*, **24**, 336-343.
91. Anderson, E.M., Miller, P., Ilesley, D., Marshall, W., Khvorova, A., Stein, C.A. and Benimetskaya, L. (2005) Gene profiling study of G3139- and Bcl-2-targeting siRNAs identifies a unique G3139 molecular signature. *Cancer Gene Ther*, **13**, 406-414.
92. Elbashir, S.M., Martinez, J., Patkaniowska, A., Lendeckel, W. and Tuschl, T. (2001) Functional anatomy of siRNAs for mediating efficient RNAi in *Drosophila melanogaster* embryo lysate. *The EMBO journal*, **20**, 6877-6888.
93. Parrish, S., Fleenor, J., Xu, S., Mello, C. and Fire, A. (2000) Functional anatomy of a dsRNA trigger: differential requirement for the two trigger strands in RNA interference. *Mol Cell*, **6**, 1077-1087.
94. Jovin, T.M. (1991) in: *Nucleic Acids and Molecular Biology* (ed. By Eckstein, F. and Lilley, D. M. J.), Springer-Verlag, Berlin.
95. Stryer, L. and Haugland, R.P. (1967) Energy transfer: a spectroscopic ruler. *Proceedings of the National Academy of Sciences of the United States of America*, **58**, 719-726.
96. Selvin, P.R. (1995) In Kenneth, S. (ed.), *Methods in enzymology*. Academic Press, Vol. Volume 246, pp. 300-334.

97. Chirio-Lebrun, M.-C. and Prats, M. (1998) Fluorescence resonance energy transfer (FRET): Theory and experiments. *Biochemical Education*, **26**, 320-323.
98. Ishikawa-Ankerhold, H.C., Ankerhold, R. and Drummen, G.P.C. (2012) Advanced Fluorescence Microscopy Techniques—FRAP, FLIP, FLAP, FRET and FLIM. *Molecules*, **17**, 4047-4132.
99. Lima, Walt F., Prakash, Thazha P., Murray, Heather M., Kinberger, Garth A., Li, W., Chappell, Alfred E., Li, Cheryl S., Murray, Susan F., Gaus, H., Seth, Punit P. *et al.* (2012) Single-Stranded siRNAs Activate RNAi in Animals. *Cell*, **150**, 883-894.
100. Yu, D., Pendergraff, H., Liu, J., Kordasiewicz, H.B., Cleveland, Don W., Swayze, Eric E., Lima, Walt F., Crooke, Stanley T., Prakash, Thazha P. and Corey, David R. (2012) Single-Stranded RNAs Use RNAi to Potently and Allele-Selectively Inhibit Mutant Huntingtin Expression. *Cell*, **150**, 895-908.
101. Jackson, A.L., Burchard, J., Leake, D., Reynolds, A., Schelter, J., Guo, J., Johnson, J.M., Lim, L., Karpilow, J., Nichols, K. *et al.* (2006) Position-specific chemical modification of siRNAs reduces “off-target” transcript silencing. *RNA*, **12**, 1197-1205.
102. Whitehead, K.A., Dahlman, J.E., Langer, R.S. and Anderson, D.G. (2011) Silencing or stimulation? siRNA delivery and the immune system. *Annual review of chemical and biomolecular engineering*, **2**, 77-96.
103. Czauderna, F., Fechtner, M., Dames, S., Aygün, H., Klippel, A., Pronk, G.J., Giese, K. and Kaufmann, J. (2003) Structural variations and stabilising modifications of synthetic siRNAs in mammalian cells. *Nucleic Acids Research*, **31**, 2705-2716.
104. Amarzguioui, M., Holen, T., Babaie, E. and Prydz, H. (2003) Tolerance for mutations and chemical modifications in a siRNA. *Nucleic Acids Research*, **31**, 589-595.
105. Braasch, D.A., Jensen, S., Liu, Y., Kaur, K., Arar, K., White, M.A. and Corey, D.R. (2003) RNA Interference in Mammalian Cells by Chemically-Modified RNA[†]. *Biochemistry*, **42**, 7967-7975.
106. Kenski, D.M., Cooper, A.J., Li, J.J., Willingham, A.T., Haringsma, H.J., Young, T.A., Kuklin, N.A., Jones, J.J., Cancilla, M.T., McMasters, D.R. *et al.* (2010) Analysis of acyclic nucleoside modifications in siRNAs finds sensitivity at position 1 that is restored by 5'-terminal phosphorylation both in vitro and in vivo. *Nucleic Acids Research*, **38**, 660-671.
107. Hall, A.H.S., Wan, J., Spesock, A., Sergueeva, Z., Shaw, B.R. and Alexander, K.A. (2006) High potency silencing by single-stranded boranophosphate siRNA. *Nucleic Acids Research*, **34**, 2773-2781.
108. Watts, J.K., Deleavey, G.F. and Damha, M.J. (2008) Chemically modified siRNA: tools and applications. *Drug Discovery Today*, **13**, 842-855.
109. Deleavey, G.F., Watts, J.K. and Damha, M.J. (2001), *Current Protocols in Nucleic Acid Chemistry*. John Wiley & Sons, Inc.
110. Deleavey, G.F. and Damha, M.J. (2012) Designing chemically modified oligonucleotides for targeted gene silencing. *Chemistry and Biology*, **19**, 937-954.
111. Watts, J.K. and Corey, D.R. (2012) Silencing disease genes in the laboratory and the clinic. *The Journal of Pathology*, **226**, 365-379.
112. Peacock, H., Kannan, A., Beal, P.A. and Burrows, C.J. (2011) Chemical Modification of siRNA Bases To Probe and Enhance RNA Interference. *The Journal of Organic Chemistry*, **76**, 7295-7300.

113. Damha, M. and Ogilvie, K. (1993) In Agrawal, S. (ed.), *Protocols for Oligonucleotides and Analogs*. Humana Press, Vol. 20, pp. 81-114.
114. Westman, E. and Stromberg, R. (1994) Removal of t-butyldimethylsilyl protection in RNA-synthesis. Triethylamine trihydrofluoride (TEA, 3HF) is a more reliable alternative to tetrabutylammonium fluoride (TBAF). *Nucleic Acids Research*, **22**, 2430-2431.
115. Felber, A.E., Bayo-Puxan, N., Deleavey, G.F., Castagner, B., Damha, M.J. and Leroux, J.C. (2012) The interactions of amphiphilic antisense oligonucleotides with serum proteins and their effects on in vitro silencing activity. *Biomaterials*, **33**, 5955-5965.

CHAPTER 6: CONTRIBUTIONS TO KNOWLEDGE

6.1 Summary of Research

6.1.1 Structural Effects Determining the High Thermal Stability of 2'F-ANA:RNA Hybrids

There is much debate over whether organic fluorine can form energetically important hydrogen bonds in aqueous environments. This work led to the unexpected finding that the high binding affinity of 2'F-ANA towards RNA is, in part, due to a hydrogen bonding interaction between the organic fluorine at 2'-position of the 2'F-ANA nucleotides and the H8 of the proximal purine (i.e. C-H8...2'F-C). Comparisons of the melting profiles of several 2'F-ANA modified duplexes with an identical base composition but a rearranged sequence confirmed that energetically important fluorine-mediated “pseudohydrogen” bonding is in operation in these sequences, and that the effect is more pronounced when the H-bond donor (purine H8) is activated (intrinsically acidic) by the presence of electronegative fluorine at its own 2'-position. These results have been used as an additional design rule for the creation of therapeutically relevant 2'F-ANA modified antisense oligonucleotides.

6.1.2 Directing the Folding of Human Telomeric Quadruplex with a single 2'F-arabinose substitution

Human telomeric DNA quadruplexes have garnered considerable attention due to their involvement in telomere maintenance and gene regulation. These unique structures can adopt different conformations in solution. We have shown that a single 2'F-ANA, ANA, or RNA substitution stabilizes the propeller parallel G-quadruplex form over all competing conformers, allowing NMR structural determination of this particularly important nucleic acid structure.

We have found that 2'F-ANA substitution provides the greatest stabilization among all studied chemical modifications, which is in most part related to the formation of 2'F-CH...O4' and C-H8...2'F-C noncovalent interactions.

6.1.3 Effect of ANA and 2'F-ANA on Duplex-Hairpin Interconversion

Through a combination of thermal denaturation experiments, high resolution NMR and restrained molecular dynamics, we have demonstrated for the first time that while stable ANA:ANA duplexes are too unstable to form via ANA+ANA bimolecular association, an appropriate combination of 2'F-ANA and ANA nucleotides in a sequence containing a central segment ('gap') of ANA nucleotides flanked by two 2'F-ANA 'wings' can force ANAs to bind with sufficient stability and to an extent that allows its structural characterization by NMR. We have shown that such 'gapmer' design can adopt both a monomeric hairpin (with a loop consisting of unpaired ANA nucleotides) and a bimolecular duplex structure of comparable thermal stabilities. The co-existence of the duplex and hairpin structures may be a particularly useful tool in applications where a duplex/hairpin conformational switch is desirable. Our NMR analysis of this gapmer has once again revealed the formation favourable C-2'F...H8-C pseudohydrogen bonding interactions in the 2'F-ANA modified segments.

6.1.4 ANA as Modulators of siRNA Activity

We have shown for the first time that the arabinonucleic acid (ANA) modification has a place among chemically modified oligonucleotides known to be compatible with siRNA-mediated gene silencing in mammalian cells. We took advantage of ANA's destabilizing effects, and through combining ANA with its 2'-epimer (RNA) and its 2'F-analogue (2'F-ANA) in the siRNA

passenger strand and in patterns which bias duplex thermal stability, we have produced chemically modified duplexes that were capable of potent silencing of Luciferase and DRR, a gene linked to malignant glioma.

6.1.5 Development of Novel Chemically Modified Parallel-Stranded Duplexes

We have investigated the stability and helical structure of several reverse Watson-Crick parallel duplexes via circular dichroism (CD) and UV binding studies. Our study is the first to incorporate isoguanosine and isocytidine into an RNA strand, in order to assess whether formation of stable *ps*-RNA or *ps*-DNA:RNA hybrids is possible under physiological-like conditions. We have also examined for the first time the impact of 2'-fluorinated sugar modifications (2'F-ANA, and its epimer 2'F-RNA) on parallel duplex strength, and have shown that similar stabilization to what is gained with these modifications in the conventional antiparallel arrangement, is obtained, in most cases, in the parallel pattern as well.

6.1.6 Parallel-Stranded Duplexes are Compatible with RNAi

The results obtained from structural analysis and thermal stability measurements of parallel hybrids at physiological conditions inspired us to assess the ability of these duplexes for stimulation of RNAi activity. As such, we have introduced parallel hybridization as a completely different base pairing system to design a new class of siRNAs. Our preliminary results from gene silencing assays against the expression of the oncoprotein Bcl-2 have indicated that a parallel siRNA is capable of RNAi activation and eliciting gene silencing activity.

6.2 Papers, and Conference Presentations

6.2.1 Papers published

Maryam Yahyaee Anzahaee, Glen F. Deleavey, Phuong Uyen Li, Johans Fakhoury, Kevin Petrecca and Masad J. Damha; (2014) Arabinonucleic Acids: 2'-Stereoisomeric Modulators of siRNA Activity; *Nucleic Acids Therapeutics*, 24: 336-343

Nerea Martín-Pintado, Maryam Yahyaee Anzahaee, Glen F. Deleavey, Guillem Portella, Modesto Orozco, Masad J. Damha, and Carlos González; (2013) Dramatic Effect of Furanose C2' Substitution on Structure and Stability: Directing the Folding of the Human Telomeric Quadruplex with a Single Fluorine Atom; *J. Am. Chem. Soc.* 135: 5344-5347.

Nerea Martín-Pintado, Maryam Yahyaee Anzahaee, Ramon Campos-Olivas, Anne M. Noronha, Christopher J. Wilds, Masad J. Damha and Carlos González (2012) The solution structure of double helical arabino-nucleic acids (ANA and 2'-F-ANA): effect of arabinoses in duplex-hairpin interconversion; *Nucleic Acids Research*, 40: 9329–9339.

Maryam Yahyaee Anzahaee, Jonathan K. Watts, Nageswara R. Alla, Allen W. Nicholson, and Masad J. Damha; (2011) Energetically Important C-H...F-C Pseudohydrogen Bonding in Water: Evidence and Application to Rational Design of Oligonucleotides with High Binding Affinity; *J. Am. Chem. Soc.* 133: 728–731.

6.2.2 Papers in preparation

Maryam Yahyaee Anzahaee, Nerea Martín-Pintado, Elena Moroz, Jean-Christophe Leroux, Carlos González and Masad J. Damha; (2014) Structural properties and gene silencing activity of parallel-stranded nucleic acid duplexes; *manuscript in preparation*.

6.2.3 Conference Attendance

“Structural properties and gene silencing activity of parallel-stranded nucleic acid duplexes”, Maryam Yahyaee Anzahaee, Nerea Martín-Pintado, Elena Moroz, Jean-Christophe Leroux, Carlos González and Masad J. Damha; Oral Presentation in 248th American Chemical Society National Meeting & Exposition (ACS) in San Francisco, USA (August 2014).

“Structural properties and gene silencing activity of parallel-stranded nucleic acid duplexes”, Maryam Yahyaee Anzahaee, Nerea Martín-Pintado, Elena Moroz, Jean-Christophe Leroux, Carlos González and Masad J. Damha; Oral Presentation in 97th Canadian Chemistry Conference and Exhibition (CSC) in Vancouver, Canada (June 2014).

“Evidence for C-H \cdots F-C Pseudohydrogen Bonding in F2' Modified Single-Stranded Nucleic Acids”, Maryam Yahyaee Anzahaee, Nerea Martín-Pintado, Carlos González and Masad J. Damha; Poster presentation in the International Roundtable of Nucleosides, Nucleotides and Nucleic Acids in Montreal, Canada (August 2012).

“Energetically Important C-H...F-C Pseudohydrogen Bonding in Water: Evidence and Application to Rational Design of Oligonucleotides with High Binding Affinity”, Maryam Yahyae Anzahaee, Jonathan K. Watts, Nageswara R. Alla, Allen W. Nicholson, and Masad J. Damha; Oral presentation in 94th Canadian Chemistry Conference and Exhibition (CSC) in Montreal, Canada (June 2011).

“Role of pseudohydrogen bonding in the stabilization of nucleic acid double helices”, Jonathan K. Watts, Maryam Yahyae Anzahaee, Nerea Martin-Pintado, Carlos Gonzalez and Masad J. Damha; Poster Presentation in 93rd Canadian Chemistry Conference and Exhibition (CSC) in Toronto, Canada (June 2010).

